Molecular mechanisms

of therapy resistance and recurrence

in glioblastoma multiforme

Inaugural-Dissertation

zur Erlangung des Doktorgrades
der gesamten Naturwissenschaften (Dr. rer. nat.)
dem Fachbereich Medizin der Philipps-Universität Marburg

vorgelegt von

Agnes Schäfer
aus Siegen

Marburg, 2023

Angenommen vom Fachbereich Medizin der Philipps-Universität Marburg am: 10.07.2023

Gedruckt mit Genehmigung des Fachbereichs Medizin

Dekanin: Frau Prof. Dr. Denise Hilfiker-Kleiner

Referent: Herr Prof. Dr. Jörg-Walter Bartsch

1. Korreferent: Herr Prof. Dr. Leon Schulte

Für mein Rudel

Table of Contents

List of abbreviations

ABC	ATP binding cassette
ABCG2	ABC subfamily member 2
ACZ	Acetazolamide
ADAM	A disintegrin and metalloproteinase
AKT	Protein kinase B
ATG5	Autophagy related 5
ATM	Ataxia telangiectasia gene
ATP	Adenosine triphosphate
BBB	Blood-brain barrier
BCL-2	B-cell lymphoma 2
BRZ	Brinzolamide
CA	Carbonic anhdrasey
CAI	Carbonic anhydrase inhibitor
CCL	Chemokine (C-C motif) ligand
CD	Cytopplasmatic tail
CD44	Cluster of differentiation 44
CD81	Cluster of differentiation 81
CD133	Prominin-1-positive
CFSE	Carboxyfluorescein succinimidyl ester
CNS	Central nervous system
CTG	CellTiter-Glo®
CREB-1	Cyclic adenosine monophosphate responsive element-binding protein 1
CREBL2	cAMP responsive element binding protein-like 2
CRISPR	Clustered regulatory interspaced short palindromic repeats
CRISPR/Cas	Clustered regularly interspaced short palindromic repeats/ CRISPR associated protein
CXCL	Chemokine (C-X-C motif) ligand
DFO	Deferoxamine
DNA	Desoxyribonucleic acid
DRAM	Damage-regulated autophagy modulator
DUSP6	Dual specificity phosphatase 6
ECAR	Extracellular acidification rate
ECM	Extracellular matrix
EGF	Epidermal growth factor
EGFR	Epidermal growth factor receptor

ELISA	Enzyme-linked immunosorbent assay
ERK1/2	Extracellular signal-regulated 1/2 kinases
EVs	Extracellular vesicles
FAK	Focal adhesion kinase
FDA	Food-and-drug-administration
GBM	Glioblastoma multiforme
GFAP	Glial fibrillary acidic protein
GSC	Glioblastoma stem-like cell
HIF-1α	Hypoxia-induced factor 1 Alpha
IDH	Isocitrate dehydrogenase
IFN	Interferon
iGBM	Initial glioblastoma multiforme
IHC	Immunohistochemistry
IL	Interleukin
JAK2	Janus kinase 2
JAG2	Jagged-2
KD	Kilodalton
KEGG	Kyoto Ecyclopedia of Genes and Genomes
KRAS	Kirsten rat sarcoma virus
LC3	Microtubule-associated protein 1A/1B-light chain 3
LCN2	Lipocalin 2
Let	Lethal
MAPK	Mitogen-activated protein kinase
MCT	Monocarboxylate transporter
MEK	Mitogen-activated protein kinase kinase
MiRNA	MicroRNA
MMP	Matrix metalloprotease
MPO	Myeloperoxidase
MRI	Magnetic resonance imaging
NF-κB	Nuclear factor 'kappa-light-chain-enhancer' of activated B cells
NRAS	Neuroblastoma RAS viral oncogene homolog
OCR	Oxygen consumption rate
Oct4	Octamer-binding transcription factor 4
P53	Transformation-related protein 53
PCR	Polymerase chain reaction
p-gp	Permeability glycoprotein

pH	Pondus hydrogenii
PI3K	Phosphoinositide-3-kinase
PTEN	Phosphatase and tensin homolog
qPCR	Quantitative polymerase chain reaction
RAF	Rat fibrosarcoma
RAS	Rat sarcoma
rGBM	Recurrent glioblastoma multiforme
RISC	RNA-induced silencing complex
RNA	Ribonucleic acid
ROS	Reactive oxygen species
SCR	Protein tyrosine kinases like proto-oncogene tyrosine-protein kinase Src
SH3	Src homology 3
siRNA	small interfering RNA
SLC4A4	Solute Carrier Family 4 Member 4
SOCS3	Suppressor of cytokine signaling 3
SOX2	Sex determining region Y box 2
STAT3	Signal transducer and activator of transcription 3
Src	Sarcoma
TAM	Tumor-associated macrophage
TERT	Telomerase-reverse-transcriptase
TGF-β1	Tumor growth factor Beta 1
TME	Tumor microenvironment
TMZ	Temozolomide
TNFα	Tumor necrosis factor alpha
UTR	Untranslated region
VEGF	Vascular endothelial growth factor
VEGFR	Vascular endothelial growth factor receptor
WHO	World Health Organization
ZNF117	Zinc finger protein 117

List of figures

1 Zusammenfassung

Das Glioblastom (GBM) WHO Grad 4 ist der bösartigste und häufigste primäre Hirntumor mit einer Gesamtüberlebensrate von 9,8 % nach fünf Jahren. Praktisch jedes Mal scheitert die Standardbehandlung bestehend aus Operation und Radio- und Chemotherapie mit Temozolomid (TMZ), und der Tumor entwickelt sich weiter, bildet Resistenzmechanismen aus und kehrt in Form eines Rezidivs zurück. Daher ist es von entscheidender Bedeutung, das Forschungsfeld auszuweiten, um diese Mechanismen besser zu verstehen, den Tumor tiefer zu klassifizieren, kombinatorische Biomarker zu erstellen und neue therapeutische Ansätze zur Überwindung der Therapieresistenzen zu entwickeln.

Die hier aufgeführte erste Veröffentlichung thematisiert TMZ-Resistenzmechanismen, die auf dem veränderten Stoffwechsel des Tumors und der pH-Wert Regulierung beruhen. Die Carboanhydrase 2 (CA2) wurde zuvor als konsistent und signifikant hochreguliert in rezidiviertem GBM-Gewebe und in TMZ-resistenten GBM-Stammzellen (GSZs) beschrieben. In CA2-hochexprimierenden GBM-Zelllinien, die durch CRISPR/Cas9 induziert wurden, konnte ein erhöhter Sauerstoffverbrauch und eine erhöhte extrazelluläre Ansäuerung festgestellt werden. Diese Beobachtung ergibt sich aus der bekannten Funktion des Protonenaustauschers CA2, die aerobe Glykolyse (Warburg Effekt) und den Protonenausstoß mit voranzutreiben. Dies führt zu einem niedrigen extrazellulären pH-Wert und zu einer pro-invasiven und pro-entzündlichen Tumormikroumgebung. Der pan-CA Inhibitor Acetazolamid (ACZ) unterdrückte den Sauerstoffverbrauch und die extrazelluläre Übersäuerung effizienter als der selektivere CA2-Inhibitor Brinzolamid (BRZ) in CA2-überexprimierenden GBM-Zellen, was auf die entscheidende Rolle zusätzlicher CA-Isoenzyme hinweist, die zur pH-Regulierung und damit zum Warburg-Effekt beitragen. Im Gegensatz dazu reduzierte BRZ die Infiltrationsrate effizienter und verstärkte die TMZ-induzierte und Zelltod-vermittelnde Autophagie in CA2-überexprimierenden Zellen sowie in hoch CA2-exprimierenden und in TMZ-resistenten GSZ deutlicher. Diese Daten deuten darauf hin, dass eine BRZ-induzierte pH-Wert-Verschiebung auf ein physiologisches Niveau die TMZ-Behandlung optimieren könnte.

In einem weiteren Manuskript wurden die Signalwege, die zur Tumorprogression und Resistenzentwicklung beitragen, auf den Einfluss der Disintegrin- und Metalloproteinase 8 (ADAM8) untersucht. Neben seiner Fähigkeit, extrazelluläre Matrixproteine zu spalten und dadurch die Tumormikroumgebung mitzugestalten, kann ADAM8 als Multidomänenenzym an Integrine binden und so verschiedene Signalwege modulieren. Hier wurde untersucht, wie ADAM8 die microRNA (miRNA) Expressionsprofile durch intra- und extrazellulare Signalübertragung reguliert. Beim Vergleich von GBM-Zellen mit endogener ADAM8 Expression zu CRISPR/Cas9 induziertem Verlust der ADAM8 Expression wurden mehrere dysregulierte miRNAs identifiziert. Die Expression des Tumorsuppressors miR-181a-5p war in Zellen mit fehlender ADAM8 Expression hochreguliert. Es wurde festgestellt, dass ADAM8 die Unterdrückung von miR-181a-5p über STAT3 und MAPK-

Signalwege vermittelt. Die Transfektion einer miR-181a-5p Mimik unterdrückte die GBM-Zellproliferation teilweise durch die post-transkriptionelle Hemmung von MEK1/2, ERK1/2 und CREB-1, was indirekt auf die MMP9 Expressionsunterdrückung abzielte. Bei der Aufschlüsselung der ADAM8-vermittelten Signalübertragung unter der Beteiligung von miR-181a-5p wurde eine ADAM8/STAT3/miR-181a-5p/Osteopontin- und ADAM8/ERK1/2/CREB-1/miR/181a-5p Achse mit einer negativen Rückkopplungsschleife auf MMP9 untersucht. Mit dem Verlust der zellulären ADAM8 Expression gingen niedrigere miR-181a-5p Mengen in extrazellulären Vesikeln einher. Somit könnte die ADAM8-vermittelte Unterdrückung von miR-181a-5p in den benachbarten Zellen eine Runterregulation von MMP9 verhindern und dadurch Invasivität und Proliferation fördern. Klinisch wurde miR-181a-5p in Serum-EVs nachgewiesen und in GBM-Gewebeproben im Vergleich zu ADAM8 herunterreguliert vorgefunden, wobei *ADAM8* mit der *MMP9* mRNA Expression korrelierte. Die vielseitigen Einflüsse von ADAM8 auf progressions- und resistenzfördernde Signalwege, auch durch miRNA Regulation, rechtfertigen weitere experimentelle Ansätze, die auf ADAM8 beim GBM abzielen.

Schließlich wurden die miRNA-Expressionsmuster von drei von Patienten stammenden GSZs im Vergleich zu den entsprechenden differenzierten astrozytären Zelllinien untersucht. Einundreißig signifikant veränderte miRNAs wurden identifiziert, darunter zehn stark dysregulierte miRNAs, die an der GBM-Progression und der Ausbildung eines Stammzellphänotyps beteiligt sind. Die Transfektion von miR-425-5p reduzierte die PTEN- und GFAP-Proteinexpression in von Patienten stammenden GBM-Zelllinien, was darauf hindeutet, dass sie den GSC-Phänotyp teilweise induziert. Eine KEGG-Anreicherungsanalyse der miRNA-mRNA-Beziehung offenbarte einen Teil des dynamischen miRNA/Signalnetzwerks, das über die Differenzierung von Stammzellen entscheidet. Diese Daten führen zu einer weiteren Klassifizierung des zellulären Subtyps. Ferner deuten sie auf potenzielle Zielmoleküle, die zur Stimulation der SZ-Differenzierung beitragen können, um den Tumor anfälliger für Behandlungsstrategien zu machen.

2 Summary

Glioblastoma multiforme (GBM) WHO grade 4 is the most malignant and frequent primary brain tumor with a five-year overall survival rate of 9.8%. Virtually every time, the standard treatment with surgery and radio-/chemotherapy applying temozolomide (TMZ) fails, and the tumor progresses, develops resistance mechanisms, and recurs. Thus, it is crucial to further expand the research field for a proper understanding of those mechanisms enabling deeper classifications, the assembly of combinatorial biomarkers, and the development of new therapeutic approaches to overcome therapy resistances.

The first publication thematizes TMZ-resistance mechanisms based on the tumor's changed metabolism and pH-value regulation. Carbonic anhydrase 2 (CA2) was previously identified as highly upregulated in TMZ-resistant glioblastoma stem-like cells (GSCs) as well as recurrent GBM tissue samples. Here, the metalloenzyme was functionally analyzed. Increased oxygen consumption and extracellular acidification rates were detected in CA2-overexpressing GBM cell lines induced *via* CRISPR/Cas9. This observation underlines the known function of the proton exchanger to enhance aerobic glycolysis (Warburg effect) and proton efflux, thereby leading to extracellular acidification and a pro-invasive and pro-inflammatory microenvironment in cancer. The pan-CA inhibitor acetazolamide (ACZ) repressed the oxygen consumption and extracellular acidification rates more efficiently than the more selective CA2 inhibitor brinzolamide (BRZ) in CA2-overexpressing GBM cells, indicating the crucial role of additional CA isozymes mediating tumor pH regulation and contributing to the Warburg effect. On the contrary, BRZ reduced infiltrative rates and augmented TMZ-induced autophagy causing cell death more efficiently than ACZ in CA2-overexpressing cells, CA2-highly expressing GSCs and TMZ-resistant GSCs. Those data provide evidence for a BRZ-induced pH shift to a physiological level, optimizing the conditions for an efficient TMZ treatment.

In the second publication, signaling pathways contributing to tumor progression and resistance were examined for the influence of the disintegrin and metalloproteinase 8 (ADAM8). Next to its ability to cleave extracellular matrix proteins thereby shaping the tumor microenvironment, ADAM8 is characterized as a multi-domain enzyme and can bind to integrins thereby modulating various signaling pathways. Here, the mechanism of ADAM8 regulating miRNA expression profiles through intra- and extracellular signaling was investigated. Several dysregulated miRNAs were identified, comparing GBM cells with endogenous ADAM8 expression or a CRISPR/Cas9-induced ADAM8 knockout. In GBM, miR-181a-5p is described as a tumor-suppressor. Here, this miRNA was identified being upregulated in ADAM8 knockout cells. Mechanistically, ADAM8 was found to mediate miR-181a-5p repression *via* STAT3 and MAPK signaling. MiR-181a-5p mimic transfection suppressed GBM cell proliferation partially through the post-transcriptional inhibition of MEK1/2, ERK1/2, and CREB-1, indirectly targeting MMP9. Breaking down the ADAM8-mediated signaling

involving miR-181a-5p, an ADAM8/STAT3/miR-181a-5p/osteopontin and ADAM8/ERK1/2/CREB-1/miR-181a-5p axis with a negative feedback loop targeting MMP9 was examined. Upon loss of ADAM8 expression, enriched miR-181a-5p levels were detected in extracellular vesicles. Thus, the ADAM8-mediated repression of miR-181a-5p could prevent surrounding cells from MMP9 repression, stimulating invasion and proliferation. Clinically, miR-181a-5p was detected in serum-EVs and downregulated in GBM tissue samples compared to *ADAM8,* which correlated with *MMP9* mRNA expression. The versatile influences of ADAM8 on progression- and resistance-driving signaling pathways, also *via* miRNA regulation, justifies further experimental approaches targeting ADAM8 in GBM.

Lastly, the miRNA expression patterns of three patient-derived GSCs compared to their differentiated astrocytic states were investigated. Thirty-one significantly changed miRNAs were identified, including ten highly dysregulated miRNAs involved in GBM progression and stem cell fate. Among them, miR-425-5p was highly expressed in GSCs, and miR-425-5p mimic transfection reduced the PTEN and GFAP protein expression in patient-derived GBM cell lines, suggesting to induce the GSC phenotype partially. A miRNA-target relationship KEGG enrichment analysis revealed a section of the dynamic miRNA/signaling network deciding about stem cell fate. Thus, we further classified the cellular subtype GSCs revealing potential targets to stimulate GSC differentiation, which could modulate the sensitivity towards GBM treatment strategies.

3 Introduction

3.1 Glioblastoma multiforme (GBM)

Glioblastoma multiforme (GBM) is the most frequent and lethal primary brain tumor with an incidence of 3.19/100,000 per year, increasing with age and male sex, and the median age at diagnosis of 65 years (Leece *et al.*, 2017; Ostrom *et al.*, 2019; Torrisi *et al.*, 2022). Diagnosed patients have a progression-free survival of seven to eight months and five-year overall survival of 9.8% (Stupp *et al.*, 2009; Michaelsen *et al.*, 2013; Nørøxe *et al.*, 2016). GBM can develop as a primary or secondary tumor arising from lower-grade gliomas, often facilitating isocitrate dehydrogenase (IDH) mutation (Nørøxe *et al.*, 2016). Currently, the World Health Organization (WHO) defined former GBM WHO central-nervous-system (CNS) grade 4 tumors harboring an IDH R132H mutation as diffuse astrocytomas IDH-mutant WHO CNS grade 4 tumors (Stoyanov *et al.*, 2022). This reclassification of formerly GBM WHO CNS grade IV leaves O^6-methylguanine-DNA methyltransferase (MGMT) promotor methylation as the only significant prognostic marker in clinical use predicting patient survival (Stupp *et al.*, 2017; Stoyanov *et al.*, 2022). Although there are approaches to expand the diagnostic to a more personalized manner utilizing molecular and genomic characteristics leading to classical, mesenchymal, and proneural GBM subtypes (Verhaak *et al.*, 2010), the current diagnosis consists of histopathological examination. Nuclear atypia, high mitotic activity, cellular pleomorphism, microvascular proliferation, necrosis, and vascular thrombosis are crucial for diagnosing GBM WHO CNS grade 4 (Wirsching *et al.*, 2016; Louis *et al.*, 2016; Gilard *et al.*, 2021).

The clinical manifestation highly depends on the tumor location and size at diagnosis. GBM often occurs in the supra-tentorial space (>85%) (Wirsching *et al.*, 2016). Headache and nausea are the common symptoms at diagnosis, arising from a large tumor or edema. GBM patients suffer from symptoms caused by intracranial hypertension (30%), motor deficits (20%), loss of body weight (17%), epilepsy (15% - 20%), confusion (15%), and speech and visual restrictions (13%) (Yuile *et al.*, 2006; Vecht *et al.*, 2014; Gilard *et al.*, 2021). The standard adjuvant treatment is based on the Stupp regimen (Stupp *et al.*, 2005) consisting of surgery and subsequent treatment with the alkylating agent temozolomide (TMZ) in combination with a fractionated exposure to 60 Gray X-ray irradiation (Torrisi *et al.*, 2022). Since 2017, tumor-treating fields have amended the Stupp regimen. Its usage improved the progression-free and overall-survival significantly (Stupp *et al.*, 2017). Additional therapeutic approaches can be grouped into molecular or chemotherapeutic drugs and immunotherapies (Torrisi *et al.*, 2022). Not only finding common signatures for GBM subgroup classification enabling personalized treatment decisions but also understanding the hallmarks of GBM is proposed to lead to advanced treatment strategies (Nørøxe *et al.*, 2016; Torrisi *et al.*, 2022).

3.1.1 The molecular hallmarks of GBM

Based on the definition of cancer hallmarks by Hanahan and Weinberg (Hanahan and Weinberg, 2000; Hanahan and Weinberg, 2011) and later adapted by Fouad and Aanei (Fouad and Aanei, 2017), seven hallmarks can be described for GBM (Torrisi *et al.*, 2022) defining the aggressiveness, complexity and heterogeneity of GBM. According to Torrisi and colleagues, the hallmarks are illustrated in Figure 1.
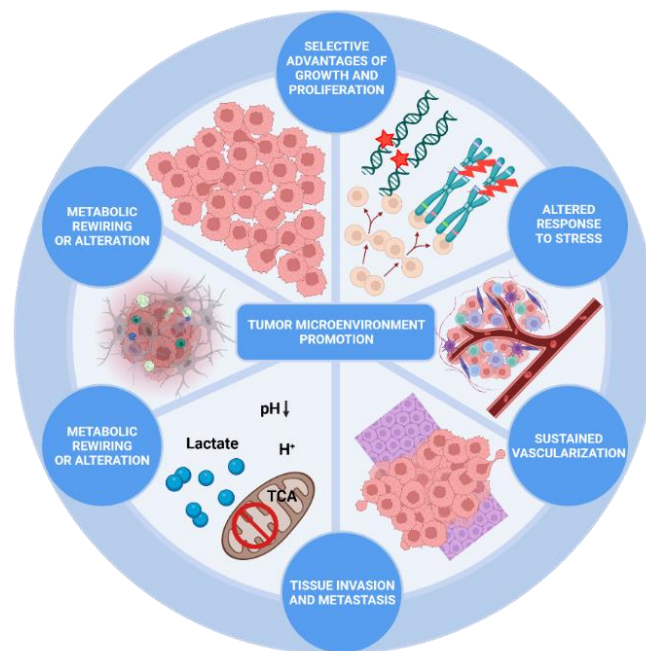
Figure 1. The hallmarks of glioblastoma multiforme. According to the definition of Torrisi and colleagues, mainly six hallmarks are deeply interconnected to ensure the seventh summarizing hallmark called 'tumor microenvironment promotion.' Created with BioRender.com. Modified and adapted from Torrisi *et al.*, 2022.

3.1.2.1 Uncontrolled growth and proliferation

Firstly, uncontrolled growth and proliferation are summarized as one essential GBM hallmark, which arises from the deregulation of signaling pathways resulting in the activation of oncogenes and the inactivation of tumor-suppressor genes (Mao *et al.*, 2012; Torrisi *et al.*, 2022). One driving signaling pathway is the Rat sarcoma–Rat fibrosarcoma–mitogen-activated protein kinase kinases–extracellular signal-regulated kinase (Ras-Raf-MEK-ERK) pathway, which promotes tumor growth, cellular proliferation, vascularization and the modulation of the tumor microenvironment (TME) (Chappell *et al.*, 2011). Moreover, the amplification of receptor tyrosine kinases like the vascular endothelial growth receptor (VEGFR) and the epidermal growth factor receptor (EGFR), including its mutated and constitutively active form EGFRvIII (Haynes *et al.*, 2014), leads to downstream effects including the stimulation of protein tyrosine kinases like proto-oncogene tyrosine-protein kinase Src (SCR) proteins stimulating not only uncontrolled tumor growth but also migration, invasion, and cell survival (Ahluwalia *et al.*, 2010; Oikonomou *et al.*, 2014). Among others, the retinoblastoma protein (RB) pathway plays a significant role. Once inactivated, it stimulates

autophagy, resistance to desoxyribonucleic acid (DNA) damage, and apoptosis evasion (Biasoli *et al.*, 2013).

3.1.2.2 Altered response to stress

Secondly, the 'altered response to stress' is ascribed to a hallmark of GBM (Torrisi *et al.*, 2022). GBM cells have an efficient DNA damage and repair system. MGMT activity is the prime example, removing alkylating agents induced by chemotherapeutic agents like TMZ (Gerson, 2004). Moreover, DNA damage response molecules are active for single-strand and double-strand breaks. Naming one example, ataxia-telangiectasia mutated (ATM) is constitutively active in glioblastoma stem-like cells (Jackson and Bartek, 2009; Carruthers *et al.*, 2018; Ferri *et al.*, 2020). Rapid growth distant from blood vessels can lead to undersupply of nutrients and oxygen before the tumor can adapt to the TME *via* neovascularization. Hence, tumor cells learn to handle and exploit the hypoxic TME. Using hypoxia-inducible factor 1-alpha (HIF-1α), GBM cells sustain reactive oxygen species (ROS) and control their export *via* controlled lactate export (Olivier *et al.*, 2020). Autophagy, a catabolic process recycling cellular constituents and promoting cellular balance recovery (Escamilla-Ramírez *et al.*, 2020), is induced under hypoxic conditions promoting tumor survival (Jawhari *et al.*, 2016). Yet, the role of autophagy in GBM remains controversial (Escamilla-Ramírez *et al.*, 2020) since it is also discussed to inhibit tumor initiation avoiding necrosis, genomic instability and inflammation by removing damaged proteins and organelles (Choi *et al.*, 2013; Escamilla-Ramírez *et al.*, 2020). Moreover, induced autophagy can promote apoptosis and senescence by type-II programmed cell death, thereby functioning as a tumor suppressor (Escamilla-Ramírez *et al.*, 2020).

3.1.2.3 Metabolic alteration

Different metabolic modulations coexist within the heterogenous tumor GBM, including the Warburg effect (aerobe glycolysis), fatty acid oxidation, glutaminolysis, and oxidative phosphorylation (Torrisi *et al.*, 2022). Given the hypoxic TME, HIF-1α ubiquitination is inhibited by prolyl hydroxylase activation. It forms stable heterodimers with HIF-1β enabling the transcription of several glycolytic enzymes and glucose transporter (Nagao *et al.*, 2019), contributing to the Warburg effect. Importantly, the conversion of pyruvate to lactate and inhibition of pyruvate oxidation is also supported by the inhibition of pyruvate dehydrogenase 1, leading to reduced mitochondrial oxygen-consumption rates (Olivier *et al.*, 2020). As a connection to another GBM hallmark, lactate promotes the M2-like immunosuppressive polarization of macrophages (La Cruz-López *et al.*, 2019). Moreover, metabolic reshaping is linked to an increased invasion through energy delivery and lactate production, causing increased acidification (Torrisi *et al.*, 2022).

3.1.2.4 Vascularization

GBM is a highly vascularized tumor triggered by many factors, including the main axis of hypoxia/hypoxia response element sequence transcription/VEGF activation. Noticeably, acidification of the TME stimulates VEGF and fibroblast growth factor β expression causing

increased proliferation and motility of endothelial cells due to increased lactate release promoting hyaluronic acid production and supporting vessel formation (Vallée *et al.*, 2021; Torrisi *et al.*, 2022).

3.1.2.5 Invasion

The GBM hallmark invasion is described as a local infiltration through healthy parenchyma and stroma mainly responsible for a recurrency rather than forming metastasis to secondary organs due to the short patient survival rate and physical barriers like the blood-brain-barrier (BBB) (Kim *et al.*, 2014; Da Cunha and Maldaun, 2019; Torrisi *et al.*, 2022) Here, the extracellular matrix (ECM) remodeling is crucial and partially achieved by matrix metalloproteinases (MMPs) like the gelatinase MMP9, whose expression is associated with the primary GBM subtype (Choe *et al.*, 2002). Through its proteolytic cleavage of cell surface proteins, proteins of the ECM, and proteins maintaining the cell-cell and cell-ECM interactions, MMP9 contributes to invasion and proliferation, angiogenesis, inflammation, migration and tumor metastasis (Huang, 2018).

3.1.2.6 Immune modulation

Due to the BBB, GBM's TME was described as 'cold TME.' Recently, many immune-cell types have been associated with GBM progression, passing the BBB due to weakened tight junctions and endothelial cells (Couto *et al.*, 2019). Among these immune cells comprising myeloid-derived suppressor cells, dendritic cells, and neutrophils (Daubon *et al.*, 2020), tumor-associated macrophages (TAMs) make up the largest immune cell population and account for up to 40% of the tumor mass (Chhor *et al.*, 2013; Buonfiglioli and Hambardzumyan, 2021; Torrisi *et al.*, 2022). Immunosuppressive TAMs promote invasion, vascularization, proliferation and immunosuppression (Grégoire *et al.*, 2020). Moreover, hypoxia is one of the main stimuli for an immunosuppressive microenvironment. For instance, periostin is highly expressed under hypoxia, inducing the phosphoinositide-3-kinase/protein kinase B (PI3K/AKT) pathway and shifting recruited TAMs to the immunosuppressive M2 phenotype (Ma *et al.*, 2018; Torrisi *et al.*, 2022).

3.1.2.7 Promotion of the tumor microenvironment

Torrisi and colleagues define the complex interplay of all six hallmarks as the seventh hallmark (Torrisi *et al.*, 2022). On the cellular level, extracellular vesicles (EVs) support the GBM hallmarks and contribute to their interplay due to their crucial role in cellular communication (Yekula *et al.*, 2019). EVs are small membrane-bound vesicles secreted by all cells into the extracellular space. They contain nucleic acids like miRNAs as well as proteins and lipids and, thus, contribute to several GBM hallmarks like angiogenesis and reprogramming the metabolic activity as well as drug resistance (van Niel *et al.*, 2018; Yekula *et al.*, 2019).

3.2 Recurrent GBM

Despite the standard treatment of GBM according to the Stupp regimen (Stupp *et al.*, 2005; Stupp *et al.*, 2017), virtually every tumor recurs (Campos *et al.*, 2016; Birzu *et al.*, 2020). Diagnostically,

magnetic resonance imaging (MRI) with the patient's clinical status serves to detect a recurrent GBM (rGBM) (Piper *et al.*, 2018). In about 80% of the cases, GBM recurs at the initial tumor location, but also distant and unifocal or multifocal leptomeningeal or parenchymal spread is described (Bordignon *et al.*, 2006). Here, it remains challenging to distinguish between an rGBM or a complication occurring in treatment related to pseudoprogression and radionecrosis (Weller *et al.*, 2013), underlying the need for additional biomarkers to detect an rGBM. In less than 50% of rGBM patients, a second surgery is possible due to the tumor's feasibility and the patient's condition (Birzu *et al.*, 2020). The National Comprehensive Cancer Network suggests clinical trials to treat rGBM since the lack of validated standard treatment (Wen *et al.*, 2020a; Birzu *et al.*, 2020). Therapeutic options are also re-irradiation (Shi *et al.*, 2018), re-treatment with TMZ (Perry *et al.*, 2010), treatment with lomustine and bevacizumab (Wick *et al.*, 2017), and tumor-treating fields (Stupp *et al.*, 2012; Birzu *et al.*, 2020). Although at first it was thought that rGBM differs significantly from initial GBM (iGBM) since shared mutations variated from eleven to ninety-seven percent (Kim *et al.*, 2015; Campos *et al.*, 2016), it is now acknowledged that the rGBM shares a mostly similar genetic and epigenetic landscape with its iGBM, slightly facilitating therapy decisions (Birzu *et al.*, 2020). Little evidence for rGBM-specific mutations was found, and the strongest selective pressure was supposed to be exerted on the iGBM (Barthel *et al.*, 2019). The observed heterogeneity resulted partially from the heterogeneity in the tumor itself since analyzing several samples in parallel taken from the same surgery can cause significant molecular profile differences and crucial changes in the microenvironment and immune cell infiltration (Campos *et al.*, 2016; Birzu *et al.*, 2020). Nevertheless, rarer distant rGBMs resulting from infiltrating tumor cells share fewer mutations with their iGBMs (Kim *et al.*, 2015), and individual genes can show different mutation retentions. Whereas *telomerase-reverse-transcriptase (TERT)* promotor mutations are commonly retained in around 90% of investigated cases, *EGFR* mutations are less maintained in rGBM in around 50% (Draaisma *et al.*, 2020; Barthel *et al.*, 2019; van den Bent *et al.*, 2015; Birzu *et al.*, 2020), and the mutations in the same gene can differ (Draaisma *et al.*, 2020; Birzu *et al.*, 2020). Moreover, hypermutated rGBMs show significant differences from their iGBMs caused by TMZ treatment and inactivating mutations in repair enzymes resulting in extraordinarily high numbers of mutations (Birzu *et al.*, 2020). However, a gross total resection at the first surgery is not always possible, and many studies do not refer to the terms gross- and subtotal resection, although the significant impact of the surgery's extent is well known (Shonka and Aizenberg, 2017; Han *et al.*, 2020). Therefore, an rGBM may often be a progression of iGBM. Nevertheless, the gained therapy resistance mechanisms of the progression or recurrence are crucial for the poor patients' overall survival.

3.3 Resistance mechanisms

Virtually every time, the treatment of GBM patients according to the Stupp regimen (Stupp *et al.*, 2005; Stupp *et al.*, 2017) eventually fails, and the tumor progresses or results in a recurrence, which is associated with resistance mechanisms (Ortiz *et al.*, 2021). Hence, it is crucial to understand and overcome those adapted mechanisms. The development of radioresistances can be withdrawn to key factors, including DNA damage repair, cell cycle, metabolic alteration, hypoxia, TME, glioblastoma stem-like cells (GSCs), microRNAs (miRNAs), and tumor heterogeneity (Ali *et al.*, 2020). Similarly, mainly five resistance mechanisms are intensively studied that counteract the TMZ-induced apoptosis, autophagy, or senescence: MGMT promotor methylation, DNA mismatch repairment, base excision repair pathway, acquired resistance through the induction and selection of genes or cell clones requiring survival, and the presence of GSCs (Ortiz *et al.*, 2021).

3.3.1 Glioblastoma stem-like cells

GSCs are described as a source of rGBM (Lathia *et al.*, 2015) inducing radio- and chemoresistance (Garnier *et al.*, 2019), angiogenesis and invasion (Boyd *et al.*, 2021), and contributing to GBM's heterogeneity by their potential of multi-lineage differentiation (Lathia *et al.*, 2015). Singh and colleagues, among other researchers, initially described GSCs as prominin-1-positive (CD133$^+$) tumor-initiating cells *in vivo* (Singh *et al.*, 2003; Singh *et al.*, 2004). This small cellular subpopulation is classified by its self-renewal capacity forming tumor spheres *in vitro* and tumors in xenograft experiments *in vivo*. Moreover, GSCs are multipotent and can initiate tumors contributing to GBM heterogeneity (Bayin *et al.*, 2014). Stem cell maintenance occurs through the interaction with TME components, mesenchymal stem cells, vascular compartments and immunity (Torrisi *et al.*, 2022) involving signaling pathways like the Notch, transforming-growth-factor β (TGF-β), PI3K/AKT and mitogen-activated protein kinase (MAPK) kinase signaling. Within GBM, bone morphogenic protein functions as a differentiation signal. Although also involved in the maintenance of GSCs, Notch-Signaling is described as an important signaling cascade for the differentiation into tumor-derived endothelium (Bayin *et al.*, 2014). Their slow cell cycle kinetics (Jackson et al., 2015) make them less attackable for chemotherapeutics targeting high-proliferative cells. Residing in stem cell niches, they benefit from favorable conditions interacting with the ECM and non-tumor cells while not being recognized by the immune system. Moreover, GSCs are known to overexpress adenosine triphosphate (ATP) binding cassette (ABC) transporter. Here, ABC subfamily member 2 (ABCG2) was found to bind matrix metalloproteinases delivering increased migration and cell invasion (Ortiz *et al.*, 2021). Multidrug resistance is ascribed to GSCs expressing the breast cancer resistance protein 1 (BCRP1). GSCs highly express hypoxia-inducible factors (HIFs), favoring survival, self-renewal, and tumor initiation, mimicking the molecular phenotype of cells under hypoxic conditions (Jackson *et al.*, 2015). Furthermore, GSCs facilitate extensive DNA repair and higher mitochondrial reserve (Rodriguez *et al.*, 2022).

3.3.2 Carbonic anhydrase 2

Carbonic anhydrases (CAs) contribute to TMZ-resistance by playing a significant role in hypoxia, metabolic changes, and extracellular acidification, which combines several hallmarks of GBM. Their crucial role in pH regulation has been known for almost a century (KEILIN and MANN, 1939; Haapasalo *et al.*, 2020), catalyzing the chemical key reaction: $CO_2 + H_2O <=> HCO_3- + H^+$ (Meldrum and Roughton, 1933; Lindskog, 1997). Fifteen family members of the human α-CA family are described as differing in their intra- or extracellular localization and enzymatic activity. Especially the isozymes CA2, CA9, and CA12 are reported to be involved in neoplastic growth and GBM progression (Haapasalo *et al.*, 2020).
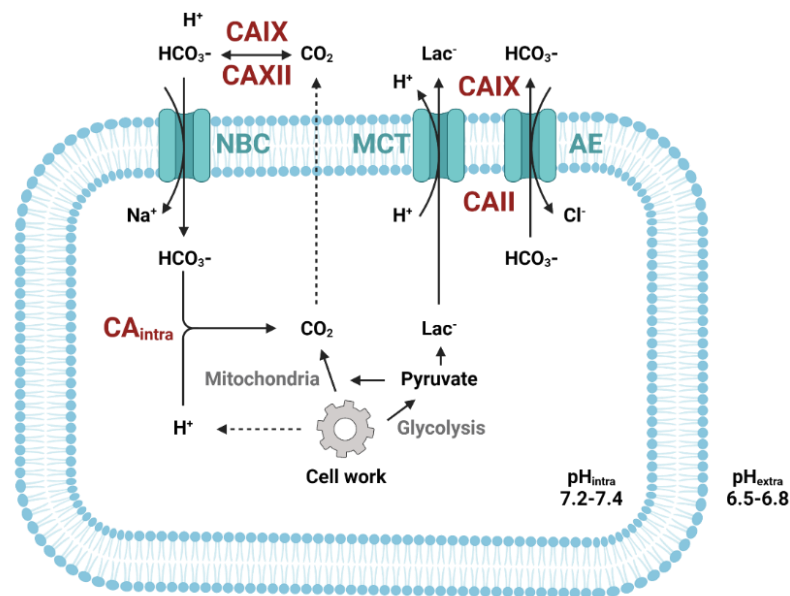
Figure 2. The mechanistic role of carbonic anhydrases in tumor pH regulation. The interplay of carbonic anhydrases (CAs) with transport proteins ensures extracellular acidification and slightly alkaline to physiological intracellular pH values. Anaerobic and aerobic glycolysis (Warburg effect) leads to elevated lactate production. Subsequently, lactate and protons are secreted through monocarboxylate transporters (MCTs). Aerobic mitochondrial respiration yields CO_2, which can diffuse passively into the extracellular space, where it gets hydrated through CA9 and CA12 enzymatic activity leading to further extracellular acidification through proton production. HCO_3- can be imported with Na^+ through sodium bicarbonate transporter (NBCs), where intracellular CAs (CA_{intra}) catalyze the reverse reaction and close the cycle. Anion exchangers (AEs) and not illustrated Na^+/H^+ exchangers and H^+-ATPases contribute to this machinery. CA2 is localized on the inner cell membrane and is a 'proton collecting antenna.' Directly bound to MCT1 and MCT4, it supports the lactate and proton symport, contributing to extracellular acidification and the Warburg effect. Created with BioRender.com. Modified and adapted from Haapasalo *et al.*, 2020.

Under physiological conditions, CA2 is mainly expressed by oligodendrocytes and thus in myelin sheaths (Kumpulainen and Korhonen, 1982; Haapasalo *et al.*, 2020), but it was also found in reactive microglial cells (Nógrádi, 1993), and shows variable expression patterns in astrocytes (Roussel *et al.*, 1979; Kimelberg *et al.*, 1982; Haapasalo *et al.*, 2020; Ghandour *et al.*, 1981; Stridh *et al.*, 2012). In astrocytes, CA2 hydrolyzes CO_2, which was secreted by neurons before. The produced proton is then shuttled to monocarboxylate transporter 1 (MCT1) and MCT4 *via* CA2 as a 'proton collecting antenna' with a concomitant efflux together with lactate. Afterward, neurons take up lactate through MCT2 and convert it to pyruvate ensuring energy balance (Becker *et al.*, 2010;

Stridh *et al.*, 2012). CA2 was found directly bound to the C-terminus of MCT1 (Becker *et al.*, 2005; Stridh *et al.*, 2012) and MCT4 (Becker *et al.*, 2010), inducing the lactate and proton symport. Moreover, CA2 is suggested to interact with the vacuolar ATPase, the main proton pump, controlling the energy flow and inducing extracellular acidification (Paunescu *et al.*, 2008). CA2 is described in oligodendrogliomas, meningiomas, low-grade astrocytomas and WHO grade 4 GBMs (Proescholdt *et al.*, 2005; Haapasalo *et al.*, 2007; Korhonen *et al.*, 2009; Haapasalo *et al.*, 2020). The zinc-dependent metalloenzyme has a dual role in promoting tumor progression. For one, the proton exchanger contributes to extracellular acidification linked to tumor progression (Parkkila, 2008). As a second role, CA2 enhances the lactate transport directly bound to MCT1/4 (Becker *et al.*, 2005; Becker *et al.*, 2010) non-enzymatically, contributing to the Warburg effect (illustrated in Figure 2). Extracellular acidification stimulates HIF (Filatova *et al.*, 2016), inducing MMP transcription (Cong *et al.*, 2014) and resulting in ECM degradation (Zhong *et al.*, 2010), inducing invasion. Hannen and colleagues described CA2 linked to TMZ-resistant GSCs and upregulated in rGBM tissue samples. Since the efficiency of several drugs, including TMZ, is highly dependent on the pH value (Stéphanou and Ballesta, 2019), targeting carbonic anhydrases like CA2 regulating the pH value could favor TMZ efficiency (Hannen *et al.*, 2019).

3.3.3 A disintegrin and metalloproteinase 8

Resistance mechanisms can be caused by selection of genes essential for cellular survival (Ortiz *et al.*, 2021). A disintegrin and metalloproteinase 8 (ADAM8) was previously associated with TMZ-resistance causing elevated pERK1/2 and pAKT levels in GBM (Dong *et al.*, 2015). Given its low expression under physiological conditions, targeting ADAM8 is discussed as very attractive, suggesting minor side effects (Conrad *et al.*, 2019). ADAM8 is a multidomain enzyme (Figure 3) with mainly two functions: proteolytic cleavage of extracellular matrix proteins shaping the TME and signal transduction influencing various tumor-driving pathways. Elevated expression of ADAM8 has been associated with invasiveness and poor prognosis in several tumor entities, including breast-, brain-, gastric-, pancreatic cancer and leukemia (Conrad *et al.*, 2019), with an especially high expression pattern in immune cells like macrophages and neutrophils (Gjorgjevski *et al.*, 2019; Jaworek *et al.*, 2021; Liu *et al.*, 2022b). ADAM8 mediates invasion and cell motility partially through its cleavage of collagen I, fibronectin, and cell adhesion molecules like vascular endothelial (VE)-cadherin. Shedding membrane-bound cytokines and chemokines like chemokine (C-X-C motif) ligand 1 (CXCL1) and tumor necrosis factor alpha (TNFα), ADAM8 shapes the TME, promoting inflammation and tumor progression (Conrad *et al.*, 2019). Moreover, the disintegrin domain of ADAM8 enables a multimerization with β_1 Integrin and the stimulation of focal adhesion kinase (FAK), ERK1/2, and PI3/AKT signaling pathways mediating cellular survival, inducing MMP activity and transmitting chemoresistance (Schlomann *et al.*, 2015; Dong *et al.*, 2015; Conrad *et al.*, 2018;

Cook *et al.*, 2022). In GBM, ADAM8 was described to mediate STAT3 signaling, promoting osteopontin expression and angiogenesis (Li *et al.*, 2021).
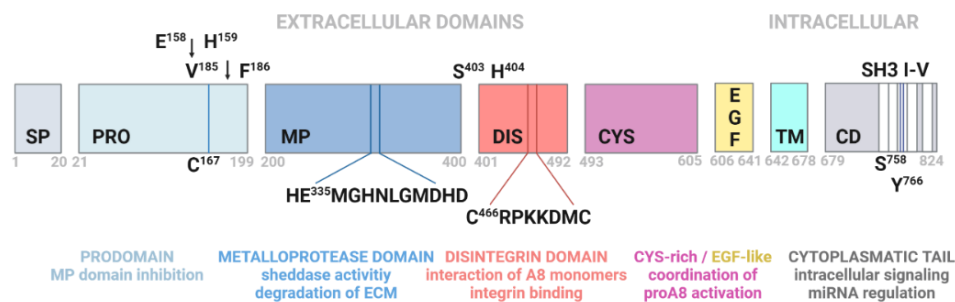
Figure 3. Schematic illustration of the domain structure of human ADAM8. Processing and activation of the multidomain enzyme require the removal of the prodomain (light blue), which can be achieved by homophilic multimerization of disintegrin (orange) and cysteine-rich (CYS-rich, purple) domains and subsequent autocatalytic cleavage. Thus, the 120 kilodalton (kDa) proform of ADAM8 becomes a 90 kDa active form. The metalloprotease domain (around 30 kDa) can be released, leaving a 60 kDa remnant form of human ADAM8. Additionally depicted are domain functions and borders. The cytoplasmic tail (CD) is essential for the mediation of intracellular signaling, also influencing miRNA expression profiles, containing src homology three (SH3) binding motifs and potential phosphorylation sites at S^{758} and Y^{766}. Created with BioRender.com. Modified and adapted from Conrad *et al.*, 2019.

Recently, ADAM8 was found to activate heparin-binding-EGF/EGFR signaling, thereby inducing chemokine (C-C motif) ligand 2 (CCL2)-mediated TAM recruitment in GBM (Liu *et al.*, 2022b). In breast and pancreatic cancer, ADAM8 influences miRNA expression profiles (Das *et al.*, 2016; Verel-Yilmaz *et al.*, 2021). In detail, Das and colleagues revealed that ADAM8-mediated ERK signaling induces miR-720 expression in breast cancer cell lines, describing a new function exercised through its ability of intracellular signaling. As a crucial factor in the TME, ADAM8 is expressed as an active protease in pancreatic cancer-derived EVs (Verel-Yilmaz *et al.*, 2021; Cook *et al.*, 2022) and is associated with the systematic packaging of specific molecules into EVs, like LCN2 and MMP9 (Cook *et al.*, 2022) or miR-720 and miR-451 (Verel-Yilmaz *et al.*, 2021). Koller and Bartsch developed a specific ADAM8 inhibitor, BK-1361, mimicking the β₁ Integrin binding loop structure and preventing ADAM8 multimerization and autocatalytic activation (Schlomann *et al.*, 2015). BK-1361 treatment revealed promising results in pancreatic cancer (Schlomann *et al.*, 2015) and asthma (Chen *et al.*, 2016), which could be transferred to GBM considering the ability of ADAM8 to transmit TMZ-resistance in GBM (Dong *et al.*, 2015).

3.3.4 MicroRNAs

MicroRNAs (miRNAs) consists of around twenty-two nucleotides and are non-coding. Binding to complementary or partially complementary target-mRNAs, they modulate protein expression post-transcriptionally (reviewed in O'Brien *et al.*, 2018). Their impact on translational regulation is revealed by participating in the regulation of more than 50% of the human genome (reviewed in Mahinfar *et al.*, 2022). Indeed, around 2,600 mature human miRNA sequences are supposed to target hundreds to thousands of mRNAs respectively (reviewed in Shea *et al.*, 2016). Functionally,

miRNAs bind to the 3' untranslated region (UTR) of selected mRNAs in most cases. Thereby, miRNAs cause translational inhibition, deadenylation or decapping of target mRNAs. MiRNAs are also reported to bind to 5' UTRs and coding regions causing post-transcriptional inhibiton. The interactions with promotor regions were shown to induce proliferation. Mostly, miRNAs function as part of the miRNA induced silencing complex (RISC). Here, miRNAs guide to target mRNAs and enable the mRNA cleavage through endonuclease argonaute 2 (AGO2) (reviewed in O'Brien *et al.*, 2018). Depending on their target genes, miRNAs can feature tumor-suppressive or tumor-promoting roles (reviewed in Mahinfar *et al.*, 2022). MiRNAs themselves are regulated by promotor methylation, influenced during their biogenesis or through extrinsic molecules like exogenous xenobiotics, hormones, and cytokines (Gulyaeva and Kushlinskiy, 2016). Dysregulated miRNAs are associated with several cancer hallmarks facilitating invasion, metastasis, growth, proliferation, metabolic reprogramming and avoiding the immune system in GBM (reviewed in Mahinfar *et al.*, 2022). Influencing multidrug resistance, for instance, miR-328 was described directly targeting the multidrug resistance protein ABCG2, ascribing a tumor suppressive role and its possible utilization as a predictive marker (reviewed in Shea *et al.*, 2016). Moreover, EVs carry high amounts of miRNAs (reviewed in O'Brien *et al.*, 2018; Mahinfar *et al.*, 2022). Mahinfar and colleagues reviewed and listed specific miRNAs dynamically involved in GBM progression and resistance (Mahinfar *et al.*, 2022). Therapeutically, utilizing tumor-suppressor miRNAs carried by nanoparticles is discussed (reviewed in O'Neill and Dwyer, 2020), but also targeting oncogenic miRNAs through the transfection of single-stranded RNA-oligonucleotides leading to miRNA degradation are conceivable (reviewed in Shea *et al.*, 2016).

3.4 Aim of this thesis

Given the high mortality rate due to the incurability of GBM, the progression, recurrence, and resistance mechanisms, it is crucial to deepen our understanding of molecular mechanisms of TMZ-resistance in order to overcome them. Thus, different molecular mechanisms of GBM progression and resistance were aimed to elucidate. In the case of CA2, metabolic mechanisms leading to resistance were analyzed. Specifically, targeting CA2 using brinzolamide (BRZ) was probed as a potential co-treatment augmenting TMZ-induced cell death. Moreover, signaling mechanisms leading to tumor survival, proliferation, and progression were investigated on ADAM8. ADAM8 was found to influence various pathways partially by its miRNA regulation. Lastly, GSCs as a source of rGBM were analyzed regarding their changing miRNA profile through differentiation, suggesting a deeper GBM classification and potential elucidation of different targeting strategies.

4 Summary of the publications

4.1 Inhibition of Carbonic Anhydrase 2 Overcomes Temozolomide Resistance in Glioblastoma Cells

Kai Zhao, **Agnes Schäfer**, Zhuo Zhang, Katharina Elsässer, Carsten Culmsee, Li Zhong, Axel Pagenstecher,

Christopher Nimsky and Jörg W. Bartsch

4.1.1 Scientific summary

Despite the standard treatment of GBM comprising surgical resection, radiotherapy, and chemotherapy with TMZ (Stupp *et al.*, 2005), nearly every tumor recurs (Campos *et al.*, 2016). A small subpopulation of tumor cells, GSCs, is considered to contribute to the recurrence showing several resistance mechanisms (Lathia *et al.*, 2015; Campos *et al.*, 2016). For instance, these self-renewing cells have metabolic features that enable them to grow under hypoxic conditions. They overexpress DNA repair enzymes and have an upregulated drug efflux, thereby escaping radio- and chemotherapy (Bao *et al.*, 2006; Liu *et al.*, 2006; Campos *et al.*, 2016). Previously, our group identified CA2 as being consistently upregulated in TMZ-resistant GSCs and recurrent GBM tissue using a transcriptomic approach (Hannen *et al.*, 2019). However, the function of CA2 in GBM therapy resistance was unknown at this stage. As a member of the carbonic anhydrase family, CA2 is a proton exchange protein involved in regulating pH homeostasis (Haapasalo *et al.*, 2020). Additionally, CA2 takes part in the symport of, for instance, lactate, pyruvate and protons *via* its location at the inner cell membrane and its association with the monocarboxylate transporters MCT1/4 (Becker *et al.*, 2005). Thus, CA2 supports the maintenance of aerobic glycolysis (Warburg effect) (La Cruz-López *et al.*, 2019). In this study, we performed subsequent functional experiments focusing on the metabolism, proliferation, invasion, TMZ-resistance, and inhibition of CA2 in GBM cells and primary GSCs.

First, we verified an enriched *CA2* mRNA expression in rGBM *via* testing ten matched GBM patients' tissue samples ($p < 0.001$, Figure 1A and patients' information are in Table S1). The significantly higher *CA2* mRNA expression in GBM tumor tissue compared to normal brain tissue is notable *via* "TCGA" and "GTEx" database analysis (Figure S1). Next to *CA2*, the well-established GSC marker *CD133* (Liu *et al.*, 2006) was tested in ten matched tissue samples with no differences detectable in mRNA expression (Figure 1C). In contrast, the efflux transport protein and multidrug-resistance protein permeability-glycoprotein (p-gp) was slightly upregulated in rGBM tissue samples on mRNA level ($p < 0.05$, Figure 1B). *Via* immunohistochemistry analysis in paraffin-embedded tissue slides, the co-localization of CA2 with the stem cell marker (sex determining region Y)-box 2 (SOX2) (Liu *et al.*, 2009) indicated the partial expression of CA2 by SOX2-positive GSCs (Figure 1D). The information on patients used for immunohistochemistry stainings is summarized in Table S2. An enriched *CA2* mRNA expression was observed in three out of four patient-derived GSC cell lines

compared to the levels in the GBM cell line U87 (Figure 1E), which was also seen on the protein level (Figure S1B). Interestingly, testing other two critical members of the carbonic anhydrase family described in GBM and other tumor entities (Haapasalo *et al.*, 2020) showed *CA9* as highly downregulated in all four tested GSC cell lines (p < 0.001, Figure 1F) and *CA12* as upregulated in two of four GSC cell lines (Figure 1G) compared to U87 cells. The independent expression of *CA9* and *CA12* to *CA2* was also described in Figure S2. Here, deferoxamine (DFO) induced hypoxia stimulates their mRNA expression in GBM cells and GSCs in a very different manner, protruding CA9 induced up to around 2,000 fold.

To deeper analyze the function of CA2 in GBM cells, gain-of-function experiments were performed, generating stable cell clones expressing CA2 (U87_CA2 and U251_CA2) and control vector-transfected cells (U87_Ctrl and U251_Ctrl). One representative clone was picked for further experiments, respectively. The stable overexpression of CA2 was confirmed on protein and mRNA levels in both cell lines (Figure 2A&C). Moreover, a higher proliferation rate was measured in U87_CA2 and U251_CA2 cells compared to their control transfected cell lines (Figure 2B&D), and CA2 expressing U251 cell lines showed an elevated invasion into Matrigel (Figure 2E&F). Metabolic changes induced by a stable CA2 expression were measured *via* "Seahorse Analysis" determining the mitochondrial oxygen consumption rate (OCR) and the extracellular acidification rate (ECAR) (Figure 2G-J). A higher OCR with stable CA2 expression was manifested by higher ATP production, maximal respiration, and basal respiration. In addition, a higher ECAR was shown through more elevated glycolysis and glycolytic capacity in both cell lines ($p < 0.001$).

To investigate whether those metabolic changes depend on the enzymatic activity of CA2, cells were treated with either the pan-CA inhibitor acetazolamide (ACZ) or the more selective CA2 inhibitor brinzolamide (BRZ) (Supuran, 2007, 2008). In Table S3&S4, the inhibitory effects of ACZ and BRZ are listed. Their molecular structures are depicted in Figure 3 A&B. After applying 100 µM or 400 µM ARZ or BRZ, metabolic changes in U251_Ctrl (Figure S3) and U251_CA2 (Figure 3C&D) were investigated. Interestingly, no differences in the OCR or ECAR of U251_Ctrl cells were detectable, whereas, in U251_CA2 cells, the OCRs and ECARs diminished with BRZ and even more with ACZ treatment. In a direct comparison of U251_Ctrl and U251_CA2 cells, significant decreases in the OCRs after ACZ (Figure 3E) and BRZ (Figure 3G) and the ECARs after ACZ (Figure 3F) and BRZ (Figure 3H) treatment were visible in CA2 expressing cells. Noticeably, the pan-CA inhibitor ACZ was more potent than the CA2 inhibitor BRZ. Next, we wondered if the induced invasion through stable CA2 expression could be inhibited *via* ACZ or BRZ treatment. Interestingly, with 400 µM ACZ and 100 and 400 µM BRZ, a significantly reduced invasive behavior was observed in U251_CA2 cells (Figure 3I-L). In contrast, 100 µM ACZ caused no changes in the invasive behavior of U251_CA2 cells (Figure 3K), showing BRZ to be more potent in inhibiting invasiveness in CA2-expressing cells. In

comparison, no differences in invasive behavior were observed without a stable CA2 expression (Figure S4).

Next, we investigated if sensitization to TMZ through BRZ treatment can be achieved, as previously shown for ACZ (Hannen *et al.*, 2019). Thus, U87_Ctrl and U87_CA2 cells were treated with 500 µM TMZ, and U251_Ctrl and U251_CA2 cells with 30 µM TMZ, combined with 100 or 400 µM ACZ or BRZ for five days with subsequent measurement of cell viability *via* "CellTiter-Glo® (CTG) assay". Interestingly, the TMZ co-treatment with BRZ caused synergistic effects at even lower concentrations with stable CA2 expression in both cell lines (Figure 4A&C). In contrast, only ACZ at a high dosage of 400 µM could augment the effect of TMZ in U87_CA2 compared to U87_Ctrl (Figure 4A), and in U251, the stable CA2 expression did not reinforce the synergistic effect of ACZ at all (Figure 4C). Moreover, stable CA2 expression leads to a more TMZ-resistant phenotype in both cell lines (Figure 4A&C). The synergistic effects of BRZ and TMZ are visible in both CA2-expressing cell lines, whereas ACZ caused reduced cell viability only in high dosage (Figure 4B&D). Regarding cytotoxicity, treating ACZ and BRZ alone did not impact cell viability. Only 400 µM BRZ showed a slow cytotoxic effect in U87_CA2 cells (Figure 4B).

The higher capacity of BRZ than ARZ to sensitize to TMZ therapy was also observed in GSCs (Figure 5). Here, three GSC cell lines were stimulated with TMZ for three or five days leading to an upregulation of the *CA2* mRNA level (Figure 5A-C). GCS cell lines were treated with TMZ, ACZ, or BRZ in combination or alone for ten days (Figure 5D-G). Interestingly, in all three GSC cell lines, BRZ in co-treatment with TMZ significantly reduced cell viability compared to TMZ monotherapy (Figure 5E-G) with striking morphological changes in sphere size and form (Figure 5D). As for ACZ, only a higher dosage in co-treatment enhanced the TMZ effect on cell viability significantly in two of three cell lines (Figure 5E-G) with striking morphological changes (Figure 5D). Speaking for the low cytotoxicity of ACZ and BRZ, no changes in morphology (Figure 5D) nor cell viability (Figure 5E-G) were detected after mono treatment. Whether combined BRZ would be more effective than combined ACZ in long-term TMZ-resistant GSCs (GSC_TMZ) (Hannen *et al.*, 2019) was investigated next. With TMZ-resistance, strongly upregulated *CA2* and *CA12* mRNA levels were observed ($p <$ 0.001, Figure 6A&C), whereas CA9, on the contrary, was downregulated ($p < 0.05$ compared to DMSO, Figure 6B). Moreover, the *p-gp* and the bicarbonate cotransporter *solute carrier family 4 member 4 (SLC4A4)* mRNA levels were elevated with TMZ-resistance (Figure 6D&G), whereas the mRNA level of *MCT1* and *MCT4* did not change (Figure 6E&F). The combined treatment of high-dose BRZ with TMZ inhibited cell viability significantly compared to TMZ mono treatment (Figure 6J) in those TMZ-resistant cells with high *CA2* mRNA (Figure 6A) and protein levels (Figure S5). In contrast, the combinatorial treatment of ACZ and TMZ did not reduce cell viability significantly (Figure 6J). In addition, the GSC_DMSO cell line did not show any significant inhibitory effects with ACZ, BRZ, ACZ + TMZ, or BRZ + TMZ compared to TMZ treatment alone. Microscopic pictures

showed morphological changes with TMZ monotherapy and combinatorial therapy of ACZ and BRZ but not with ACZ or BRZ monotherapy (Figure 6H).

Lastly, we aimed to discover the mechanism of how BRZ augments cell death in combination with TMZ. Since TMZ can induce autophagy (Escamilla-Ramírez *et al.*, 2020; Hu *et al.*, 2020), we wondered if BRZ can enhance this effect, thereby overcoming resistance mechanisms preventing autophagy. To target this, we tested for microtubule-associated protein 1A/1B-light chain 3 (LC3) II puncta formation visible *via* immunohistochemistry (Figure 7A) and LC3II protein expression (Figure 7C-G). LC3II is the lapidated form of LC3I and is autophagosome-related. An enhancement of autophagy is measurable *via* the conversation from LC3I to LC3II (Scherz-Shouval *et al.*, 2007)**.** Next to LC3II, p62 protein levels were quantified to mark autophagic flux (Figure 7C-G, (Bjørkøy *et al.*, 2009). Interestingly, with a combinatorial BRZ treatment, LC3II puncta formation was enhanced in U251_CA2 cells (Figure 7A&B). Moreover, an increased LC3II and decreased p62 protein expression after combinatorial BRZ treatment were observed in U251_CA2 but not U251_Ctrl cells (Figure 7C&D). Similar results were found in U87_Ctrl and U87_CA2 cells (Figure S6). Moreover, three GCS cell lines were tested with increased LC3II and decreased p62 protein expression. As for the CA2 protein level, an increased signal was observed with TMZ monotherapy and a significant reduction after combinatorial treatment of BRZ and TMZ (Figure 7D-G).

4.1.2 Description of own contribution

I participated in the development of the experimental design and methodology and elaborated and analyzed the data shown in Figure 1A-C. I compiled the information on the patients (Table S1&S2).

4.2 The Metalloprotease-Disintegrin ADAM8 Alters the Tumor Suppressor miR-181a-5p Expression Profile in Glioblastoma Thereby Contributing to Its Aggressiveness

Agnes Schäfer*, Lara Evers*, Lara Meier, Uwe Schlomann, Miriam H. A. Bopp, Gian-Luca Dreizner, Olivia Lassmann, Aaron Ben Bacha, Andreea-Cristina Benescu, Mirza Pojskic, Christian Preußer, Elke Pogge von Strandmann, Barbara Carl, Christopher Nimsky and Jörg W. Bartsch

* These authors have contributed equally to this work.

4.2.1 Scientific summary

Disintegrin and metalloproteases (ADAMs) participate in the mediation of tumor cell adhesion and migration as well as intracellular signaling (Murphy, 2008). ADAM8 is one particular family member contributing to the aggressiveness and progression leading to a poor prognosis in several tumor entities including GBM, breast cancer and pancreatic ductal adenocarcinoma (Valkovskaya *et al.*, 2007; He *et al.*, 2012; Romagnoli *et al.*, 2014; Conrad *et al.*, 2019). As a multidomain enzyme, ADAM8 mediates signaling pathways *via* its cytoplasmatic domain (CD) and disintegrin/cysteine-rich domain (DIS/CYS-rich). This occurs either in an EGFR-independent manner (Schlomann *et al.*, 2015; Conrad *et al.*, 2018) or EGFR-dependent manner (Liu *et al.*, 2022b). Moreover, ADAM8

interacts with β$_1$ integrin, activating FAK and the PI3K/AKT signaling pathway (Schlomann *et al.*, 2015; Awan *et al.*, 2021) and it mediates the STAT3 signaling cascade (Li *et al.*, 2021). Given this diverse and critical influence of ADAM8 on signaling pathways, we hypothesized whether the regulation of miRNAs by ADAM8 plays a role in mediating this influence. MiRNAs can modify many cancer progression-related pathways (Ali Syeda *et al.*, 2020) by post-transcriptionally regulating protein expression (O'Brien *et al.*, 2018). Through binding to specific target mRNAs, miRNAs lead to the inhibition of translation or even to the degradation of mRNAs as part of the RISC complex (Fabian *et al.*, 2010). In GBM, the tumor-suppressor miR-181a-5p is downregulated and targets oncogenic proteins like osteopontin (Ciafrè *et al.*, 2005; Wang *et al.*, 2015; Marisetty *et al.*, 2020) and B-cell lymphoma 2 (BCL2) (Shi *et al.*, 2008; Hu, 2010). Moreover, miR-181a-5p is predicted to regulate members of the MAPK pathway (Liu *et al.*, 2013; Wang *et al.*, 2017b). The MMP9 expression correlates with ADAM8 in GBM and breast-cancer-derived brain metastasis (Conrad *et al.*, 2018; Gjorgjevski *et al.*, 2019). MMP9 is upregulated in GBM (Musumeci *et al.*, 2015) and promotes especially tumor invasion, migration, metastasis, and proliferation (Huang, 2018). Exploring also the influence of ADAM8 on extracellular signaling, we thematized EVs, which are critical mediators of cellular communication in the tumor microenvironment as they contain proteins, lipids, and nucleic acids like miRNAs as cargo (van Niel *et al.*, 2018). In this study, we investigated the influence of ADAM8 on intra- and extracellular signaling pathways through its alteration of miRNA expression profiles, further exploring its correlation to MMP9 and its effect on tumor cell proliferation in GBM.

To investigate the influence of ADAM8 on the expression of miRNAs, we generated stable ADAM8 knockout clones of U87 cells (U87_KO) with the clustered regularly interspaced short palindromic repeats/CRISPR associated protein 9 (CRISPR/Cas9) homologous recombinant method using two guide RNAs. Two representative KO clones (U87_KO1 and U87_KO2) were selected for further analysis and compared to U87_CTRL cells with endogenous ADAM8 expression. The successful KO of ADAM8 was verified on mRNA level (Figure 1A), protein level (Figure 1B), and in cell culture supernatants *via* enzyme-linked immunosorbent assay (ELISA, Figure 1C). Next, a miRNA PCR Array (Human Finder) was conducted, screening 84 different miRNAs with additional controls in U87_ clones and U87_CTRL cells (Figure 1D). Especially four miRNAs, miR-19a-3p, miR-29b-3p, miR-130a-3p, and miR-181a-5p, were highly upregulated in U87_KO1 and U87_KO2 compared to U87_CTRL cells. Since only miR-181a-5p was upregulated *via* ERK1/2 inhibition (Supplementary Figure 2), we focused on this miRNA repressed by ADAM8. First, we confirmed the highly significant miR-181a-5p upregulation in the two representatives KO clones compared to CTRL (Figure 1E) and ten KO clones compared to ten ADAM8-expressing clones (Supplementary Figure 1). To expand this observation on other GBM cell lines, we tested U251, G28, G112, three patient-derived GBM cell lines (GBM29, GBM98, GBM42), and three patient-derived GSCs (GSC 2016/240, GSC 2017/74, GSC 2017/151) for

miR-181a-5p (Figure 1F) and *ADAM8* mRNA expression (Figure 1G). Results were normalized to the expression in U87, respectively. Interestingly, a higher expression of miR-181a-5p in GSCs ($p < 0.01$) was observed, whereas the *ADAM8* level was comparatively low. Pearson correlation analysis revealed a negative association between miR-181a-5p and *ADAM8* in GSCs (Figure 1J), which was not verified in GBM cells (Figure 1H) and primary GBM cells (Figure 1I). Additionally, the downregulation of ADAM8, accomplished through small interfering RNA (siRNA) in GBM42 (Supplementary Figure 3A), revealed an elevated miR-181a-5p expression (Supplementary Figure 3B). Since U87 and GBM42 showed the highest *ADAM8* level, those cells were selected for further analysis.

Next, we aimed to investigate the miR-181a-5p downregulation through ADAM8 mechanistically. To target this, ADAM8-expressing U87 cells were treated with either Batimastat (BB-94) (Brown, 1995) as broad-spectrum inhibitor of metalloproteases or with the selective ADAM8 inhibitor BK-1361 (Schlomann *et al.*, 2015) (Figure 2A). Treating cells with BB-94 led to a slight, not significant tendency of higher miR-181a-5p values, whereas the treatment with 5 or 10 µM BK-1361 conducted in a significantly higher miR-181a-5p expression ($p < 0.05$). Focusing on ADAM8 mediated signaling through its CD domain, a transient re-expression of ADAM8 lacking this critical domain (Delta CD) or a full-length transient rescue of ADAM8 (hA8) was accomplished in U87_KO2 cells and confirmed *via* western blot (Figure 2B). Interestingly, the full-length ADAM8 rescue resulted in miR-181a-5p downregulation (Figure 2B, right). Contrary to this observation, the transfection of the Delta CD variant of ADAM8 did not change the miR-181a-5p expression (Figure 2B, right). Moreover, a slight tendency of higher pSTAT3 occurrence was observed with full-length ADAM8 but not Delta CD variant rescue (Figure 2B). Treating U87 (Figure 2D) and GBM42 cells (Figure 2E) with the STAT3 inhibitor WP1066 (Iwamaru *et al.*, 2007) resulted in elevated miR-181a-5p levels ($p < 0.05$ and $p < 0.001$, respectively). In addition, MEK1/2 inhibitor U0126 (Favata *et al.*, 1998) treatment resulted in a slight upregulation of miR-181a-5p in U87 (Supplementary Figure 4A, $p < 0.05$) and no significant trend of higher miR-181a-5p level in GBM42 (Supplementary Figure 4B, $p = 0.052$).

The question appeared whether the ADAM8-induced downregulation of miR-181a-5p contributed to the aggressiveness of GBM *in vitro*. The upregulation of miR-181a-5p in U87_KO2 cells was accompanied with a reduced proliferation rate (Figure 3A, $p < 0.0001$). MiR-181a-5p mimic transfection also attenuated the cellular proliferation in U87 cells (Figure 3B, $p < 0.05$). MMP9 expression levels are associated with elevated proliferation in GBM (Xue *et al.*, 2017; Huang, 2018), and a strong downregulation of *MMP9* mRNA was seen in U87_KO1 and U87_KO2 (Figure 3C, left, $p < 0.001$). This effect was partially recapitulated with the miR-181a-5p mimic transfection in U87 cells (Figure 3C, right, $p < 0.001$). Next to significantly decreased *MMP9* mRNA levels, less secreted MMP9 was measurable in cellular supernatants (Figure 3D, left, $p < 0.05$), and less MMP9 was

detected *via* western blot analysis in cell lysates (Figure 3D, right). Comparably, miR-181a-5p mimic transfection induced decreased *SPP1* and secreted osteopontin levels (Supplementary Figure 7). Since there is no direct binding side of miR-181a-5p to the potential target mRNA of *MMP9*, we aimed to investigate an indirect influence of miR-181a-5p on the MMP9 expression. Interestingly, critical members of the MAPK pathway, *CREB-1*, *MEK1*, and *ERK2*, are distinguished by a complementary sequence and binding side for miR-181a-5p predicted by "miRDB" and "TargetScan" prediction tools (Supplementary Table 1). Western blot analysis revealed decreased protein levels of pERK1/2 and pCREB-1 and no influence on their unphosphorylated forms induced by miR-181a-5p mimic transfection (Figure 3E). Moreover, the inhibition of MEK1/2 by U0126 resulted in decreased MMP9 protein level in U87 and GBM42 (Supplementary Figure 5), whereas the miR-181a-5p mimic transfection had no influence on STAT3 or pSTAT3 status in U87 and GBM42 (Supplementary Figure 6).

Next to the intracellular influence of ADAM8 on signaling cascades *via* miR-181a-5p inhibition, we aimed to explore its extracellular effects in the TME through EV secretion. Firstly, we separated EVs from cellular supernatants of U87_CTRL, U87_KO1, and U87_KO2 and characterized them regarding their size and concentration (Figure 4A&B). Interestingly, a higher occurrence of smaller EVs secreted from both KO clones was observed compared to secreted EVs from U87_CTRL cells. The successful EV separation was verified with the presence of FLOTILLIN-1 and CD81 EV markers (Figure 4C) and the absence of CALNEXIN and β-TUBULIN known to be predominantly expressed in the cellular fractions. After characterization, EVs were tested for miR-181a-5p occurrence (Figure 4D). The presence of miR-181a-5p was measurable in EVs derived from U87_CTRL, U87_KO1, and U87_KO2 cells, with a tendency of a higher amount in KO-derived EVs. To ensure that higher miR-181a-5p occurrence in U87_KO derived EVs is due to the higher cellular amounts of miR-181a-5p, we transfected U87_CTRL cells with miR-181a-5p mimic before EV separation resulting in twenty-eight-fold higher miR-181a-5p presence in EVs (Supplementary Figure 8). Moreover, the possible uptake of EVs was demonstrated *via* carboxyfluorescein succinimidyl ester (CFSE) staining and immunofluorescence (Supplementary Figure 9A). The incubation of U87 cells with U87_KO2-derived EVs decreased MMP9 expression (Supplementary Figure 9B). Moreover, incubating U87 cells with EVs derived from miR-181a-5p mimic or inhibitor-transfected cells demonstrated the cross-cell influence of miR-181a-5p wrapped in EVs (Supplementary Figure 9C). EVs from mimic-transfected cells showed an inhibitory effect on soluble MMP9 occurrence, whereas EVs from inhibitor-transfected cells did not.

Lastly, we examined the possibility of transferring our *in vitro* results to clinical observations investigating tumor tissue samples derived from twenty-two patients diagnosed with primary GBM IDH wildtype (Table 1). Comparing the mRNA expression levels of *ADAM8* and *MMP9* with miR-181a-5p, the high upregulation of these oncogenes was visible (Figure 5A, *p* < 0.001). Afterward,

the patients were divided into subgroups according to high or low *ADAM8* or miR-181a-5p levels (Supplementary Figure 10). Interestingly, *MMP9* was upregulated in the subgroup with high *ADAM8* expression (Figure 5B, p = 0.001). This strong connection was confirmed by their high positive correlation in mRNA expression levels (Figure 5D). In contrast, no high or low miR-181a-5p association was observed with high or low *ADAM8* and *MMP9* levels (Figure 5B). The mRNA levels of *ADAM8* and *MMP9* showed no correlation to miR-181a-5p (Figure 5D). The single miR-181a-5p expression patterns listing each patient are demonstrated in Figure 5C. To limit the high heterogeneity of GBM to a certain extent, we determined the *ADAM8*, *MMP9*, and miR-181a-5p levels in tissue samples obtained by MR-spectroscopy-guided surgery from a selected patient (Figure 5E). Detailed histological and spectroscopic information on every tissue part are summarized in Supplementary Table 2. Interestingly, starting from non-tumorous access tissue, high miR-181a-5p and low *ADAM8* and *MMP9* values were detected, but with further approaching the tumor core, low miR-181a-5p and high *ADAM8* and *MMP9* values were measured (Figure 5F&G). Moreover, analyzing miR-181a-5p occurrence in serum-derived EVs of three selected patients suffering from initial GBM with a subsequent recurrence, decreased levels after the first surgery (Figure 5H) and a tendency of elevated levels after the second surgery (Figure 5I) were measured. Moreover, comparing the occurrence of serum-EVs separated before the first and second surgery, a significant decrease of the tumor-suppressor miR-181a-5p was measured before the second surgery (Figure 5J).

In conclusion, we summarized our findings schematically in Figure 6, describing the ADAM8/STAT3&MAPK/miR-181a-5p/MAPK/MMP9 axis and a new mechanism of ADAM8 regulating critical pathways promoting GBM progression.

4.2.2 Description of own contribution

As a personal contribution to the publication, experiments were performed, including planning their setup and analyzing and designing the results of Figures 1A-C, Figure 1E-J, Figure 2, Figure 3, Figure 4, Figure 5A-C, Figure 5F-J, and Supplementary Figures 1, 3-10. I participated in writing the manuscript. In addition, the medical doctoral candidate and human biology students Lara Evers, Gian-Luca Dreizner, Olivia Lassmann, and Aaron Ben Bacha worked under my supervision.

4.3 Identification of Dysregulated microRNAs in Glioblastoma Stem-like Cells

Lara Evers*, **Agnes Schäfer***, Raffaella Pini, Kai Zhao, Susanne Stei,

Christopher Nimsky and Jörg W. Bartsch

* These authors have contributed equally to this work.

4.3.1 Scientific summary

GSCs are distinguished as a small but powerful self-renewing subpopulation of GBM tumor cells (Lathia *et al.*, 2015). They are partially responsible for developing GBM recurrence due to their

inducement of radio-/chemoresistance (Garnier *et al.*, 2019) or occurrence in perivascular niches. Their ability to differentiate into multi-lineages contributes to GBM heterogeneity (Lathia *et al.*, 2015). The miRNA expression pattern changes during GSC differentiation into astrocytic tumor cells, and GCSs are proposed to have a unique miRNA expression profile (Shea *et al.*, 2016). As miRNAs are significant post-transcriptionally modulators of gene expression (O'Brien *et al.*, 2018), they highly influence critical cancer progression-related pathways like proliferation, apoptosis, and angiogenesis (Buruiană *et al.*, 2020). Here, we investigated the changes in miRNA expression pattern during GSC differentiation and revealed essential miRNAs involved in the GSC maintenance and GBM progression.

Firstly, three patient-derived GSC cell lines (2016/240, 2017/74, and 2017/151) were characterized regarding their stem cell phenotype and property of differentiation. The clinical information and histopathological features are depicted in Table 1. Based on their morphological characteristics, GSCs grew as non-adherent neurospheres (Figure 1A, left). After their differentiation, the cells grew as attached monolayers and exhibited long and star-shaped protrusions (Figure 1A, right). On the molecular level, high mRNA levels of the established cancer stem-like cell marker *CD133* (Singh *et al.*, 2004; Liu *et al.*, 2006; Barzegar Behrooz *et al.*, 2019) were detected in GSC cells with a significant decrease during differentiation (Figure 1B, left). On the contrary, the mRNA expression of *glial fiber acid protein (GFAP)* as a hallmark of reactive astrocytes and intermediate filament (BIGNAMI and DAHL, 1976) was low in all three GSCs and elevated with differentiation highly significantly (Figure 1B, right). To deeper characterize the stemness, more cancer-stem-like markers were tested (Lathia *et al.*, 2015). At the mRNA level, SOX2 and Nestin showed less consistent trends (Figure S1B&C) and CD44 was increased in differentiated cells (Figure S1A). SOX2 protein was highly expressed in all three GCS cell lines with diminished occurrence in differentiated cells, whereas the GFAP levels were induced with differentiation (Figure 1C&D). Noticeable is the clear distinction of those protein markers in 2017/74 and 2017/151, whereas 2016/240 showed fewer intrinsic differences and shallow GFAP levels.

A pathway-focused miRNA PCR array was conducted to analyze the changes in miRNA expression patterns with GSC differentiation (Figure 2A). To realize this, miRNA samples from all three GSC cell lines or their corresponding differentiated cells were pooled and used at the same miRNA concentration. The heatmap in Figure 2A describes all eighty-four tested miRNAs with an upregulation (green) and downregulation (red) in GSCs. *Via* scatter plot analysis, twenty-two miRNAs were found to be overexpressed in GSCs, whereas nine miRNAs were overexpressed in differentiated astrocytic tumor cells (Figure 2B). MiRNAs were interpreted as dysregulated with exhibiting fold regulation > 2 or < 2 using the "Qiagen" analysis tool. Detailed analysis of those thirty-one miRNAs revealed ten highly dysregulated miRNAs (Figure 2C and Table 2). Table 2 summarizes the thorough literature research on those ten miRNAs focusing on their general role

and current status in GBM and GSCs. Notably, four members of the let-7a miRNA family and miR-223-3p were highly expressed in differentiated cells, known as tumor-suppressor miRNA. In particular, miR-223-3p enhances the radiation sensitivity by targeting the *ATM* (Liang *et al.*, 2014), and all four let-7a miRNA family members and miR-223-3p are predicted to target the stem-like marker *Musashi-2* (Kehl *et al.*, 2020). Contrary, miR-425-5p, miR-17-5p, miR-30c-5p, miR-424-5p, and miR-195-5p feature a strongly elevated expression in GSCs.

Of those ten highly dysregulated miRNAs, miR-425-5p, miR-17-5p, miR-223-3p, and let-7a-5p were considered most potentially involved in GSC differentiation (Table 2). Before further functional analysis, we aimed to validate the observations of up- or downregulation with differentiation in each GSC cell line separately (Figure 3A&B, Figure S2). MiR-425-5p was the most consistently and significantly upregulated in each GSC cell line except 2016/240, showing only a trend of lower expression in differentiated cells (Figure 3A&B). Also, miR-17-5p was verified as highly upregulated in GSCs except for 2016/240 (Figure S2A). The upregulation of let-7a-5p and miR-223-3p in differentiated cells could not be validated (Figure S2B&C).

Focusing on miR-425-5p as the most consistently overexpressed miRNA in GSCs, we aimed to explore its potential role in maintaining the GSC phenotype by targeting *GFAP*. For this purpose, we transiently transfected the patient-derived GBM42 and GBM100 cell lines with a miR-425-5p mimic (Figure 3C) and tested for protein levels of the known target PTEN (Zhou *et al.*, 2020) and the "miRPathDB 2.0" predicted candidate GFAP (Kehl *et al.*, 2020) (Figure 3D-G). Indeed, the miR-425-5p transfection significantly reduced GFAP and PTEN expression in GBM100 (Figure 3D&E, $p <$ 0.05). Contrary, the inhibition of GFAP and PTEN by miR-425-5p mimic-transfection was not verified in GBM42 cells (Figure 3F&G).

The ten most dysregulated miRNAs with GSC differentiation (Table 2) were further analyzed bioinformatically by "Kyoto Ecyclopedia of Genes and Genomes (KEGG)" enrichment analysis (Figure 4A). Depicting the numbers and significance of miRNAs involved in critical cancer progression-related pathways, the pathways "Signaling pathways regulating pluripotency of stem cells" and "PI3-AKT signaling pathway" turned out to be the most significant and in GBM important influenced signaling cascades. The miRNA/mRNA target relationship including all ten miRNAs modulating "Signaling pathways regulating pluripotency of stem cells" (Figure 4A) is depicted in Figure 4B as a chord plot, visualizing the miRNA contribution to either GSC differentiation or maintenance.

4.3.2 Description of own contribution

I designed, performed, and analyzed the experiments in Figure 1C&D, Figure 3A-G, Figure S1A-C, and Figure S2A-C. Moreover, I contributed to reviewing and editing the writing part of the manuscript. The medical doctoral candidate Lara Evers worked under my supervision.

5 Discussion

5.1 Inhibition of Carbonic Anhydrase 2 Overcomes Temozolomide Resistance in Glioblastoma Cells

Based on our group's previous publication (Hannen *et al.*, 2019), we aimed to explore the mechanistic background of the sensitization to TMZ treatment *via* ACZ in TMZ-resistant GSCs. For the first time, Hannen *et al.* revealed CA2 to be induced in TMZ-resistant GSCs and patient-matched rGBM tissues compared to their iGBM, respectively (n=8). We expanded the patient cohort with additional ten patient-matched samples and confirmed the upregulation of CA2 in rGBM. Under physiological conditions, CA2 is mainly expressed by oligodendrocytes and, therefore, in myelin sheaths (Kumpulainen and Korhonen, 1982; Haapasalo *et al.*, 2020) and shows variable expression patterns in astrocytes suggesting relatively low levels (Roussel *et al.*, 1979; Kimelberg *et al.*, 1982; Snyder *et al.*, 1983; Haapasalo *et al.*, 2020). Contrary, Ghandour and colleagues found CA2 highly expressed in astrocytes (Ghandour *et al.*, 1981; Stridh *et al.*, 2012). Interestingly, CA2 was also found in amoeboid and reactive microglial cells, while resting microglial cells were negative for CA2 (Nógrádi, 1993; Haapasalo *et al.*, 2020). Although the CA2 expression by reactive microglia must be further validated, an accumulation of CA2 in rGBM could be partially due to the expansion of TAMs in rGBM (Cosenza-Contreras, manuscript in preparation) since TAMs consist of tissue-resident microglia and invaded bone marrow-derived macrophages. TAMs can make up to 40% of the tumor mass and are known to support tumor growth by releasing a broad panel of factors stimulating tumor growth and invasion in GBM (Buonfiglioli and Hambardzumyan, 2021). Hence, it would be interesting to investigate the CA2 expression in TAMs and their influence on glial tumor cells. For instance, Ye *et al.* observed a higher invasive potential of CD133^{+} GSCs after being cocultured with TAMs and traced this observation back to the release of TGF-β1 by TAMs inducing MMP-9 expression in GSCs (Ye *et al.*, 2012). Thus, extracellular acidification as one significant tumor-promoting result of CA2 overexpression (Lindskog, 1997; Parkkila, 2008) could be caused by CA2-expressing tumor cells, GSCs, and also by CA2-expressing tumor-promoting TAMs activating signal transduction and proteolytic pathways, which lead to more aggressiveness facilitating invasion and metastatic behavior (Martínez-Zaguilán *et al.*, 1996; Raghunand *et al.*, 2003). In a study of two hundred-fifty-five diffuse astrocytic and seventy-one oligodendroglial tumors, Haapasalo *et al.* demonstrated the highest expression of CA2 in glioblastoma and oligodendroglioma with an accumulation in tumor cells' cytoplasm or neovascular endothelial cells, which underlines the metabolic function of CA2 (Haapasalo *et al.*, 2007). In meningiomas, CA2 was positively correlated with tumor proliferation rates and histological grade (Korhonen et al., 2009), which highly underlines the oncogenic role of CA2. In agreement with these findings, our "TCGA" and "GTEx" analysis revealed a significantly higher expression of *CA2* in GBM tumor tissues compared to normal brain samples.

In low-grade astrocytomas and grade 4 glioblastoma, CA9 immunostaining is the most dominant compared to CA2 and CA12 showing only faint signals (Haapasalo *et al.*, 2020). Proescholdt and colleagues found 97% of tested GBMs to be CA9 positive (Proescholdt *et al.*, 2005; Haapasalo *et al.*, 2020). We observed an opposite expression trend of *CA2* and *CA12* to *CA9*. Our patient-derived GSCs expressed significantly higher *CA2* and *CA12* mRNA levels than GBM cells, whereas *CA9* was enriched in GBM cells. The small subpopulation GSCs distinguished as a source of rGBM (Lathia *et al.*, 2015) could make up the faint CA2 immunohistochemical staining indicated in Haapasalo *et al.*, 2020, in line with our observation of higher mRNA levels in this subpopulation compared to GBM cell lines and in line with the CA2 co-localization with SOX2$^+$ expressing GSCs in three selected patients. Even though we did not detect changes in *CD133* levels comparing rGBM and iGBM, which indicates no increase of CD133$^+$ GSCs in rGBM, we saw a significant increase in the *p-gp* mRNA expression in rGBM. For one thing, the upregulation of this drug-efflux protein displays the multidrug-resistance mechanism (Seelig, 2020). On the other hand, this also might indicate the evaluated presence of a GCS fraction since p-gp is highly activated in GSCs (Daood *et al.*, 2008; Rodriguez *et al.*, 2022). As expected, we saw *CA9* highly upregulated with DFO-induced hypoxia, independent of *CA2* and *CA12* expression, which were comparably low affected. This observation indicates the critical role of CA9 during hypoxia, a hallmark of GBM (Harris, 2002; Park and Lee, 2022). CA9 is located on the surface of hypoxic tumor cells, where it can hydrate carbon dioxide to bicarbonate and a proton. Bicarbonate can be converted back to carbon dioxide by cytoplasmatic CA2 and diffuse back into the extracellular space, closing the circle (Parkkila, 2008) and leading to proton accumulation in the extracellular compartment, thereby contributing to acidification (Swietach *et al.*, 2007). RNAi experiments also show that CA9 is crucial for tumor survival and growth in hypoxia (Robertson *et al.*, 2004), and CA9 is described in several brain tumors, including astrocytomas as a hypoxia-induced factor (Haapasalo *et al.*, 2020). In one particular study, Erpolat *et al.* verified CA9 evaluated with hypoxia or as a single factor in high-grade astrocytomas (n = 172), indicating shorter overall survival and suggested using a combination of hypoxic predictive markers such as CA9, osteopontin, and HIF-1α (Erpolat *et al.*, 2013). Thus, we confirmed the strong induction and a critical role for CA9 under hypoxic conditions in GBM.

Nevertheless, we mainly aimed to describe the CA2 expression in GSCs and rGBM. Its upregulation in rGBM tissue, together with p-gp, the co-expression with SOX2, and the upregulation in GSCs, speaks for it. But there is a need to validate our results by exploiting an expanded patient cohort and, for instance, testing a co-expression of CA2 with a marker for GSCs, but also a marker expressed by the broad tumor bulk such as GFAP. Our results support the initial findings in Hannen *et al.* that CA2 is upregulated in rGBM and associated with GSCs. More importantly, Hannen *et al.* found CA2 enriched in TMZ-resistant GSCs, indicating that CA2 is part of a critical resistance mechanism that urgently needs further exploration.

Unlike the isozymes CA9 and CA12, CA2 is a cytosolic protein located at the inner cell membrane (Haapasalo *et al.*, 2020). The zinc-containing enzymes catalyze the key reaction for pH regulation, the reverse hydration of carbon dioxide ($CO_2 + H_2O <=> HCO_3^- + H^+$) (Meldrum and Roughton, 1933; Lindskog, 1997). Many of them, also the widely expressed CA2, are associated with specific tumor entities (Haapasalo *et al.*, 2020). As a proton exchanger, CA2 contributes to extracellular acidification, which is linked to tumor progression (Parkkila, 2008). On the other side, CA2 is reported to enhance the lactate transport through direct binding to the C-terminus of MCT1 (Becker *et al.*, 2005; Stridh *et al.*, 2012) and MCT4 (Becker *et al.*, 2010). In cancer, carbonic anhydrases, including the isozyme CA2 contribute to aerobic glycolysis (Warburg Effect), enhancing the symport of lactate with a proton by, for instance, directly binding MCT1 (Becker *et al.*, 2005), thereby contributing to extracellular acidification (Swietach *et al.*, 2007; Becker, 2020). Recently, CA2 was suggested to interact with the main proton pump vacuolar ATPase, inducing extracellular acidification and controlling the energy flow (Paunescu *et al.*, 2008). Since many drugs, including TMZ, function under physiological pH values (Stéphanou and Ballesta, 2019), the extracellular acidification induced by CA2 is contra-productive for efficient therapy. Hence, we hypothesized that the extracellular acidification caused by CA2 is one resistance mechanism of GSCs in rGBM and can be targeted by carbonic anhydrase inhibitors. To explore the metabolic influence of CA2, we overexpressed this metalloenzyme in two GBM cell lines. Indeed, we confirmed higher mitochondrial basal respiration, ATP production, maximal respiration, and glycolytic activity by measuring the OCR and ECAR levels. Thus, we could confirm the functional overexpression of CA2 in both GBM cell lines as a basis for further experiments. Similarly, Silagi and colleagues measured the extracellular acidification associated with CA9 and CA12 and their dependency on the transcription factor HIF in nucleus pulposus cells without referencing CA2 (Silagi *et al.*, 2018).

As an additional experiment underlining the oncogenic role of CA2 in the TME, we observed higher infiltration rates with a stable CA2 overexpression in U251. This observation was particularly interesting since the aggressive invasion is one GBM hallmark shared by all GBM subtypes leading to the impossibility of removing the whole tumor by surgery (Vollmann-Zwerenz *et al.*, 2020). Extracellular acidification is induced by carbonic anhydrases, as shown by us and others. Firstly described in melanoma cells, culturing tumor cells with the medium of acidic pH value leads to higher invasion rates through relatively more activated gelatinase B (MMP9) (Martínez-Zaguilán *et al.*, 1996). Now it has been discovered that the change in pH value in the TME can stimulate the HIF function (Filatova *et al.*, 2016) and activates MMPs (Cong *et al.*, 2014), which consequently leads to enhanced degradation of extracellular matrix proteins like gelatin, collagen, laminin, and fibronectin (Zhong *et al.*, 2010), thereby causing higher invasion rates. The hypoxia-induced transcription factor HIF enhances the CA9 expression (Swietach *et al.*, 2007), creating a positive feedback loop. HIF induces glycolysis through its transcriptional upregulation of glucose transporter

and glycolytic enzymes (Pasteur, 1861; Kierans and Taylor, 2021). The resulting energy in the form of ATP and biosynthetic precursors is essential for cell division, invasion, and migration (Zhou *et al.*, 2022). This could describe an indirect mechanism of CA2 inducing glycolysis and invasion, next to its known binding to MCT1/4 supporting the lactate/proton symport (Becker *et al.*, 2005; Becker *et al.*, 2010). Because of this pH change in the TME, the high expression of CA2 in neovascularized endothelial cells (Haapasalo *et al.*, 2007), and its expression in astrocytes, which are critical for the formation of the BBB (Watkins *et al.*, 2014), one could hypothesize that CA2 also supports the infiltration of bone-marrow-derived immune cells. Haapasalo and colleagues depicted a clear association between high CA2 expression in endothelial cells and poor prognosis in patients with astrocytomas, underlining the importance of deeper analysis of invasive behavior associated with CA2 expression. Moreover, it has been studied that extracellular acidification is associated with inflammation (Okajima, 2013). For instance, an acidic tumor microenvironment was accompanied by human neutrophil activation and apoptosis repression (Trevani *et al.*, 1999). We described the role of CA2-inducing invasion in GBM for the first time. Still, Tachibana and colleagues previously saw this connection in urinary bladder cancer, finding CA2 by proteome analysis and verifying their results with immunohistochemical staining (Tachibana *et al.*, 2017). Thus, further investigations are necessary to explain the mechanistic background behind CA2-induced infiltration. Using the CA2-specific inhibitor BRZ resulted in a higher inhibition of infiltration than the broad-spectrum inhibitor ACZ in CA2 overexpressing cells, specifically indicating CA2 to be the crucial isozyme of the carbonic anhydrase family inducing extracellular acidification and subsequent infiltration, reinforcing this theory, without a stable CA2 overexpression, neither BRZ nor ACZ induced changes in infiltration patterns. Hence, an immunohistochemical or realtime-quantitative polymerase chain reaction (RT-qPCR)-based characterization regarding the specific patients' CA2 expression could enable a personalized therapy targeting CA2 and GBM infiltration, potentially contributing to the prevention of recurrence.

We deeper analyzed the mechanism behind the usage of ACZ and BRZ, starting with metabolic changes. ACZ is a pan-CAI, and a "Food and Drug Administration" (FDA) approved drug in clinical use against glaucoma (Lemon *et al.*, 2021). BRZ has been reported to have similar efficiency in treating glaucoma (Sugrue, 2000; Supuran, 2008). As in gliomas, the co-treatment of ACZ with TMZ shows synergistic effects (Das *et al.*, 2008; Amiri *et al.*, 2016; Wu *et al.*, 2018) and is now in phase I clinical study for a combined treatment of iGBM and rGBM patients in the University of Chicago, US (https://clinicaltrials.gov; Study Number NCT03011671; accessed on 06 March 2023, Zhao *et al.*, 2021). As a pan-CAI, ACZ targets carbonic anhydrases involved in tumor suppression. For instance, CA10 acts as a tumor suppressor. It is downregulated by promotor CpG methylation with an implication in cell proliferation and apoptosis, demonstrating its role as a prognostic risk factor in renal cell carcinoma (Li *et al.*, 2022). To circumvent undesirable side effects, we also tested BRZ

with a high efficiency against CA2 (K_i value = 3 nM) reported against the full-length enzyme compared to the K_i value of 12 nM in the case of ACZ (Supuran, 2008). Although BRZ also functions highly efficiently against the catalytic domain of CA12 (K_i value = 3 nM), the efficiency against the full-length enzyme is unknown and usually higher by orders of magnitude (Supuran, 2007, 2008). BRZ also features a K_i value of 0.9 nM for the full-length isoform CA6 and 2.8 nM for CA7. Although CA6 is predominantly expressed in salivary and mammalian glands (Supuran, 2008), CA7 is highly expressed in neurons and takes part in neuronal signal transduction in hippocampal neurons (Ruusuvuori *et al.*, 2004; Haapasalo *et al.*, 2020), so side effects targeting neurons have to be ruled out before clinical usage. Although we did not observe any toxic effect treating GBM cells with ACZ or BRZ alone, the combination with TMZ reduced cellular viability, which shall be discussed below. Hence, the impact of ACZ and especially BRZ in combination with TMZ on neurons and other surrounding cells should be addressed in further experiments, potentially by treating primary mouse-derived brain slices and subsequent staining for apoptotic markers like Annexin V (Rusch, manuscript in preparation). Nevertheless, treating CA2 overexpressing GBM cells with ACZ compared to BRZ resulted in the downregulation of OCRs and ECARs only in cell lines overexpressing CA2, indicating the critical role of CA2, with a higher potency observed with ACZ. We ascribed this observation to the additional inhibition of CA9 and CA12 through ACZ and not BRZ, independent of CA2 expressed and part of the regulation of the pH-value and ATP production contributing to extracellular acidification in gliomas (Parkkila, 2008; Haapasalo *et al.*, 2007).

To our knowledge, we were the first group to describe the more powerful sensitization to TMZ inducing cell death by treating CA2 overexpressing GBM cells and CA2 expressing patient-derived GSCs with BRZ than with ACZ, suggesting a potential mechanism to overcome TMZ-resistance and a critical role of CA2 in rGBM. Similar, Mujumdar and colleagues synthesized derivates from psammaplin C (1), the product of primary sulfonamide, and identified compound 55 as a potent inhibitor of CA12 (Ki = 0.56 nM) with further verification of overcoming TMZ-resistance in an orthotopic, patient-derived GBM xenograft model (Mujumdar *et al.*, 2019). In another study, Boyd and colleagues showed a regression of GBM xenografts treated with TMZ and SLC-0111, a CA9 and CA12 inhibitor inducing DNA damage and cell cycle arrest *in vitro* (Boyd *et al.*, 2017). These results highlight the promising potential of selective CAIs to target specific CA isozymes with minor side effects. Moreover, celecoxib acts as a selective CA2 inhibitor and is a cyclooxygenase inhibitor (Knudsen *et al.*, 2004; Di Fiore *et al.*, 2006; Haapasalo *et al.*, 2020) in a currently completed clinical trial combinatory with eight other repurposed drugs in the combinatorial treatment with TMZ in rGBM in Ulm, Germany (https://clinicaltrials.gov; Study Number NCT02770378, accessed on 06 March 2023). Interestingly, we observed a more TMZ-resistant phenotype in CA2 overexpressing cell lines, higher *CA2* mRNA level after TMZ treatment in GSCs, and *CA2* and *CA12* were highly upregulated in TMZ-resistant GSCs. At the same time, *CA9* was downregulated. All these results

indicate that CA2 and potentially CA12 are part of a resistance mechanism, while CA9 is downregulated as a reaction to TMZ-resistance. The CA9 downregulation as a consequence of TMZ-resistance remains to be explained. Since CA9 is highly influenced by extracellular acidification (Sedlakova *et al.*, 2014), describing the TMZ influence on extracellular pH-values would be interesting. TMZ efficiency depends highly on the pH-value, which should be optimally around the physiological level of 7.4 (Stéphanou and Ballesta, 2019). Still, the potential influence of TMZ on the pH value and, thereby, on CA9 remains to be discovered.

GSCs combine several mechanisms to avoid TMZ or radiotherapy-induced cell death, including slow cell cycle kinetics suggesting a quiescent state, DNA repair mechanisms, multidrug-resistance, and exploiting the hypoxic microenvironment expressing HIF2α (Jackson *et al.*, 2015). We ascribe the high presence of CA2 found in TMZ-resistant GSCs to a resistance mechanism (Hannen *et al.*, 2019), which can be overcome by specific CA2 inhibition with BRZ more efficiently than with the pan-CAI ACZ in a TMZ co-treatment. As also proposed by Ortiz *et al.*, we enhance the effect of TMZ by using a pH-regulating agent, directly targeting CA2 and inhibiting extracellular acidification. Still, there is a need to confirm the influence of BRZ on the intracellular pH values since we only measured pH values extracellularly. The importance of direct intracellular pH measurements emerges from a literature search since there was an assumption of acidic intracellular and extracellular pH values in the 1930s to 1980s based on the Warburg effect, but with the progression in technologies, intracellular pH measurements indicate now a mildly alkaline or near neutral pH value (Webb *et al.*, 2011; Hao *et al.*, 2018). Thus, we hypothesized that CA2 inhibition leads to intracellular acidification, shifting the mildly alkaline pH to a physiological value. The observed upregulation of the sodium bicarbonate transporter SLC4A4 is hinting for more HCO_3^- and Na^+ import and more conversion to CO_2 by intracellular carbonic anhydrases like CA2 (Becker, 2020; Haapasalo *et al.*, 2020) driving the extracellular acidification, comparably as described in Silagi *et al.*, 2018, also with the tendency of upregulation of MCT1 and MCT4. But a decrease in SLC4A4 expression with BRZ or ACZ treatment was not shown, which would be only an indirect assumption of intracellular pH values. Interestingly, we also measured highly elevated mRNA levels of *p-gp* in TMZ-resistant GSCs, indicating the additional inducement of the multidrug-resistance mechanism, highly activated in GSCs, (Seelig, 2020; Daood *et al.*, 2008; Rodriguez *et al.*, 2022) from multiple mechanisms and reminding of the heterogeneity beyond CA2. A connection between carbonic anhydrases and the expression of p-gp regarding TMZ-resistance is worth further studying since CA12 was already shown to be co-expressed with p-gp and necessary for the TMZ efflux in neurospheres building a new TMZ-resistance mechanism in GBM (Salaroglio *et al.*, 2018). We supported these promising insights by detecting significantly upregulated *g-pg* and *CA12* mRNA levels in TMZ-resistant GSCs. Collectively, our data suggest that BRZ is a more powerful synergistic agent for TMZ than ACZ, assuming high cellular CA2 levels. Although we validated the important role of CA9 in extracellular

acidification under hypoxia, we did not see a connection to TMZ-resistance as we see it for CA2, which is highly upregulated in GSCs and even higher in TMZ-resistant GSCs or after TMZ treatment in GBM cells. Conversely, CA9 was downregulated in GSCs and TMZ-resistant GSCs. Thus, we justify paying more attention to CA2, which contributes to TMZ-resistance. But more studies are arguing for a specific CA9 inhibition to overcome TMZ-resistance in GBM (Amiri *et al.*, 2016; Boyd *et al.*, 2017). Hence, there is a need to explore the isozymes of the carbonic anhydrase family in more detail to enable an efficient TMZ treatment under optimal pH conditions. So, someday there will be personalized therapy as a drug cocktail based on the expression pattern of, for instance, CA2 and CA9 as part of a personalized treatment regimen in GBM patients.

The question remained, how BRZ augments the TMZ effect reducing cell viability. Since apoptotic pathways are inhibited in GBM and hypoxia-induced HIF augments mitochondrial autophagy (Bellot *et al.*, 2009; Escamilla-Ramírez *et al.*, 2020), we wonder if the combined treatment with TMZ and CAI induces autophagy leading to cell death more than the treatment with TMZ alone. Indeed, we measured an enhancement of autophagy with the increased conversation from LC3I to LC3II (Scherz-Shouval *et al.*, 2007) and the reduction of p62 protein levels (Bjørkøy *et al.*, 2009). Comparably to our survival analysis, we saw stronger effects using BRZ/TMZ compared to ACZ/TMZ, suggesting that the unspecific inhibition of several carbonic anhydrases could cause compensatory effects leading to cell survival. Some comparable studies indicate that CAI inhibitors induce autophagy and cell death. For instance, in breast cancer, ACZ was shown to induce autophagy resulting in cell death by the increased expression of transformation-related protein 53 (p53), damage-regulated autophagy modulator (DRAM), autophagy related 5 (ATG5), beclin 1 (BCLN1) / B-cell lymphoma 2 (BCL-2) ratio, and a decrease of AKT1 along with an increase of PTEN expression (Mohammadpour *et al.*, 2014). Gul and colleagues synthesized new dibenzenesulfonamides inducing apoptosis and autophagy and inhibiting CA9 and CA12 in different tumor cell lines (Gul *et al.*, 2018). The molecular mechanism of CAs and specific CA isozymes inhibiting autophagy, or at least the molecular mechanism behind CA inhibition inducing autophagy, must be further elucidated. Here, it also have to be considered that tumor cells induce autophagy to adapt to a hypoxic microenvironment in the first stage (Escamilla-Ramírez *et al.*, 2020). Nevertheless, it is conceivable that tumor cells induce autophagy as a reaction to CA inhibition since the machinery of ATP production by glycolysis is affected. By this, the existing intra- and extracellular pH values, meaning essential TME conditions, will change. The autophagy inhibitor 3-methyladenin led to more cell death (Zhao, unpublished data), so we could postulate that autophagy might have a protective function. Noticeably, we show that the TMZ-induced autophagy is enhanced with ACZ and even more with BRZ, possibly due to the intracellular pH shift to a physiological level. Here, carbonic anhydrases like CA9 could be activated by HIF (Swietach *et*

al., 2007) to contribute to extracellular acidification and aerobic glycolysis, thereby helping to adapt to the hypoxic microenvironment and autophagy to recycle cellular organelles and proteins.

5.2 The Metalloprotease-Disintegrin ADAM8 Alters the Tumor Suppressor miR-181a-5p Expression Profile in Glioblastoma Thereby Contributing to Its Aggressiveness

Based on the indications in other tumor entities that ADAM8 can regulate specific miRNA expression profiles (Das *et al.*, 2016; Verel-Yilmaz *et al.*, 2021), we aimed to investigate its potential influence on miRNAs further exploring its tumor-promoting role in GBM. With two representative clones of a stable CRISPR/Cas9 induced ADAM8 KO in U87 GBM cells, we performed a miRNA PCR array and found four miRNAs consistently and strongly upregulated compared to U87_CTRL cells. Of these miRNAs, only miR-181a-5p was upregulated with ERK1/2 inhibition, indicating a potential regulatory pathway. Comparably, Das and colleagues described the ADAM8-dependent regulation of miR-720 expression *via* binding of ADAM8 to Integrin β_1 and subsequent activation of the ERK signaling cascade, leading to increased miR-720 expression in breast cancer cell lines (Das *et al.*, 2016). The induction of pERK levels by ADAM8 was described in brain, breast, and pancreatic cancer (Conrad *et al.*, 2019). Hence, we focused on miR-181a-5p being potentially regulated by ADAM8-induced signaling. MiR-181a is known as tumor suppressor miRNA, matching its downregulation induced by the oncoprotein and multidomain enzyme ADAM8. Recently, miR-181a-5p was described as a potential prognostic and diagnostic biomarker in glioma patients, being downregulated in elderly patients, in IDH1 WT tumors or high-grade compared to low-grade astrocytomas. Its downregulation is significantly associated with a low overall rate survival analyzed in tissue samples of seventy-eight 2 to 4 grade glioma patients (Valiulyte *et al.*, 2022). This study was in line with observations from Huang and colleagues, which investigated the downregulation of miR-181a-5p and negative correlation with target genes *via* a gene microarray in GBM (HUANG *et al.*, 2016), and we could also verify a downregulation of miR-181a-5p compared to *ADAM8* in GBM tissue samples (n = 22). Interestingly, analyzing different GBM cells, patient-derived cells, and patient-derived GSCs, we detected a negative correlation of miR-181a-5p with *ADAM8* only in GSCs with enriched miR-181a-5p and low *ADAM8* levels. Contrary to our findings of high miR-181a-5p levels in GSCs, Huang and colleagues found miR-181a-5p to be downregulated, inhibiting GSC formation by targeting Notch2 mRNA underlining its tumor-suppressor role (HUANG *et al.*, 2017). Critically viewed, they based their experiments on U87MG and U373MG GBM cells and their formation of GSCs, whereas we performed our experiments with patient-derived GSCs, but also with GSCs derived from three patients. Since miR-181a-5p can inhibit proliferation by targeting F-box protein 11 shown in U251 GBM cells (Wen *et al.*, 2020b), the high occurrence of miR-181a-5p in GSCs could contribute to the suggested quiescent state depicted by slow cell cycle kinetics (Jackson *et al.*, 2015) thereby avoiding alkylating agents like TMZ, which target high proliferative cells. Yet, this would describe an oncogenic role of miR-181a-5p in GSCs and needs further

evaluation to explain its particular role in the proliferation and survival regulation of GSCs. Contrary to this theory, Sun and colleagues recently reported that miR-181a-5p is decreased in hippocampal neural stem cells. Once overexpressed, miR-181a-5p targets PTEN, thereby supporting AKT signaling and neural stem cell proliferation (Sun *et al.*, 2023). Nevertheless, they investigated neural stem cells in the context of aging and not neoplasia, giving miR-181a-5p a "healing" role in supporting the learning and memorial abilities in aged mice. Moreover, the location of stem cells in the brain could impact the role of miR-181a-5p since the hippocampus is known to be spared by infiltrating glioma cells (Mughal *et al.*, 2018). When studying miRNAs, their localization, expression by different cell types, and diverse target genes are important to consider, showing the need to investigate the complex network of miRNAs in sufficient detail.

As a multidomain enzyme on the one hand, ADAM8 has a proteolytic function shaping the microenvironment *via* shedding of membrane-bound chemokines and cytokines like TNFα and CXCL1 or contributing to cell motility and invasion through ECM degradation, cleaving, for instance, collagen I, fibronectin, and cell adhesion molecules like VE-cadherin (Conrad *et al.*, 2019). On the other hand, ADAM8 can bind to Integrin β1 with its disintegrin domain inducing FAK, ERK1/2, and AKT/PI3 kinase signaling (Schlomann *et al.*, 2015; Dong *et al.*, 2015; Conrad *et al.*, 2018; Cook *et al.*, 2022). Here, the cytoplasmatic tail (CD) is crucial, containing SH3-binding motifs and potential phosphorylation sites (Ser[758] and Tyr[766]) (Kleino *et al.*, 2015). More recently, ADAM8 was also found to activate heparin-binding-EGF/EGFR signaling to induce CCL2 expression and TAM recruitment *in vitro* and *in vivo* in GBM (Liu *et al.*, 2022b). Given its strong regulatory influence on different signaling pathways, thereby potentially regulating the transcription of miRNA as one mechanism of regulation (Ha and Kim, 2014), we aimed to explore the ADAM8-regulated signaling pathway influencing miR-181a-5p expression. Interestingly, using the broad-spectrum MMP inhibitor batimastat (BB-94) (Brown, 1995), no significant changes in miR-181a-5p expression were verified, but with the usage of BK-1361 mimicking the structure of the Integrin $β_1$ binding loop and specifically inhibiting the ADAM8 dimerization and autocatalytic activation (Schlomann *et al.*, 2015), significantly higher miR-181a-5p levels were detected in ADAM8 expressing U87_CTRL cells suggesting the specific regulation of miR-181a-5p *via* active, homophilic multimerized ADAM8. In more detail, we showed that rescuing full-length ADAM8 in U87_KO cells significantly inhibited miR-181a-5p expression, whereas transient transfection of ADAM8 missing the CD domain failed to suppress miR-181a-5p, indicating that ADAM8 influences the miR-181a-5p profile through its participation on signaling cascades. Although we did not see significant changes in the ratios of pEGFR to EGFR, pERK1/2 to ERK1/2, and pSTAT3 to STAT3 after transient transfection of full-length ADAM8 or ADAM8 lacking the CD domain, treatment of ADAM8-expressing U87 and patient-derived GBM42 cells with the STAT3 inhibitor WP1066 (Iwamaru *et al.*, 2007) or MEK1/2 inhibitor U0126 (Favata *et al.*, 1998), which inhibits MEK1/2 upstream of ERK1/2, resulted in a dose-

dependent upregulation of miR-181a-5p. Thus, we described an unknown mechanism that explains the downregulation of miR-181a-5p in GBM (HUANG *et al.*, 2016; Valiulyte *et al.*, 2022). Summarized in Figure 6 of the manuscript, on the one hand, we have described ADAM8-dependent STAT3 signaling, shown before by Li *et al.* (2021), to possibly regulate miR-181a-5p, which is known to bind to the 3' UTR region of *SPP1* encoding osteopontin (Marisetty *et al.*, 2020), indicating an ADAM8/STAT3/miR-181a-5p/osteopontin axis. On the other hand, we suggest that ADAM8 induces the ERK1/2 signaling pathway by inhibiting miR-181a-5p *via* CREB-1, which has been shown to bind to miR-181a-5p and repress its transcription in fibrous dysplasia (Fu *et al.*, 2021), indicating an ADAM8/ERK1/2/miR-181a-5p axis. Still, there are some mechanistic gaps to be filled. Even though the direct binding of CREB-1 to miR-181a-5p *via* chromatin immunoprecipitation has been demonstrated in fibrous dysplasia (Fu *et al.*, 2021), it remains to be shown that STAT3 inhibits miR-181a-5p through direct binding. Contrary to our findings in breast cancer, it was shown that STAT3 directly binds to the promotor of miR-181a-5p, driving its transcription. Here, miR-181a-5p is an oncogene downregulating BAX, decreasing apoptosis and increasing invasion (Niu *et al.*, 2016). Nevertheless, miR-181a-5p appears to play a dual role in breast cancer, both pro- and anti-tumorigenic, which may be attributed to the complex network of diverse target genes and feedback or feedforward loops (Yang *et al.*, 2017). Moreover, with the full-length rescue of ADAM8 in U87_KO cells, it was expected to see higher pSTAT3 and pERK1/2 levels, which can be assumed from the representative western blot. Still, the quantification of three independent experiments revealed no significant differences. It is conceivable that miR-181a-5p is not only regulated by ADAM8-induced signaling, and its transcription factors remain to be fully defined. Although miRNAs were intensively studied during the last decades, the focus mostly laid on their quantification and the investigation of target genes regarding their potential role as prognostic and diagnostic markers, therapeutic targets, or potential drugs. In contrast, little is known about the regulation of miRNAs themselves. Applying the previous knowledge, miR-181a-5p could also be regulated by promotor methylation, post-transcriptionally by changes in the activities of Drosha and Dicer, hormones, cytokines, or exogenous xenobiotics (Gulyaeva and Kushlinskiy, 2016).

However, we further functionally analyzed the impacts on miR-181a-5p mimic transfection in ADAM8 expressing U87 cells and detected a decrease in cellular proliferation rates, slightly readjusting the reduced cellular proliferation observed in U87_KO2. This indicates that the reduced proliferative behavior of U87_KO cells is partially due to the upregulation of miR-181a-5p. The inhibition of proliferation by miR-181a-5p is not only known for GBM (Wen *et al.*, 2020b) but also for prostate-cancer-inducing G1 cell cycle arrest *in vitro* (Shen H, Weng XD, Liu XH, et al, 2018) and in retinoblastoma cells targeting neuroblastoma RAS (NRAS) and reducing proliferation while enhancing apoptosis (Ouyang *et al.*, 2022). The induction of apoptosis by miR-181a-5p could also be reflected in our CTG assay defining cellular proliferation rates since the assay is based on

measuring active metabolic cells secreting ATP. Accordingly, Hu and colleagues found that miR-181a-5p was downregulated when they exposed U87 cells to radiation. Here, miR-181a-5p was reported to target Bcl-2, indicating the induction of apoptosis possibly contributing to radiosensitivity (Hu, 2010). In our study, we focused on MMP9 as a potential miR-181a-5p target, given its significant role as a promotor of invasion, metastasis, angiogenesis, proliferation and possible biomarker in GBM (Xue *et al.*, 2017; Huang, 2018), aiming to explain the highly significant correlation of *ADAM8* and *MMP9* in GBM tissue samples, as shown by us, and brain metastasis derived from breast cancer (Conrad *et al.*, 2018; Gjorgjevski *et al.*, 2019) in one possible way. Conrad and colleagues previously found that ADAM8 regulates MMP9 expression *via* ERK1/2 signaling. Measurements of induced pERK1/2 and pCREB levels were significantly higher in MB-231 triple negative breast cancer cells expressing full-length ADAM8 than in cells lacking the CD domain. As a consequence, transmigration was reduced in cells without the CD domain *in vitro*. Interestingly, miR-181a-5p is known to target MEK1 (He *et al.*, 2013; Wang *et al.*, 2017b), ERK2 (He *et al.*, 2013; Wang *et al.*, 2017b; Huang *et al.*, 2016) and CREB-1 (Liu *et al.*, 2013; Fu *et al.*, 2021) and we confirmed significantly lower pERK1/2, pCREB-1 and *MMP9* levels after miR-181a-5p mimic transfection. At this point, we could not show lower total protein ERK1/2 and CREB-1 levels as expected because of miR-181a-5p binding and RISC-induced RNA degradation or translational inhibition. Aiming to explain this, a target scan analysis revealed that miR-181a-5p directly binds to cAMP-responsive element binding protein-like 2 (CREBL2), which interacts with CREB (Ma *et al.*, 2011), underlining the very complex and diverse possibility of miR-181a-5p to influence cancer-related pathways. Wang and colleagues also observed lower pAKT and pERK levels after miR-181d transfection with a western blot approach in glioma cells (Wang *et al.*, 2012), indicating a currently unknown mechanism of kinase regulation by miRNAs. In the example of miR-181a-5p targeting PTEN, thereby enabling the phosphorylation of AKT by PI3K (Sun *et al.*, 2023), elevated pAKT levels but not total AKT levels can be explained, so the reduced levels of pERK1/2 and pCREB induced by miR-181a-5p could also be explained by an indirect mechanism induced by miR-181a-5p in a network. Nevertheless, we showed that active ERK1/2 signaling promotes MMP9 expression and is inhibited by miR-181a-5p. In summary, we explained a novel mechanism of ADAM8 signaling driven through miRNA regulation with emerging influences on tumor-promoting pathways, on the example of miR-181a-5p in GBM cells. As depicted in Figure 6 in the mansucript, we propose an ADAM8/ERK1/2/CREB-1/miR-181a-5p axis with a negative feedback loop on the known ADAM8/ERK1/2/CREB-1/MMP9 (Conrad *et al.*, 2018) axis, thereby inhibiting MMP9 expression and contributing to the ADAM8 dependent regulation of MMP9. Interestingly, the suggested ADAM8/STAT3/miR-181a-5p/osteopontin axis could harbor a negative or positive feedback loop. He and colleagues confirmed the binding of miR-181a-5p on the 3'UTR of STAT3 *via* dual luciferase reporter assay in cutaneous melanoma (He *et al.*, 2020), implicating that miR-181a-5p inhibits

STAT3 signaling and thus its inhibition. On the contrary, Assmann and colleagues measured induced pSTAT3 and pERK1/2 levels with miR-181a-5p overexpression targeting suppressor of cytokine signaling 3 (SOCS3) and dual specificity phosphatase 6 (DUSP6) in T large granular lymphocyte leukemia (Assmann *et al.*, 2022). Here, it has to be reconsidered that the suppression of diverse mRNA targets by miRNAs is not necessarily ubiquitous between cell types and is dependent on several factors like the robustness of the RISC complex, the possibility of alternative splicing and polyadenylation affecting the mRNA secondary structures (O'Brien *et al.*, 2018). Expanding the possibility that ADAM8 mediates signaling involving miR-181a-5p from intra- to extracellular, we wonder if the packaging of miR-181a-5p into EVs depends on the cellular ADAM8 expression. Previous publications from our group indicated that ADAM8 itself occurs as an active protease in EVs derived from pancreatic adenocarcinoma cells (Cook *et al.*, 2022) and is detectable in serum samples from patients suffering from pancreatic ductal adenocarcinoma (Verel-Yilmaz *et al.*, 2021). Moreover, LCN2 and MMP-9 (Cook *et al.*, 2022), miR-720 and miR-451 (Verel-Yilmaz *et al.*, 2021) were considered ADAM8-dependent EV cargos, suggesting that ADAM8 shapes the TME. As expected, EVs derived from ADAM8-expressing cells carried lower amounts of miR-181a-5p. The transfection of miR-181a-5p mimic or inhibitor in U87 cells significantly affected the amounts of miR-181a-5p in EVs, suggesting that the amount of miR-181a-5p in EVs is associated with the amount in the original cell. The regulated process on the miR-181a-5p release by EVs remains to be clarified. Several mechanisms of miRNA cargo sorting are described and controlled by miRNAs and target sequences (O'Brien *et al.*, 2018; Wei *et al.*, 2021). Nevertheless, we showed that the miR-181a-5p amount in EVs depends on the cellular ADAM8 expression, enabling ADAM8 to partially shape the TME by controlling both the cellular and the EV miR-181a-5p expression, suggesting that with more availability of cellular miR-181a-5p, more miR-181a-5p gets packed into vesicles. Indeed, cytosolic miRNA's high occurrence is connected to an enriched occurrence in EVs (Munir *et al.*, 2020). With the miR-181a-5p repression by ADAM8 in cells and EVs, we hypothesized that ADAM8 protects surrounding cells from MMP9 inhibition by miR-181a-5p reduction. Indeed, we confirmed EV uptake by U87 cells and the MMP9 repression in cells treated with EVs carrying high miR-181a-5p amounts. Although there is a need to investigate this observation in different cell entities of the TME, one could hypothesize that especially TAMs, which are known to highly express ADAM8 (Gjorgjevski *et al.*, 2019; Jaworek *et al.*, 2021; Liu *et al.*, 2022b), secrete EVs with less miR-181a-5p amounts, thereby promoting MMP9 expression and MMP9-induced invasion, migration, metastasis, and proliferation (Xue *et al.*, 2017; Huang, 2018). EVs are acknowledged mediators of cell-to-cell communication, also in the TME of the brain, adapting to the hypoxic microenvironment and creating an immune-suppressive microenvironment (Simon *et al.*, 2020). Supporting our hypothesis and insights that ADAM8 inhibits miR-181a-5p EV secretion, thereby preventing MMP9 downregulation in surrounding cells, several reports declare EVs to participate in ECM

reorganization, enhancing the secretion and activation of MMPs and subsequently cellular migration and invasion (Baulch *et al.*, 2016; Oushy *et al.*, 2018; Rackov *et al.*, 2018). In one particular study, GBM-EVs decreased p53 levels in astrocytes, which led to the increase of fibronectin 1, a ligand for the upregulated receptor integrin α5 and β1 dimer associated with MMPs, invasion and poor prognosis (Kesanakurti *et al.*, 2013; Mallawaaratchy *et al.*, 2017; Simon *et al.*, 2020). In pancreatic cancer, Puolakkainen and colleagues described that macrophages enhance the expression of ADAM8 and MMP9 leading to evaluated invasion rates in a co-culture approach *in vitro* (Puolakkainen *et al.*, 2014), describing the correlation of ADAM8 and MMP9 crossing the single cell and partially describing the network of the TME. Moreover, Cook and colleagues described the influence of ADAM8-expressing cells in the TME, regulating the release of LCN2, stabilizing MMP9 in a heterodimer complex (Yan *et al.*, 2001), suggesting to support extracellular matrix degradation and invasion. Interestingly, the co-culture of pancreatic cancer cells with ADAM8-expressing macrophages even overcame ADAM8-dependent intracellular signaling in pancreatic cancer cells since LCN2 and MMP9 expression patterns in ADAM8 KO pancreatic tumor cells were induced (Cook *et al.*, 2022). This strongly argues for ADAM8 mediating the TME through the release of EVs, which are known to carry high amounts of miRNAs (O'Brien *et al.*, 2018). The regulated release of miRNAs *via* EVs expands the influence of ADAM8 enormously. Focusing on miR-181a-5p released by EVs, Sue and colleagues investigated miR-181a-5p in EVs secreted by mesenchymal stromal cells, suppressing PTEN and activating STAT5 and the inhibitory regulators SOCS1 in macrophages, which demonstrates the ability of miR-181a-5p impairing crucial inflammatory pathways cross-cellular. Interestingly, ones overexpressed in mesenchymal stromal cells, EVs carried more miR-181a-5p and therapeutically affected acute respiratory distress syndrome *in vivo*, highly underlining the possible therapeutical function of miR-181a-5p (Su *et al.*, 2022).

We clinically transferred the suggested ADAM8/miR-181a-5p/MMP9 axis and tested GBM tissue samples for miR-181a-5p, *ADAM8* and *MMP9* expression. As a result, *ADAM8* and *MMP9* expression levels significantly correlated, fitting to previous observations of our group testing another patient cohort (Gjorgjevski *et al.*, 2019) and in line with "TCGA X GTEx" dataset analysis (unpublished data). Contrary, no negative correlation between *ADAM8* and miR-181a-5p or *MMP9* and miR-181a-5p could be determined, suggesting that there are more influences regulating the miR-181a-5p expression than the exclusive inhibition through ADAM8 and more, and potentially stronger, influences on MMP9 regulation than the indirect influence of miR-181a-5p targeting MEK1/2, ERK1/2, and CREB-1 in the heterogeneity of GBM tissue. Several factors are described to regulate MMP9, for instance, inflammatory cytokines and growth factors like interleukin 1 and tumor necrosis factor α or repressors like kisspeptin, which interferes with the translocation of *MMP9* and binds to nuclear factor 'kappa-light-chain-enhancer' of activated B cells (NF-

κB) subunits to the promotor of *MMP9* (Labrie and St-Pierre, 2013). Hence, the repeated highly significant observation of the *ADAM8* and *MMP9* correlation, despite the heterogeneity of GBM and various other influences, argues for a strong connection and reciprocal influence that promotes tumor progression. Narrowing the heterogeneity of GBM tissue by analyzing the expression patterns in tissue samples derived from an MR-spectroscopy-guided surgery, a clear distinction of non-tumorous access tissue, with high miR-181a-5p and low *ADAM8* and *MMP9* levels, to the tumor core, comprising the opposite expression pattern, appeared. Therapeutically, targeting the 'dispensable' ADAM8 is considered to be very attractive since it shows low physiological expression levels suggesting low side effects (Conrad *et al.*, 2019). BK-1361, as a specific ADAM8 inhibitor, turned out to be a promising therapeutic approach in pancreatic cancer, inhibiting ERK1/2 signaling and MMP activity (Schlomann *et al.*, 2015). In line, treatment of U87 cells with BK-1361 resulted in higher miR-181a-5p levels suggesting the promotion of the ERK1/2 pathway inhibition additionally. In GBM, the ERK1/2 pathway strongly drives uncontrolled cell growth (Guo *et al.*, 2020) due to the constitutively active EGFRIII (Padfield *et al.*, 2015). Hence, inhibiting this pathway is crucial and could be targeted indirectly *via* BK-1361 usage. BK1-361 proved to be a promising novel therapeutical approach not only in pancreatic cancer (Schlomann *et al.*, 2015) but also in asthma (Chen *et al.*, 2016) and, with our data and the study of Dong and colleagues, showing that ADAM8 can cause TMZ-resistance in GBM cells with elevated pERK1/2 and pAKT levels (Dong *et al.*, 2015), we justify considering more experimental approaches to target ADAM8 in GBM. Moreover, the induced overexpression of miR-181a-5p could also serve as a therapeutical option. As tumor suppressor miRNA, miR-181a-5p is downregulated in GBM (Valiulyte *et al.*, 2022), so the therapeutically induced re-expression could restore its tumor suppressive function, and the miRNA could be degraded if overexpressed in other tissue compartments, potentially avoiding side-effects. As therapeutically thought nanoparticles (O'Neill and Dwyer, 2020), EVs are considered to carry miRNA as a therapeutical approach, either isolated especially from mesenchymal stem cells overexpressing the miRNA or loaded with miRNAs by physical or chemical techniques, potentially being able to cross the BBB (Munir *et al.*, 2020). First clinical trials demonstrated the ability of EVs to support the immune system in response to cancer. Even before EVs were thought to serve as drug carrier, their impact as biomarkers was discussed (Couch *et al.*, 2021). Our pilot study provides evidence that miR-181a-5p derived from serum-EVs could be a potential biomarker to detect an early rGBM because of changes in expression patterns before and after the first and second surgery. Nevertheless, screening a larger patient cohort would be necessary to verify this data. Next to elevated ADAM8 and low miR-181a-5p levels in GBM, high MMP9 levels are associated with high glioma grade, poor survival, and poor response to TMZ treatment (Li *et al.*, 2016). Thus, combinatorial screening of ADAM8, MMP9, and miR-181a-5p

expression patterns in paired tissue and blood samples of iGBM and rGBM could serve as a prognostic marker.

5.3 Identification of Dysregulated microRNAs in Glioblastoma Stem-like Cells

GSCs are partially responsible for the development of GBM recurrence, inducing radio-/chemoresistance (Garnier *et al.*, 2019), invasion, angiogenesis (Boyd *et al.*, 2021), and contributing to heterogeneity through their multi-lineage differentiation (Lathia *et al.*, 2015). Although it is known that miRNAs are commonly dysregulated and mostly downregulated in GBM (Møller *et al.*, 2013) and several studies aim to further classify the heterogenic GBM through its miRNA expression pattern aiming to enable a personalized therapy (Shea *et al.*, 2016), little is known about the change of miRNA expression during differentiation of GSCs into astrocytic tumor cells. We differentiated three patient-derived GSC cell lines with subsequent characterization according to morphological and specific expression pattern changes. The downregulation of the well-established cancer stem-like marker *CD133* (Singh *et al.*, 2004; Liu *et al.*, 2006; Barzegar Behrooz *et al.*, 2019) and the upregulation of the intermediate filament highly expressed in active astrocytes *GFAP* (BIGNAMI and DAHL, 1976) distinguished GSCs from differentiated astrocytic tumor cells, indicating the successful experimental performance, initially shown by Hannen *et al.*, 2019. Since the discovery that CD133$^-$ cells also has the ability to initiate GBM tumor formation and CD133$^+$ descendants *in vivo* (Wang *et al.*, 2008), it became clear that more markers needed to be involved, but the effectiveness of those markers is still controversial (Yi *et al.*, 2016). We also tested *SOX2*, *Nestin*, and *CD44* mRNA expression patterns with less consistent trends, possibly due to the high patient diversity and heterogeneity of GBM or the further need for GBM subset classification. Especially the unexpected and strong upregulation of *CD44* with GSC differentiation into astrocytes raised questions. In line with our controversy than expected observation, Wang and colleagues induced a knockdown of initially CD44$^+$ GSCs through intrinsic and extrinsic methods and observed an upregulation of GSC features like lower GFAP and higher CD133, Nestin and octamer-binding transcription factor 4 (Oct4) expression, reduced cellular proliferation and increased sphere formation (Wang *et al.*, 2017a), questioning the suitability to mark GSCs. In comparison, it was shown that both CD44^{low}/CD133^{high} and CD44^{high}/CD133^{low} form GSC typical spheres and have high tumorigenicity (Lottaz *et al.*, 2010; Fu *et al.*, 2013). Regarding molecular-based GBM classification, CD44 is assigned to the mesenchymal subtype featuring especially high angiogenesis and invasion, the activation of PI3K/AKT signaling and poor prognosis. In contrast, the signature of SOX2 belongs to the proneural subtype, which is more common in young patients and less aggressive (Zhang *et al.*, 2020). Thus, the three tested patient-derived cell lines could be classified especially to the mesenchymal phenotype additionally induced with astrocytic differentiation, fitting to the known patient age at diagnosis. The donor specificity became apparent in cell line 2016/240, which showed less but still significant distinction using CD133 and GFAP. Moreover, there were less

consistent results in further performed verifications of miRNA expression patterns. Although caution is required in drawing conclusions based on the low number of patients analyzed, it is interesting to note that cell line 2016/240 was also derived from the only female and the youngest patient with the longest survival, as sex differences affecting hormones, metabolic pathways, and the immune system lead to different outcomes and incidences (Carrano *et al.*, 2021).

Applying a pathway-focused miRNA PCR array testing eighty-four miRNAs with additional controls revealed thirty-one dysregulated miRNAs comparing pooled GCSs and their matched pooled differentiated astrocytic cell types. Focusing on ten highly dysregulated miRNAs based on a literature search regarding their potential role in GBM, four lethal (let) -7 miRNA family members were highly upregulated in astrocytic cells. Remarkably, even six out of nine initially found upregulated miRNAs in differentiated cells in the set of thirty-one dysregulated miRNAs were let-7 family members. In GBM, the let-7 miRNA family can be classified as tumor-suppressive (Wang *et al.*, 2013; Song *et al.*, 2016), and there are some studies regarding their role in GSC differentiation. Induced overexpression of let-7b reduced tumor sphere formation and inhibited proliferation, migration, and invasion of glioma cells (Song *et al.*, 2016). Directly targeting Kirsten rat sarcoma virus (K-RAS), let-7a-5p induces apoptosis, cell cycle arrest, and migration inhibition (Wang *et al.*, 2013). Thus, directly targeting K-RAS, let-7a-5p suppresses major signaling pathways like the PI3K/AKT and MAPK signaling, mediating proliferation, survival and self-renewal of GSCs (Bayin *et al.*, 2014). Moreover, neural stem stell marker Musahi-2 (Kaneko *et al.*, 2000) represents a possible target predicted by "miRPathDB v.2.0", suggesting an additional factor suppressing the GSC phenotype. Despite the heterogeneity of GBM, we confirmed the association of let-7 family members with GSC differentiation by detecting six upregulated members through a screening method using three patient-derived GSC cell lines. Therefore, we justify further experiments to induce the expression of let-7 miRNAs, thereby promoting GSC differentiation and potentially making the tumor more vulnerable to radio- and chemotherapy. Interestingly, Liu and colleagues recently discovered *zinc finger protein 117 (ZNF117)* as a genetic regulator of GSC differentiation towards an oligodendroglial lineage. ZNF117 regulates the critical Notch signaling (Bayin *et al.*, 2014) interacting with *jagged-2 (JAG2)*. The authors discussed ZNF117 as a challenging drug target regarding traditional therapy since it functions as a transcription factor (Liu *et al.*, 2022a). Thus, targeting *ZNF117* mRNA by an induced overexpression of a tumor-suppressor miRNA could contribute to an oligodendroglial differentiation and, interestingly, let-7c-3p is predicted to target *ZNF117 via* "miRPathDB v.2.0" (unpublished data). Next to the let-7 family, miR-223-3p was highly enriched in differentiated cells. Directly targeting ATM, miR-223-3p sensitizes to radio- and chemotherapy overcoming ATM-induced DNA repair mechanism sensitizing in GBM (Liang *et al.*, 2014). Yet, its potential role in controlling stem cell fate is not described, but there are some implications for the involvement of miR-223-3p. In cervical cancer, leukemia, hepatoma, oral

carcinoma, and lung cancer cells, miR-223-3p is described to suppress cell proliferation by targeting insulin-like growth factor-1 receptor (IGF-1R). Consequently, the downstream PI3K/AKT signaling or MAPK pathway was suppressed *via* miR-223-3p overexpression (Gao *et al.*, 2017), similar to the impacts of let-7 targeting K-RAS described above. Since those signaling pathways are critically involved in the maintenance of the stem cell phenotype (Bayin *et al.*, 2014), it remains to be investigated if miR-223-3p targets IGF-1R in GSCs. Thus, the low expression of tumor suppressor miR-223-3p in GCSs justifies further detailed analysis regarding co-transfection with let-7 family members, potentially inducing stem cell differentiation overcoming radio- and chemoresistance and inhibiting distant tumor formation resulting in a recurrence.

As for the most significant upregulated miRNAs in GSCs, miR-425-5p, miR-17-5p, miR-30c-5p, miR-424-5p, and miR-195-5p are all involved or potentially involved, according to "miRPathDB v.2.0" prediction analysis, in the maintenance of the GSC phenotype (Zhou *et al.*, 2020; Li and Yang, 2012; Kehl *et al.*, 2020). Whereas for miR-30c-5p, miR-424-5p, and miR-195-5p tumor-suppressive roles are also described in GBM (Liu *et al.*, 2019; Gheidari *et al.*, 2021; Wang *et al.*, 2019), miR-425-5p and miR-17-5p can be classified as onco-miRNAs targeting PTEN (Li and Yang, 2012; Zhou *et al.*, 2020). PTEN is commonly mutated or deleted in GBM, constituting active PI3K/AKT signaling with subsequent uncontrolled tumor growth as a hallmark of GBM. PTEN loss or mutation was discussed but not proven as a prognostic marker in GBM (Montano, 2016). Given the significant role of PI3K/AKT signaling in the maintenance of GSCs (Bayin *et al.*, 2014), the inactivation of PTEN partially through miRNAs like miR-17-5p and miR-425-5p could classify GSCs additionally to the loss of GFAP (BIGNAMI and DAHL, 1976), which could be additionally targeted by both miRNAs as predicted by "miRPathDB v.2.0". Since miR-425-5p was the most consistent upregulated miRNA in GSCs, we transfected patient-derived GBM cells featuring the ability to readopt to GSCs with a miR-425-5p mimic and detected significantly reduced PTEN and GFAP levels in GBM100 but were not able to verify these changes on a protein level in GBM42 cells. This could be explained by the high heterogeneity in GBM, making a statement difficult even if the results were consistent in two patient-derived cell lines. On the other hand, the need to perform a luciferase reporter assay, like conducted for PTEN (Zhou *et al.*, 2020), to verify the binding ability of miR-425-5p to the 3' UTR of GFAP becomes apparent. Since GFAP expression is induced by Janus kinase 2 (JAK2)/STAT3 signaling and leads to differentiation (Bonni *et al.*, 1997), the potential downregulation of GFAP by an induced overexpression of miR-425-5p in astrocytic tumor cells could partially lead to re-differentiation and GSC formation. Conversely, the transfection of single-stranded, antisense RNA-oligonucleotides complementary to onco-miRNAs (Shea *et al.*, 2016), like miR-425-5p and miR-17-5p, could prevent PTEN and GFAP downregulation and induce the differentiation to more attackable astrocytic tumor cells. Interestingly, clinical phase I and II trials were conducted targeting miR-122 for the first time with promising outcomes for hepatitis c virus patients (Janssen

et al., 2013), which requires miR-122 for replication. Although no side effects were reported, the widespread effects of miRNAs must be considered. For example, miR-122 functions as a tumor suppressor in GBM and decreased expression is associated with poor survival rates (Wang *et al.*, 2014; Shea *et al.*, 2016).

KEGG enrichment analysis and the illustration of the miRNA-target relationship as a chord plot showed the suggested network of all ten miRNAs and their target genes involved in pathways crucial for the GSC phenotype, like the PI3K/AKT pathway and a collection of signaling pathways mediating stem cell pluripotency. Since 2,588 mature human miRNA sequences are counted on the database 'miRbase,' each miRNA predicted to target hundreds to thousands of mRNAs (Shea *et al.*, 2016), we surely state to reveal only a small part of a very heterogenous, complex, and constantly evolving network. Comparably to our study, Tomei and colleagues performed an array-based profiling and RT-qPCR comparing three GSCs and their autologous differentiated cells, revealing fourteen significantly dysregulated miRNAs. Especially miR-21 and miR-95 were associated with overall patient survival (Tomei *et al.*, 2021). In another study, Sana and colleagues analyzed ten paired GSCs and differentiated tumor cells *via* global expression analysis *in vitro* and *in vivo*, defining a dysregulated miRNA signature (Sana *et al.*, 2018). Together with these studies, we provide evidence for a new miRNA-based GBM classification, potentially finding prognostic markers, defining new therapeutic targets associated with GSC, and overcoming associated radio- and chemoresistance.

6 References

Ahluwalia MS, Groot J de, Liu WM and Gladson CL. Targeting SRC in glioblastoma tumors and brain metastases: rationale and preclinical studies. *Cancer letters* 2010; **298**: 139–149.

Ali MY, Oliva CR, Noman ASM, Allen BG, Goswami PC, Zakharia Y, Monga V, Spitz DR, Buatti JM and Griguer CE. Radioresistance in Glioblastoma and the Development of Radiosensitizers. *Cancers* 2020; **12**.

Ali Syeda Z, Langden SSS, Munkhzul C, Lee M and Song SJ. Regulatory Mechanism of MicroRNA Expression in Cancer. *International journal of molecular sciences* 2020; **21**.

Amiri A, Le PU, Moquin A, Machkalyan G, Petrecca K, Gillard JW, Yoganathan N and Maysinger D. Inhibition of carbonic anhydrase IX in glioblastoma multiforme. *European journal of pharmaceutics and biopharmaceutics official journal of Arbeitsgemeinschaft fur Pharmazeutische Verfahrenstechnik e.V* 2016; **109**: 81–92.

Assmann JLJC, Leon LG, Stavast CJ, van den Bogaerdt SE, Schilperoord-Vermeulen J, Sandberg Y, Bellido M, Erkeland SJ, Feith DJ, Loughran TP and Langerak AW. miR-181a is a novel player in the STAT3-mediated survival network of TCRαβ+ CD8+ T large granular lymphocyte leukemia. *Leukemia* 2022; **36**: 983–993.

Awan T, Babendreyer A, Mahmood Alvi A, Düsterhöft S, Lambertz D, Bartsch JW, Liedtke C and Ludwig A. Expression levels of the metalloproteinase ADAM8 critically regulate proliferation, migration and malignant signalling events in hepatoma cells. *Journal of cellular and molecular medicine* 2021; **25**: 1982–1999.

Bao S, Wu Q, McLendon RE, Hao Y, Shi Q, Hjelmeland AB, Dewhirst MW, Bigner DD and Rich JN. Glioma stem cells promote radioresistance by preferential activation of the DNA damage response. *Nature* 2006; **444**: 756–760.

Barthel FP, Johnson KC, Varn FS, Moskalik AD, Tanner G, Kocakavuk E, Anderson KJ, Abiola O, Aldape K, Alfaro KD, Alpar D, Amin SB, Ashley DM, Bandopadhayay P, Barnholtz-Sloan JS, Beroukhim R, Bock C, Brastianos PK, Brat DJ, Brodbelt AR, Bruns AF, Bulsara KR, Chakrabarty A, Chakravarti A, Chuang JH, Claus EB, Cochran EJ, Connelly J, Costello JF, Finocchiaro G, Fletcher MN, French PJ, Gan HK, Gilbert MR, Gould PV, Grimmer MR, Iavarone A, Ismail A, Jenkinson MD, Khasraw M, Kim H, Kouwenhoven MCM, LaViolette PS, Li M, Lichter P, Ligon KL, Lowman AK, Malta TM, Mazor T, McDonald KL, Molinaro AM, Nam D-H, Nayyar N, Ng HK, Ngan CY, Niclou SP, Niers JM, Noushmehr H, Noorbakhsh J, Ormond DR, Park C-K, Poisson LM, Rabadan R, Radlwimmer B, Rao G, Reifenberger G, Sa JK, Schuster M, Shaw BL, Short SC, Smitt PAS, Sloan AE, Smits M, Suzuki H, Tabatabai G, van Meir EG, Watts C, Weller M, Wesseling P, Westerman BA, Widhalm G, Woehrer A, Yung WKA, Zadeh G, Huse JT, Groot JF de, Stead LF and Verhaak

RGW. Longitudinal molecular trajectories of diffuse glioma in adults. *Nature* 2019; **576**: 112–120.

Barzegar Behrooz A, Syahir A and Ahmad S. CD133: beyond a cancer stem cell biomarker. *Journal of drug targeting* 2019; **27**: 257–269.

Baulch JE, Geidzinski E, Tran KK, Yu L, Zhou Y-H and Limoli CL. Irradiation of primary human gliomas triggers dynamic and aggressive survival responses involving microvesicle signaling. *Environmental and molecular mutagenesis* 2016; **57**: 405–415.

Bayin NS, Modrek AS and Placantonakis DG. Glioblastoma stem cells: Molecular characteristics and therapeutic implications. *World journal of stem cells* 2014; **6**: 230–238.

Becker HM. Carbonic anhydrase IX and acid transport in cancer. *British journal of cancer* 2020; **122**: 157–167.

Becker HM, Hirnet D, Fecher-Trost C, Sültemeyer D and Deitmer JW. Transport activity of MCT1 expressed in Xenopus oocytes is increased by interaction with carbonic anhydrase. *The Journal of biological chemistry* 2005; **280**: 39882–39889.

Becker HM, Klier M and Deitmer JW. Nonenzymatic augmentation of lactate transport via monocarboxylate transporter isoform 4 by carbonic anhydrase II. *The Journal of membrane biology* 2010; **234**: 125–135.

Bellot G, Garcia-Medina R, Gounon P, Chiche J, Roux D, Pouysségur J and Mazure NM. Hypoxia-induced autophagy is mediated through hypoxia-inducible factor induction of BNIP3 and BNIP3L via their BH3 domains. *Molecular and cellular biology* 2009; **29**: 2570–2581.

Biasoli D, Kahn SA, Cornélio TA, Furtado M, Campanati L, Chneiweiss H, Moura-Neto V and Borges HL. Retinoblastoma protein regulates the crosstalk between autophagy and apoptosis, and favors glioblastoma resistance to etoposide. *Cell death & disease* 2013; **4**: e767.

BIGNAMI A and DAHL D. THE ASTROGLIAL RESPONSE TO STABBING. IMMUNOFLUORESCENCE STUDIES WITH ANTIBODIES TO ASTROCYTE-SPECIFIC PROTEIN (GFA) IN MAMMALIAN AND SUBMAMMALIAN VERTEBRATES. *Neuropathology and Applied Neurobiology* 1976; **2**: 99–110.

Birzu C, French P, Caccese M, Cerretti G, Idbaih A, Zagonel V and Lombardi G. Recurrent Glioblastoma: From Molecular Landscape to New Treatment Perspectives. *Cancers* 2020; **13**.

Bjørkøy G, Lamark T, Pankiv S, Øvervatn A, Brech A and Johansen T. Monitoring autophagic degradation of p62/SQSTM1. *Methods in enzymology* 2009; **452**: 181–197.

Bonni A, Sun Y, Nadal-Vicens M, Bhatt A, Frank DA, Rozovsky I, Stahl N, Yancopoulos GD and Greenberg ME. Regulation of gliogenesis in the central nervous system by the JAK-STAT signaling pathway. *Science (New York, N.Y.)* 1997; **278**: 477–483.

Bordignon KC, Neto MC, Ramina R, Meneses MS de, Zazula AD and Almeida LGMP de. Patterns of neuroaxis dissemination of gliomas: suggestion of a classification based on magnetic resonance imaging findings. *Surgical neurology* 2006; **65**: 472-7; discussion 477.

Boyd NH, Tran AN, Bernstock JD, Etminan T, Jones AB, Gillespie GY, Friedman GK and Hjelmeland AB. Glioma stem cells and their roles within the hypoxic tumor microenvironment. *Theranostics* 2021; **11**: 665–683.

Boyd NH, Walker K, Fried J, Hackney JR, McDonald PC, Benavides GA, Spina R, Audia A, Scott SE, Landis CJ, Tran AN, Bevensee MO, Griguer C, Nozell S, Gillespie GY, Nabors B, Bhat KP, Bar EE, Darley-Usmar V, Xu B, Gordon E, Cooper SJ, Dedhar S and Hjelmeland AB. Addition of carbonic anhydrase 9 inhibitor SLC-0111 to temozolomide treatment delays glioblastoma growth in vivo. *JCI insight* 2017; **2**.

Brown PD. Matrix metalloproteinase inhibitors: a novel class of anticancer agents. *Advances in enzyme regulation* 1995; **35**: 293–301.

Buonfiglioli A and Hambardzumyan D. Macrophages and microglia: the cerberus of glioblastoma. *Acta neuropathologica communications* 2021; **9**: 54.

Buruiană A, Florian ŞI, Florian AI, Timiş T-L, Mihu CM, Miclăuş M, Oşan S, Hrapşa I, Cataniciu RC, Farcaş M and Şuşman S. The Roles of miRNA in Glioblastoma Tumor Cell Communication: Diplomatic and Aggressive Negotiations. *International journal of molecular sciences* 2020; **21**.

Campos B, Olsen LR, Urup T and Poulsen HS. A comprehensive profile of recurrent glioblastoma. *Oncogene* 2016; **35**: 5819–5825.

Carrano A, Juarez JJ, Incontri D, Ibarra A and Guerrero Cazares H. Sex-Specific Differences in Glioblastoma. *Cells* 2021; **10**.

Carruthers RD, Ahmed SU, Ramachandran S, Strathdee K, Kurian KM, Hedley A, Gomez-Roman N, Kalna G, Neilson M, Gilmour L, Stevenson KH, Hammond EM and Chalmers AJ. Replication Stress Drives Constitutive Activation of the DNA Damage Response and Radioresistance in Glioblastoma Stem-like Cells. *Cancer research* 2018; **78**: 5060–5071.

Chappell WH, Steelman LS, Long JM, Kempf RC, Abrams SL, Franklin RA, Bäsecke J, Stivala F, Donia M, Fagone P, Malaponte G, Mazzarino MC, Nicoletti F, Libra M, Maksimovic-Ivanic D, Mijatovic S, Montalto G, Cervello M, Laidler P, Milella M, Tafuri A, Bonati A, Evangelisti C, Cocco L, Martelli AM and McCubrey JA. Ras/Raf/MEK/ERK and PI3K/PTEN/Akt/mTOR inhibitors: rationale and importance to inhibiting these pathways in human health. *Oncotarget* 2011; **2**: 135–164.

Chen J, Deng L, Dreymüller D, Jiang X, Long J, Duan Y, Wang Y, Luo M, Lin F, Mao L, Müller B, Koller G and Bartsch JW. A novel peptide ADAM8 inhibitor attenuates bronchial hyperresponsiveness

and Th2 cytokine mediated inflammation of murine asthmatic models. *Scientific reports* 2016; **6**: 30451.

Chhor V, Le Charpentier T, Lebon S, Oré M-V, Celador IL, Josserand J, Degos V, Jacotot E, Hagberg H, Sävman K, Mallard C, Gressens P and Fleiss B. Characterization of phenotype markers and neuronotoxic potential of polarised primary microglia in vitro. *Brain, Behavior, and Immunity* 2013; **32**: 70–85.

Choe G, Park JK, Jouben-Steele L, Kremen TJ, Liau LM, Vinters HV, Cloughesy TF and Mischel PS. Active matrix metalloproteinase 9 expression is associated with primary glioblastoma subtype. *Clin Cancer Res.* 2002: 2894–2901.

Choi AMK, Ryter SW and Levine B. Autophagy in human health and disease. *The New England journal of medicine* 2013; **368**: 651–662.

Ciafrè SA, Galardi S, Mangiola A, Ferracin M, Liu C-G, Sabatino G, Negrini M, Maira G, Croce CM and Farace MG. Extensive modulation of a set of microRNAs in primary glioblastoma. *Biochemical and biophysical research communications* 2005; **334**: 1351–1358.

Cong D, Zhu W, Shi Y, Pointer KB, Clark PA, Shen H, Kuo JS, Hu S and Sun D. Upregulation of NHE1 protein expression enables glioblastoma cells to escape TMZ-mediated toxicity via increased H^+ extrusion, cell migration and survival. *Carcinogenesis* 2014; **35**: 2014–2024.

Conrad C, Benzel J, Dorzweiler K, Cook L, Schlomann U, Zarbock A, Slater EP, Nimsky C and Bartsch JW. ADAM8 in invasive cancers: links to tumor progression, metastasis, and chemoresistance. *Clinical science (London, England 1979)* 2019; **133**: 83–99.

Conrad C, Götte M, Schlomann U, Roessler M, Pagenstecher A, Anderson P, Preston J, Pruessmeyer J, Ludwig A, Li R, Kamm RD, Ritz R, Carl B, Nimsky C and Bartsch JW. ADAM8 expression in breast cancer derived brain metastases: Functional implications on MMP-9 expression and transendothelial migration in breast cancer cells. *International journal of cancer* 2018; **142**: 779–791.

Cook L, Sengelmann M, Winkler B, Nagl C, Koch S, Schlomann U, Slater EP, Miller MA, Strandmann EP von, Dörsam B, Preußer C and Bartsch JW. ADAM8-Dependent Extracellular Signaling in the Tumor Microenvironment Involves Regulated Release of Lipocalin 2 and MMP-9. *International journal of molecular sciences* 2022; **23**.

Couch Y, Buzàs EI, Di Vizio D, Gho YS, Harrison P, Hill AF, Lötvall J, Raposo G, Stahl PD, Théry C, Witwer KW and Carter DRF. A brief history of nearly EV-erything - The rise and rise of extracellular vesicles. *Journal of extracellular vesicles* 2021; **10**: e12144.

Couto M, Coelho-Santos V, Santos L, Fontes-Ribeiro C, Silva AP and Gomes CMF. The interplay between glioblastoma and microglia cells leads to endothelial cell monolayer dysfunction via

the interleukin-6-induced JAK2/STAT3 pathway. *Journal of cellular physiology* 2019; **234**: 19750–19760.

Da Cunha MLV and Maldaun MVC. Metastasis from glioblastoma multiforme: a meta-analysis. *Revista da Associacao Medica Brasileira (1992)* 2019; **65**: 424–433.

Daood M, Tsai C, Ahdab-Barmada M and Watchko JF. ABC transporter (P-gp/ABCB1, MRP1/ABCC1, BCRP/ABCG2) expression in the developing human CNS. *Neuropediatrics* 2008; **39**: 211–218.

Das A, Banik NL and Ray SK. Modulatory effects of acetazolamide and dexamethasone on temozolomide-mediated apoptosis in human glioblastoma T98G and U87MG cells. *Cancer investigation* 2008; **26**: 352–358.

Das SG, Romagnoli M, Mineva ND, Barillé-Nion S, Jézéquel P, Campone M and Sonenshein GE. miR-720 is a downstream target of an ADAM8-induced ERK signaling cascade that promotes the migratory and invasive phenotype of triple-negative breast cancer cells. *Breast cancer research BCR* 2016; **18**: 40.

Daubon T, Hemadou A, Romero Garmendia I and Saleh M. Glioblastoma Immune Landscape and the Potential of New Immunotherapies. *Frontiers in immunology* 2020; **11**: 585616.

Di Fiore A, Pedone C, D'Ambrosio K, Scozzafava A, Simone G de and Supuran CT. Carbonic anhydrase inhibitors: Valdecoxib binds to a different active site region of the human isoform II as compared to the structurally related cyclooxygenase II "selective" inhibitor celecoxib. *Bioorganic & medicinal chemistry letters* 2006; **16**: 437–442.

Dong F, Eibach M, Bartsch JW, Dolga AM, Schlomann U, Conrad C, Schieber S, Schilling O, Biniossek ML, Culmsee C, Strik H, Koller G, Carl B and Nimsky C. The metalloprotease-disintegrin ADAM8 contributes to temozolomide chemoresistance and enhanced invasiveness of human glioblastoma cells. *Neuro-oncology* 2015; **17**: 1474–1485.

Draaisma K, Chatzipli A, Taphoorn M, Kerkhof M, Weyerbrock A, Sanson M, Hoeben A, Lukacova S, Lombardi G, Leenstra S, Hanse M, Fleischeuer R, Watts C, McAbee J, Angelopoulos N, Gorlia T, Golfinopoulos V, Kros JM, Verhaak RGW, Bours V, van den Bent MJ, McDermott U, Robe PA and French PJ. Molecular Evolution of IDH Wild-Type Glioblastomas Treated With Standard of Care Affects Survival and Design of Precision Medicine Trials: A Report From the EORTC 1542 Study. *Journal of clinical oncology official journal of the American Society of Clinical Oncology* 2020; **38**: 81–99.

Erpolat OP, Gocun PU, Akmansu M, Ozgun G and Akyol G. Hypoxia-related molecules HIF-1α, CA9, and osteopontin predictors of survival in patients with high-grade glioma. *Strahlentherapie und Onkologie Organ der Deutschen Rontgengesellschaft … [et al]* 2013; **189**: 147–154.

Escamilla-Ramírez A, Castillo-Rodríguez RA, Zavala-Vega S, Jimenez-Farfan D, Anaya-Rubio I, Briseño E, Palencia G, Guevara P, Cruz-Salgado A, Sotelo J and Trejo-Solís C. Autophagy as a Potential Therapy for Malignant Glioma. *Pharmaceuticals (Basel, Switzerland)* 2020; **13**.

Fabian MR, Sonenberg N and Filipowicz W. Regulation of mRNA translation and stability by microRNAs. *Annual review of biochemistry* 2010; **79**: 351–379.

Favata MF, Horiuchi KY, Manos EJ, Daulerio AJ, Stradley DA, Feeser WS, van Dyk DE, Pitts WJ, Earl RA, Hobbs F, Copeland RA, Magolda RL, Scherle PA and Trzaskos JM. Identification of a novel inhibitor of mitogen-activated protein kinase kinase. *The Journal of biological chemistry* 1998; **273**: 18623–18632.

Ferri A, Stagni V and Barilà D. Targeting the DNA Damage Response to Overcome Cancer Drug Resistance in Glioblastoma. *International journal of molecular sciences* 2020; **21**.

Filatova A, Seidel S, Böğürcü N, Gräf S, Garvalov BK and Acker T. Acidosis Acts through HSP90 in a PHD/VHL-Independent Manner to Promote HIF Function and Stem Cell Maintenance in Glioma. *Cancer research* 2016; **76**: 5845–5856.

Fouad YA and Aanei C. Revisiting the hallmarks of cancer. *Am. J. Cancer Res* 2017: 1016–1036.

Fu J, Yang Q, Sai K, Chen F, Pang JCS, Ng H, Kwan A and Chen Z. TGM2 inhibition attenuates ID1 expression in CD44-high glioma-initiating cells. *Neuro-oncology* 2013; **15**: 1353–1365.

Fu Y, Xin Z, Ling Z, Xie H, Xiao T, Shen X, Lin J, Xu L and Jiang H. A CREB1-miR-181a-5p loop regulates the pathophysiologic features of bone marrow stromal cells in fibrous dysplasia of bone. *Molecular medicine (Cambridge, Mass.)* 2021; **27**: 81.

Gao Y, Le Lin, Li T, Yang J and Wei Y. The role of miRNA-223 in cancer: Function, diagnosis and therapy. *Gene* 2017; **616**: 1–7.

Garnier D, Renoult O, Alves-Guerra M-C, Paris F and Pecqueur C. Glioblastoma Stem-Like Cells, Metabolic Strategy to Kill a Challenging Target. *Frontiers in oncology* 2019; **9**: 118.

Gerson SL. MGMT: its role in cancer aetiology and cancer therapeutics. *Nature reviews. Cancer* 2004; **4**: 296–307.

Ghandour MS, Derer P, Labourdette G, Delaunoy JP and Langley OK. Glial cell markers in the reeler mutant mouse: a biochemical and immunohistological study. *Journal of neurochemistry* 1981; **36**: 195–200.

Gheidari F, Arefian E, Adegani FJ, Kalhori MR, Seyedjafari E, Kabiri M, Teimoori-Toolabi L and Soleimani M. miR-424 induces apoptosis in glioblastoma cells and targets AKT1 and RAF1 oncogenes from the ERBB signaling pathway. *European journal of pharmacology* 2021; **906**: 174273.

Gilard V, Tebani A, Dabaj I, Laquerrière A, Fontanilles M, Derrey S, Marret S and Bekri S. Diagnosis and Management of Glioblastoma: A Comprehensive Perspective. *Journal of personalized medicine* 2021; **11**.

Gjorgjevski M, Hannen R, Carl B, Li Y, Landmann E, Buchholz M, Bartsch JW and Nimsky C. Molecular profiling of the tumor microenvironment in glioblastoma patients: correlation of microglia/macrophage polarization state with metalloprotease expression profiles and survival. *Bioscience reports* 2019; **39**.

Grégoire H, Roncali L, Rousseau A, Chérel M, Delneste Y, Jeannin P, Hindré F and Garcion E. Targeting Tumor Associated Macrophages to Overcome Conventional Treatment Resistance in Glioblastoma. *Frontiers in pharmacology* 2020; **11**: 368.

Gul HI, Yamali C, Bulbuller M, Kirmizibayrak PB, Gul M, Angeli A, Bua S and Supuran CT. Anticancer effects of new dibenzenesulfonamides by inducing apoptosis and autophagy pathways and their carbonic anhydrase inhibitory effects on hCA I, hCA II, hCA IX, hCA XII isoenzymes. *Bioorganic chemistry* 2018; **78**: 290–297.

Gulyaeva LF and Kushlinskiy NE. Regulatory mechanisms of microRNA expression. *Journal of translational medicine* 2016; **14**: 143.

Guo Y-J, Pan W-W, Liu S-B, Shen Z-F, Xu Y and Hu L-L. ERK/MAPK signalling pathway and tumorigenesis. *Experimental and therapeutic medicine* 2020; **19**: 1997–2007.

Ha M and Kim VN. Regulation of microRNA biogenesis. *Nature reviews. Molecular cell biology* 2014; **15**: 509–524.

Haapasalo J, Nordfors K, Haapasalo H and Parkkila S. The Expression of Carbonic Anhydrases II, IX and XII in Brain Tumors. *Cancers* 2020; **12**.

Haapasalo J, Nordfors K, Järvelä S, Bragge H, Rantala I, Parkkila A-K, Haapasalo H and Parkkila S. Carbonic anhydrase II in the endothelium of glial tumors: a potential target for therapy. *Neuro-oncology* 2007; **9**: 308–313.

Han Q, Liang H, Cheng P, Yang H and Zhao P. Gross Total vs. Subtotal Resection on Survival Outcomes in Elderly Patients With High-Grade Glioma: A Systematic Review and Meta-Analysis. *Frontiers in oncology* 2020; **10**: 151.

Hanahan D and Weinberg RA. The hallmarks of cancer. *Cell* 2000; **100**: 57–70.

Hanahan D and Weinberg RA. Hallmarks of cancer: the next generation. *Cell* 2011; **144**: 646–674.

Hannen R, Selmansberger M, Hauswald M, Pagenstecher A, Nist A, Stiewe T, Acker T, Carl B, Nimsky C and Bartsch JW. Comparative Transcriptomic Analysis of Temozolomide Resistant Primary GBM Stem-Like Cells and Recurrent GBM Identifies Up-Regulation of the Carbonic Anhydrase CA2 Gene as Resistance Factor. *Cancers* 2019; **11**.

Hao G, Xu ZP and Li L. Manipulating extracellular tumour pH: an effective target for cancer therapy. *RSC advances* 2018; **8**: 22182–22192.

Harris AL. Hypoxia--a key regulatory factor in tumour growth. *Nature reviews. Cancer* 2002; **2**: 38–47.

Haynes HR, Camelo-Piragua S and Kurian KM. Prognostic and predictive biomarkers in adult and pediatric gliomas: toward personalized treatment. *Frontiers in oncology* 2014; **4**: 47.

He Q, Zhou X, Li S, Jin Y, Chen Z, Chen D, Cai Y, Liu Z, Zhao T and Wang A. MicroRNA-181a suppresses salivary adenoid cystic carcinoma metastasis by targeting MAPK-Snai2 pathway. *Biochimica et biophysica acta* 2013; **1830**: 5258–5266.

He S, Ding L, Cao Y, Li G, Deng J, Tu Y and Wang B. Overexpression of a disintegrin and metalloprotease 8 in human gliomas is implicated in tumor progression and prognosis. *Medical oncology (Northwood, London, England)* 2012; **29**: 2032–2037.

He Y, Yang Y, Xu J, Liao Y, Liu L, Deng L and Xiong X. IL22 drives cutaneous melanoma cell proliferation, migration and invasion through activation of miR-181/STAT3/AKT axis. *Journal of Cancer* 2020; **11**: 2679–2687.

Hu. MicroRNA-181a sensitizes human malignant glioma U87MG cells to radiation by targeting Bcl-2. *Oncology Reports* 2010; **23**.

Hu Z, Mi Y, Qian H, Guo N, Yan A, Zhang Y and Gao X. A Potential Mechanism of Temozolomide Resistance in Glioma-Ferroptosis. *Frontiers in oncology* 2020; **10**: 897.

Huang H. Matrix Metalloproteinase-9 (MMP-9) as a Cancer Biomarker and MMP-9 Biosensors: Recent Advances. *Sensors (Basel, Switzerland)* 2018; **18**.

Huang X, Schwind S, Santhanam R, Eisfeld A-K, Chiang C-L, Lankenau M, Yu B, Hoellerbauer P, Jin Y, Tarighat SS, Khalife J, Walker A, Perrotti D, Bloomfield CD, Wang H, Lee RJ, Lee LJ and Marcucci G. Targeting the RAS/MAPK pathway with miR-181a in acute myeloid leukemia. *Oncotarget* 2016; **7**: 59273–59286.

HUANG S-X, ZHAO Z-Y, WENG G-H, HE X-Y, WU C-J, FU C-Y, SUI Z-Y, Ma Y-S and Liu T. Upregulation of miR-181a suppresses the formation of glioblastoma stem cells by targeting the Notch2 oncogene and correlates with good prognosis in patients with glioblastoma multiforme. *Biochemical and biophysical research communications* 2017; **486**: 1129–1136.

HUANG S-X, ZHAO Z-Y, WENG G-H, HE X-Y, WU C-J, FU C-Y, SUI Z-Y, ZHONG X-M and LIU TA. The correlation of microRNA-181a and target genes with poor prognosis of glioblastoma patients. *International Journal of Oncology* 2016; **49**: 217–224.

Iwamaru A, Szymanski S, Iwado E, Aoki H, Yokoyama T, Fokt I, Hess K, Conrad C, Madden T, Sawaya R, Kondo S, Priebe W and Kondo Y. A novel inhibitor of the STAT3 pathway induces apoptosis in malignant glioma cells both in vitro and in vivo. *Oncogene* 2007; **26**: 2435–2444.

Jackson M, Hassiotou F and Nowak A. Glioblastoma stem-like cells: at the root of tumor recurrence and a therapeutic target. *Carcinogenesis* 2015; **36**: 177–185.

Jackson SP and Bartek J. The DNA-damage response in human biology and disease. *Nature* 2009; **461**: 1071–1078.

Janssen HLA, Reesink HW, Lawitz EJ, Zeuzem S, Rodriguez-Torres M, Patel K, van der Meer AJ, Patick AK, Chen A, Zhou Y, Persson R, King BD, Kauppinen S, Levin AA and Hodges MR. Treatment of HCV infection by targeting microRNA. *The New England journal of medicine* 2013; **368**: 1685–1694.

Jawhari S, Ratinaud M-H and Verdier M. Glioblastoma, hypoxia and autophagy: a survival-prone 'ménage-à-trois'. *Cell death & disease* 2016; **7**: e2434.

Jaworek C, Verel-Yilmaz Y, Driesch S, Ostgathe S, Cook L, Wagner S, Bartsch DK, Slater EP and Bartsch JW. Cohort Analysis of ADAM8 Expression in the PDAC Tumor Stroma. *Journal of personalized medicine* 2021; **11**.

Kaneko Y, Sakakibara S, Imai T, Suzuki A, Nakamura Y, Sawamoto K, Ogawa Y, Toyama Y, Miyata T and Okano H. Musashi1: an evolutionarily conserved marker for CNS progenitor cells including neural stem cells. *Developmental neuroscience* 2000; **22**: 139–153.

Kehl T, Kern F, Backes C, Fehlmann T, Stöckel D, Meese E, Lenhof H-P and Keller A. miRPathDB 2.0: a novel release of the miRNA Pathway Dictionary Database. *Nucleic acids research* 2020; **48**: D142-D147.

KEILIN D and MANN T. Carbonic Anhydrase. *Nature* 1939; **144**: 442–443.

Kesanakurti D, Chetty C, Dinh DH, Gujrati M and Rao JS. Role of MMP-2 in the regulation of IL-6/Stat3 survival signaling via interaction with α5β1 integrin in glioma. *Oncogene* 2013; **32**: 327–340.

Kierans SJ and Taylor CT. Regulation of glycolysis by the hypoxia-inducible factor (HIF): implications for cellular physiology. *The Journal of Physiology* 2021; **599**: 23–37.

Kim J, Lee I-H, Cho HJ, Park C-K, Jung Y-S, Kim Y, Nam SH, Kim BS, Johnson MD, Kong D-S, Seol HJ, Lee J-I, Joo KM, Yoon Y, Park W-Y, Lee J, Park PJ and Nam D-H. Spatiotemporal Evolution of the Primary Glioblastoma Genome. *Cancer cell* 2015; **28**: 318–328.

Kim W, Yoo H, Shin SH, Gwak HS and Lee SH. Extraneural Metastases of Glioblastoma without Simultaneous Central Nervous System Recurrence. *Brain tumor research and treatment* 2014; **2**: 124–127.

Kimelberg HK, Stieg PE and Mazurkiewicz JE. Immunocytochemical and biochemical analysis of carbonic anhydrase in primary astrocyte cultures from rat brain. *Journal of neurochemistry* 1982; **39**: 734–742.

Kleino I, Järviluoma A, Hepojoki J, Huovila AP and Saksela K. Preferred SH3 domain partners of ADAM metalloproteases include shared and ADAM-specific SH3 interactions. *PloS one* 2015; **10**: e0121301.

Knudsen JF, Carlsson U, Hammarström P, Sokol GH and Cantilena LR. The cyclooxygenase-2 inhibitor celecoxib is a potent inhibitor of human carbonic anhydrase II. *Inflammation* 2004; **28**: 285–290.

Korhonen K, Parkkila A-K, Helen P, Välimäki R, Pastorekova S, Pastorek J, Parkkila S and Haapasalo H. Carbonic anhydrases in meningiomas: association of endothelial carbonic anhydrase II with aggressive tumor features. *Journal of neurosurgery* 2009; **111**: 472–477.

Kumpulainen T and Korhonen LK. Immunohistochemical localization of carbonic anhydrase isoenzyme C in the central and peripheral nervous system of the mouse. *The journal of histochemistry and cytochemistry official journal of the Histochemistry Society* 1982; **30**: 283–292.

La Cruz-López KG de, Castro-Muñoz LJ, Reyes-Hernández DO, García-Carrancá A and Manzo-Merino J. Lactate in the Regulation of Tumor Microenvironment and Therapeutic Approaches. *Frontiers in oncology* 2019; **9**: 1143.

Labrie M and St-Pierre Y. Epigenetic regulation of mmp-9 gene expression. *Cellular and molecular life sciences CMLS* 2013; **70**: 3109–3124.

Lathia JD, Mack SC, Mulkearns-Hubert EE, Valentim CLL and Rich JN. Cancer stem cells in glioblastoma. *Genes & development* 2015; **29**: 1203–1217.

Leece R, Xu J, Ostrom QT, Chen Y, Kruchko C and Barnholtz-Sloan JS. Global incidence of malignant brain and other central nervous system tumors by histology, 2003-2007. *Neuro-oncology* 2017; **19**: 1553–1564.

Lemon N, Canepa E, Ilies MA and Fossati S. Carbonic Anhydrases as Potential Targets Against Neurovascular Unit Dysfunction in Alzheimer's Disease and Stroke. *Frontiers in aging neuroscience* 2021; **13**: 772278.

Li H and Yang BB. Stress response of glioblastoma cells mediated by miR-17-5p targeting PTEN and the passenger strand miR-17-3p targeting MDM2. *Oncotarget* 2012; **3**: 1653–1668.

Li Q, Chen B, Cai J, Sun Y, Wang G, Li Y, Li R, Feng Y, Han B, Li J, Tian Y, Yi L and Jiang C. Comparative Analysis of Matrix Metalloproteinase Family Members Reveals That MMP9 Predicts Survival and Response to Temozolomide in Patients with Primary Glioblastoma. *PloS one* 2016; **11**: e0151815.

Li Q, Zhang L, Zhang Z, Fan Y and Zhang Q. Carbonic anhydrase 10 functions as a tumor suppressor in renal cell carcinoma and its methylation is a risk factor for survival outcome. *Urologic oncology* 2022; **40**: 168.e1-168.e9.

Li Y, Guo S, Zhao K, Conrad C, Driescher C, Rothbart V, Schlomann U, Guerreiro H, Bopp MH, König A, Carl B, Pagenstecher A, Nimsky C and Bartsch JW. ADAM8 affects glioblastoma progression by regulating osteopontin-mediated angiogenesis. *Biological chemistry* 2021; **402**: 195–206.

Liang L, Zhu J, Zaorsky NG, Deng Y, Wu X, Liu Y, Liu F, Cai G, Gu W, Shen L and Zhang Z. MicroRNA-223 enhances radiation sensitivity of U87MG cells in vitro and in vivo by targeting ataxia telangiectasia mutated. *International journal of radiation oncology, biology, physics* 2014; **88**: 955–960.

Lindskog S. Structure and mechanism of carbonic anhydrase. *Pharmacology & therapeutics* 1997; **74**: 1–20.

Liu G, Yuan X, Zeng Z, Tunici P, Ng H, Abdulkadir IR, Lu L, Irvin D, Black KL and Yu JS. Analysis of gene expression and chemoresistance of CD133+ cancer stem cells in glioblastoma. *Molecular cancer* 2006; **5**: 67.

Liu J, Wang X, Chen AT, Gao X, Himes BT, Zhang H, Chen Z, Wang J, Sheu WC, Deng G, Xiao Y, Zou P, Zhang S, Liu F, Zhu Y, Fan R, Patel TR, Saltzman WM and Zhou J. ZNF117 regulates glioblastoma stem cell differentiation towards oligodendroglial lineage. *Nature communications* 2022a; **13**: 2196.

Liu Q, Nguyen DH, Dong Q, Shitaku P, Chung K, Liu OY, Tso JL, Liu JY, Konkankit V, Cloughesy TF, Mischel PS, Lane TF, Liau LM, Nelson SF and Tso C-L. Molecular properties of CD133+ glioblastoma stem cells derived from treatment-refractory recurrent brain tumors. *Journal of neuro-oncology* 2009; **94**: 1–19.

Liu S, Li X and Zhuang S. miR-30c Impedes Glioblastoma Cell Proliferation and Migration by Targeting SOX9. *Oncology research* 2019; **27**: 165–171.

Liu X, Huang Y, Qi Y, Wu S, Hu F, Wang J, Shu K, Zhang H, Bartsch JW, Nimsky C, Dong F and Lei T. The GBM Tumor Microenvironment as a Modulator of Therapy Response: ADAM8 Causes Tumor Infiltration of Tams through HB-EGF/EGFR-Mediated CCL2 Expression and Overcomes TMZ Chemosensitization in Glioblastoma. *Cancers* 2022b; **14**.

Liu Y, Zhao Z, Yang F, Gao Y, Song J and Wan Y. microRNA-181a is involved in insulin-like growth factor-1-mediated regulation of the transcription factor CREB1. *Journal of neurochemistry* 2013; **126**: 771–780.

Lottaz C, Beier D, Meyer K, Kumar P, Hermann A, Schwarz J, Junker M, Oefner PJ, Bogdahn U, Wischhusen J, Spang R, Storch A and Beier CP. Transcriptional profiles of CD133+ and CD133- glioblastoma-derived cancer stem cell lines suggest different cells of origin. *Cancer research* 2010; **70**: 2030–2040.

Louis DN, Perry A, Reifenberger G, Deimling A von, Figarella-Branger D, Cavenee WK, Ohgaki H, Wiestler OD, Kleihues P and Ellison DW. The 2016 World Health Organization Classification of

Tumors of the Central Nervous System: a summary. *Acta neuropathologica* 2016; **131**: 803–820.

Ma Q, Long W, Xing C, Chu J, Luo M, Wang HY, Liu Q and Wang R-F. Cancer Stem Cells and Immunosuppressive Microenvironment in Glioma. *Frontiers in immunology* 2018; **9**: 2924.

Ma X, Zhang H, Yuan L, Jing H, Thacker P and Li D. CREBL2, interacting with CREB, induces adipogenesis in 3T3-L1 adipocytes. *The Biochemical journal* 2011; **439**: 27–38.

Mahinfar P, Mansoori B, Rostamzadeh D, Baradaran B, Cho WC and Mansoori B. The Role of microRNAs in Multidrug Resistance of Glioblastoma. *Cancers* 2022; **14**.

Mallawaaratchy DM, Hallal S, Russell B, Ly L, Ebrahimkhani S, Wei H, Christopherson RI, Buckland ME and Kaufman KL. Comprehensive proteome profiling of glioblastoma-derived extracellular vesicles identifies markers for more aggressive disease. *Journal of neuro-oncology* 2017; **131**: 233–244.

Mao H, Lebrun DG, Yang J, Zhu VF and Li M. Deregulated signaling pathways in glioblastoma multiforme: molecular mechanisms and therapeutic targets. *Cancer investigation* 2012; **30**: 48–56.

Marisetty A, Wei J, Kong L-Y, Ott M, Fang D, Sabbagh A and Heimberger AB. MiR-181 Family Modulates Osteopontin in Glioblastoma Multiforme. *Cancers* 2020; **12**.

Martínez-Zaguilán R, Seftor EA, Seftor RE, Chu YW, Gillies RJ and Hendrix MJ. Acidic pH enhances the invasive behavior of human melanoma cells. *Clinical & experimental metastasis* 1996; **14**: 176–186.

Meldrum NU and Roughton FJW. Carbonic anhydrase. Its preparation and properties. *The Journal of Physiology* 1933; **80**: 113–142.

Michaelsen SR, Christensen IJ, Grunnet K, Stockhausen M-T, Broholm H, Kosteljanetz M and Poulsen HS. Clinical variables serve as prognostic factors in a model for survival from glioblastoma multiforme: an observational study of a cohort of consecutive non-selected patients from a single institution. *BMC cancer* 2013; **13**: 402.

Mohammadpour R, Safarian S, Ejeian F, Sheikholya-Lavasani Z, Abdolmohammadi MH and Sheinabi N. Acetazolamide triggers death inducing autophagy in T-47D breast cancer cells. *Cell biology international* 2014; **38**: 228–238.

Møller HG, Rasmussen AP, Andersen HH, Johnsen KB, Henriksen M and Duroux M. A systematic review of microRNA in glioblastoma multiforme: micro-modulators in the mesenchymal mode of migration and invasion. *Molecular neurobiology* 2013; **47**: 131–144.

Montano N. Biomarkers in Glioblastoma multiforme. Evidences from a literature review. *Journal of Clinical and Translational Research* 2016; **2**.

Mughal AA, Zhang L, Fayzullin A, Server A, Li Y, Wu Y, Glass R, Meling T, Langmoen IA, Leergaard TB and Vik-Mo EO. Patterns of Invasive Growth in Malignant Gliomas-The Hippocampus Emerges as an Invasion-Spared Brain Region. *Neoplasia (New York, N.Y.)* 2018; **20**: 643–656.

Mujumdar P, Kopecka J, Bua S, Supuran CT, Riganti C and Poulsen S-A. Carbonic Anhydrase XII Inhibitors Overcome Temozolomide Resistance in Glioblastoma. *Journal of medicinal chemistry* 2019; **62**: 4174–4192.

Munir J, Yoon JK and Ryu S. Therapeutic miRNA-Enriched Extracellular Vesicles: Current Approaches and Future Prospects. *Cells* 2020; **9**.

Murphy G. The ADAMs: signalling scissors in the tumour microenvironment. *Nature reviews. Cancer* 2008; **8**: 929–941.

Musumeci G, Magro G, Cardile V, Coco M, Marzagalli R, Castrogiovanni P, Imbesi R, Graziano ACE, Barone F, Di Rosa M, Castorina S and Castorina A. Characterization of matrix metalloproteinase-2 and -9, ADAM-10 and N-cadherin expression in human glioblastoma multiforme. *Cell and tissue research* 2015; **362**: 45–60.

Nagao A, Kobayashi M, Koyasu S, Chow CCT and Harada H. HIF-1-Dependent Reprogramming of Glucose Metabolic Pathway of Cancer Cells and Its Therapeutic Significance. *International journal of molecular sciences* 2019; **20**.

Niu J, Xue A, Chi Y, Xue J, Wang W, Zhao Z, Fan M, Yang CH, Shao Z-M, Pfeffer LM, Wu J and Wu Z-H. Induction of miRNA-181a by genotoxic treatments promotes chemotherapeutic resistance and metastasis in breast cancer. *Oncogene* 2016; **35**: 1302–1313.

Nógrádi A. Differential expression of carbonic anhydrase isozymes in microglial cell types. *Glia* 1993; **8**: 133–142.

Nørøxe DS, Poulsen HS and Lassen U. Hallmarks of glioblastoma: a systematic review. *ESMO open* 2016; **1**: e000144.

O'Brien J, Hayder H, Zayed Y and Peng C. Overview of MicroRNA Biogenesis, Mechanisms of Actions, and Circulation. *Frontiers in endocrinology* 2018; **9**: 402.

Oikonomou E, Koustas E, Goulielmaki M and Pintzas A. BRAF vs RAS oncogenes: are mutations of the same pathway equal? Differential signalling and therapeutic implications. *Oncotarget* 2014; **5**: 11752–11777.

Okajima F. Regulation of inflammation by extracellular acidification and proton-sensing GPCRs. *Cellular signalling* 2013; **25**: 2263–2271.

Olivier C, Oliver L, Lalier L and Vallette FM. Drug Resistance in Glioblastoma: The Two Faces of Oxidative Stress. *Frontiers in molecular biosciences* 2020; **7**: 620677.

O'Neill CP and Dwyer RM. Nanoparticle-Based Delivery of Tumor Suppressor microRNA for Cancer Therapy. *Cells* 2020; **9**.

Ortiz R, Perazzoli G, Cabeza L, Jiménez-Luna C, Luque R, Prados J and Melguizo C. Temozolomide: An Updated Overview of Resistance Mechanisms, Nanotechnology Advances and Clinical Applications. *Current neuropharmacology* 2021; **19**: 513–537.

Ostrom QT, Cioffi G, Gittleman H, Patil N, Waite K, Kruchko C and Barnholtz-Sloan JS. CBTRUS Statistical Report: Primary Brain and Other Central Nervous System Tumors Diagnosed in the United States in 2012-2016. *Neuro-oncology* 2019; **21**: v1-v100.

Oushy S, Hellwinkel JE, Wang M, Nguyen GJ, Gunaydin D, Harland TA, Anchordoquy TJ and Graner MW. Glioblastoma multiforme-derived extracellular vesicles drive normal astrocytes towards a tumour-enhancing phenotype. *Philosophical transactions of the Royal Society of London. Series B, Biological sciences* 2018; **373**.

Ouyang M, Liu G, Xiong C and Rao J. microRNA-181a-5p impedes the proliferation, migration, and invasion of retinoblastoma cells by targeting the NRAS proto-oncogene. *Clinics (Sao Paulo, Brazil)* 2022; **77**: 100026.

Padfield E, Ellis HP and Kurian KM. Current Therapeutic Advances Targeting EGFR and EGFRvIII in Glioblastoma. *Frontiers in oncology* 2015; **5**: 5.

Park JH and Lee HK. Current Understanding of Hypoxia in Glioblastoma Multiforme and Its Response to Immunotherapy. *Cancers* 2022; **14**.

Parkkila S. Significance of pH regulation and carbonic anhydrases in tumour progression and implications for diagnostic and therapeutic approaches. *BJU international* 2008; **101 Suppl 4**: 16–21.

Pasteur. Exp´eriences et vues nouvelles sur la nature des fermentations. *C R Acad Sci* 1861: 1260–1264.

Paunescu TG, Jones AC, Tyszkowski R and Brown D. V-ATPase expression in the mouse olfactory epithelium. *American journal of physiology. Cell physiology* 2008; **295**: C923-30.

Perry JR, Bélanger K, Mason WP, Fulton D, Kavan P, Easaw J, Shields C, Kirby S, Macdonald DR, Eisenstat DD, Thiessen B, Forsyth P and Pouliot J-F. Phase II trial of continuous dose-intense temozolomide in recurrent malignant glioma: RESCUE study. *Journal of clinical oncology official journal of the American Society of Clinical Oncology* 2010; **28**: 2051–2057.

Piper RJ, Senthil KK, Yan J-L and Price SJ. Neuroimaging classification of progression patterns in glioblastoma: a systematic review. *Journal of neuro-oncology* 2018; **139**: 77–88.

Proescholdt MA, Mayer C, Kubitza M, Schubert T, Liao S-Y, Stanbridge EJ, Ivanov S, Oldfield EH, Brawanski A and Merrill MJ. Expression of hypoxia-inducible carbonic anhydrases in brain tumors. *Neuro-oncology* 2005; **7**: 465–475.

Puolakkainen P, Koski A, Vainionpää S, Shen Z, Repo H, Kemppainen E, Mustonen H and Seppänen H. Anti-inflammatory macrophages activate invasion in pancreatic adenocarcinoma by increasing the MMP9 and ADAM8 expression. *Medical oncology (Northwood, London, England)* 2014; **31**: 884.

Rackov G, Garcia-Romero N, Esteban-Rubio S, Carrión-Navarro J, Belda-Iniesta C and Ayuso-Sacido A. Vesicle-Mediated Control of Cell Function: The Role of Extracellular Matrix and Microenvironment. *Frontiers in physiology* 2018; **9**: 651.

Raghunand N, Howison C, Sherry AD, Zhang S and Gillies RJ. Renal and systemic pH imaging by contrast-enhanced MRI. *Magnetic resonance in medicine* 2003; **49**: 249–257.

Robertson N, Potter C and Harris AL. Role of carbonic anhydrase IX in human tumor cell growth, survival, and invasion. *Cancer research* 2004; **64**: 6160–6165.

Rodriguez SMB, Staicu G-A, Sevastre A-S, Baloi C, Ciubotaru V, Dricu A and Tataranu LG. Glioblastoma Stem Cells-Useful Tools in the Battle against Cancer. *International journal of molecular sciences* 2022; **23**.

Romagnoli M, Mineva ND, Polmear M, Conrad C, Srinivasan S, Loussouarn D, Barillé-Nion S, Georgakoudi I, Dagg Á, McDermott EW, Duffy MJ, McGowan PM, Schlomann U, Parsons M, Bartsch JW and Sonenshein GE. ADAM8 expression in invasive breast cancer promotes tumor dissemination and metastasis. *EMBO molecular medicine* 2014; **6**: 278–294.

Roussel G, Delaunoy JP, Nussbaum JL and Mandel P. Demonstration of a specific localization of carbonic anhydrase C in the glial cells of rat CNS by an immunohistochemical method. *Brain research* 1979; **160**: 47–55.

Ruusuvuori E, Li H, Huttu K, Palva JM, Smirnov S, Rivera C, Kaila K and Voipio J. Carbonic anhydrase isoform VII acts as a molecular switch in the development of synchronous gamma-frequency firing of hippocampal CA1 pyramidal cells. *The Journal of neuroscience the official journal of the Society for Neuroscience* 2004; **24**: 2699–2707.

Salaroglio IC, Mujumdar P, Annovazzi L, Kopecka J, Mellai M, Schiffer D, Poulsen S-A and Riganti C. Carbonic Anhydrase XII Inhibitors Overcome P-Glycoprotein-Mediated Resistance to Temozolomide in Glioblastoma. *Molecular cancer therapeutics* 2018; **17**: 2598–2609.

Sana J, Busek P, Fadrus P, Besse A, Radova L, Vecera M, Reguli S, Stollinova Sromova L, Hilser M, Lipina R, Lakomy R, Kren L, Smrcka M, Sedo A and Slaby O. Identification of microRNAs differentially expressed in glioblastoma stem-like cells and their association with patient survival. *Scientific reports* 2018; **8**: 2836.

Scherz-Shouval R, Shvets E, Fass E, Shorer H, Gil L and Elazar Z. Reactive oxygen species are essential for autophagy and specifically regulate the activity of Atg4. *The EMBO journal* 2007; **26**: 1749–1760.

Schlomann U, Koller G, Conrad C, Ferdous T, Golfi P, Garcia AM, Höfling S, Parsons M, Costa P, Soper R, Bossard M, Hagemann T, Roshani R, Sewald N, Ketchem RR, Moss ML, Rasmussen FH, Miller MA, Lauffenburger DA, Tuveson DA, Nimsky C and Bartsch JW. ADAM8 as a drug target in pancreatic cancer. *Nature communications* 2015; **6**: 6175.

Sedlakova O, Svastova E, Takacova M, Kopacek J, Pastorek J and Pastorekova S. Carbonic anhydrase IX, a hypoxia-induced catalytic component of the pH regulating machinery in tumors. *Frontiers in physiology* 2014; **4**: 400.

Seelig A. P-Glycoprotein: One Mechanism, Many Tasks and the Consequences for Pharmacotherapy of Cancers. *Frontiers in oncology* 2020; **10**: 576559.

Shea A, Harish V, Afzal Z, Chijioke J, Kedir H, Dusmatova S, Roy A, Ramalinga M, Harris B, Blancato J, Verma M and Kumar D. MicroRNAs in glioblastoma multiforme pathogenesis and therapeutics. *Cancer medicine* 2016; **5**: 1917–1946.

Shen H, Weng XD, Liu XH, et al. miR-181a-5p is downregulated and inhibits proliferation and the cell cycle in prostate cancer. *International Journal of Clinical and Experimental Pathology.* 2018: 3969–3976.

Shi L, Cheng Z, Zhang J, Li R, Zhao P, Fu Z and You Y. hsa-mir-181a and hsa-mir-181b function as tumor suppressors in human glioma cells. *Brain research* 2008; **1236**: 185–193.

Shi W, Scannell Bryan M, Gilbert MR, Mehta MP, Blumenthal DT, Brown PD, Valeinis E, Hopkins K, Souhami L, Andrews DW, Tzuk-Shina T, Howard SP, Youssef EF, Lessard N, Dignam JJ and Werner-Wasik M. Investigating the Effect of Reirradiation or Systemic Therapy in Patients With Glioblastoma After Tumor Progression: A Secondary Analysis of NRG Oncology/Radiation Therapy Oncology Group Trial 0525. *International journal of radiation oncology, biology, physics* 2018; **100**: 38–44.

Shonka NA and Aizenberg MR. Extent of Resection in Glioblastoma. *Journal of oncology practice* 2017; **13**: 641–642.

Silagi ES, Schoepflin ZR, Seifert EL, Merceron C, Schipani E, Shapiro IM and Risbud MV. Bicarbonate Recycling by HIF-1-Dependent Carbonic Anhydrase Isoforms 9 and 12 Is Critical in Maintaining Intracellular pH and Viability of Nucleus Pulposus Cells. *Journal of bone and mineral research the official journal of the American Society for Bone and Mineral Research* 2018; **33**: 338–355.

Simon T, Jackson E and Giamas G. Breaking through the glioblastoma micro-environment via extracellular vesicles. *Oncogene* 2020; **39**: 4477–4490.

Singh SK, Clarke ID, Terasaki M, Bonn VE, Hawkins C, Squire J and Dirks PB. Identification of a cancer stem cell in human brain tumors. *Cancer Res.* 2003: 5821–5828.

Singh SK, Hawkins C, Clarke ID, Squire JA, Bayani J, Hide T, Henkelman RM, Cusimano MD and Dirks PB. Identification of human brain tumour initiating cells. *Nature* 2004; **432**: 396–401.

Snyder DS, Zimmerman TR, Farooq M, Norton WT and Cammer W. Carbonic anhydrase, 5'-nucleotidase, and 2',3'-cyclic nucleotide-3'-phosphodiesterase activities in oligodendrocytes, astrocytes, and neurons isolated from the brains of developing rats. *Journal of neurochemistry* 1983; **40**: 120–127.

Song H, Zhang Y, Liu N, Zhang D, Wan C, Zhao S, Kong Y and Yuan L. Let-7b inhibits the malignant behavior of glioma cells and glioma stem-like cells via downregulation of E2F2. *Journal of physiology and biochemistry* 2016; **72**: 733–744.

Stéphanou A and Ballesta A. pH as a potential therapeutic target to improve temozolomide antitumor efficacy A mechanistic modeling study. *Pharmacology research & perspectives* 2019; **7**: e00454.

Stoyanov GS, Lyutfi E, Georgieva R, Georgiev R, Dzhenkov DL, Petkova L, Ivanov BD, Kaprelyan A and Ghenev P. Reclassification of Glioblastoma Multiforme According to the 2021 World Health Organization Classification of Central Nervous System Tumors: A Single Institution Report and Practical Significance. *Cureus* 2022; **14**: e21822.

Stridh MH, Alt MD, Wittmann S, Heidtmann H, Aggarwal M, Riederer B, Seidler U, Wennemuth G, McKenna R, Deitmer JW and Becker HM. Lactate flux in astrocytes is enhanced by a non-catalytic action of carbonic anhydrase II. *The Journal of Physiology* 2012; **590**: 2333–2351.

Stupp R, Hegi ME, Mason WP, van den Bent MJ, Taphoorn MJB, Janzer RC, Ludwin SK, Allgeier A, Fisher B, Belanger K, Hau P, Brandes AA, Gijtenbeek J, Marosi C, Vecht CJ, Mokhtari K, Wesseling P, Villa S, Eisenhauer E, Gorlia T, Weller M, Lacombe D, Cairncross JG and Mirimanoff R-O. Effects of radiotherapy with concomitant and adjuvant temozolomide versus radiotherapy alone on survival in glioblastoma in a randomised phase III study: 5-year analysis of the EORTC-NCIC trial. *The Lancet. Oncology* 2009; **10**: 459–466.

Stupp R, Mason WP, van den Bent MJ, Weller M, Fisher B, Taphoorn MJB, Belanger K, Brandes AA, Marosi C, Bogdahn U, Curschmann J, Janzer RC, Ludwin SK, Gorlia T, Allgeier A, Lacombe D, Cairncross JG, Eisenhauer E and Mirimanoff RO. Radiotherapy plus concomitant and adjuvant temozolomide for glioblastoma. *The New England journal of medicine* 2005; **352**: 987–996.

Stupp R, Taillibert S, Kanner A, Read W, Steinberg D, Lhermitte B, Toms S, Idbaih A, Ahluwalia MS, Fink K, Di Meco F, Lieberman F, Zhu J-J, Stragliotto G, Tran D, Brem S, Hottinger A, Kirson ED, Lavy-Shahaf G, Weinberg U, Kim C-Y, Paek S-H, Nicholas G, Bruna J, Hirte H, Weller M, Palti Y, Hegi ME and Ram Z. Effect of Tumor-Treating Fields Plus Maintenance Temozolomide vs Maintenance Temozolomide Alone on Survival in Patients With Glioblastoma: A Randomized Clinical Trial. *JAMA* 2017; **318**: 2306–2316.

Stupp R, Wong ET, Kanner AA, Steinberg D, Engelhard H, Heidecke V, Kirson ED, Taillibert S, Liebermann F, Dbalý V, Ram Z, Villano JL, Rainov N, Weinberg U, Schiff D, Kunschner L, Raizer J,

Honnorat J, Sloan A, Malkin M, Landolfi JC, Payer F, Mehdorn M, Weil RJ, Pannullo SC, Westphal M, Smrcka M, Chin L, Kostron H, Hofer S, Bruce J, Cosgrove R, Paleologous N, Palti Y and Gutin PH. NovoTTF-100A versus physician's choice chemotherapy in recurrent glioblastoma: a randomised phase III trial of a novel treatment modality. *European journal of cancer (Oxford, England 1990)* 2012; **48**: 2192–2202.

Su Y, Silva JD, Doherty D, Simpson DA, Weiss DJ, Rolandsson-Enes S, McAuley DF, O'Kane CM, Brazil DP and Krasnodembskaya AD. Mesenchymal stromal cells-derived extracellular vesicles reprogramme macrophages in ARDS models through the miR-181a-5p-PTEN-pSTAT5-SOCS1 axis. *Thorax* 2022.

Sugrue MF. Pharmacological and ocular hypotensive properties of topical carbonic anhydrase inhibitors. *Progress in retinal and eye research* 2000; **19**: 87–112.

Sun Q, Ma L, Qiao J, Wang X, Li J, Wang Y, Tan A, Ye Z, Wu Y, Xi J and Kang J. MiR-181a-5p promotes neural stem cell proliferation and enhances the learning and memory of aged mice. *Aging cell* 2023: e13794.

Supuran CT. Therapeutic applications of the carbonic anhydrase inhibitors. *Therapy* 2007; **4**: 355–378.

Supuran CT. Carbonic anhydrases: novel therapeutic applications for inhibitors and activators. *Nature Reviews Drug Discovery* 2008; **7**: 168–181.

Swietach P, Vaughan-Jones RD and Harris AL. Regulation of tumor pH and the role of carbonic anhydrase 9. *Cancer metastasis reviews* 2007; **26**: 299–310.

Tachibana H, Gi M, Kato M, Yamano S, Fujioka M, Kakehashi A, Hirayama Y, Koyama Y, Tamada S, Nakatani T and Wanibuchi H. Carbonic anhydrase 2 is a novel invasion-associated factor in urinary bladder cancers. *Cancer science* 2017; **108**: 331–337.

Tomei S, Volontè A, Ravindran S, Mazzoleni S, Wang E, Galli R and Maccalli C. MicroRNA Expression Profile Distinguishes Glioblastoma Stem Cells from Differentiated Tumor Cells. *Journal of personalized medicine* 2021; **11**.

Torrisi F, Alberghina C, D'Aprile S, Pavone AM, Longhitano L, Giallongo S, Tibullo D, Di Rosa M, Zappalà A, Cammarata FP, Russo G, Ippolito M, Cuttone G, Li Volti G, Vicario N and Parenti R. The Hallmarks of Glioblastoma: Heterogeneity, Intercellular Crosstalk and Molecular Signature of Invasiveness and Progression. *Biomedicines* 2022; **10**.

Trevani AS, Andonegui G, Giordano M, López DH, Gamberale R, Minucci F and Geffner JR. Extracellular Acidification Induces Human Neutrophil Activation. *The Journal of Immunology* 1999; **162**: 4849–4857.

Valiulyte I, Pranckeviciene A, Bunevicius A, Tamasauskas A, Svitina H, Skrypkina I and Vaitkiene P. Associations of miR-181a with Health-Related Quality of Life, Cognitive Functioning, and Clinical

Data of Patients with Different Grade Glioma Tumors. *International journal of molecular sciences* 2022; **23**.

Valkovskaya N, Kayed H, Felix K, Hartmann D, Giese NA, Osinsky SP, Friess H and Kleeff J. ADAM8 expression is associated with increased invasiveness and reduced patient survival in pancreatic cancer. *Journal of cellular and molecular medicine* 2007; **11**: 1162–1174.

Vallée A, Lecarpentier Y and Vallée J-N. The Key Role of the WNT/β-Catenin Pathway in Metabolic Reprogramming in Cancers under Normoxic Conditions. *Cancers* 2021; **13**.

van den Bent MJ, Gao Y, Kerkhof M, Kros JM, Gorlia T, van Zwieten K, Prince J, van Duinen S, Sillevis Smitt PA, Taphoorn M and French PJ. Changes in the EGFR amplification and EGFRvIII expression between paired primary and recurrent glioblastomas. *Neuro-oncology* 2015; **17**: 935–941.

van Niel G, D'Angelo G and Raposo G. Shedding light on the cell biology of extracellular vesicles. *Nature reviews. Molecular cell biology* 2018; **19**: 213–228.

Vecht CJ, Kerkhof M and Duran-Pena A. Seizure prognosis in brain tumors: new insights and evidence-based management. *The oncologist* 2014; **19**: 751–759.

Verel-Yilmaz Y, Fernández JP, Schäfer A, Nevermann S, Cook L, Gercke N, Helmprobst F, Jaworek C, Pogge von Strandmann E, Pagenstecher A, Bartsch DK, Bartsch JW and Slater EP. Extracellular Vesicle-Based Detection of Pancreatic Cancer. *Frontiers in cell and developmental biology* 2021; **9**: 697939.

Verhaak RGW, Hoadley KA, Purdom E, Wang V, Qi Y, Wilkerson MD, Miller CR, Ding L, Golub T, Mesirov JP, Alexe G, Lawrence M, O'Kelly M, Tamayo P, Weir BA, Gabriel S, Winckler W, Gupta S, Jakkula L, Feiler HS, Hodgson JG, James CD, Sarkaria JN, Brennan C, Kahn A, Spellman PT, Wilson RK, Speed TP, Gray JW, Meyerson M, Getz G, Perou CM and Hayes DN. Integrated genomic analysis identifies clinically relevant subtypes of glioblastoma characterized by abnormalities in PDGFRA, IDH1, EGFR, and NF1. *Cancer cell* 2010; **17**: 98–110.

Vollmann-Zwerenz A, Leidgens V, Feliciello G, Klein CA and Hau P. Tumor Cell Invasion in Glioblastoma. *International journal of molecular sciences* 2020; **21**.

Wang G, Zhao Y and Zheng Y. MiR-122/Wnt/β-catenin regulatory circuitry sustains glioma progression. *Tumour biology the journal of the International Society for Oncodevelopmental Biology and Medicine* 2014; **35**: 8565–8572.

Wang H, Ren S, Xu Y, Miao W, Huang X, Qu Z, Li J, Liu X and Kong P. MicroRNA-195 reverses the resistance to temozolomide through targeting cyclin E1 in glioma cells. *Anti-cancer drugs* 2019; **30**: 81–88.

Wang H, Tao T, Yan W, Feng Y, Wang Y, Cai J, You Y, Jiang T and Jiang C. Upregulation of miR-181s reverses mesenchymal transition by targeting KPNA4 in glioblastoma. *Scientific reports* 2015; **5**: 13072.

Wang H-H, Liao C-C, Chow N-H, Huang LL-H, Chuang J-I, Wei K-C and Shin J-W. Whether CD44 is an applicable marker for glioma stem cells. *Am J Transl Res* 2017a: 4785–4806.

Wang J, Sakariassen PØ, Tsinkalovsky O, Immervoll H, Bøe SO, Svendsen A, Prestegarden L, Røsland G, Thorsen F, Stuhr L, Molven A, Bjerkvig R and Enger PØ. CD133 negative glioma cells form tumors in nude rats and give rise to CD133 positive cells. *International journal of cancer* 2008; **122**: 761–768.

Wang P, Chen D, Ma H and Li Y. LncRNA SNHG12 contributes to multidrug resistance through activating the MAPK/Slug pathway by sponging miR-181a in non-small cell lung cancer. *Oncotarget* 2017b; **8**: 84086–84101.

Wang X-F, Shi Z-M, Wang X-R, Cao L, Wang Y-Y, Zhang J-X, Yin Y, Luo H, Kang C-S, Liu N, Jiang T and You Y-P. MiR-181d acts as a tumor suppressor in glioma by targeting K-ras and Bcl-2. *Journal of cancer research and clinical oncology* 2012; **138**: 573–584.

Wang X-R, Luo H, Li H-L, Cao L, Wang X-F, Yan W, Wang Y-Y, Zhang J-X, Jiang T, Kang C-S, Liu N and You Y-P. Overexpressed let-7a inhibits glioma cell malignancy by directly targeting K-ras, independently of PTEN. *Neuro-oncology* 2013; **15**: 1491–1501.

Watkins S, Robel S, Kimbrough IF, Robert SM, Ellis-Davies G and Sontheimer H. Disruption of astrocyte-vascular coupling and the blood-brain barrier by invading glioma cells. *Nature communications* 2014; **5**: 4196.

Webb BA, Chimenti M, Jacobson MP and Barber DL. Dysregulated pH: a perfect storm for cancer progression. *Nature reviews. Cancer* 2011; **11**: 671–677.

Wei H, Chen Q, Lin L, Sha C, Li T, Liu Y, Yin X, Xu Y, Chen L, Gao W, Li Y and Zhu X. Regulation of exosome production and cargo sorting. *International journal of biological sciences* 2021; **17**: 163–177.

Weller M, Cloughesy T, Perry JR and Wick W. Standards of care for treatment of recurrent glioblastoma--are we there yet? *Neuro-oncology* 2013; **15**: 4–27.

Wen PY, Weller M, Lee EQ, Alexander BM, Barnholtz-Sloan JS, Barthel FP, Batchelor TT, Bindra RS, Chang SM, Chiocca EA, Cloughesy TF, DeGroot JF, Galanis E, Gilbert MR, Hegi ME, Horbinski C, Huang RY, Lassman AB, Le Rhun E, Lim M, Mehta MP, Mellinghoff IK, Minniti G, Nathanson D, Platten M, Preusser M, Roth P, Sanson M, Schiff D, Short SC, Taphoorn MJB, Tonn J-C, Tsang J, Verhaak RGW, Deimling A von, Wick W, Zadeh G, Reardon DA, Aldape KD and van den Bent MJ. Glioblastoma in adults: a Society for Neuro-Oncology (SNO) and European Society of Neuro-

Oncology (EANO) consensus review on current management and future directions. *Neuro-oncology* 2020a; **22**: 1073–1113.

Wen X, Li S, Guo M, Liao H, Chen Y, Kuang X, Liao X, Ma L and Li Q. miR-181a-5p inhibits the proliferation and invasion of drug-resistant glioblastoma cells by targeting F-box protein 11 expression. *Oncology letters* 2020b; **20**: 1.

Wick W, Gorlia T, Bendszus M, Taphoorn M, Sahm F, Harting I, Brandes AA, Taal W, Domont J, Idbaih A, Campone M, Clement PM, Stupp R, Fabbro M, Le Rhun E, Dubois F, Weller M, Deimling A von, Golfinopoulos V, Bromberg JC, Platten M, Klein M and van den Bent MJ. Lomustine and Bevacizumab in Progressive Glioblastoma. *The New England journal of medicine* 2017; **377**: 1954–1963.

Wirsching H-G, Galanis E and Weller M. Glioblastoma. *Handbook of clinical neurology* 2016; **134**: 381–397.

Wu L, Bernal GM, Cahill KE, Pytel P, Fitzpatrick CA, Mashek H, Weichselbaum RR and Yamini B. BCL3 expression promotes resistance to alkylating chemotherapy in gliomas. *Science translational medicine* 2018; **10**.

Xue Q, Cao L, Chen X-Y, Zhao J, Gao L, Li S-Z and Fei Z. High expression of MMP9 in glioma affects cell proliferation and is associated with patient survival rates. *Oncology letters* 2017; **13**: 1325–1330.

Yan L, Borregaard N, Kjeldsen L and Moses MA. The high molecular weight urinary matrix metalloproteinase (MMP) activity is a complex of gelatinase B/MMP-9 and neutrophil gelatinase-associated lipocalin (NGAL). Modulation of MMP-9 activity by NGAL. *The Journal of biological chemistry* 2001; **276**: 37258–37265.

Yang C, Tabatabaei SN, Ruan X and Hardy P. The Dual Regulatory Role of MiR-181a in Breast Cancer. *Cellular physiology and biochemistry international journal of experimental cellular physiology, biochemistry, and pharmacology* 2017; **44**: 843–856.

Ye X, Xu S, Xin Y, Yu S, Ping Y, Chen L, Xiao H, Wang B, Yi L, Wang Q, Jiang X, Yang L, Zhang P, Qian C, Cui Y, Zhang X and Bian X. Tumor-associated microglia/macrophages enhance the invasion of glioma stem-like cells via TGF-β1 signaling pathway. *Journal of immunology (Baltimore, Md. 1950)* 2012; **189**: 444–453.

Yekula A, Yekula A, Muralidharan K, Kang K, Carter BS and Balaj L. Extracellular Vesicles in Glioblastoma Tumor Microenvironment. *Frontiers in immunology* 2019; **10**: 3137.

Yi Y, Hsieh I-Y, Huang X, Li J and Zhao W. Glioblastoma Stem-Like Cells: Characteristics, Microenvironment, and Therapy. *Frontiers in pharmacology* 2016; **7**: 477.

Yuile P, Dent O, Cook R, Biggs M and Little N. Survival of glioblastoma patients related to presenting symptoms, brain site and treatment variables. *Journal of clinical neuroscience official journal of the Neurosurgical Society of Australasia* 2006; **13**: 747–751.

Zhang P, Xia Q, Liu L, Li S and Dong L. Current Opinion on Molecular Characterization for GBM Classification in Guiding Clinical Diagnosis, Prognosis, and Therapy. *Frontiers in molecular biosciences* 2020; **7**: 562798.

Zhao K, Schäfer A, Zhang Z, Elsässer K, Culmsee C, Zhong L, Pagenstecher A, Nimsky C and Bartsch JW. Inhibition of Carbonic Anhydrase 2 Overcomes Temozolomide Resistance in Glioblastoma Cells. *International journal of molecular sciences* 2021; **23**.

Zhong J, Paul A, Kellie SJ and O'Neill GM. Mesenchymal migration as a therapeutic target in glioblastoma. *Journal of oncology* 2010; **2010**: 430142.

Zhou D, Duan Z, Li Z, Ge F, Wei R and Kong L. The significance of glycolysis in tumor progression and its relationship with the tumor microenvironment. *Frontiers in pharmacology* 2022; **13**: 1091779.

Zhou J-S, Yang Z-S, Cheng S-Y, Yu J-H, Huang C-J and Feng Q. miRNA-425-5p enhances lung cancer growth via the PTEN/PI3K/AKT signaling axis. *BMC pulmonary medicine* 2020; **20**: 223.

Article

Inhibition of Carbonic Anhydrase 2 Overcomes Temozolomide Resistance in Glioblastoma Cells

Kai Zhao [1], Agnes Schäfer [1], Zhuo Zhang [1], Katharina Elsässer [2], Carsten Culmsee [2,3], Li Zhong [4], Axel Pagenstecher [3,5], Christopher Nimsky [1,3] and Jörg W. Bartsch [1,3,*]

[1] Department of Neurosurgery, Uniklinikum Giessen and Marburg (UKGM), University of Marburg, Baldingerstraße, 35033 Marburg, Germany; Zhouk@students.uni-marburg.de (K.Z.); Schaef4g@students.uni-marburg.de (A.S.); zhzmclaren@gmail.com (Z.Z.); nimsky@med.uni-marburg.de (C.N.)
[2] Department of Pharmacology and Clinical Pharmacology, Biochemical-Pharmacological Center, University of Marburg, Karl-von-Frisch-Strasse 2, 35032 Marburg, Germany; elsaessk@staff.uni-marburg.de (K.E.); culmsee@staff.uni-marburg.de (C.C.)
[3] Center for Mind, Brain and Behavior, 35032 Marburg, Germany; pagenste@med.uni-marburg.de
[4] College of Bioengineering, Chongqing University, Shazheng Street 174, Shapingba District, Chongqing 400044, China; jlzhong@cqu.edu.cn
[5] Department of Neuropathology, Uniklinikum Giessen and Marburg (UKGM), University of Marburg, Baldingerstraße, 35033 Marburg, Germany
* Correspondence: jbartsch@med.uni-marburg.de

Abstract: About 95% of Glioblastoma (GBM) patients experience tumor relapse as a consequence of resistance to the first-line standard chemotherapy using temozolomide (TMZ). Recent studies reported consistently elevated expression levels of carbonic anhydrase CA2 in recurrent glioblastoma and temozolomide-resistant glioblastoma stem-like cells (GSCs). Here we show that CA2 is preferentially expressed in GSCs and upregulated by TMZ treatment. When expressed in GBM cell lines, CA2 exerts significant metabolic changes reflected by enhanced oxygen consumption and increased extracellular acidification causing higher rates of cell invasion. Notably, GBM cells expressing CA2 respond to combined treatment with TMZ and brinzolamide (BRZ), a non-toxic and potent CA2 inhibitor. Interestingly, brinzolamide was more effective than the pan-CA inhibitor Acetazolamide (ACZ) to sensitize naïve GSCs and TMZ-resistant GSCs to TMZ induced cell death. Mechanistically, we demonstrated that the combined treatment of GBM stem cells with TMZ and BRZ caused autophagy of GBM cell lines and GSCs, reflected by enhanced LC3 cleavage (LC3-II) and p62 reduction. Our findings illustrate the potential of CA2 as a chemo-sensitizing drug target in recurrent GBM and propose a combined treatment of TMZ with CA2 inhibitor to tackle GBM chemoresistance and recurrence.

Keywords: glioblastoma; GBM stem-like cells; carbonic anhydrase 2; temozolomide; chemoresistance; GBM recurrence; acetazolamide; brinzolamide; autophagy

1. Introduction

Glioblastoma (GBM) is the most common and lethal brain tumor with a median survival of around 15 months after diagnosis [1,2]. Despite an aggressive therapy regimen consisting of surgical resection, adjuvant radiation, and chemotherapy with temozolomide (TMZ) [3] virtually all GBMs recur [4,5].

GBM is characterized by a high degree of heterogeneity on phenotypic, genetic, and cellular levels [6]. Like other solid tumors, GBM is composed of various brain resident, as well as transformed cell types: there are rapidly multiplying tumor cells that make up the bulk of the tumor mass and, on the other hand, there are self-renewing cell types, often termed Glioblastoma stem-like cells (GSCs) [6–8]. Whereas differentiated GBM cells are responsive to chemotherapy due to their high proliferation rate, GSCs are thought to

exert increased resistance to adjuvant therapy and tumor-initiating capacity as a source of glioma recurrence [3,5,9]. There are several proposed resistance mechanisms, such as metabolic inactivation of drugs, inhibition of conversion from prodrug to bioactive drug, increased drug efflux, and increased DNA repair [10,11]. In this regard, by analyzing GSCs resistant to TMZ treatment, we and others have shown previously that a major factor of TMZ resistance in GBM stem cells and recurrent tumor tissue is Carbonic Anhydrase 2 (CA2). More recently, two lines of evidence identified CA2 as another important carbonic anhydrase functionally important for TMZ resistance as a downstream target gene of BCL-3 activation [12,13]. CA2 is a member of a greater family of Carbonic Anhydrases which are highly conserved proteins in animals and plants [14–16]. Carbonic Anhydrases constitute a family of structurally divergent proton exchange proteins and particularly CA9 and CA12 have been previously described in GBM and other tumor entities as tumor cell-intrinsic carbonic anhydrases [17,18] and a current clinical trial uses acetazolamide in conjunction with TMZ (trial number NCT03011671) in GBM patients. CA9 has been identified as a hypoxia-dependent gene that is particularly relevant for the stem cell niche, in which GSCs can survive tumor-targeted therapies [19,20]. While CA9 and CA12 are transmembrane proteins, CA2 is located at the inner cell membrane and is associated with monocarboxylate transporter proteins MCT1/4, which are important in the symport of monocarboxylic acids (e.g., lactate, pyruvate) and protons (H$^+$) [21]. This supports the notion that CA2 could be involved in proton/lactate symport in GBM cells thereby supporting the so-called "Warburg effect" in tumor cells by maintaining glycolysis as a major source of metabolic energy [22].

As no functional data on CA2 in GBM cells are available so far, we analyzed the functional effects of CA2 expression in GBM cells by assessing metabolic parameters, such as the oxygen consumption rate (OCR) and the extracellular acidification rate (ECAR) in cells expressing CA2. Moreover, we investigated how CA2 affects proliferation, invasion, and TMZ resistance. As a potent inhibitor of CA2 with a K_i value of 3 nM for the full-length enzyme, we utilized brinzolamide (BRZ) in cell viability assays in comparison to the well-established pan-CA inhibitor acetazolamide (ACZ) and analyzed the potential and the mechanism of CA2 inhibition on TMZ sensitivity. We show that the therapeutic effect of brinzolamide is advantageous compared to acetazolamide.

2. Results

*Expression of CA2 in GBM Patients and GBM Stem-like Cells*

A TCGA X GTEx dataset comparing normal brain tissue with that of GBM revealed significantly higher expression levels of CA2 in GBM tissue (Figure S1A, $p < 0.01$). Glioblastoma stem-like cells (GSCs) are the major tumor cell type exerting chemoresistance with a strong capacity for self-renewal, one of the main reasons for GBM recurrence. For this reason, we analyzed patient-matched GBM samples from initial and from recurrent GBMs (20 samples from 10 patients). In this particular patient cohort, we observed that CA2 is significantly up-regulated (Figure 1A) while the expression of P-gp, an efflux transport protein is slightly up-regulated, and that of CD133, a GSC marker, is not significantly changed (Figure 1B,C), patient information is shown in Table S1.

To characterize the CA2 producing cells in recurrent glioblastoma (rGBM), the localization of CA2 was determined by immunofluorescence in paraffin slides of rGBM patients (Figure 1D). In combination with Sox-2, a stem-like cell marker, co-localization with CA2 was observed in representative GBM sections (Figure 1D), suggesting that CA2 is expressed in GSCs of recurrent tumors or differentiated tumor cells (Patient 3, Figure 1D), patient information is shown in Table S2. Expression levels of CA2 were further investigated in GBM cell lines U87 and U251 and in four patient-derived GSC lines (Figure 1E) and compared to those of CA9 (Figure 1F) and CA12 (Figure 1G), the protein level of CA2 also increased in GSCs (Figure S1B).

Notably, higher expression levels of CA2 mRNA were detected in all GSCs compared to the GBM cell lines, whereas mRNA expression of CA9 was lower in all GSCs, and only

one GSC line showed a higher expression level of CA12 while two of them were lower compared to GBM cell lines (Figure 1G). From all three carbonic anhydrase genes, CA9 is the typical gene induced by hypoxia (Figure S2). Based on these observations, the high expression levels of CA2 in GSCs suggest a functional role of CA2.
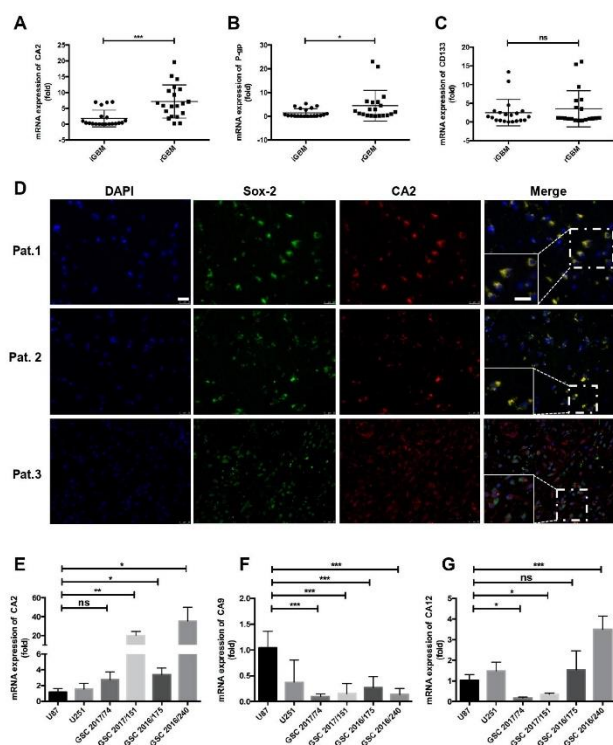
Figure 1. Expression levels of CA2 (**A**), P-gp (**B**), and CD133 (**C**) in patient-matched initial (i) vs. recurrent (r) GBM ($n = 20$ from 10 matched patients); (**D**) Representative IF staining of CA2 and stem cell marker SOX2 in three GBM tissue sections. Co-staining of CA2 (red) and SOX2 (green) confirmed CA2 in stem-like cells of GBM patients ($n = 3$ from 10 recurrent GBM patients), scale bar: 25 μm. (**E–G**) mRNA expression of GBM related carbonic anhydrase genes *CA2* (**E**), *CA9* (**F**), and *CA12* (**G**) in GBM cell lines U87 and U251 and patient-derived GSCs. Carbonic Anhydrase expression levels were detected by qPCR ($n = 3$). For all genes, expression levels determined in U87 cells were set to 1. qPCR results were obtained from three independent experiments. In (**A–C,E–G**), data are presented as mean $\pm$ SD, student's *t*-test was used to analyze (**A–C**), One-way ANOVA was used to analyze (**E–G**), * $p < 0.05$; ** $p < 0.01$; *** $p < 0.001$, ns: not significant.

To characterize the function of CA2 in GBM cells by gain-of-function analyses, stable cell clones of U87 and U251 GBM cell lines were generated by transfection with either a control vector (U87_Ctrl and U251_Ctrl) or with a CA2 plasmid (U87_CA2 and U251_CA2). After selection with G418, stable cell clones were generated and analyzed for CA2 expression by Western Blot and qPCR (Figure 2A,C), and one representative cell clone from each condition was selected for further analysis. U87_CA2 and U251_CA2 cells gave rise to a 29 kD band of CA2, whereas the control cells were negative for CA2.
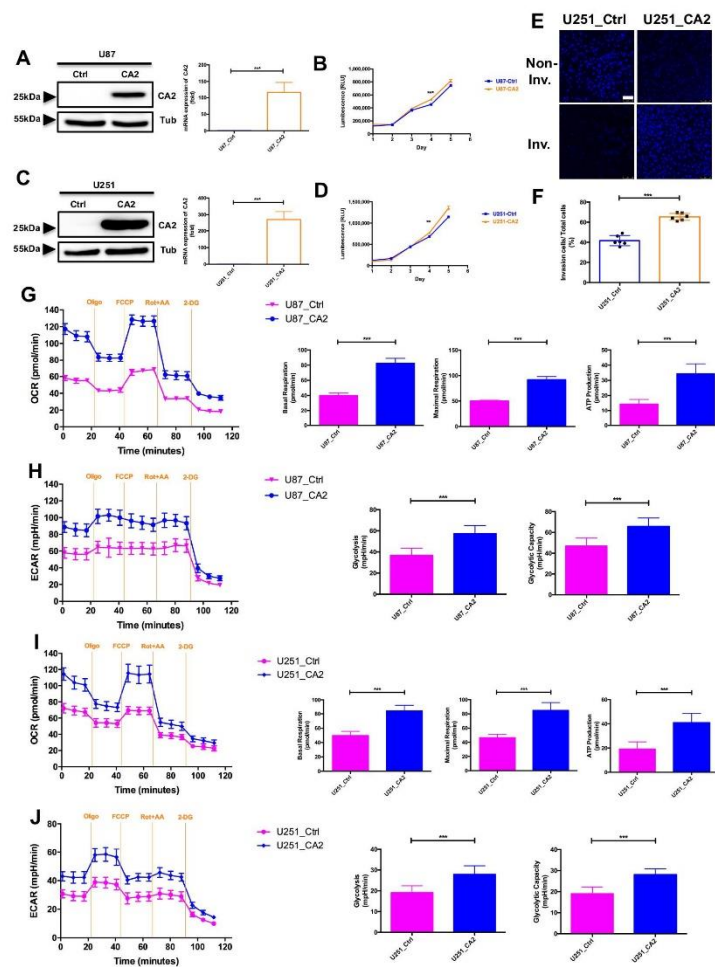
Figure 2. (**A,C**) Generation of stable CA2 overexpressing U87 and U251 cell lines as confirmed by Western Blot and qPCR. (**B,D**) The proliferation of control cells (U87_Ctrl, U251_Ctrl) and CA2 overexpressing (U87_CA2, U251_CA2) cells was measured by CellTiter Glo (*n* = 3 independent replicates). (**E**) Invasion of U251_Ctrl (Left panel) and U251_CA2 (Right panel) cells stained with DAPI (scale bar: 75 μm). (**F**) Relative invasion of U251_Ctrl and U251_CA2 cells (*n* = 6). (**G,I**) CA2 overexpressing cells have increased oxidative mitochondrial metabolism. The oxygen consumption rate (OCR) was measured by a seahorse XFe96 metabolic-flux analyzer. U87_CA2 cells (**G**) and U251_CA2 cells (**I**) significantly increased mitochondrial basal respiration, maximal respiration, and ATP production (*n* = 7–8). (**H,J**) CA2 overexpressing cells have elevated levels of glycolysis rate. The extracellular acidification rates (ECAR) were measured by a seahorse XFe96 metabolic-flux analyzer. U87_CA2 cells (**H**) and U251_CA2 cells (**J**) significantly increased glycolytic activity (*n* = 7–8). Results were obtained from three independent experiments. Data are presented as mean ± SD, student's *t*-test was used to analyze the data ** $p < 0.01$; *** $p < 0.001$, ns: not significant.

Cell proliferation of these cell clones was determined using a CellTiter-Glo® assay (Figure 2B,D). Both CA2 overexpressing GBM cell types show significantly higher proliferation rates than their respective control clones (Figure 2B,D, with $p < 0.001$ and $p < 0.01$, respectively). In addition, the invasive GBM cell line U251 shows higher rates of cell invasion into Matrigel when expressing CA2 (Figure 2E,F, $p < 0.001$).

To analyze whether CA2 expression affects the cellular metabolism of U87 and U251 cells, we used a Seahorse Analyzer that continuously measures oxygen concentration as oxygen consumption rate (OCR) and the proton flux into the cell supernatant determined as extracellular acidification rate (ECAR) enabling quantification of mitochondrial respiration, ATP production, and glycolysis. Indicative for CA2 function, a notable increase in OCR (Figure 2G,I) and ECAR (Figure 2H,J) was observed in both GBM lines U87 and U251 expressing CA2 compared to their control clones.

To test if these metabolic changes and the observed invasive behavior can be specifically ascribed to CA2 function, either the pan-CA inhibitor acetazolamide (ACZ, Figure 3A) or the potent CA2 inhibitor brinzolamide (BRZ, Figure 3B) were used in concentrations of 100 and 400 μM, respectively in U251_Ctrl and U251_CA2 cells (Figure 3). The inhibitory effects of ACZ and BRZ clinically used drugs against the carbonic anhydrase isoforms are shown in Table S3 [23,24] and Table S4 (https://www.selleckchem.com/carbonic-anhydrase.html; accessed on 12 December 2021). OCR and ECAR rates were determined after adding either ACZ or BRZ. Metabolic changes were hardly observed in U251_Ctrl cells (Figure S3). In contrast, U251_CA2 cells respond well to the treatment after 24 h with a significantly reduced basal OCR and ECAR (Figure 3C,D), however, to a greater extent with ACZ, but at the higher dose of 400 μM BRZ, cells also responded with a significantly reduced OCR and ECAR. The maximal respiration capacity, after the addition of FCCP, was reduced by 400 μM ACZ (Figure 3E) and 400 μM BRZ (Figure 3G) in U251_CA2 cells compared to U251_Ctrl cells. ACZ and BRZ effectively inhibited the activity of carbonic anhydrase, which decreased cellular respiration, ATP production (Figure 3E, G), and extracellular acidification (Figure 3F,H) in U251_CA2 cells compared to U251_Ctrl cells. However, this effect was more pronounced after ACZ stimulation, which might be based on the fact that ACZ is much more potent than BRZ to modulate mitochondrial activity, since ACZ inhibits CA2 and other CA family members, such as CA9, CA12 which are expressed in both GBM cell lines independent of CA2 expression (Figure S2) and are involved in the mitochondrial metabolism.

To analyze the role of CA2 for invasion behavior of U251 cells, U251_Ctrl cells (Figure S4) and U251_CA2 cells (Figure 3I,J) were analyzed in their response to 100 μM, 400 μM ACZ and 100 μM, 400 μM BRZ stimulation. Whereas ACZ (Figure 3K) had no significant effect on the invasion of U251_CA2 cells, BRZ (Figure 3L) was much more effective in reducing invasion by 10% in a concentration of 400 μM while treatment of U251_Ctrl with ACZ or BRZ did not affect cellular invasiveness (Figure S4). Taken together, these findings indicate that ACZ and BRZ effectively inhibit mitochondrial metabolism with ACZ being more potent than BRZ, whereas BRZ is more effective in reducing the invasiveness of CA2 expressing GBM cells.
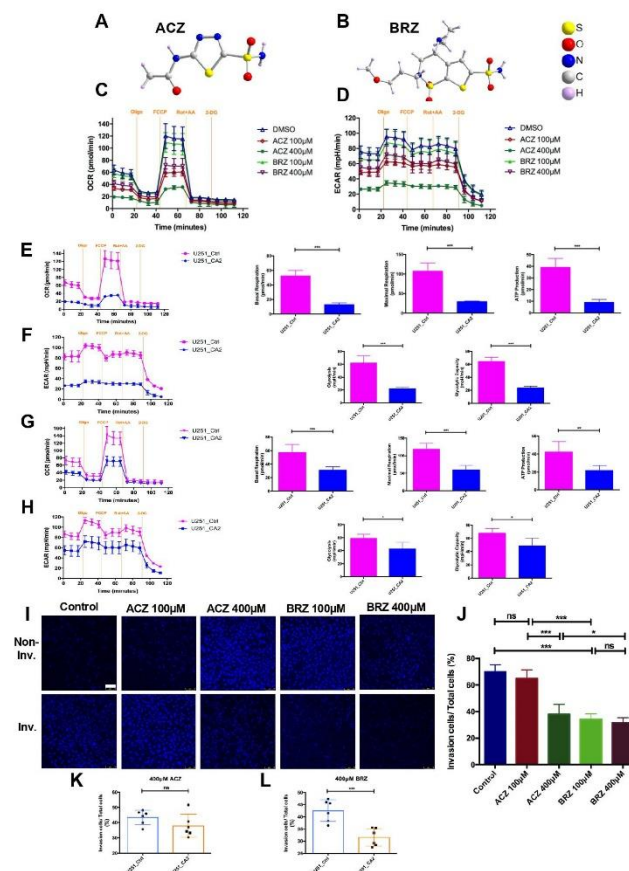
Figure 3. Effect of the pan-CA inhibitor acetazolamide (ACZ) and a potent CA2 inhibitor brinzolamide (BRZ) on invasion and energy metabolism in GBM cell lines. (**A**,**B**) Molecular structures of ACZ and BRZ. (**C**,**D**) U251_CA2 cells' overall metabolism after ACZ and BRZ stimulation was measured by a seahorse XFe96 metabolic-flux analyzer. ACZ and BRZ significantly decreased oxidative metabolism (**C**) and also reduced the level of glycolysis rate (**D**) in U251_CA2 cells (n = 5–6). U251_CA2 cells significantly decreased mitochondrial basal respiration, maximal respiration, and ATP production compared to U251_Ctrl cells after a 24 h stimulation with either 400 μM ACZ (**E**) or 400 μM BRZ (**G**). U251_CA2 cells also significantly reduced glycolytic activity compared to U251_Ctrl cells after 400 μM ACZ (**F**) and BRZ (**H**) stimulation for 24 h. (**I**) Invasion assay of U251_CA2 cells stained with DAPI after ACZ and BRZ stimulation for 24 h with concentrations indicated (scale bar: 75 μm). (**J**) Quantification of the proportion of invasive cells. Both 100 μM and 400 μM BRZ significantly decreased cell invasion of U251_CA2 cells, whereas only 400 μM ACZ reduced the invasiveness of cells (n = 6). (**K**,**L**) U251_CA2 cell significantly reduced cell invasiveness compared to U251_Ctrl cells after treatment with 400 μM BRZ. However, 400 μM ACZ did not change the invasiveness of U251_CA2 cells compared to the control group. Results were obtained from three independent experiments. Data are presented as mean ± SD, student's *t*-test was used to analyze (**E**–**H**,**K**,**L**) One-way ANOVA was used to analyze (**J**), * $p < 0.05$; ** $p < 0.01$; *** $p < 0.001$, ns: not significant.

To address the major question of whether CA2 inhibition can sensitize GBM cells to TMZ treatment as demonstrated for ACZ [12], we tested the combined application of BRZ with TMZ and hypothesized that CA2 overexpressing U87 and U251 cells can be sensitized to TMZ when CA2 is simultaneously inhibited. We compared the effects of ACZ and BRZ alone or in combination with TMZ on GBM cell lines U87_Ctrl and U87_CA2, and U251_Ctrl and U251_CA2. As previously, two doses of ACZ and BRZ, 100 μM and 400 μM, combined with TMZ (500 μM for U87 and 30 μM for U251) were applied to GBM cell lines for 5 d, and cell viability was determined by a CellTiter-Glo® assay (Figure 4). We observed a synergistic effect of TMZ and BRZ, already at the lower concentration of BRZ on the cell viability of U87_CA2 cells as compared to U87_Ctrl cells, whereas ACZ, combined with TMZ reduced cell viability in U87_CA2 cells than U87_Ctrl cells only at the higher concentration of 400 μM, and there was no change at 100 μM ACZ (Figure 4A). Similarly, BRZ at concentrations of 100 μM and 400 μM combined with TMZ significantly augmented cell death of U251_CA2 cells compared to U251_Ctrl cells (Figure 4C). Interestingly, we also found that monotherapy with TMZ significantly decreased the growth of U87_Ctrl and U251_Ctrl cells compared to U87_CA2 and U251_CA2 cells, respectively, including that U87 and U251 control cells might be more sensitive than CA2 cells in response to TMZ treatment. Concerning toxicity, we show that ACZ alone has no effect on U87_CA2 and U251_CA2 growth, and BRZ alone treatment on U251_CA2 cells also showed no cytotoxic, however, 400 μM BRZ show a slight cytotoxic effect on U87_CA2 cells (Figure 4B,D).

Together, these data confirm that BRZ in combination with TMZ is more effective than the pan-CA inhibitor ACZ. However, this needs to be demonstrated on GSCs, as this cell type is a major source of TMZ therapy resistance in GBM. Therefore, to analyze the possibility that CA2 induced by TMZ could cause chemoresistance, we first evaluated the mRNA expression of CA2 in three independent patient-derived GSC lines after stimulation with TMZ and determined CA2 expression levels by qPCR (Figure 5A–C). After stimulating the GSCs with 500 μM TMZ for 3 d and 5 d, expression of CA2 was found to be significantly up-regulated in GSC151 cells after 3 and 5 days, in GSC175 cells only after 5 days and GSC 240 cells 3 days after TMZ treatment (Figure 5A–C).
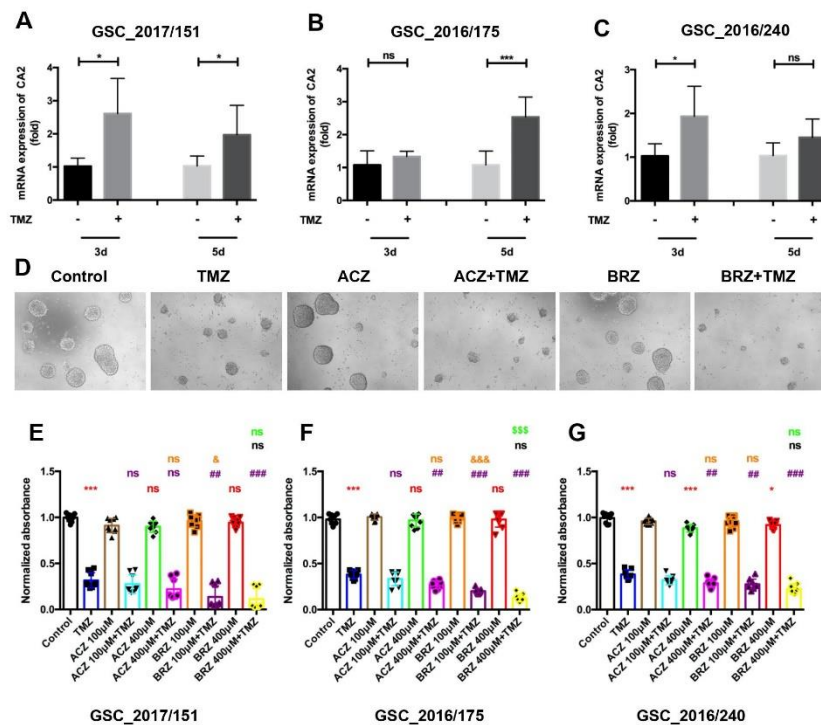
Considering that CA2 expression is induced by TMZ stimulation in GSCs, inhibition of CA2 expression might overcome TMZ resistance. To confirm our hypothesis, we determined cell viability using a CellTiter-Glo® assay after treatment with TMZ, ACZ, BRZ alone or in combination for 10 days (Figure 5D–G). Visualization of the morphology of GSCs using light microscopy identified differences in cell growth with TMZ alone, ACZ/BRZ alone, or combined ACZ/BRZ plus TMZ treatment (Figure 5D).

Our quantitative results show that TMZ alone diminishes cell numbers by more than 50% as compared to the control group in all three GSCs, whereas ACZ alone or BRZ alone did not have any cytotoxic effect on GSCs, even at higher concentrations of 400 μM. The combination of TMZ with ACZ at 100 μM did not cause growth inhibition compared to TMZ alone, whereas co-treatment with 400 μM ACZ and TMZ significantly reduced cell viability than single treatment with TMZ. However, BRZ, at both concentrations (100 μM and 400 μM) significantly augments TMZ cytotoxicity in all GSC lines. These results indicate that co-treatment with the CA inhibitor BRZ and TMZ leads to a better re-sensitization of GBM stem cells than ACZ applied in combination with TMZ (Figure 5E–G).
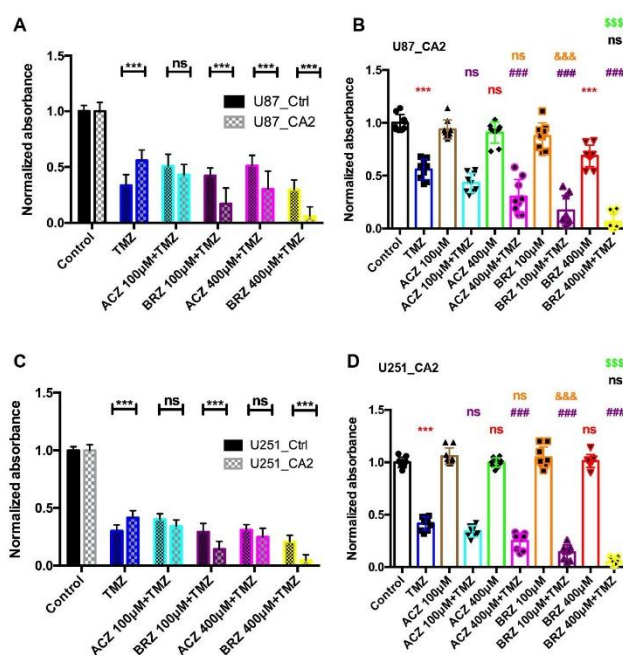
Figure 4. Effect of combined treatment with TMZ and either ACZ or BRZ on CA2 overexpressing GBM cell lines U87 and U251. (**A**) Co-treatment with 500 μM TMZ and ACZ/BRZ on U87_Ctrl cells and U87_CA2 cells for 5 d. U87_CA2 cells significantly decreased cell viability compared to U87_Ctrl cells after BRZ + TMZ treatment. However, only 400 μM ACZ + TMZ decreased cell viability compared to the U87_Ctrl group (*n* = 3). (**B**) In U87_CA2 cells treated with TMZ, ACZ/BRZ, or TMZ + ACZ/BRZ, TMZ plus 400 μM ACZ decreased the viability compared to TMZ alone. However, 100 μM ACZ in combination with TMZ did not change the cell viability. Both 100 μM and 400 μM BRZ in combination with 500 μM TMZ decreased the viability significantly compared to TMZ treatment alone (*n* = 3). (**C**) Co-treatment with 30 μM TMZ and ACZ/BRZ on U251_Ctrl cells and U251_CA2 cells for 5 d. U251_CA2 cells decreased cell viability compared to U251_Ctrl cells after 400 μM BRZ + TMZ treatment. However, ACZ + TMZ did not change cell viability compared to the U251_Ctrl group (*n* = 3). (**D**) In U251_CA2 cells, ACZ/BRZ has no cytotoxic effect, TMZ plus 400 μM ACZ decreased the viability compared to TMZ alone. Both 100 μM and 400 μM BRZ in combination with 500 μM TMZ decreased the viability significantly compared to TMZ treatment alone (*n* = 3). * (Red): compared to Control group; # (Purple): compared to TMZ group; & (Orange): compared to ACZ 100 μM + TMZ group; % (Black): compared to BRZ 100 μM + TMZ group; $ (Green): compared to ACZ 400 μM + TMZ group. Results were obtained from 3 independent experiments. Data are presented as mean ± SD, Two-way ANOVA was used to analyze (**A,C**), One-way ANOVA was used to analyze (**B,D**), ***, $$$, &&&, ###, *p* < 0.001, ns: not significant.

Figure 5. Combined treatment of BRZ and TMZ increases cell death in GBM stem-like cells. (**A–C**) mRNA expression of CA2 after TMZ treatment at 3 d and 5 d were detected by RT-PCR, the mRNA level of CA2 increased after TMZ stimulation (*n* = 3). (**D**) Visualization of the morphology of GSCs (Nr. 2016/175) using light microscopy after TMZ and CA inhibitor stimulation for 10 d. (**E–G**) Cell viability of co-treatment measured by CellTiter-Glo assay. Co-treatment with 500 µM TMZ and 400 µM ACZ decreased the viability compared to TMZ alone. However, 100 µM ACZ in combination with TMZ did not change the cell viability. Both 100 µM and 400 µM BRZ in combination with 500 µM TMZ decreased the viability significantly compared to TMZ treatment alone (*n* = 3). * (Red): compared to Control group; # (Purple): compared to TMZ group; & (Orange): compared to ACZ 100 µM + TMZ group; % (Black): compared to BRZ 100 µM + TMZ group; $ (Green): compared to ACZ 400 µM + TMZ group. Results were obtained from 3 independent experiments. In (**A–C,E–G**), data are presented as mean ± SD, student's *t*-test was used to analyze (**A–C**), One-way ANOVA was used to analyze (**E–G**), *, & $p < 0.05$; ## $p < 0.01$; ***, ###, &&&, $$$ $p < 0.001$, ns: not significant.

Next, we sought to explore the cytotoxic effects of single TMZ treatment and co-treatment with ACZ or BRZ in a GSC line with a high TMZ resistance (GSC_TMZ), resembling a GSC type present in recurrent GBM in comparison to the naïve GSC line (GSC_DMSO) [12]. Firstly, to explore the changes in mRNA expression levels of carbonic anhydrases CA2, CA9, CA12 (Figure 6A–C), monocarboxylate transporter molecules MCT1, MCT4, SLC4A4 (Figure 6D–F), and drug-resistant protein molecule (P-gp, Figure 6G) as a consequence of long-term treatment with TMZ and acquired chemoresistance, the lines GSC175_Ctrl, CSC175_DMSO, and GSC175_TMZ resistant GSCs were analyzed by q PCR (Figure 6A–G). We noticed that GSC_TMZ cells significantly up-regulated CA2, CA12, P-gp,

SLC4A4 expression levels compared to GSC_DMSO or GSC_Ctrl cells, while MCT1 and MCT4 mRNA transcripts were not changed, even CA9 mRNA expression was reduced in GSC_TMZ cells, confirming that the activation of CA2 and CA12 might be involved in TMZ-mediated GSC resistance, meanwhile, Western blot also shown an upregulation of CA2 in GSC_TMZ cell (Figure S5). On the contrary, GSC_TMZ did not up-regulate CA9, MCT1, MCT4 mRNA expression, indicating that these proteins mediating intracellular pH and lactate transport may require a hypoxic microenvironment in glioblastomas. To test for the viability of these cells, they were observed under the light microscope after 14 d stimulated with ACZ, BRZ alone, and in combination with TMZ (Figure 6H). Here, cells were treated with the IC_{50} value of TMZ as shown previously [12]. Similar to the reported combined treatment regimens, 100 μM and 400 μM of CA inhibitors ACZ and BRZ were applied. As expected, single TMZ treatment almost reduced half of the cells compared to the control group, which was significant in GSC_DMSO cells and GSC_TMZ cells (Figure 6I,J). Neither 100 μM nor 400 μM ACZ or BRZ alone caused any cytotoxicity in these cells. Noticeably, the combined treatment of ACZ with TMZ did not have any effect on cell viability compared to TMZ treatment alone, either in GSC_DMSO cells or in GSC_TMZ cells (Figure 6I,J). However, co-treatment with BRZ was more cytotoxic at lower concentrations in GSC_TMZ cells than GSC_DMSO cells and significantly inhibited cell viability (Figure 6I,J), which might be due to CA2 overexpression in GSC_TMZ cells, while BRZ more specifically inhibits CA2 expression than ACZ. Collectively, these data indicated that BRZ combinatorial treatment might be most potent in long-term TMZ-resistant GSCs and that BRZ is synergistic to TMZ to cause increased cytotoxicity of TMZ to reduce chemoresistance of GSCs.

As established previously, autophagy is altered in GBM cells and can be induced by TMZ, so that many resistance mechanisms exist to prevent chemotherapy-induced autophagy. Autophagy itself might exert either a pro-tumor or an anti-tumor effect. We, therefore, asked whether this phenomenon that we observed above might be due to co-treatment with CA inhibitors promoting cell death via enhanced activation of autophagy. To test our hypothesis, LC3II, the lipidated autophagosome-associated form of LC3, and p62, a marker of autophagic flux were measured by Western Blot and as LC3-II puncta formation by immunocytochemistry. We noticed that BRZ/TMZ but not ACZ or BRZ enhanced autophagy of U251_CA2 cells (ratio of LC3II to LC3I) (Figure 7A,B).

We also examined the effects of the combined treatment with TMZ/ACZ or TMZ/BRZ on CA2, LC3, p62 expression in U87_CA2 and U251_CA2 cells (Figure S6 and Figure 7). Our results show that TMZ significantly up-regulates the protein level of CA2 while we found that co-treatment with BRZ effectively inhibited CA2 expression compared to TMZ, BRZ, ACZ alone, or to combined TMZ/ACZ treatment (Figure 7D–G), which demonstrated that BRZ more specifically inhibits CA2 expression than ACZ after TMZ stimulation. Moreover, BRZ + TMZ significantly increased the conversion of LC3I to LC3II compared with TMZ alone or ACZ + TMZ, and also decreased p62 expression. The LC3 and p62 expression in U251_Ctrl cells as well as U87_Ctrl cells enhanced autophagy by single TMZ treatment but not by co-treatment (Figure 7C and Figure S6B) suggesting that CA2 is required to exert this effect. For U251_CA2 cells, we observed that TMZ in combination with BRZ significantly increased the LC3II/LC3I ratio and reduced CA2 and p62 expression (Figure 7D), which suggests that BRZ in combination with TMZ strongly increases autophagic flux and promotes the occurrence of autophagy thereby causing enhanced cell death.
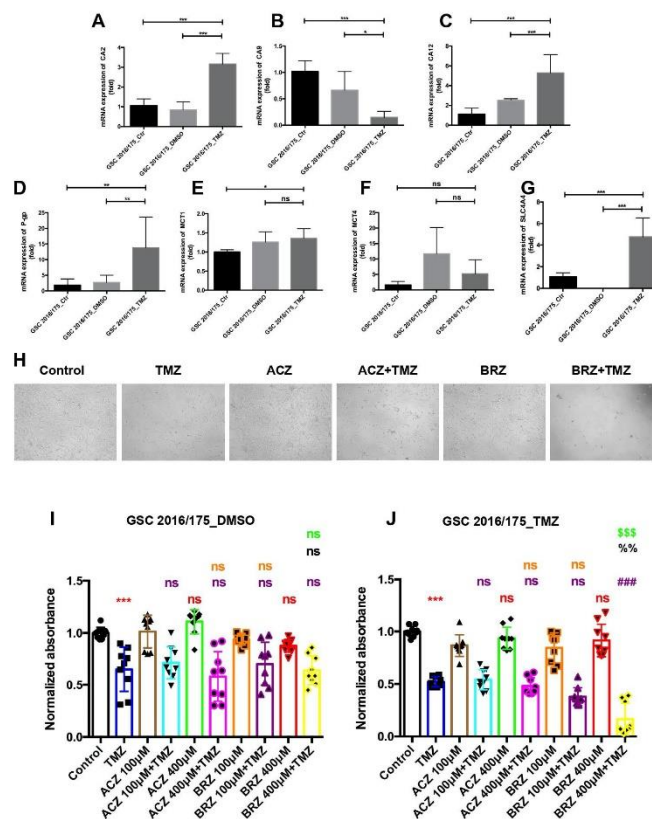
Figure 6. BRZ is more effective than ACZ in causing re-sensitization of long-term TMZ-resistant GSCs. (**A**–**G**) qPCR measurement for three GBM-related *CA* genes (*CA2*, *CA9*, and *CA12*), three monocarboxylate transporters (*MCT-1*, *MCT-4*, and *SLC4A4*), and drug-resistance gene (*P-gp*) which showed differential expression between TMZ resistant cell and its paired control/DMSO cells (*n* = 3). (**H**) Cell morphology changes after TMZ and CA inhibitor stimulation for 14 d. (**I**) Co-treatment with C50 dose (3 μM) of TMZ and 100 μM/400 μM ACZ or BRZ did not decrease the cell viability compared to single treatment with TMZ on DMSO control cells (*n* = 3). (**J**) Both 100 μM and 400 μM BRZ in combination with IC50 dose (250 μM) TMZ decreased the viability significantly compared to TMZ treatment alone on TMZ-resistant cells, however, ACZ in combination with TMZ did not change the cell viability (*n* = 3). * (Red): compared to Control group; # (Purple): compared to TMZ group; & (Orange): compared to ACZ 100 μM + TMZ group; % (Black): compared to BRZ100 μM + TMZ group; $ (Green): compared to ACZ 400 μM + TMZ group. Results were obtained from 3 independent experiments. Data are presented as mean ± SD, One-way ANOVA was used to analyze the data, * $p < 0.05$; **, %% $p < 0.01$; ***, ###, $$$ $p < 0.001$, ns: not significant.
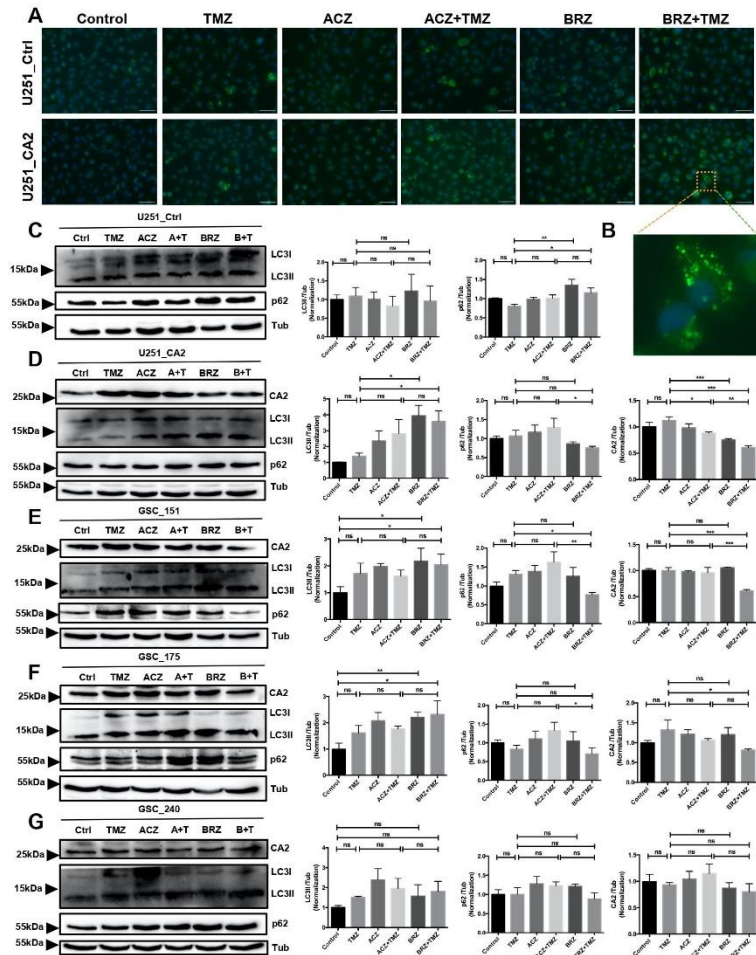
Figure 7. The combination of BRZ and TMZ increased cell death in GBM stem-like cells by activating autophagy (**A**,**B**) Autophagy marker LC3 immunostaining of U251_Ctrl and U251_CA2 cells after TMZ and ACZ/BRZ stimulation for 24 h. Co-treatment with TMZ and BRZ induced the expression of LC3 puncta in U251_CA2 cells (scale bar: 50 μm). (**C**,**D**) Western Blotting of autophagy-related proteins and CA2 protein in U251_Ctrl and U251_CA2 cells with the same treatment as in (**A**). TMZ plus BRZ did not increase the protein expression of LC3II in U251_Ctrl cells compared to TMZ treatment alone (**C**) but increased in U251_CA2 cells (**D**) (*n* = 3). (**E**–**G**) Western Blotting of autophagy-related proteins and CA2 protein in GBM stem cells with the same treatment as in Figure 5E–G for 24 h stimulation. Compared with the control group, TMZ monotherapy has a tendency to increase the protein level of LC3II, but the expression of it is significantly increased in BRZ alone and TMZ combined with BRZ treatment (*n* = 3). Results were obtained from three independent experiments. Data are presented as mean ± SEM, One-way ANOVA was used to analyze the data, * $p < 0.05$; ** $p < 0.01$; *** $p < 0.001$, ns: not significant.

These results indicate that BRZ might be involved in mediating TMZ chemosensitivity of CA2 overexpressing GBM cell lines through enhanced activation of autophagy. This mechanism is similar in GSCs, as the combination of BRZ and TMZ also increased cell death of GSCs. For a precise evaluation of the autophagic progress in GSCs, CA2, LC3, p62 were measured by Western Blot after treatment with TMZ alone, ACZ/BRZ alone, or co-treatment for 24 h and compared to controls. All three GSCs showed, in the presence of BRZ, a significant increase in LC3II that was accompanied by a decrease in LC3I in Western Blots (Figure 7E–G). This was even more pronounced in cells treated with TMZ/BRZ. We also found that p62 was reduced under TMZ/BRZ co-treatment. Furthermore, CA2 was significantly decreased in TMZ combined with BRZ in all three GSCs. These patterns are consistent with an increase in autophagy.

3. Discussion

The current standard strategies for patients with newly diagnosed GBM glioma include surgical resection, radiation therapy, and chemotherapy [3]. However, in most patients, tumor recurrence is an inevitable problem. Singh et al. first demonstrated the existence of glioma stem-like cells (GSCs) in human brain tumors [25,26]. Further research established that GSCs play important roles in therapeutic resistance, including invasion [27], chemo-resistance [28], radio-resistance [11], and recurrence [28]. As general properties of all stem cells, a GSC has the potential for self-renewal, a capacity for undirected differentiation and tumor initiation, and GSC chemo-resistance is related to drug efflux transporter and GSC diversity [29,30], GSCs have been identified to be relatively resistant to the first-line chemotherapeutic drug TMZ compared to their non-stem-like counterparts [31]. Glioma GSCs have higher expression levels of O6-methyl-guanine- DNA-methyltransferase, the key repair enzyme for TMZ-induced DNA damage, compared to non-stem cells [32]. Therefore, improving the efficacy of TMZ to overcome GSCs resistance is an urgent problem that needs to be solved.

In our study, we identified a strategy to overcome GBM chemoresistance by pharmaco-logical targeting of carbonic anhydrase 2 (CA2) for the improvement of TMZ efficacy which could have implications for further clinical strategies in GBM treatment. Transcriptomic data from recurrent tumor tissues and TMZ-resistant GSCs previously revealed consistently enhanced levels of CA2, however, no functional data on CA2 in GBM cells and GSCs were available. Firstly, we found higher expression levels of CA2 in GSCs compared to GBM cell lines, U87 and U251. To investigate the functional consequences of CA2 expression in these cells, we established stable CA2 overexpressing cell clones of U87 and U251 cells and determined their cellular behavior.

As evolutionary highly conserved zinc-dependent proteins with one of the highest substrate turnover rates, CAs catalyze the conversion of CO_2 and H_2O into bicarbonate. Hence, CAs are involved in cellular processes, such as mitochondrial respiration and acid-base regulation, electrolyte secretion, bone reabsorption, and calcification, also in lipogenesis and gluconeogenesis [33]. As a highly active cytosolic isoform, CA2 is expressed in almost all tissues throughout the body including the brain [34,35]. It was shown that CA2 interacts with monocarboxylate transporter proteins e.g., MCT-1/4 thereby symporting protons with monocarboxylic acids, such as lactate [21]. As a metabolic consequence, CA2 maintains glycolysis in tumor cells, thus supporting the "Warburg effect", prioritizing glycolysis as a major source of energy. Interestingly, it has been proposed that CA2 interacts with V-ATPase [36] to control intracellular energy flow and cellular autophagy. Our data demonstrate that, in GBM cells, high expression of CA2 leads to an increase in mitochondrial basal respiration, maximal respiration, ATP production, and glycolytic activity that these alterations may link to patient outcome, this finding allows us to further clarify the role of CA2 in GBM.

Acetazolamide (ACZ) has been reported to have synergistic effects when combined with TMZ [13,37,38] and is currently in clinical studies for GBM co-treatment with TMZ (https:clinicaltrials.gov; Study Number NCT03011671; accessed on 9 November 2021) in

a dose of 500 mg per day and escalated to 1000 mg per day between cycle day 1–21. However, due to its pan-CA characteristics, ACZ could inhibit carbonic anhydrases which could have beneficial effects, i.e., by sensitizing GBM cells to TMZ, so that the ACZ effect might be less significant as more specific CA2 inhibition. Indeed, depending on the cell type investigated, there is a difference in the efficacy of BRZ/TMZ treatment compared to ACZ/TMZ treatment, which is highly significant in U251_CA2 cells and two of the three patient-derived GSC lines. Given these results, we hypothesize that a combination of the CA2 inhibitor brinzolamide (BRZ) in conjunction with TMZ might provide an improved patient benefit by acting on several cellular processes in which carbonic anhydrases are involved.

Concerning carbonic anhydrases known to be physiologically relevant, the specificity of CA-inhibitors needs to be evaluated (Tables S3 and S4). In contrast to acetazolamide, brinzolamide is considered to be the most specific CA2 inhibitor with a K_i value of 3 nM for the full-length enzyme. However, brinzolamide is also able to inhibit CA12 with a K_i value of 3 nM for the catalytic domain. As an argument for higher specificity of brinzolamide for CA2 over CA12, the K_i value for the full-length enzyme of CA12 is unknown and K_i values for the full-length enzyme are likely by an order of magnitude higher than for the isolated catalytic domain [23,24]. Nevertheless, we can state an improved therapeutic effect of brinzolamide compared to acetazolamide when combined with TMZ.

In this respect, our study demonstrates the differences between the application of a pan-CA and a more specific CA2 inhibitor. Metabolic processes in GSCs were more severely impaired by ACZ as compared to BRZ. This can be explained by the fact that all CAs present in GBM cells (at least CA2, CA9, and CA12) are part of the inside/out regulation of protons and the monocarboxylate transport mechanism. Thus, as observed in GBM cells, ACZ reduces OCR and ECAE in CA2 overexpressing cells, but the effects of ACZ are significantly stronger than those of BRZ.

However, there might be a certain "hierarchy" in CAs, in which CA2 might have stronger effects on cellular processes apart from metabolism, and this is the induced invasion seen under CA2 expression. It is, therefore, interesting to notice that in this particular cellular process, the effect of BRZ is stronger than that of ACZ.

Both CA inhibitors, ACZ and BRZ, are not cytotoxic as our data suggest in all cell lines investigated. However, both inhibitors can increase TMZ efficacy. The highest TMZ efficacy is achieved at physiological pH. However, tumor cells often exhibit an alkaline pH, so that acidification as a result of CA2 inhibition leads to a physiological pH, thereby enhancing the uptake of TMZ into tumor cells. The described alterations of metabolism in vivo often causally correlate with hypoxia [13,38]. Hypoxia is a characteristic feature of the GBM microenvironment and impacts several processes which lead to the progression of tumors, such as differentiation, invasion, and angiogenesis [39]. It was shown that TMZ induces autophagy in GBM cells, and additional compounds leading to augmented TMZ-induced autophagy are of great value for the optimization of GBM chemotherapy strategies [30,40].

In our study, we confirmed that in GBM cells expressing CA2 and in GSCs, CA2 can suppress autophagy, as autophagy is activated after treatment with the CA inhibitor BRZ [41,42]. Similar, although weaker effects were observed with ACZ. The metabolic changes in ACZ treated cells are more pronounced compared to BRZ, and yet, the effects of BRZ are stronger for invasion behavior and autophagy regulation. The somewhat surprising outcome of this study was that a preferential CA2 inhibition, in contrast to combined inhibition of GBM-relevant CAs (CA2, CA9 and CA12) with ACZ provides a stronger effect on cell viability when combined with TMZ. The strongest effect of BRZ over ACZ was observed for autophagy regulation in CA2 expressing U251 cells and in GSCs. Both CA inhibitors can induce autophagy, and in some cell lines, BRZ was the stronger inducer. However, when TMZ induced the so-called chemotherapy-induced autophagy that leads to cell death, the combined treatment with BRZ showed significantly stronger effects on cell viability than the combination of TMZ with ACZ suggesting that inhibition of other CAs apart from CA2 could cause compensatory effects that can support cell survival.

In addition to autophagy regulation, we show in our study that inhibition of CA2 by brinzolamide has a strong effect on the invasive behavior of GBM cells which is superior to ACZ. Whether this effect is solely based on metabolic effects remains to be determined.

These findings have implications for clinical studies. Firstly, we show that ACZ is only effective in higher doses of 400 µM. As an estimate, the ACZ concentration of current clinical studies is in the range of 100 µM so that autophagy induction is most likely not sufficient to exert a significant clinical benefit to patients, as these ACZ doses used for co-treatment with TMZ are shown to be inefficient in our cell-based studies as demonstrated here. Based on these data, a TMZ/BRZ co-treatment would be a more promising approach. However, so far, pharmacological use of BRZ is only approved for ophthalmologic applications [43] and it remains to be established whether it can be applied to patients systemically.

4. Materials and Methods

4.1. Clinical Specimens

All tumor tissue samples from patients obtained approval from the ethics committee of the Medical Faculty, Philipps University of Marburg (Institutional review board number 185/11).

4.2. Gene Expression Analysis

We checked the CA2 gene expression in the "Gene-DE" part of the TIMER2 website and observed the CA2 difference expression between different tumor tissues and adjacent normal tissues in the TCGA database (http://timer.cistrome.org/; 12 December 2021), data are not shown. For GBM only 5 normal tissues, we used the "Expression analysis Box Plots" part of the GEPIA2 website (http://gepia2.cancer-pku.cn/#analysis, 12 December 2021) to obtain the CA2 expression difference between GBM tumor tissues and the normal tissues of the GETx (Genotype-Tissue Expression) database.

4.3. Cell Culture

U87 and U251 glioblastoma cell lines (identity of cell lines was verified by karyotyping and STR profiling) were obtained from ECACC and were cultured in DMEM cell medium (DMEM-HA, Capricorn Scientific, Ebsdorfergrund, Germany) supplemented with 10% fetal bovine serum (FBS) (S0615, Sigma, Dreieich, Germany), 1% penicillin/streptomycin (2321115, Gibco, Carlsbad, CA, USA), 1% Non-essential amino acids (NEAA) (11140050, Gibco, Carlsbad, USA) and 1% Sodium pyruvate (NPY-B, Capricorn Scientific, Ebsdorfergrund, Germany). Glioblastoma stem-like cells were isolated as described previously [12]. Cells were cultured in DMEM/F12 medium (DMEM-12-A, Capricorn Scientific, Ebsdorfergrund, Germany) including 2% B27 supplement (117504044, Gibco, Carlsbad, USA), 1% amphotericin (152290026, Gibco, Carlsbad, USA), 0.5% HEPES (H0887, Sigma, Dreieich, Germany) and 0.1% gentamycin (A2712, Biochrom, Berlin, Germany) with EGF (100-18B, Peprotech, Hamburg, Germany) and bFGF (315-09, Peprotech, Hamburg, Germany) in a concentration of 20 ng/mL, respectively. All cells were incubated at 37 °C under 5% CO_2 humidified incubator.

4.4. Generation of CA2 Expressing Stable GBM Cell Lines

U87 and U251 CA2 expressing cells were generated by transfection with CA2 plasmid (RC201974, ORIGENE, Rockville, MD, USA) using 2.5 µg of plasmid DNA mix Lipofectamine LTX Reagent (15338100, Invitrogen, Waltham, MA, USA). After 48 h, the medium was changed to complete DMEM with G418 (A2912, Biochrom, Berlin, Germany) (400 µg/mL for U87 cells and 600 µg/mL for U251 cells) for 3 weeks. Positive clones were picked and further selected for stable integration. The plasmid pCMV6-LacZ-Bbsl (114,671, Addgene, Watertown, MA, USA) was used for vector control cell lines.

4.5. Invasion Assay

Acetazolamide (ACZ, A6011, Sigma, Dreieich, Germany) and Brinzolamide (BRZ, SML0216, Sigma, Dreieich, Germany) were used for cell treatment 24 h before cell invasiveness analysis. An 8 μm pore transwell insert (662638, Greiner Bio-One, Monroe, Austria) in conjunction with a 24-well plate was used. Transwells were coated with 50 μL matrigel Mix (matrigel mixed 1:1 with cold DMEM) (Corning, 354230, Corning, NY, USA), transwell was turned upside down after 1 h after solidification, and 2.5×10^3 cells in 50 μL medium were seeded on the other side of the insert, turn the transwell right side up again after 4 h adherence. Around 250 μL medium containing 20% FBS was supplied to the transwell on the upper chamber whereas 750 μL medium containing 0.5% FBS was added into the 24-well plate to create a concentration gradient. Cells invaded along the FBS gradient into the matrigel for 24 h, and cells were fixed with 4% PFA, permeabilized with 0.3% Triton (T8787, Sigma, Dreieich, Germany), and nuclei were stained with Hoechst 33342 (1:10,000 dilution, 62249, ThermoFisher, Waltham, MA, USA) for 15 min at RT in the dark. Images were acquired using Leica confocal microscope. Cells were counted in six random areas and were calculated as the percentage of cells that passed across the membrane.

4.6. Cell Viability Assay

The survival effect of cells was determined using the CellTiter-Glo 3D cell viability assay (G7571, Promega, Walldorf, Germany). GBM cell lines were seeded at a density of 2.0×10^3 cells per well, GSCs were seeded at a density of 1.0×10^4 cells per well, TMZ-resistant GSCs were seeded as described previously [12]. All cells were stimulated by overnight incubation. 50 μL CellTiter-Glo 3D Reagent was added to the well before measurement, mixed shaking for 15 min, and incubated for 15 min at RT to avoid light. Luminescence was measured with a Microplate Reader luminometer (FLUOstar OPTIMA Microplate Reader, Offenburg, Germany).

4.7. Seahorse Assay

The seahorse system XF96-Analyzer (Agilent Technologies, Waldbronn, Germany) was used to measure alterations in the metabolism of cells to analyze mitochondrial oxygen consumption rate (OCR) and extracellular acidification rate (ECAR), 9000 cells were seeded in micro-plate overnight, after inhibitor treatment 24 h, the conditional medium was replaced by seahorse medium and incubated for 1 h before measurement. The whole detailed steps were executed as described before [44]

4.8. RNA Isolation, Reverse Transcription, and Quantitative Real-Time PCR

Total RNA was isolated by QIAzol reagent (79306, Qiagen, Hilden, Germany) and absorbance was measured with OD 260/280 ratio between 1.8 and 2.1. For qPCR analysis, 2 μg of RNA was subjected to the synthesis of cDNA by using RNA to cDNA EcoDry Premix (Clontech, Saint-Germain-en-Laye, France) according to the manufacturer's instructions. Total reaction volume (20 μL) includes 10 μL SYBR Green/Rox Master Mix (Primer Design, Southhampton, UK), 2 μL primers synthesized by Qiagen GmbH (Hilden, Germany), 6 μL nuclease-free water, and 2 μL cDNA. The qPCR protocol set initial denaturation at 95 °C for 10 min, then 40 amplification cycles including 95 °C for 15 s and 60 °C for 1 min. The XS-13 was used as an internal reference for all reactions. The fold changes in gene expression relative to control were calculated by $2^{-\Delta\Delta CT}$.

4.9. Protein Extraction and Western Blot Analysis

After cells were washed 3 times with ice-cold PBS, total proteins were extracted with RIPA buffer including a protease inhibitor (A32955, Thermo Scientific, Waltham, MA, USA) and phosphatase inhibitor (A32957, Thermo Scientific, Waltham, MA, USA). Protein lysates were boiled in Laemmli and sample reducing buffer (B0009, Invitrogen, Waltham, MA, USA) for 5 min. An equal amount of protein samples were separated by 12.5% SDS polyacrylamide gel electrophoresis and transferred onto nitrocellulose (NC)

membranes (A29591442, GE Healthcare Life science, Solingen, Germany). After blocking with 5% non-fat milk (X968.1, Carl Roth, Karlsruhe, Germany) for 1 h at RT, and membrane were incubated overnight at 4 °C with primary antibody, the following antibodies were used: anti-CA2 (1:2000 dilution, ab124687, Abcam, Cambridge, UK), anti-MAP LC3 (1:500 dilution, sc-271625, Santa Cruz Biotechnology, Dallas, TX, USA), anti-p62 (2 ug/mL dilution, MAB8028, R&D Systems, Minneapolis, MN, USA), and anti-β-Tubulin (1:2000 dilution, NB600-936, Novus Biologicals, Littleton, CO, USA) in 5% milk in TBST. Subsequently, the NC membranes were incubated with secondary antibody Donkey (Dnk) pAb to Mouse (Ms) IgG (HRP) (ab97030, Abcam, Cambridge, UK) and Dnk pAb to Rabbit (Rb) IgG (HRP) (ab97064, Abcam, Cambridge, UK) for 1 h at RT. The membranes were washed with TBS-T and scanned with Chemostar Imager (Intas, Goettingen, Germany).

4.10. Immunofluorescence Staining

Paraffin sections (5 μm thick) were obtained from GBM patients. All slides were blocked to avoid non-specific binding with 1% BSA (A7030, Sigma, Dreieich, Germany), and incubated with Rabbit Anti-CA2 antibody (1:250 dilution, ab124687, Abcam, Cambridge, UK) and Mouse Anti-Sox2 antibody (1:100 dilution, MA1-014, ThermoFisher, Waltham, MA, USA) at 4 °C overnight, washed in PBS 3 times, and incubated with secondary antibody Donkey anti-Rabbit 550 (1:200 dilution, ab98489, Abcam, Cambridge, UK), Donkey anti-Mouse 488 (1:200 dilution, ab98794, Abcam, Cambridge, UK) at least 1 h at RT avoid night. Nuclei were stained with Hoechst 33342 (1:10,000 dilution, 62249, ThermoFisher, Waltham, MA, USA) 15 min at RT avoid night before cover with anti-fade mounting medium (S3023, Agilent, Santa Clara, CA, USA) was done. Images were acquired using a Leica DM 5500 microscope.

For IF, cells were cultured on collagen I (C7661, Sigma, Dreieich, Germany) coated coverslips in a 24-well plate overnight, cells were washed in PBS 3X, fixed with 4% paraformaldehyde 15 min at RT, permeabilized with 0.3% Triton X100 (T8787, Sigma, Dreieich, Germany) 15 min at RT, blocked to avoid non-specific binding with 5% BSA 1 h, and incubated with Mouse anti-MAP LC3 (1:250 dilution, sc-271625, Santa Cruz Biotechnology, Dallas, USA) at 4 °C overnight, washed, and incubated with secondary antibody donkey anti-Mouse 488 (1:200 dilution, ab98794, Abcam, Cambridge, UK) at least 1 h at RT avoid night. Nuclei were stained with Hoechst 33342 15 min at RT in the dark before covering with the anti-fade mounting medium was done.

4.11. Statistical Analyses

All data were shown as the mean $\pm$ SD or SEM and analyzed using GraphPad Prism software (GraphPad Software Inc., San Diego, CA, USA). Unpaired Student's *t*-tests were used for statistical comparison among two groups. Analysis of variance (ANOVA) test was performed for multicomponent comparisons (one-way or two-way ANOVA), all statistical tests have been indicated in the figure legends. *p*-value < 0.05 was considered statistically significant.

5. Conclusions

As recurrence caused by TMZ resistance is almost unavoidable for GBM patients, there is an urgent need for improved treatment options. Here we show the functional consequences of CA2 in GBM cell lines and GSCs and provide a rationale for inhibition of CA2 bearingf a novel therapeutic potential by sensitizing GBM cell lines and GSCs for TMZ treatment more efficiently as pan-CA inhibition using acetazolamide.

Supplementary Materials: The following supporting information can be downloaded at: https://www.mdpi.com/article/10.3390/ijms23010157/s1.

References

1. Gramatzki, D.; Dehler, S.; Rushing, E.J.; Zaugg, K.; Hofer, S.; Yonekawa, Y.; Bertalanffy, H.; Valavanis, A.; Rohrmann, S.; Oberle, J.; et al. Glioblastoma in the Canton of Zurich, Switzerland, revisited (2005–2009). *J. Clin. Oncol.* **2015**, *33*, e13025. [CrossRef]
2. Rajaratnam, V.; Islam, M.M.; Yang, M.; Slaby, R.; Ramirez, H.M.; Mirza, S.P. Glioblastoma: Pathogenesis and current status of chemotherapy and other novel treatments. *Cancers* **2020**, *12*, 937. [CrossRef] [PubMed]
3. Stupp, R.; Mason, W.P.; van den Bent, M.J.; Weller, M.; Fisher, B.; Taphoorn, M.J.B.; Belanger, K.; Brandes, A.A.; Marosi, C.; Bogdahn, U.; et al. Radiotherapy plus concomitant and adjuvant temozolomide for glioblastoma. *N. Engl. J. Med.* **2005**, *352*, 987–996. [CrossRef] [PubMed]
4. Kim, J.; Lee, I.H.; Cho, H.J.; Park, C.K.; Jung, Y.S.; Kim, Y.; Nam, S.H.; Kim, B.S.; Johnson, M.D.; Kong, D.S.; et al. Spatiotemporal evolution of the primary glioblastoma genome. *Cancer Cell* **2015**, *28*, 318–328. [CrossRef]
5. Campos, B.; Olsen, L.R.; Urup, T.; Poulsen, H.S. A comprehensive profile of recurrent glioblastoma. *Oncogene* **2016**, *35*, 5819–5825. [CrossRef]
6. Stieber, D.; Golebiewska, A.; Evers, L.; Lenkiewicz, E.; Brons, N.H.; Nicot, N.; Oudin, A.; Bougnaud, S.; Hertel, F.; Bjerkvig, R.; et al. Glioblastomas are composed of genetically divergent clones with distinct tumourigenic potential and variable stem cell-associated phenotypes. *Acta Neuropathol.* **2014**, *127*, 203–219. [CrossRef]
7. Dey, M.; Ulasov, I.V.; Lesniak, M.S. Virotherapy against malignant glioma stem cells. *Cancer Lett* **2010**, *289*, 1–10. [CrossRef]
8. Lathia, J.D.; Mack, S.C.; Mulkearns-Hubert, E.E.; Valentim, C.L.L.; Rich, J.N. Cancer stem cells in glioblastoma. *Genes Dev.* **2015**, *29*, 1203–1217. [CrossRef]
9. Ahmad, G.; Amiji, M.M. Cancer stem cell-targeted therapeutics and delivery strategies. *Expert Opin. Drug Deliv.* **2017**, *14*, 997–1008. [CrossRef]
10. Sharifzad, F.; Ghavami, S.; Verdi, J.; Mardpour, S.; Mollapour Sisakht, M.; Azizi, Z.; Taghikhani, A.; Aos, M.J.; Fakharian, E.; Ebrahimi, M.; et al. Glioblastoma cancer stem cell biology: Potential theranostic targets. *Drug Resist. Updates Rev. Comment. Antimicrob. Anticancer. Chemother.* **2019**, *42*, 35–45. [CrossRef] [PubMed]
11. Bao, S.; Wu, Q.; McLendon, R.E.; Hao, Y.; Shi, Q.; Hjelmeland, A.B.; Dewhirst, M.W.; Bigner, D.D.; Rich, J.N. Glioma stem cells promote radioresistance by preferential activation of the DNA damage response. *Nature* **2006**, *444*, 756–760. [CrossRef]
12. Hannen, R.; Selmansberger, M.; Hauswald, M.; Pagenstecher, A.; Nist, A.; Stiewe, T.; Acker, T.; Carl, B.; Nimsky, C.; Bartsch, J.W. Comparative transcriptomic analysis of temozolomide resistant primary GBM stem-like cells and recurrent GBM identifies up-regulation of the carbonic anhydrase CA2 gene as resistance factor. *Cancers* **2019**, *11*, 921. [CrossRef] [PubMed]
13. Wu, L.; Bernal Giovanna, M.; Cahill Kirk, E.; Pytel, P.; Fitzpatrick Carrie, A.; Mashek, H.; Weichselbaum Ralph, R.; Yamini, B. BCL3 expression promotes resistance to alkylating chemotherapy in gliomas. *Sci. Transl. Med.* **2018**, *10*, eaar2238. [CrossRef] [PubMed]
14. Tetu, S.G.; Tanz, S.K.; Vella, N.; Burnell, J.N.; Ludwig, M. The flaveria bidentis β-carbonic anhydrase gene family encodes cytosolic and chloroplastic isoforms demonstrating distinct organ-specific expression patterns. *Plant Physiol.* **2007**, *144*, 1316–1327. [CrossRef]

15. Mustaffa, N.I.; Latif, M.T.; Wurl, O. The role of extracellular carbonic anhydrase in biogeochemical cycling: Recent advances and climate change responses. *Int. J. Mol. Sci.* **2021**, *22*, 7413. [CrossRef]
16. Sly, W.S.; Hu, P.Y. Human carbonic anhydrases and carbonic anhydrase deficiencies. *Annu. Rev. Biochem.* **1995**, *64*, 375–401. [CrossRef] [PubMed]
17. Alterio, V.; Di Fiore, A.; D'Ambrosio, K.; Supuran, C.T.; De Simone, G. Multiple binding modes of inhibitors to carbonic anhydrases: How to design specific drugs targeting 15 different isoforms? *Chem. Rev.* **2012**, *112*, 4421–4468. [CrossRef]
18. Haapasalo, J.; Nordfors, K.; Haapasalo, H.; Parkkila, S. The expression of carbonic anhydrases II, IX and XII in brain tumors. *Cancers* **2020**, *12*, 1723. [CrossRef]
19. Boyd, N.H.; Walker, K.; Fried, J.S.; Hackney, J.R.; McDonald, P.C.; Benavides, G.A.; Spina, R.; Audia, A.; Scott, S.E.; Libby, C.J.; et al. Addition of carbonic anhydrase 9 inhibitor SLC-0111 to temozolomide treatment delays glioblastoma growth In Vivo. *JCI Insight* **2017**, *2*, e92928. [CrossRef]
20. Said, H.M.; Hagemann, C.; Carta, F.; Katzer, A.; Polat, B.l.; Staab, A.; Scozzafava, A.; Anacker, J.; Vince, G.H.; Flentje, M.; et al. Hypoxia induced CA9 inhibitory targeting by two different sulfonamide derivatives including acetazolamide in human glioblastoma. *Bioorg. Med. Chem.* **2013**, *21*, 3949–3957. [CrossRef] [PubMed]
21. Becker, H.M.; Hirnet, D.; Fecher-Trost, C.; Sültemeyer, D.; Deitmer, J.W. Transport activity of MCT1 expressed in Xenopus oocytes is increased by interaction with carbonic anhydrase. *J. Biol. Chem.* **2005**, *280*, 39882–39889. [CrossRef] [PubMed]
22. de la Cruz-López, K.G.; Castro-Muñoz, L.J.; Reyes-Hernández, D.O.; García-Carrancá, A.; Manzo-Merino, J. Lactate in the regulation of tumor microenvironment and therapeutic approaches. *Front. Oncol.* **2019**, *9*, 1143. [CrossRef]
23. Supuran, C.T. Therapeutic applications of the carbonic anhydrase inhibitors. *Therapy* **2007**, *4*, 355–378. [CrossRef]
24. Supuran, C.T. Carbonic anhydrases: Novel therapeutic applications for inhibitors and activators. *Nat. Rev. Drug Discov.* **2008**, *7*, 168–181. [CrossRef] [PubMed]
25. Singh, S.K.; Clarke, I.D.; Terasaki, M.; Bonn, V.E.; Hawkins, C.; Squire, J.; Dirks, P.B. Identification of a cancer stem cell in human brain tumors. *Cancer Res.* **2003**, *63*, 5821.
26. Singh, S.K.; Hawkins, C.; Clarke, I.D.; Squire, J.A.; Bayani, J.; Hide, T.; Henkelman, R.M.; Cusimano, M.D.; Dirks, P.B. Identification of human brain tumour initiating cells. *Nature* **2004**, *432*, 396–401. [CrossRef]
27. Wakimoto, H.; Kesari, S.; Farrell, C.J.; Curry, W.T.; Zaupa, C.; Aghi, M.; Kuroda, T.; Stemmer-Rachamimov, A.; Shah, K.; Liu, T.-C.; et al. Human glioblastoma–derived cancer stem cells: Establishment of invasive glioma models and treatment with oncolytic herpes simplex virus vectors. *Cancer Res.* **2009**, *69*, 3472. [CrossRef]
28. Chen, J.; Li, Y.; Yu, T.-S.; McKay, R.M.; Burns, D.K.; Kernie, S.G.; Parada, L.F. A restricted cell population propagates glioblastoma growth after chemotherapy. *Nature* **2012**, *488*, 522–526. [CrossRef] [PubMed]
29. Oberstadt, M.C.; Bien-Möller, S.; Weitmann, K.; Herzog, S.; Hentschel, K.; Rimmbach, C.; Vogelgesang, S.; Balz, E.; Fink, M.; Michael, H.; et al. Epigenetic modulation of the drug resistance genes MGMT, ABCB1 and ABCG2 in glioblastoma multiforme. *BMC Cancer* **2013**, *13*, 617. [CrossRef]
30. Hu, Z.; Mi, Y.; Qian, H.; Guo, N.; Yan, A.; Zhang, Y.; Gao, X. A potential mechanism of temozolomide resistance in glioma–Ferroptosis. *Front. Oncol.* **2020**, *10*, 897. [CrossRef] [PubMed]
31. Gong, X.; Schwartz, P.H.; Linskey, M.E.; Bota, D.A. Neural stem/progenitors and glioma stem-like cells have differential sensitivity to chemotherapy. *Neurology* **2011**, *76*, 1126. [CrossRef]
32. Bleau, A.M.; Hambardzumyan, D.; Ozawa, T.; Fomchenko, E.I.; Huse, J.T.; Brennan, C.W.; Holland, E.C. PTEN/PI3K/Akt pathway regulates the side population phenotype and ABCG2 activity in glioma tumor stem-like cells. *Cell Stem Cell* **2009**, *4*, 226–235. [CrossRef] [PubMed]
33. Neri, D.; Supuran, C.T. Interfering with pH regulation in tumours as a therapeutic strategy. *Nat. Rev. Drug Discov.* **2011**, *10*, 767–777. [CrossRef] [PubMed]
34. Nordfors, K.; Haapasalo, J.; Korja, M.; Niemelä, A.; Laine, J.; Parkkila, A.-K.; Pastorekova, S.; Pastorek, J.; Waheed, A.; Sly, W.S.; et al. The tumour-associated carbonic anhydrases CA II, CA IX and CA XII in a group of medulloblastomas and supratentorial primitive neuroectodermal tumours: An association of CA IX with poor prognosis. *BMC Cancer* **2010**, *10*, 148. [CrossRef]
35. Nortunen, M.; Huhta, H.; Helminen, O.; Parkkila, S.; Kauppila, J.H.; Karttunen, T.J.; Saarnio, J. Carbonic anhydrases II, IX, and XII in Barrett's esophagus and adenocarcinoma. *Virchows Arch.* **2018**, *473*, 567–575. [CrossRef] [PubMed]
36. Păunescu, T.G.; Jones, A.C.; Tyszkowski, R.; Brown, D. V-ATPase expression in the mouse olfactory epithelium. *Am. J. Physiol.-Cell Physiol.* **2008**, *295*, C923–C930. [CrossRef]
37. Das, A.; Banik, N.L.; Ray, S.K. Modulatory effects of acetazolamide and dexamethasone on temozolomide mediated apoptosis in human glioblastoma T98G and U87MG Cells. *Cancer Investig.* **2008**, *26*, 352–358. [CrossRef]
38. Amiri, A.; Le, P.U.; Moquin, A.; Machkalyan, G.; Petrecca, K.; Gillard, J.W.; Yoganathan, N.; Maysinger, D. Inhibition of carbonic anhydrase IX in glioblastoma multiforme. *Eur. J. Pharm. Biopharm.* **2016**, *109*, 81–92. [CrossRef]
39. Proescholdt, M.A.; Merrill, M.J.; Stoerr, E.-M.; Lohmeier, A.; Pohl, F.; Brawanski, A. Function of carbonic anhydrase IX in glioblastoma multiforme. *Neuro-Oncology* **2012**, *14*, 1357–1366. [CrossRef]
40. Escamilla-Ramírez, A.; Castillo-Rodríguez, R.A.; Zavala-Vega, S.; Jimenez-Farfan, D.; Anaya-Rubio, I.; Briseño, E.; Palencia, G.; Guevara, P.; Cruz-Salgado, A.; Sotelo, J.; et al. Autophagy as a potential therapy for malignant glioma. *Pharmaceuticals* **2020**, *13*, 156. [CrossRef]

41. Gul, H.I.; Yamali, C.; Bulbuller, M.; Kirmizibayrak, P.B.; Gul, M.; Angeli, A.; Bua, S.; Supuran, C.T. Anticancer effects of new dibenzenesulfonamides by inducing apoptosis and autophagy pathways and their carbonic anhydrase inhibitory effects on hCA I, hCA II, hCA IX, hCA XII isoenzymes. *Bioorg. Chem.* **2018**, *78*, 290–297. [CrossRef]
42. Mohammadpour, R.; Safarian, S.; Ejeian, F.; Sheikholya-Lavasani, Z.; Abdolmohammadi, M.H.; Sheinabi, N. Acetazolamide triggers death inducing autophagy in T-47 D breast cancer cells. *Cell Biol. Int.* **2014**, *38*, 228–238. [CrossRef] [PubMed]
43. Greig, S.L.; Deeks, E.D. Brinzolamide/Brimonidine: A review of its use in patients with open-angle glaucoma or ocular hypertension. *Drugs Aging* **2015**, *32*, 251–260. [CrossRef] [PubMed]
44. Hoffmann, L.; Waclawczyk, M.S.; Tang, S.; Hanschmann, E.-M.; Gellert, M.; Rust, M.B.; Culmsee, C. Cofilin1 oxidation links oxidative distress to mitochondrial demise and neuronal cell death. *Cell Death Dis.* **2021**, *12*, 953. [CrossRef] [PubMed]

The Metalloprotease-Disintegrin ADAM8 Alters the Tumor Suppressor miR-181a-5p Expression Profile in Glioblastoma Thereby Contributing to Its Aggressiveness

Agnes Schäfer[1†], Lara Evers[1†], Lara Meier[1], Uwe Schlomann[1], Miriam H. A. Bopp[1,2], Gian-Luca Dreizner[1], Olivia Lassmann[1], Aaron Ben Bacha[1], Andreea-Cristina Benescu[1], Mirza Pojskic[1], Christian Preußer[3], Elke Pogge von Strandmann[3], Barbara Carl[1], Christopher Nimsky[1,2] and Jörg W. Bartsch[1,2*]

[1] Department of Neurosurgery, Philipps University Marburg, Marburg, Germany, [2] Marburg Center for Mind, Brain and Behavior (MCMBB), Marburg, Germany, [3] Core Facility Extracellular Vesicles, Philipps University of Marburg – Medical Faculty, Marburg, Germany

Glioblastoma (GBM) as the most common and aggressive brain tumor is characterized by genetic heterogeneity, invasiveness, radio-/chemoresistance, and occurrence of GBM stem-like cells. The metalloprotease-disintegrin ADAM8 is highly expressed in GBM tumor and immune cells and correlates with poor survival. In GBM, ADAM8 affects intracellular kinase signaling and increases expression levels of osteopontin/SPP1 and matrix metalloproteinase 9 (MMP9) by an unknown mechanism. Here we explored whether microRNA (miRNA) expression levels could be regulators of MMP9 expression in GBM cells expressing ADAM8. Initially, we identified several miRNAs as dysregulated in ADAM8-deficient U87 GBM cells. Among these, the tumor suppressor miR-181a-5p was significantly upregulated in ADAM8 knockout clones. By inhibiting kinase signaling, we found that ADAM8 downregulates expression of miR-181a-5p *via* activation of signal transducer and activator of transcription 3 (STAT3) and mitogen-activated protein kinase (MAPK) signaling suggesting an ADAM8-dependent silencing of miR-181a-5p. In turn, mimic miR-181a-5p transfection caused decreased cell proliferation and lower MMP9 expression in GBM cells. Furthermore, miR-181a-5p was detected in GBM cell-derived extracellular vesicles (EVs) as well as patient serum-derived EVs. We identified miR-181a-5p downregulating MMP9 expression *via* targeting the MAPK pathway. Analysis of patient tissue samples (n=22) revealed that in GBM, miR-181a-5p is strongly downregulated compared to *ADAM8* and *MMP9* mRNA expression, even in localized tumor areas. Taken together, we provide evidence for a functional axis involving ADAM8/miR-181a-5p/ MAPK/MMP9 in GBM tumor cells.

Keywords: glioblastoma, tumor microenvironment, extracellular vesicles, miRNA, MR spectroscopy, ADAM8, miR-181a-5p, MMP9

85

INTRODUCTION

Glioblastoma multiforme (GBM) is the most common malignant primary brain tumor in adults. Despite a standard multimodal therapeutic strategy combining maximum safe surgical resection and radio-/chemotherapy with temozolomide, the median survival remains low between 12 and 15 months (1). To improve the poor prognosis of GBM patients it is crucial to identify new therapeutic targets and their underlying dysregulated signaling pathways.

GBM is characterized as a highly invasive, heterogeneously composed, and rapidly growing tumor (2). At the molecular level, a disintegrin and metalloproteinases (ADAMs) mediate tumor cell adhesion and migration as well as intracellular signaling (3). One such proteolytically active family member is the metalloproteinase-disintegrin 8 (ADAM8), strongly associated with tumor aggressiveness, progression, and reduced survival in various cancers including breast cancer, pancreatic ductal adenocarcinoma (PDAC), and GBM (4–7). ADAM8, in particular, the cytoplasmic domain (CD) and the disintegrin/cysteine-rich domain (DC) can activate central signaling pathways in carcinogenesis. First, ADAM8 activates the mitogen-activated protein kinase (MAPK) signaling cascade, epidermal growth factor receptor (EGFR) independently (8, 9). Second, ADAM8 mediates angiogenesis by inducing the expression of osteopontin (SPP1) via STAT3 signaling (10). Moreover, ADAM8 interacts with integrin ß1 (ITGB1) and thereby activates its downstream targets focal adhesion kinase (FAK), and the PI3K/AKT pathway (9, 11). Interestingly, ADAM8 dependent activation of the MAPK pathway as well the PI3K/AKT pathway enhanced temozolomide-chemoresistance in GBM cell lines (12). Considering these diverse functions of ADAM8 in intracellular signaling, we and others hypothesized that ADAM8 mediates these functions through the regulation of microRNAs and indeed, initial evidence came from a study in MDA-MB-231 breast cancer cells showing that ADAM8 regulates expression levels of miR-720 (13).

MicroRNAs (miRNAs) are small non-coding RNA molecules that regulate protein expression on a post-transcriptional level by binding and thereby silencing their target messenger RNAs (mRNAs) (14). In most cases, miRNAs lead to translational repression or even degradation of their specific target mRNAs (15). Therefore, dysregulated miRNA expression profiles alter many critical pathways related to cancer progression (16). Consequently, in GBM, a large number of miRNAs are reported to be dysregulated (17, 18). In GBM, miR-181a-5p is downregulated and functions as a tumor suppressor miRNA that inhibits the translation of oncogenic proteins that are linked to tumor progression such as osteopontin (SPP1) (19–21). This type of sialoprotein is highly expressed in GBM and plays a key role in tumor-tumor microenvironment communication by attracting macrophages and mediating their immune response (22). Furthermore, miR-181a-5p regulates cell apoptosis and cell colony formation by targeting B-cell lymphoma 2 (BCL-2), so that high expression levels of miR-181a-5p can induce radiosensitivity of U87 GBM cells (23, 24). In addition, miR-

181a-5p contains inhibitory binding sites to members of the MAPK family and its downstream targets, namely mitogen-activated protein kinase kinase 1 (MEK1), cAMP response element-binding protein 1 (CREB-1), and extracellular signal-regulated kinase 2 (ERK2) (25, 26). Given an important functional role in GBM, the signaling pathways regulating miR-181a-5p itself, however, remain unclear.

Matrix metalloproteinase 9 (MMP9), a zinc-dependent endopeptidase, plays a central role in the process of tumor cell migration, infiltration, and metastasis (27). Matrix metalloproteinases degrade extracellular matrix molecules and basement membrane components and thereby contribute to glioma progression (28). Consequently, MMP9 is upregulated in GBM compared to its expression in the normal brain parenchyma (29). Gliomas that display high MMP9 levels are associated with an aggressive course and are linked to reduced survival (30). Previous studies demonstrated that MMP9 expression can be elevated via MAPK-signaling (31, 32). ADAM8 and MMP9 levels are correlated in GBM tissue samples as well breast cancer-derived brain metastasis (8, 33). Whether MMP9 can be directly targeted by miR-181a-5p or indirectly via miR-181a-5p induced downregulation of the MAPK pathway has not been explored yet.

Cancer invasion is closely associated with the interaction of infiltrating tumor cells and the tumor microenvironment (TME) (34). As a means of communication, extracellular vesicles (EVs) are secreted by tumor cells as well as by cells of the TME. Their cargo contains lipids and proteins as well as nucleic acids including miRNAs (35). Because EVs modulate tumor growth, immune-escape, and tumor cell niche formation, they function as central regulators of the TME (34).

In the current work, we explored the mechanism by which ADAM8 modulates intracellular and extracellular signaling through the regulation of miR-181a-5p expression and uncovered MMP9 as a miR-181a-5p dependent target gene in GBM.

MATERIAL AND METHODS

Patient Specimens

In accordance with the local ethics committee (Philipps University Marburg, medical faculty, file number 185/11), tumor tissue samples of GBM patients were obtained during surgical resection and serum specimens were collected one to three days prior and three to five days after surgical resection. Each patient gave written informed consent before resection. Tissue samples were shock frozen in liquid nitrogen and then stored at -80°C. Serum samples were centrifuged at 2,000 g for 10 min prior to storage at -80°C. All included tissue and serum samples were from primary, isocitrate dehydrogenase (IDH) wild-type GBM tumors, further patient information and histopathological characteristics are summarized in **Table 1**. In three cases, we analyzed the expression of miR-181a-5p in serum-derived EVs at the time of initial manifestation and tumor recurrence (Patient 9, 23, 24 in **Table 1**).

TABLE 1 | Clinical data on patient included tumor tissue samples showed isocitrate dehydrogenase (IDH) wild-type expression.

Number	Age at diagnosis (years)	Sex	Tumor localization	Type of resection	MGMT promoter meth ylation	EGFR vIII	Ki67-Li	Survival (days)
1	71	m	Septum pellucidum	Subtotal	Methylated	–	Up to 30%	114
2	65	m	Left parietal lobe	Subtotal	Not methylated	+	Up to 40%	119
3	77	w	Right frontal lobe	Subtotal	Methylated	–	Up to 20%	79
4	75	m	Right temporal and parietal lobe	Subtotal	Methylated	–	10%	476
5	63	w	Left frontal lobe	Subtotal	Methylated	–	Up to 30%	76
6	87	m	Right parietal and occipital lobe	Gross Total	Methylated	++	5%	135
7	78	w	Butterfly glioma, predominantly right frontal lobe	Subtotal	Not methylated	unknown	20%	63
8	66	m	Left frontal lobe	Subtotal	Methylated	–	25%	49
9*	66	m	Right occipital lobe	Gross total	Not methylated	+	20%	336
10	65	w	Left temporal lobe	Subtotal	Not methylated	–	Up to 15%	84
11	70	w	Left frontal lobe	Subtotal	Methylated	+	Up to 25%	278
12	61	m	Right temporal lobe	Gross total	Methylated	–	30%	626
13	64	w	Right frontal and temporal lobe	Gross total	Methylated	–	20%	930
14	65	m	Left temporal lobe	Subtotal	Methylated	–	30%	579
15	66	m	Right temporal lobe and right Insula	Subtotal	Methylated	–	Up to 20%	126
16	61	m	Left temporal lobe	Gross total	Not methylated	–	50%	398
17	57	w	Right frontal lobe	Gross total	Weakly methylated	+	20%	410
18	62	m	Right temporal and parietal lobe	Gross total	Not methylated	–	Up to 20%	457
19	56	m	Left temporal lobe	Gross total	Methylated	–	20%	578
20	69	m	Right parietal and occipital lobe	Gross total	Weakly methylated	–	Up to 50%	388
21	61	m	Right frontal lobe	Gross total	Weakly methylated	–	30%	94
22	76	m	Right frontal lobe	Gross total	Not methylated	–	30%	225
23*	76	f	Left parietal	Gross total	Methylated	–	20%	unknown
24*	54	m	Right frontal lobe	Gross total	Methylated	–	30%	450
25	74	f	Left parietal lobe	Gross total	Methylated	–	40%	unknown

*Only initial manifested primary glioblastomas were included. Here, we show further parameters regarding the patient cohort including age at diagnosis, sex, survival in days, and type of surgical resection (gross total or subtotal). Furthermore, histopathological data such as methylation status of the O^6-methylguanine-DNA-methyltransferase (MGMT), Ki67-Labelling index (Ki67-Li), and expression of epidermal growth factor variant III (EGFRvIII) are presented here. Patients' 1 to 22 tissue samples were analyzed for miR-181a-5p, ADAM8, and MMP9 mRNA expression (**Figures 5A–D**), matched samples (initial and recurrence GBM) from patients 9, 23, and 24 (*) were used for serum-EV separation and analysis (**Figures 5H–J**) and patient 25 was used for the analysis via MR-spectroscopy (**Figures 5E–G**).*

Cell Culture

Established GBM cell lines U87 and U251 were purchased from the American Type Culture Collection (ATCC) and cell lines G112 and G28 were obtained from the Westphal Lab (UKE Hamburg). All GBM cell lines were cultivated in Dulbecco's modified Eagle's medium (DMEM) high glucose (4.5 g/L) phenol red (Capricorn Scientific, Germany), supplemented with 10% fetal calf serum (FCS, S0615, Sigma, Germany), 1% penicillin/streptomycin (2321115, Gibco, US), 1% sodium pyruvate (NPY-B, Capricorn Scientific, Germany) and 1% non-essential amino acids (11140050, Gibco, US). Primary GBM cell lines and primary glioblastoma stem-like cells (GSCs) were obtained during surgical resection. The isolation and preparation process of GSCs and primary differentiated patient-derived GBM tumor cells were each described previously by our group (12, 36). GSC lines 2017/151, 2017/74, and 2016/240 were cultivated in DMEM/F12 (DMEM-12-A, Capricorn Scientific, Germany) and supplemented with 2% B27 supplement (117504044, Gibco, US), 1% amphotericin (152290026, Gibco,

US), 0.5% HEPES (H0887, Sigma, Taufkirchen, Germany) and 0.1% Gentamycin (A2712, Biochrom, Germany). Moreover, a final concentration of 0.02 ng/μL EGF (100-18B, Peprotech, Germany) and bFGF (315-09, Peprotech, Germany) was added, and GSCs were cultivated in non-cell-culture-treated petri dishes. Primary differentiated GBM cell lines GBM98, GBM42, and GBM29 were cultivated in DMEM high glucose (4.5 g/L) without phenol red (Capricorn Scientific, Germany) supplemented with 10% FCS (S0615, Sigma, Germany), 1% penicillin/streptomycin (2321115, Gibco, US), 1 mM sodium pyruvate (NPY-B, Capricorn Scientific, Germany), 1% L-glutamine (200 mM) (25030-024, Gibco, US) and 1% non-essential amino acids (11140050, Gibco, US). All cell lines were cultured in a humidified atmosphere at 37°C under 5% CO_2.

Generation of Stable U87 CRISPR/Cas9 ADAM8 KO (KO) Clones

U87 cells were transfected with two different gRNAs using the CRISPR/Cas9 knockout/knockin kit from OriGene (#

KN213386) as described previously (37). Cell clones were selected by treatment with antibiotics (1 mg/ml puromycin). The ADAM8 knockout was confirmed through RT-qPCR, western blot, and ELISA analysis. U87 wild-type cells were used as control cells.

Transient Transfection to Induce an ADAM8 Rescue in U87 ADAM8 KO Cells

To rescue ADAM8 in U87 ADAM8 KO clones, cells were seeded in 6-well-plates at a density of 500,000 cells in 2 ml. After 24 h, the transfection was performed with either ADAM8 lacking the cytoplasmatic domain or the full-length ADAM8 using LTX Lipofectamine (Invitrogen) according to the manufacturer's instructions. Cells were harvested and analyzed by RT-qPCR and western blot after 48 h of transfection.

MiR-181a-5p Mimic Transfection

To transiently overexpress miR-181a-5p, U87 cells were seeded in 6-well-plates at a density of 400,000 cells in 2 ml and were transfected with 0.01 µM miR-181a-5p mimic (miScript, Qiagen) after 24 h. 0.01 µM ON-TARGET *plus* non-targeting Control Pool (Dharmacon, US) was used as control RNA. Transfection was performed utilizing Lipofectamine RNAimax (Invitrogen, UK) according to the manufacturer's instructions. After 24 h, the transfection was repeated. Transfected cells and their controls were harvested 48 h after the second transfection. To evaluate the success of transfection, miRNA expression was analyzed by RT-qPCR.

Inhibitors

Batimastat was used as a broad-spectrum MMP-inhibitor and was purchased from Tocris (Biotechne, Wiesbaden, Germany). As a specific ADAM8-inhibitor, BK-1361 (Peptide 2.0) was utilized and described by our group previously (9). WP´066 (Sigma Aldrich, US) was used as a JAK2/STAT3 inhibitor. Cells were seeded in a 6-well-format (500,000 cells in 2 ml) and harvested 16 h after treatment with inhibitors. The concentrations used are indicated in the graphs.

Separation of Extracellular Vesicles (EVs)

EVs were separated from cellular supernatants and GBM patients' serum samples *via* sequential ultracentrifugation. Cells were incubated with 30 ml DMEM supplemented with 1% L-glutamine (200 mM), 1% penicillin/streptomycin, 1 mM sodium pyruvate solution, and 1% nonessential amino acids for 48 h. Prior to EV separation, serum samples were diluted 1:3 with HBSS (Gibco™, Life Technologies, US) (500 µl serum diluted with 1 ml HBSS). The conditioned medium and the diluted serum sample were centrifuged first at 2,000 g for 10 min at RT and then at 10,000 g for 60 min at 4°C. After a subsequent filtration (0.2 µm filter), EVs were pelleted *via* high-speed centrifugation at 100,000 g for 90 min at 4°C using an Optima XPN-80 ultracentrifuge (Beckman Coulter, Germany). Next, the EV pellet was washed with HBSS at 100,000 g for 90 min at 4°C using the Optima MAX-XP (Beckman Coulter, Germany) ultracentrifuge with a TLA-55 fixed angle rotor. EVs were resuspended in 50 µl HBSS and stored at -80°C until further

use. A 5 µl aliquot was sent to the FACS Core Facility, Marburg, for determining the size and concentration of the particles by usage of nano-flow cytometry (NanoFCM Co. Ltd., Nottingham, UK).

Real-Time Quantitative Polymerase Chain Reaction (qPCR)

Total RNA with an enriched fraction of miRNAs from tumor tissue samples and cellular pellets was isolated using the miRNeasy Tissue/Cells Advanced Mini Kit (217684, Qiagen, Germany) according to the manufacturer's instructions. To quantify the miRNA expression in cells, miRCURY LNA RT Kit (Cat. Number 339340, Qiagen, Germany) and miRCURY LNA SYBR® Green PCR Kit (Cat. Number 339345, Qiagen, Germany) were used according to manufacturer's instructions. YP00203_U6 snRNA miRCURY LNA PCR Assay (YP00203907, Qiagen, Germany) and miRCURY miRNA Assay hsa-181a-5p (YP00206081, Qiagen, Germany) was used for the quantification of relative miR-181a-5p expression. In the case of tissue samples (**Figure 5**), miScript II RT Kit (218161, Qiagen, Germany) and miScript SYBR Green PCR Kit (218073, Qiagen, Germany) were used according to the manufacturer's protocols. Here, Hs_RNU6-2_11 miScript Primer Assay (MS00033740, Qiagen, Germany) and Hs_miR-181a_2 miScript Primer Assay (MS00008827, Qiagen, Germany) were used. To assess gene expression on an mRNA level, RNA was reverse transcribed with RNA to cDNA EcoDry™ Premix (Takara Bio. Inc.). Quantitative real-time PCR was performed with iTaq™ Universal SYBR Green Supermix (Bio-rad Laboratories GmbH, US). QuantiTect Primer Assay (Qiagen) or forward and reverse primer were used in a total reaction volume of 20 µl. XS13 was used as a housekeeping gene. All PCR experiments were performed on the Applied Biosystems StepOnePlus Real-time PCR system (Thermo Fisher Scientific, US). Relative gene expression was calculated utilizing either the $2^{-\Delta Ct}$- or the $2^{-\Delta\Delta Ct}$-method as indicated.

MiRNA PCR Array – Human Finder

A pathway-focused miRNA PCR Array/Human Finder (331221 miScript, MIHS-001ZC, Qiagen, Germany) was conducted according to the manufacturer's instructions. Data analysis was performed with the online miScript miRNA Data Analysis program from Qiagen using the $2^{-\Delta\Delta Ct}$-method. Results are presented in a heatmap.

Protein Extraction and Western Blot Analysis

Cells were washed with PBS (Sigma-Aldrich, US) and detached by cell scraping. Whole cell lysates were homogenized by an incubation for 30 min in RIPA buffer (50 mM HEPES pH 7.4; 150 mM NaCl; 1% (v/v) NP-40; 0.5% (w/v) Natriumdeoxycholate; 0.1% (w/v) SDS; 10 mM Phenantrolin; 10 mM EDTA; Pierce™ Protease Inhibitor Mini Tablets, EDTA-free, Thermo Fisher Scientific; Pierce™ Phosphatase Inhibitor Mini Tablets, Thermo Fisher Scientific). Protein samples or EVs in a concentration of 1.5×10^9 particles were prepared in 5x Laemmli buffer [60 mM Tris-HCl pH

6.8; 2% (w/v) SDS; 10% (w/v) Glycerol; 5% (v/v) ß-Mercaptoethanol; 0.01% (w/v) Bromophenol-Blue] and 10x NuPAGE™ sample reducing reagent (Thermo Fisher Scientific, US) and denatured at 95°C for 5 min before SDS PAGE. For this, a 10% SDS polyacrylamide gel was used. Separated proteins were transferred on nitrocellulose membranes (A29591442, GE Healthcare Life science, Germany) followed by blocking in 5% (w/v) milk powder (MP) in TBST (50 mM Tris, pH 7.5; 150 mM NaCl; 0.1% (w/v) Tween-20) for 1 h. The detection of proteins was performed utilizing the following primary antibodies diluted as indicated in 5% MP in TBST: anti-ADAM8 (PA5-47047, Thermo Fisher Scientific, 1:1000), anti-MMP9 (IM09L, Calbiochem, 1:1,000), anti- β-Tubulin (NB600-936, Novus Biological, 1:2,000) anti-EGFR (4267, Cell Signaling, 1:1,000), anti-pEGFR (3777, Cell Signaling, 1:1,000), anti-MAPK (4696, Cell Signaling, 1:2,000), anti-pMAPK (4370, Cell Signaling, 1:2000), anti-CALNEXIN (2679, Cell Signaling, 1:1,000), anti-FLOTILLIN-1 (PA5-18053, Thermo Scientific, 1:2,000) anti-CD81 (sc166029, Santa Cruz, 1:500), anti-STAT3 (ab68153, Abcam, 1:5,000), anti-pSTAT3 (ab76315, Abcam, 1:5,000), anti-CREB-1 (H74) (sc-25785, Santa Cruz, 1:500 in 5% MP) and anti-pCREB-1(Ser133) (4276, Cell Signaling, 1:1000 in 5% BSA in TBST). Nitrocellulose membranes were incubated with primary antibodies at 4°C overnight. After washing three times with TBST, membranes were incubated with horseradish peroxidase (HRP) conjugated antibodies (Abcam, 1:5,000) for 1 h followed by a next washing step. Chemiluminescence detection was performed by adding Western Bright Sirius substrate (Advansta, US) and using the ChemiDoc MP Imaging System (Bio-rad Laboratories GmbH, US). Western blots were quantified using Image J (NIH, Maryland).

Enzyme-Linked Immunosorbent Assay (ELISA)

Soluble ADAM8 (DY1031, R&D Systems, UK) and soluble MMP9 (DY911, R&D Systems, UK) from cell culture supernatants were determined by Sandwich-ELISA method with DuoSet ELISA Kits. All ELISA experiments were performed according to the manufacturer's instructions.

Proliferation Assay

The proliferation and survival effects on U87 cells were determined using CellTiter-Glo 3D cell viability assay (G7571, Promega, Germany). Cells were seeded in triplicates on a 96-well plate. After 24 h, miR-181a-5p mimic was transfected according to section 2.5. After 48 h, 50 µl of CellTiter-Glo 3D Reagent was added to each well and mixed while shaking for 15 min. After an additional 15 min without shaking avoiding light, Luminescence was measured with a Microplate Reader luminometer (FLUOstar OPTIMA Microplate Reader, BMG Labtech, Germany).

Spectroscopy

A T2-weighted magnetic resonance (MR) tomography together with 1H-MR spectroscopy was performed on a 3T MR System (Trio, Siemens, Erlangen, Germany) for in detail analyses of tumor heterogeneity in patient 25. Thereby, a navigated extraction of tissue samples by co-registration of MR data and

integration into the neuronavigation system (Curve Ceiling-Mounted, Brainlab, Munich, Germany) was enabled.
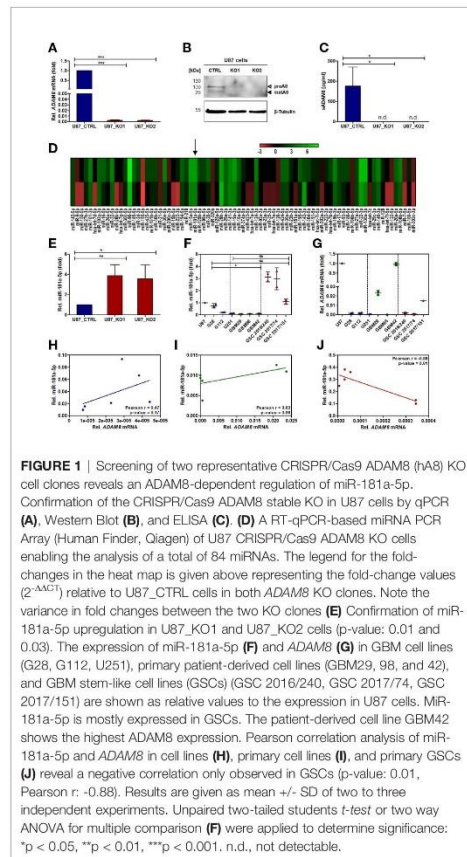
Statistical Analysis

Student's t-tests were applied for statistical analysis. For multiple comparisons, two-way ANOVA tests were used. A Wilcoxon-signed rank test and Pearson correlation were performed to determine differences or correlation in gene expression. Results were considered as not significant (ns) ($p > 0.05$), significant (*) ($p < 0.05$), highly significant (**) ($p < 0.01$), or very highly significant (***) ($p < 0.001$). Data from multiple replicates are presented as mean ± SD and statistical analyses were performed with GraphPad Prism (version 9.1.0) and Microsoft Excel.

RESULTS

ADAM8 Regulates Expression Levels of miR-181a-5p in GBM Cells

To determine potential ADAM8 correlated miRNAs, we generated stable ADAM8 knockout (KO) U87 cell clones using two guide RNAs (U87 gRNA cl. 1, U87 gRNA cl. 2) for the CRISPR/Cas9 homologous recombination method. U87 cells expressing high endogenous levels of ADAM8 were subjected to CRISPR/Cas9 induced genomic editing. After cell selection with puromycin, independent cell clones were grown and compared to U87 cells (in the following termed U87_CTRL) for morphological features and ADAM8 expression levels. From around 30 individual cell clones, two U87 gRNA clones were selected for further analyses (**Supplementary Figure 1**). Confirmation of successful ADAM8 knockout in these two U87 gRNA cell clones was provided by qPCR, Western Blot, and ELISA (**Figures 1A–C**). U87 gRNA cl. 1 and U87 gRNA cl. 2 (termed U87_KO1 and U87_KO2) showed a strong downregulation of *ADAM8* mRNA compared to U87_CTRL, $p < 0.001$ (**Figure 1A**). Western Blots confirmed successful ADAM8 knockout on the protein level (**Figure 1B**). In addition, ELISA measurements from cell supernatants revealed soluble ADAM8 levels below the detection limit in U87_KO clones compared to U87_CTRL ($p < 0.05$, **Figure 1C**). For two representative KO clones as well as a U87 control clone, a microRNA PCR Array (Human Finder) was screened. Differences in miRNA expression (given a ratio KO/CTRL) for both U87_KO clones are presented in a heatmap (**Figure 1D**) with green color representing upregulation of miRNA in U87_KO cells.

Several miRNAs were consistently upregulated in both KO clones and miR-181a-5p was selected for further investigations due to its reported regulation of osteopontin/SPP1 which also applies to ADAM8. Moreover, of all four miRNAs upregulated in U87 *ADAM8* KO cells, miR-181a-5p was the only one regulated after treatment of U87 wild-type cells with an ERK1/2 inhibitor indicating its influence in ADAM8-mediated signaling (**Supplementary Figure 2**). To further validate our miRNA screening, qPCR experiments were performed to detect miR-181a-5p expression in U87_KO and U87_CTRL cells. We

FIGURE 1 | Screening of two representative CRISPR/Cas9 ADAM8 (hA8) KO cell clones reveals an ADAM8-dependent regulation of miR-181a-5p. Confirmation of the CRISPR/Cas9 ADAM8 stable KO in U87 cells by qPCR **(A)**, Western Blot **(B)**, and ELISA **(C)**. **(D)** A RT-qPCR-based miRNA PCR Array (Human Finder, Qiagen) of U87 CRISPR/Cas9 ADAM8 KO cells enabling the analysis of a total of 84 miRNAs. The legend for the fold-changes in the heat map is given above representing the fold-change values ($2^{-\Delta\Delta CT}$) relative to U87_CTRL cells in both *ADAM8* KO clones. Note the variance in fold changes between the two KO clones **(E)** Confirmation of miR-181a-5p upregulation in U87_KO1 and U87_KO2 cells (p-value: 0.01 and 0.03). The expression of miR-181a-5p **(F)** and *ADAM8* **(G)** in GBM cell lines (G28, G112, U251), primary patient-derived cell lines (GBM29, 98, and 42), and GBM stem-like cell lines (GSCs) (GSC 2016/240, GSC 2017/74, GSC 2017/151) are shown as relative values to the expression in U87. MiR-181a-5p is mostly expressed in GSCs. The patient-derived cell line GBM42 shows the highest ADAM8 expression. Pearson correlation analysis of miR-181a-5p and *ADAM8* in cell lines **(H)**, primary cell lines **(I)**, and primary GSCs **(J)** reveal a negative correlation only observed in GSCs (p-value: 0.01, Pearson r: -0.88). Results are given as mean +/- SD of two to three independent experiments. Unpaired two-tailed students *t-test* or two way ANOVA for multiple comparison **(F)** were applied to determine significance: *p < 0.05, **p < 0.01, ***p < 0.001. n.d., not detectable.

confirmed upregulation of miR-181a-5p in U87_KO1 and U87_KO2 compared to U87_CTRL cells, p < 0.05 and p < 0.01, respectively (**Figure 1E**).

Next, we analyzed the expression profiles of ADAM8 and miR-181a-5p in several GBM cell lines, including U87, U251, G112, G28, three primary patient-derived cell lines GBM42, GBM29, GBM98, and three patient-derived Glioblastoma stem-like cell lines (GSCs), 2016/240, 2017/151 and 2017/74 (**Figures 1F, G**). GSCs showed low ADAM8 mRNA and high miR-181a-5p expression levels. Primary GBM cell lines showed great variability in ADAM8 and miR-181a-5p expression with GBM42 with the highest ADAM8 levels. Interestingly, knocking ADAM8 down with siRNA showed elevated levels of miR-181a-5p in GBM42 (**Supplementary Figure 3**). Pearson correlation analyses revealed exclusively in the case of GSCs a clear negative correlation of ADAM8 and miR-181a-5p expression (**Figures 1H–J**). U87_CTRL

cells as well as primary GBM42 cells showed the highest endogenous ADAM8 levels in qPCR experiments compared to all other cell lines and were selected for further experiments.

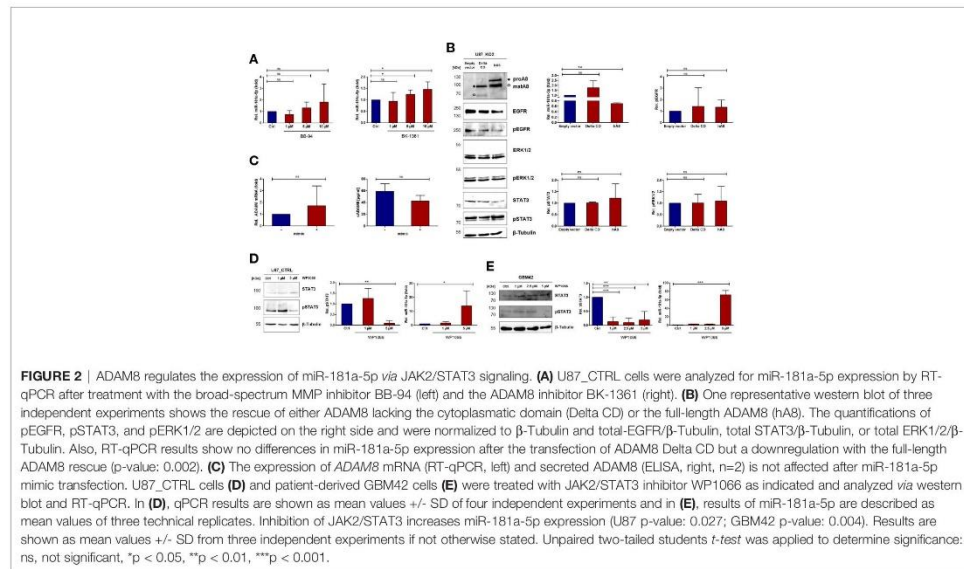## ADAM8 Regulates miR-181a-5p Expression *via* STAT3 and MAPK Signaling

To analyze the apparent ADAM8/miR-181a-5p dependence on the mechanistic level, we tested the contribution of either the metalloprotease activity or the functions of the non-proteolytic domains (DC/CD) of ADAM8 on miR-181a-5p expression. To address this, U87 cells were treated with either a broad-range metalloprotease inhibitor BB-94 (Batimastat) or with BK-1361, a selective ADAM8 inhibitor. While BB-94 did not affect miR-181a-5p expression, treatment with 10 μM and even 5 μM BK-1361 led to an increase in miR-181a-5p expression, p < 0.05 (**Figure 2A**) suggesting a contribution of the DC/CD domain on miR-181a-5p regulation by ADAM8. Moreover, we transiently re-expressed ADAM8 in U87_KO1 and analyzed the effect on miR-181a-5p expression. U87 gRNA_KO2 was transfected with either wild-type ADAM8 (hA8) or with an ADAM8 variant lacking the cytoplasmic domain (Delta CD). Western Blots confirmed re-expression of ADAM8 variants (**Figure 2B**).

Re-expression of wild-type ADAM8 caused a downregulation of miR-181a-5p, p < 0.01 (**Figure 2B**). In contrast, cells expressing the ADAM8 delta CD variant showed no downregulation of miR-181a-5p (**Figure 2B**). These results indicate that the cytoplasmic domain of ADAM8 triggers signaling cascades that lead to the downregulation of miR-181a-5p concomitant with a trend of increased pSTAT3 in cells transfected with wild-type ADAM8 (**Figure 2B**). Interestingly, this regulation only works in one direction, as changes in miR-181a-5p expression, i.e. by mimic transfection, do not affect expression levels of ADAM8 in U87 cells (**Figure 2C**). We explored the role of two downstream signaling pathways of ADAM8 CD, STAT3 signaling and MAPK signaling. For this purpose, U87 cells and primary GBM cells GBM42 were treated with either U0126 (MEK1/2 inhibitor) or WP1066 (STAT3 inhibitor). MEK1/2 inhibition caused an increase in miR-181a-5p expression in U87_CTRL cells (p < 0.05), and a tendency to increase in primary GBM42 cells (p-value: 0.052) (**Supplementary Figure 4**). More prominently, STAT3 inhibition by WP1066 was confirmed for both cell lines *via* western blot and resulted in increased expression levels of miR-181a-5p in both cell lines with p < 0.05 (**Figures 2D, E**).

MiR-181a-5p Regulates Cell Proliferation and MMP9 Expression

We further analyzed whether miR-181a-5p can affect the cell proliferation of GBM cells. Exemplified for U87_KO2, a decrease in cell proliferation was observed (p < 0.001, **Figure 3A**). This effect can be recapitulated when mimic miR-181a-5p was transfected into U87 cells (p < 0.01, **Figure 3B**). As an oncoprotein able to promote GBM cell proliferation, we analyzed *MMP9* expression in U87_KO2 and mimic transfected U87 cells (**Figures 3C, D**) (27). *MMP9* mRNA levels in U87_KO2 and mimic transfected cells are strongly downregulated as revealed by qPCR (p < 0.001, **Figure 3C**).
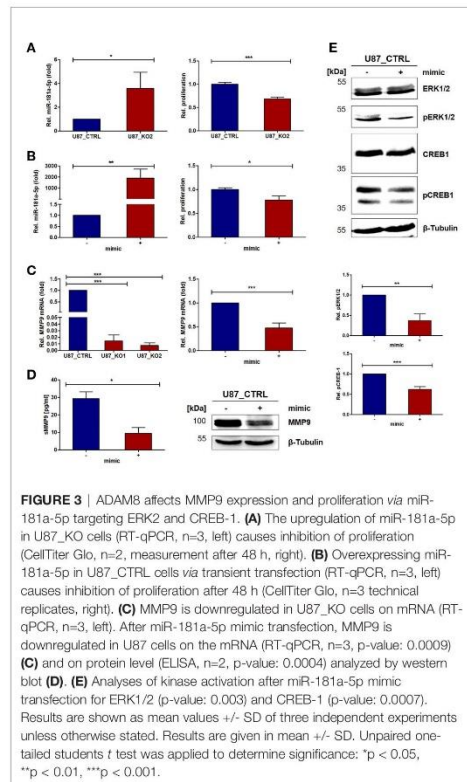
FIGURE 2 | ADAM8 regulates the expression of miR-181a-5p *via* JAK2/STAT3 signaling. **(A)** U87_CTRL cells were analyzed for miR-181a-5p expression by RT-qPCR after treatment with the broad-spectrum MMP inhibitor BB-94 (left) and the ADAM8 inhibitor BK-1361 (right). **(B)** One representative western blot of three independent experiments shows the rescue of either ADAM8 lacking the cytoplasmatic domain (Delta CD) or the full-length ADAM8 (hA8). The quantifications of pEGFR, pSTAT3, and pERK1/2 are depicted on the right side and were normalized to β-Tubulin and total-EGFR/β-Tubulin, total STAT3/β-Tubulin, or total ERK1/2/β-Tubulin. Also, RT-qPCR results show no differences in miR-181a-5p expression after the transfection of ADAM8 Delta CD but a downregulation with the full-length ADAM8 rescue (p-value: 0.002). **(C)** The expression of *ADAM8* mRNA (RT-qPCR, left) and secreted ADAM8 (ELISA, right, n=2) is not affected after miR-181a-5p mimic transfection. U87_CTRL cells **(D)** and patient-derived GBM42 cells **(E)** were treated with JAK2/STAT3 inhibitor WP1066 as indicated and analyzed *via* western blot and RT-qPCR. In **(D)**, qPCR results are shown as mean values +/- SD of four independent experiments and in **(E)**, results of miR-181a-5p are described as mean values of three technical replicates. Inhibition of JAK2/STAT3 increases miR-181a-5p expression (U87 p-value: 0.027; GBM42 p-value: 0.004). Results are shown as mean values +/- SD from three independent experiments if not otherwise stated. Unpaired two-tailed students *t-test* was applied to determine significance: ns, not significant, *p < 0.05, **p < 0.01, ***p < 0.001.

After mimic miR-181a-5p transfection of U87 cells, ELISA experiments revealed less soluble MMP9 levels in cellular supernatants (p < 0.05, **Figure 3D**). Comparable results were obtained for osteopontin (**Supplementary Figure 7**). Next, we explored whether miR-181a-5p dependent MMP9 downregulation is a result of direct miR-181-a/*MMP9* mRNA interaction. Three target prediction tools, miRDB, TargetScan, and TargetMiner, predicted no miR-181a-5p binding site. Also, bioinformatic analysis of the MMP9 3' UTR did not reveal a sufficiently long binding site for miR-181a-5p. Thus, we conclude that MMP9 is most likely indirectly regulated by miR-181a-5p. Indeed, literature research and the utilization of the target prediction tools miRDB and TargetScan revealed that miR-181a-5p directly targets three kinases of the MAPK pathway, CREB-1, MEK1, and ERK2 (**Supplementary Table 1**, 38, 39). To demonstrate that, transfection of U87_CTRL cells with a miR-181a-5p mimic was performed and revealed downregulation of pERK1/2 and p-CREB-1 in three independent Western Blot experiments, with p < 0.01 and p < 0.001, respectively (**Figure 3E**). Notably unphosphorylated levels of ERK1/2 and CREB-1 were not influenced by mimic transfection (**Figure 3E**). Thus, our results further support ERK2 and CREB-1 as downstream targets of miR-181a-5p.

EVs Derived From U87_KO Cells Are Associated With Higher miR-181a-5p Levels

Having demonstrated the intracellular effects of ADAM8 on miR-181a-5p and *MMP9* as a target gene, we further investigated

whether EVs derived from cellular supernatants of U87_CTRL (CTRL_EVs), U87_KO1 (KO1_EVs), and U87_KO2 (KO2_EVs) are associated with miR-181a-5p expression. By Nanoflow Cytometry Measurement (NanoFCM), the size and concentration of EVs prepared from cellular supernatants were analyzed (**Figures 4A, B**). Western Blot experiments further confirmed the presence of EVs using FLOTILLIN-1 and CD81 as EV markers, CALNEXIN as a negative control, and ß-Tubulin as a predominant lysate marker (**Figure 4C**). MiR-181a-5p was detected in all three EV populations (CTRL_EVs, KO1_EVs, KO2_EVs) and consistent with our observation in U87_CTRL and U87_KO cells, KO1_EVs and KO2_EVs displayed higher miR-181a-5p levels than CTRL_EVs (**Figure 4D**). To ensure that more miR-181a-5p is packed in EVs with higher cellular expression, we separated EVs from ctrl and mimic transfected cells with a 28-fold enrichment of miR-181a-5p in EVs derived from mimic transfected cells (**Supplementary Figure 8**). Furthermore, we confirmed the uptake of KO2_EVs by U87_CTRL cells *via* immunofluorescent microscopy by incubating CFSE-stained KO2_EVs as well as CTRL_EVs with Hoechst-stained U87_CTRL cells (**Supplementary Figure 9A**). Western blot analysis showed downregulation of MMP9 in U87_CTRL cells incubated with both CTRL_EVs and KO2_EVs in comparison to the HBSS control but did not confirm a significant difference of MMP9 expression comparing cells incubated with KO2_EVs or CTRL-EVs (**Supplementary Figure 9B**). We treated U87_KO2 cells with either miR-181a-5p-mimics or a miR181a-5p inhibitor and incubated the corresponding EVs with U87_CTRL cells. An
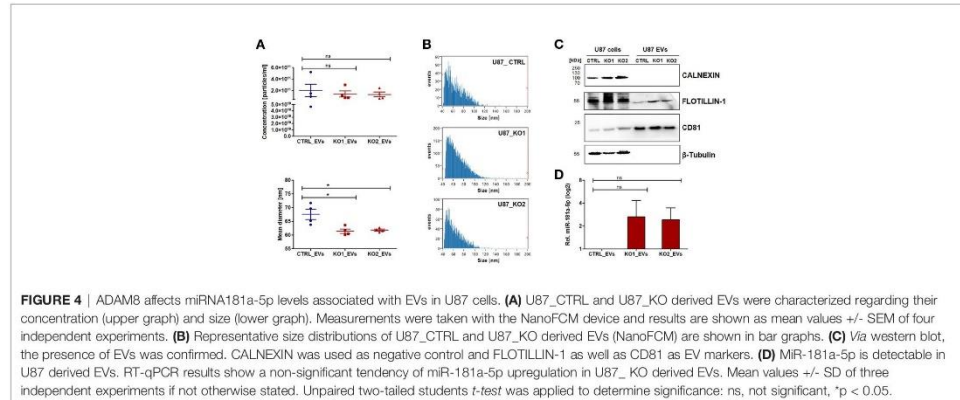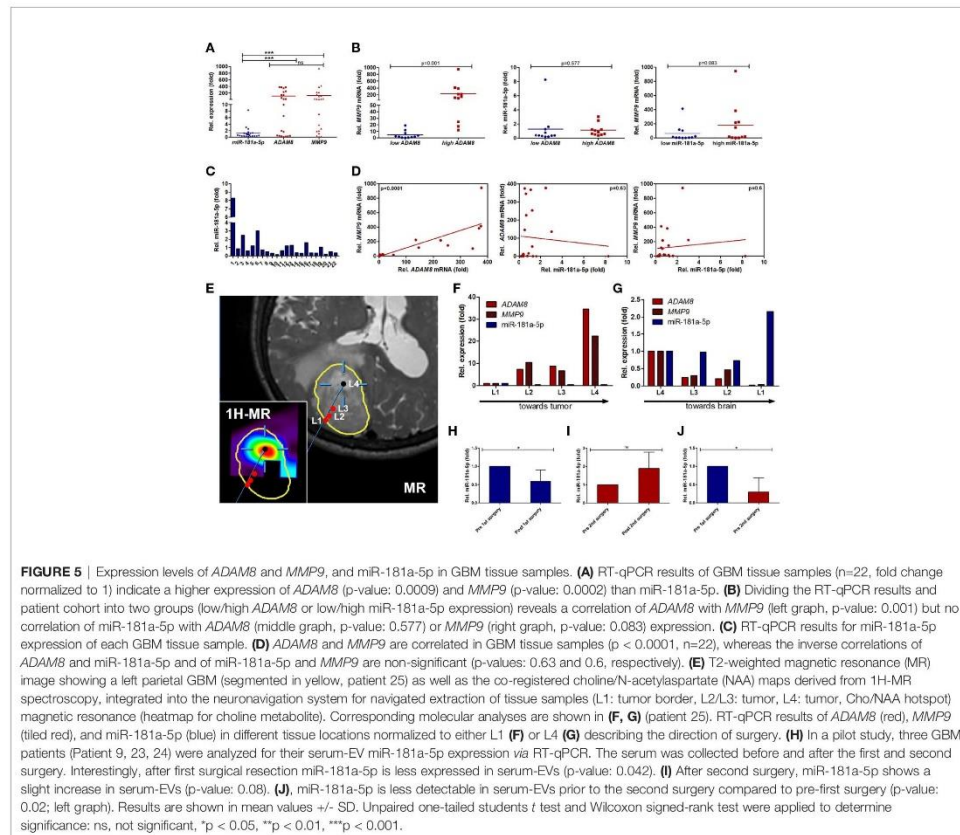
FIGURE 3 | ADAM8 affects MMP9 expression and proliferation *via* miR-181a-5p targeting ERK2 and CREB-1. **(A)** The upregulation of miR-181a-5p in U87_KO cells (RT-qPCR, n=3, left) causes inhibition of proliferation (CellTiter Glo, n=2, measurement after 48 h, right). **(B)** Overexpressing miR-181a-5p in U87_CTRL cells *via* transient transfection (RT-qPCR, n=3, left) causes inhibition of proliferation after 48 h (CellTiter Glo, n=3 technical replicates, right). **(C)** MMP9 is downregulated in U87_KO cells on mRNA (RT-qPCR, n=3, left). After miR-181a-5p mimic transfection, MMP9 is downregulated in U87 cells on the mRNA (RT-qPCR, n=3, p-value: 0.0009) **(C)** and on protein level (ELISA, n=2, p-value: 0.0004) analyzed by western blot **(D)**. **(E)** Analyses of kinase activation after miR-181a-5p mimic transfection for ERK1/2 (p-value: 0.003) and CREB-1 (p-value: 0.0007). Results are shown as mean values +/- SD of three independent experiments unless otherwise stated. Results are given in mean +/- SD. Unpaired one-tailed students *t* test was applied to determine significance: *p < 0.05, **p < 0.01, ***p < 0.001.

ELISA experiment revealed that incubation of inhibitor-treated EVs led to increased soluble MMP9 levels whilst incubation of miR-181a-5p-mimic treated EVs caused a decrease in soluble MMP9 (**Supplementary Figure 9C**).

Characterization of ADAM8, MMP9, and miR-181a-5p Expression in GBM Tumor Tissue Samples

RT-qPCR experiments were conducted on 22 tumor tissue samples from patients admitted to our clinical department to analyze the expression profiles of *ADAM8*, *MMP9*, and miR-181a-5p in GBM tissue. Further information on the patient cohort and histopathological data are listed in **Table 1**. For normalization of data (set to 1 in **Figures 5A–D**), we utilized tissue samples localized most remote from the tumor core. The majority of the examined tumor tissue samples showed downregulation of miR-181a-5p (**Figure 5C**). In contrast, mean *ADAM8* and *MMP9* expression levels were upregulated in the investigated tumor samples (**Figure 5A**). High *ADAM8* correlated with elevated *MMP9* expression levels, p < 0.0001 (**Figure 5D**). In the patient cohort, neither *ADAM8* mRNA levels nor *MMP9* mRNA levels correlated with miR-181a-5p expression, p = 0.6 and p = 0.63 respectively (**Figure 5D**). We then divided the patient cohort into subgroups, high *ADAM8* expression, and low *ADAM8* expression group, as well as high miR-181a-5p expression and low miR-181a-5p expression group (**Supplementary Figure 9**). *MMP9* expression was elevated in the high *ADAM8* group, p = 0.01 (**Figure 5B**). MiR-181a-5p expression was similar in the high *ADAM8* and low *ADAM8* groups (**Figure 5B**). *MMP9* expression was also similar in both miR-181a-5p subgroups (**Figure 5B**). To further investigate if this trend is due to the strong heterogeneity of the GBM tissue, we explored the connection between ADAM8, MMP9, and miR-181a-5p in a pilot experiment using MR-spectroscopy guided surgery at different locations in a GBM tumor tissue

FIGURE 4 | ADAM8 affects miRNA181a-5p levels associated with EVs in U87 cells. **(A)** U87_CTRL and U87_KO derived EVs were characterized regarding their concentration (upper graph) and size (lower graph). Measurements were taken with the NanoFCM device and results are shown as mean values +/- SEM of four independent experiments. **(B)** Representative size distributions of U87_CTRL and U87_KO derived EVs (NanoFCM) are shown in bar graphs. **(C)** *Via* western blot, the presence of EVs was confirmed. CALNEXIN was used as negative control and FLOTILLIN-1 as well as CD81 as EV markers. **(D)** MiR-181a-5p is detectable in U87 derived EVs. RT-qPCR results show a non-significant tendency of miR-181a-5p upregulation in U87_ KO derived EVs. Mean values +/- SD of three independent experiments if not otherwise stated. Unpaired two-tailed students *t-test* was applied to determine significance: ns, not significant, *p < 0.05.

92

FIGURE 5 | Expression levels of *ADAM8* and *MMP9*, and miR-181a-5p in GBM tissue samples. **(A)** RT-qPCR results of GBM tissue samples (n=22, fold change normalized to 1) indicate a higher expression of *ADAM8* (p-value: 0.0009) and *MMP9* (p-value: 0.0002) than miR-181a-5p. **(B)** Dividing the RT-qPCR results and patient cohort into two groups (low/high *ADAM8* or low/high miR-181a-5p expression) reveals a correlation of *ADAM8* with *MMP9* (left graph, p-value: 0.001) but no correlation of miR-181a-5p with *ADAM8* (middle graph, p-value: 0.577) or *MMP9* (right graph, p-value: 0.083) expression. **(C)** RT-qPCR results for miR-181a-5p expression of each GBM tissue sample. **(D)** *ADAM8* and *MMP9* are correlated in GBM tissue samples (p < 0.0001, n=22), whereas the inverse correlations of *ADAM8* and miR-181a-5p and of miR-181a-5p and *MMP9* are non-significant (p-values: 0.63 and 0.6, respectively). **(E)** T2-weighted magnetic resonance (MR) image showing a left parietal GBM (segmented in yellow, patient 25) as well as the co-registered choline/N-acetylaspartate (NAA) maps derived from 1H-MR spectroscopy, integrated into the neuronavigation system for navigated extraction of tissue samples (L1: tumor border, L2/L3: tumor, L4: tumor, Cho/NAA hotspot) magnetic resonance (heatmap for choline metabolite). Corresponding molecular analyses are shown in **(F, G)** (patient 25). RT-qPCR results of *ADAM8* (red), *MMP9* (tiled red), and miR-181a-5p (blue) in different tissue locations normalized to either L1 **(F)** or L4 **(G)** describing the direction of surgery. **(H)** In a pilot study, three GBM patients (Patient 9, 23, 24) were analyzed for their serum-EV miR-181a-5p expression *via* RT-qPCR. The serum was collected before and after the first and second surgery. Interestingly, after first surgical resection miR-181a-5p is less expressed in serum-EVs (p-value: 0.042). **(I)** After second surgery, miR-181a-5p shows a slight increase in serum-EVs (p-value: 0.08). **(J)**, miR-181a-5p is less detectable in serum-EVs prior to the second surgery compared to pre-first surgery (p-value: 0.02; left graph). Results are shown in mean values +/- SD. Unpaired one-tailed students *t* test and Wilcoxon signed-rank test were applied to determine significance: ns, not significant, *p < 0.05, **p < 0.01, ***p < 0.001.

sample of one selected patient. In the non-tumorous access tissue (L1), miR-181a-5p showed the highest expression whereas *ADAM8* and *MMP9* expression is at the lowest level (**Figures 5E–G**). Analysis of tumor edge (L2 and L3) and core tumor (L4) with strongly proliferating and vascularized zones revealed reversed expression patterns for *MMP9*, *ADAM8*, and miR-181a-5p (**Figures 5E–G**). Tumor locations in L3 and L4 were also confirmed by 1H-MR spectroscopy (**Supplementary Table 2**).

MiR-181a-5p Expression in Serum-Derived EVs From GBM Patients

In a further pilot study, serum specimens from three GBM patients were obtained before and after surgical resection. All three patients suffered from tumor recurrence and underwent surgical resection for a second time. In all cases, the highest miR-181a-5p expression levels were observed in serum samples prior to the first surgical resection (**Figure 5H**). After the first

surgery, a reduction in miR-181a-5p levels was observed in post-surgery serum-derived EVs, p < 0.05 (5H). In contrast, after the second surgery, miR-181a-5p expression was slightly upregulated (**Figure 5I**). A comparison of primary manifested GBM and recurrent GBM revealed a decrease in miR-181a-5p expression in EVs, p < 0.05 (5K). These results suggest that miR-181a-5p could serve as a tumor marker, but needs to be sufficiently powered in further studies.

DISCUSSION

ADAM8 as a multidomain enzyme exhibits numerous tumor-supporting characteristics by promoting invasion, angiogenesis, and chemoresistance in GBM (10, 12). Due to these multiple functions, ADAM8 affects several intracellular pathways involving several important kinases and transcription factors

such as JAK2/STAT, AKT/PI3K, ERK1/2, and CREB-1 (8–12). Mechanistically, the ADAM8 metalloprotease domain cleaves extracellular membrane components while the cytoplasmic domain activates crucial signaling cascades in carcinogenesis (4). Thereby, ADAM8 induces the expression of several oncoproteins including MMP9 and *SPP1*/osteopontin (8, 10). Previously, we demonstrated that ADAM8-dependent MMP9 expression is mediated *via* the MAPK pathway and resulted in a strong correlation of ADAM8 and MMP9 in breast cancer-derived brain metastasis (8). By characterizing the expression profile of ADAM8 and MMP9 in GBM tissue samples, we confirmed these observations for GBM. To dissect the effects of ADAM8 on oncoproteins mechanistically, we hypothesized that ADAM8 could alter the expression levels of distinct miRNAs such as miR-720, as previously shown for breast cancer cells (13). Generation of stable ADAM8 KO clones with subsequent miRNA screening revealed that the tumor suppressor miRNA miR-181a-5p shows a significantly higher expression in GBM cells deficient in ADAM8. Since high ADAM8 levels are correlated with GBM progression, a downregulation of miRNA181a-5p would be expected. Indeed, a recent study linked the poor prognosis of GBM patients with low miRNA181a-5p expression levels (40). Together, these findings qualified miRNA181a-5p as a candidate for a detailed molecular analysis, as presented here. Transient re-expression of ADAM8 in U87_KO cells resulted in downregulation of miR-181a-5p, suggesting that ADAM8 actively suppresses the expression of miR-181a-5p. Downregulation of miR-181a-5p by ADAM8 is dependent on the presence of the cytoplasmatic domain. In GBM, miR-181a-5p acts as a tumor suppressor miRNA by reducing invasiveness and enhancing radio- and chemosensitivity (23, 41). We confirmed that overexpression of miR-181a-5p led to reduced proliferation rates in U87 cells. Moreover, a similar effect on cell proliferation was observed in ADAM8 deficient GBM cells. It was shown that miR-181a-5p suppresses cell colony formation and tumor growth, and regulates apoptosis by targeting BCL-2 (23, 41). It is interesting to note that GSCs express relatively high levels of miRNA181a-5p compared to differentiated GBM cells, which could be instrumental in regulating proliferation and cell survival of this particular cell type. We have evidence that ADAM8 and, negatively correlated, miRNA181a-5p levels change in GSCs under conditions favoring differentiation of GSCs (Schäfer, unpublished data). However, the mechanisms that lead to miR-181a-5p downregulation in GBM remained elusive until now. As ADAM8 is a membrane-anchored protein, we concluded that ADAM8 downregulates the expression of miR-181a-5p by downstream signaling and activation of transcription factors. Indeed, our results revealed that miR-181a-5p can be downregulated by the activation of STAT3 and MAPK pathways. Conversely, miRNA181a-5p can regulate either total STAT3 levels in U87 cells and, notably, affect levels of p-STAT3 in the primary GBM cell line GBM42, indicating an unknown mechanism of kinase regulation by miRNA, similar to an observation made for phospho-AKT and p-ERK in a previous study in glioma (42) Previously, the importance of STAT3

signaling in GBM has been demonstrated in numerous studies whilst our group showed that ADAM8 dependent activation of STAT3 signaling led to increased angiogenesis by upregulation of osteopontin (10, 43, 44, reviewed in 45). In agreement with these findings, the 3'UTR of *SPP1*/osteopontin contains a binding site for miR-181a-5p and can be downregulated upon miR-181a-5p overexpression (19). All these results support the existence of a possible ADAM8/STAT3/miR-181a/osteopontin axis in GBM (**Figure 6** left). In addition, increased activation of the MAPK pathway is observed in numerous malignant tumors and leads to uncontrolled cell growth and mitosis (46). One of the best-known activators of the MAPK signaling pathway is the EGFR. Frequently, primary GBM tumors display a constitutively active variant, EGFRvIII (47). Apart from EGFR dependent MAPK activation, ADAM8 can activate the MAPK pathway EGFR independently (9). Interestingly, two kinases of the MAPK pathway, ERK2, and MEK1 as well as the downstream transcription factor CREB-1 are known to contain binding sites for miR-181a-5p (25, 26). In our experiments, phosphorylated and thus activated pCREB and pERK1/2 were downregulated in U87 cells transfected with miR-181a-5p mimics. We did not observe any effects on unphosphorylated CREB-1 and ERK1/2 as well as on MEK1/2 expression. Since miRNAs are post-transcriptional regulators of protein expression, we do not fully understand these results, but a TargetScan search revealed that CRBL2, a protein regulating phosphorylation of CREB1 is directly regulated by miR181a-5p, adding one more level of complexity to the network we have described here. A study by Fu et al. showed that CREB-1 suppresses miR-181a-5p transcription by directly binding to its promoter region (48). Thus, the interaction of miR-181a-5p and the MAPK pathway may constitute a regulatory loop that requires further investigation. Furthermore, we can postulate that our results describing the regulation of miR-181a-5p by ADAM8 are not restricted to the role of ADAM8 in GBM, as all other tumor cell lines that we investigated so far such as the triple-negative breast cancer cell line MDA-MB-231 and the PDAC cell line Panc89 show elevated levels of miR-181a-5p upon ADAM8 deficiency (unpublished observations). In accordance, MDA-MB-231 were among those cell lines that showed a strong correlation between ADAM8 and MMP9 expression in our previous study on breast cancer-derived brain metastases (8).

MMP9 plays a central role in tumor progression, especially for cell proliferation and invasion (27). Moreover, MMP9 expression is a prognostic factor in GBM and negatively correlated with patient survival (30). Thus, exploring the miR-181a-5p dependent *MMP9* downregulation was particularly interesting. U87 cells overexpressing miR-181a-5p exhibited decreased MMP9 levels. This was observed in U87 ADAM8 knockout cells as well as U87_CTRL cells incubated with miR-181a-5p mimics. To further establish whether *MMP9* mRNA contains a binding site for miR-181a-5p, we utilized target prediction tools and analyzed the mRNA sequence of MMP9. However, this analysis revealed that the *MMP9* mRNA does not contain an authentic binding site for miR-181a-5p.
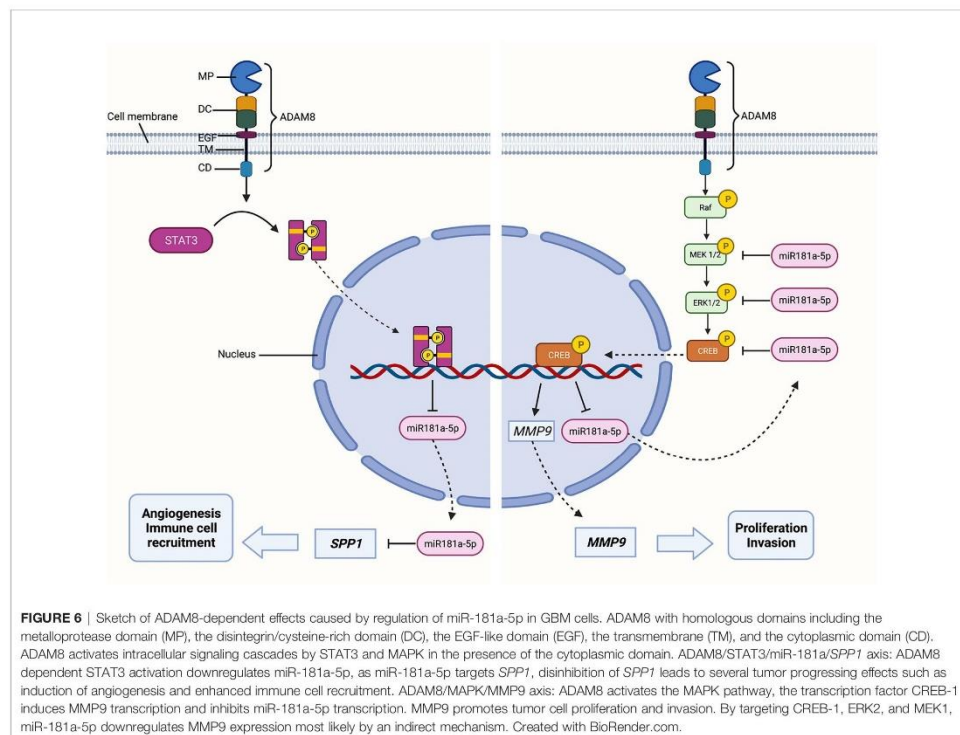
Consequently, we concluded that miR-181a-5p can indirectly downregulate MMP9 expression by silencing the MAPK cascade (**Figure 6** right). This conclusion is supported by data showing that ERK1/2 inhibition led to decreased MMP9 levels in U87 and GBM42 cells (**Supplementary Figure 5**).

All these results demonstrate intracellular regulatory mechanisms of ADAM8/miR-181a-5p signaling so far. Cell-cell communication in the tumor microenvironment is essential for shaping either an immunosuppressive or a tumor-supportive microenvironment (34). As one mode of cell-cell communication, tumor cells release EVs. These heterogeneous nanoparticles contain a great variety of different molecules including miRNAs (35). Clinically, EVs received increasing attention, as their function as novel diagnostic and prognostic biomarkers is discussed (49). In our study, we analyzed the miR-181a-5p expression in U87 cells and serum-derived EVs. We recapitulated the higher abundance of miR-181a-5p in EVs from ADAM8 KO cells. Concerning patient sera, miR-181-5p expression in EVs dropped after the first surgical tumor resection. Moreover, miR-181a-5p expression was downregulated in serum-derived EVs from recurrent GBM.

These results suggest that miR-181a-5p is further downregulated along with tumor progression. However, additional analyses must be carried out in a larger patient cohort to support this conclusion. The uptake of EVs can alter the behavior of recipient cells (50). Therefore, EVs might also be utilized as therapeutic vehicles (51). In our experiments, miR-181a-5p enriched vesicles were taken up by naive U87 cells demonstrating a role for ADAM8 in the tumor microenvironment. It remains to be determined if GBM resident immune cells such as macrophages that constitutively express ADAM8 could release EVs that might fail to suppress MMP9 expression in target cells, in conjunction with the possible tumor-promoting role of ADAM8 in macrophages (33).

Due to limited therapeutic options as well as the absence of early diagnostic biomarkers, GBM remains challenging as an incurable disease with a grim prognosis. Therefore, the identification of potential biomarkers as well as new therapeutic targets is of high importance. In summary, we identified that ADAM8 downregulates miR-181a-5p by activation of STAT3 and MAPK signaling. Considering that miR-181a-5p is a tumor suppressor miRNA in GBM, ADAM8 dependent silencing of miR-181a-5p could further contribute to

FIGURE 6 | Sketch of ADAM8-dependent effects caused by regulation of miR-181a-5p in GBM cells. ADAM8 with homologous domains including the metalloprotease domain (MP), the disintegrin/cysteine-rich domain (DC), the EGF-like domain (EGF), the transmembrane (TM), and the cytoplasmic domain (CD). ADAM8 activates intracellular signaling cascades by STAT3 and MAPK in the presence of the cytoplasmic domain. ADAM8/STAT3/miR-181a/*SPP1* axis: ADAM8 dependent STAT3 activation downregulates miR-181a-5p, as miR-181a-5p targets *SPP1*, disinhibition of *SPP1* leads to several tumor progressing effects such as induction of angiogenesis and enhanced immune cell recruitment. ADAM8/MAPK/MMP9 axis: ADAM8 activates the MAPK pathway, the transcription factor CREB-1 induces MMP9 transcription and inhibits miR-181a-5p transcription. MMP9 promotes tumor cell proliferation and invasion. By targeting CREB-1, ERK2, and MEK1, miR-181a-5p downregulates MMP9 expression most likely by an indirect mechanism. Created with BioRender.com.

tumor progression. We showed that overexpression of miR-181a-5p decreased cell proliferation and suppressed MMP9 expression by downregulation of the MAPK pathway Moreover, the presence of miR-181a-5p in clinical samples and EVs isolated from cellular supernatants as well as patient sera justifies further studies to reveal a potential role of miR-181a-5p in GBM diagnosis and progression.

DATA AVAILABILITY STATEMENT

The raw data supporting the conclusions of this article will be made available by the authors, without undue reservation.

ETHICS STATEMENT

The studies involving human participants were reviewed and approved by Local Ethics Committee (Philipps University Marburg, medical faculty, file number 185/11). The patients/participants provided their written informed consent to participate in this study.

AUTHOR CONTRIBUTIONS

JWB, ES, BC, CN, and MB conceived this study. AS, LE, LM, US, GLD, ABB, OL, and CP performed experiments and evaluated the data. ACB, MP, CN, and BC provided resources and clinical data. AS, LE, and JWB wrote the manuscript draft. MB, CN, and

MP reviewed and edited the manuscript. All authors contributed to the article and approved the submitted version.

FUNDING

ACKNOWLEDGMENTS

SUPPLEMENTARY MATERIAL

The Supplementary Material for this article can be found online at: https://www.frontiersin.org/articles/10.3389/fonc.2022.826273/full#supplementary-material

REFERENCES

1. Alifieris C, Trafalis DT. Glioblastoma Multiforme: Pathogenesis and Treatment. *Pharmacol Ther* (2015) 152:63–82. doi: 10.1016/j.pharmthera.2015.05.005
2. Vollmann-Zwerenz A, Leidgens V, Feliciello G, Klein CA, Hau P. Tumor Cell Invasion in Glioblastoma. *Int J Mol Sci* (2020) 21(6):1932. doi: 10.3390/ijms21061932
3. Murphy G. The ADAMs: Signalling Scissors in the Tumour Microenvironment. *Nat Rev Cancer* (2008) 8(12):929–41. doi: 10.1038/nrc2459
4. Conrad C, Benzel J, Dorzweiler K, Cook L, Schlomann U, Zarbock A, et al. ADAM8 in Invasive Cancers: Links to Tumor Progression, Metastasis, and Chemoresistance. *Clin Sci (Lond)* (2019) 133(1):83–99. doi: 10.1042/CS20180906
5. He S, Ding L, Cao Y, Li G, Deng J, Tu Y, et al. Overexpression of a Disintegrin and Metalloprotease 8 in Human Gliomas is Implicated in Tumor Progression and Prognosis. *Med Oncol* (2012) 29(3):2032–7. doi: 10.1007/s12032-011-0084-9
6. Romagnoli M, Mineva ND, Polmear M, Conrad C, Srinivasan S, Loussouarn D, et al. ADAM8 Expression in Invasive Breast Cancer Promotes Tumor Dissemination and Metastasis. *EMBO Mol Med* (2014) 6(2):278–94. doi: 10.1002/emmm.20130337
7. Valkovskaya N, Kayed H, Felix K, Hartmann D, Giese NA, Osinsky SP, et al. ADAM8 Expression is Associated With Increased Invasiveness and Reduced Patient Survival in Pancreatic Cancer. *J Cell Mol Med* (2007) 11(5):1162–74. doi: 10.1111/j.1582-4934.2007.00082.x
8. Conrad C, Götte M, Schlomann U, Roessler M, Pagenstecher A, Anderson P, et al. ADAM8 Expression in Breast Cancer Derived Brain Metastases: Functional Implications on MMP-9 Expression and Transendothelial Migration in Breast Cancer Cells. *Int J Cancer* (2018) 142(4):779–91. doi: 10.1002/ijc.31090
9. Schlomann U, Koller G, Conrad C, Ferdous T, Golfi P, Garcia AM, et al. ADAM8 as a Drug Target in Pancreatic Cancer. *Nat Commun* (2015) 6:6175. doi: 10.1038/ncomms7175
10. Li Y, Guo S, Zhao K, Conrad C, Driescher C, Rothbart V, et al. ADAM8 Affects Glioblastoma Progression by Regulating Osteopontin-Mediated Angiogenesis. *Biol Chem* (2021) 402(2):195–206. doi: 10.1515/hsz-2020-0184
11. Awan T, Babendreyer A, Mahmood Alvi A, Düsterhöft S, Lambertz D, Bartsch JW, et al. Expression Levels of the Metalloproteinase ADAM8 Critically Regulate Proliferation, Migration and Malignant Signalling Events in Hepatoma Cells. *J Cell Mol Med* (2021) 25(4):1982–99. doi: 10.1111/jcmm.16015
12. Dong F, Eibach M, Bartsch JW, Dolga AM, Schlomann U, Conrad C, et al. The Metalloprotease-Disintegrin ADAM8 Contributes to Temozolomide Chemoresistance and Enhanced Invasiveness of Human Glioblastoma Cells. *Neuro Oncol* (2015) 17(11):1474–85. doi: 10.1093/neuonc/nov042
13. Das SG, Romagnoli M, Mineva ND, Barillé-Nion S, Jézéquel P, Campone M, et al. miR-720 is a Downstream Target of an ADAM8-Induced ERK Signaling Cascade That Promotes the Migratory and Invasive Phenotype of Triple-Negative Breast Cancer Cells. *Breast Cancer Res* (2016) 18(1):40. doi: 10.1186/s13058-016-0699-z
14. O'Brien J, Hayder H, Zayed Y, Peng C. Overview of MicroRNA Biogenesis, Mechanisms of Actions, and Circulation. *Front Endocrinol (Lausanne)* (2018) 9:402:402. doi: 10.3389/fendo.2018.00402
15. Fabian MR, Sonenberg N, Filipowicz W. Regulation of mRNA Translation and Stability by microRNAs. *Annu Rev Biochem* (2010) 79:351–79. doi: 10.1146/annurev-biochem-060308-103103
16. Ali Syeda Z, Langden SSS, Munkhzul C, Lee M, Song SJ. Regulatory Mechanism of MicroRNA Expression in Cancer. *Int J Mol Sci* (2020) 21(5):1723. doi: 10.3390/ijms21051723

17. Møller HG, Rasmussen AP, Andersen HH, Johnsen KB, Henriksen M, Duroux M. A Systematic Review of microRNA in Glioblastoma Multiforme: Micro-Modulators in the Mesenchymal Mode of Migration and Invasion. *Mol Neurobiol* (2013) 47(1):131–44. doi: 10.1007/s12035-012-8349-7

18. Shea A, Harish V, Afzal Z, Chijioke J, Kedir H, Dusmatova S, et al. MicroRNAs in Glioblastoma Pathogenesis and Therapeutics. *Cancer Med* (2016) 5(8):1917–46. doi: 10.1002/cam4.775

19. Marisetty A, Wei J, Kong LY, Ott M, Fang D, Sabbagh A, et al. MiR-181 Family Modulates Osteopontin in Glioblastoma Multiforme. *Cancers (Basel)* (2020) 12(12):3813. doi: 10.3390/cancers12123381

20. Ciafrè SA, Galardi S, Mangiola A, Ferracin M, Liu CG, Sabatino G, et al. Extensive Modulation of a Set of microRNAs in Primary Glioblastoma. *Biochem Biophys Res Commun* (2005) 334(4):1351–8. doi: 10.1016/j.bbrc.2005.07.030

21. Wang H, Tao T, Yan W, Feng Y, Wang Y, Cai J, et al. Upregulation of miR-181s Reverses Mesenchymal Transition by Targeting KPNA4 in Glioblastoma. *Sci Rep* (2015) 5:13072. doi: 10.1038/srep13072

22. Wei J, Marisetty A, Schrand B, Gabrusiewicz K, Hashimoto Y, Ott M, et al. Osteopontin Mediates Glioblastoma-Associated Macrophage Infiltration and is a Potential Therapeutic Target. *J Clin Invest* (2019) 129(1):137–49. doi: 10.1172/jci121266

23. Chen G, Zhu W, Shi D, Lv L, Zhang C, Liu P, et al. MicroRNA-181a Sensitizes Human Malignant Glioma U87MG Cells to Radiation by Targeting Bcl-2. *Oncol Rep* (2010) 23(4):997–1003. doi: 10.3892/or_00000725

24. Shi L, Cheng Z, Zhang J, Li R, Zhao P, Fu Z, et al. Hsa-Mir-181a and Hsa-Mir-181b Function as Tumor Suppressors in Human Glioma Cells. *Brain Res* (2008) 1236:185–93. doi: 10.1016/j.brainres.2008.07.085

25. Wang P, Chen D, Ma H, Li Y. LncRNA SNHG12 Contributes to Multidrug Resistance Through Activating the MAPK/Slug Pathway by Sponging miR-181a in non-Small Cell Lung Cancer. *Oncotarget* (2017) 8(48):84086–101. doi: 10.18632/oncotarget.20475

26. Liu Y, Zhao Z, Yang F, Gao Y, Song J, Wan Y. microRNA-181a is Involved in Insulin-Like Growth Factor-1-Mediated Regulation of the Transcription Factor CREB1. *J Neurochem* (2013) 126(6):771–80. doi: 10.1111/jnc.12370

27. Huang H. Matrix Metalloproteinase-9 (MMP-9) as a Cancer Biomarker and MMP-9 Biosensors: Recent Advances. *Sensors (Basel)* (2018) 18(10):3249. doi: 10.3390/s18103249

28. Hagemann C, Anacker J, Ernestus RI, Vince GH. A Complete Compilation of Matrix Metalloproteinase Expression in Human Malignant Gliomas. *World J Clin Oncol* (2012) 3(5):67–79. doi: 10.5306/wjco.v3.i5.67

29. Musumeci G, Magro G, Cardile V, Coco M, Marzagalli R, Castrogiovanni P, et al. Characterization of Matrix Metalloproteinase-2 and -9, ADAM-10 and N-Cadherin Expression in Human Glioblastoma Multiforme. *Cell Tissue Res* (2015) 362(1):45–60. doi: 10.1007/s00441-015-2197-5

30. Li Q, Chen B, Cai J, Sun Y, Wang G, Li Y, et al. Comparative Analysis of Matrix Metalloproteinase Family Members Reveals That MMP9 Predicts Survival and Response to Temozolomide in Patients With Primary Glioblastoma. *PLoS One* (2016) 11(3):e0151815. doi: 10.1371/journal.pone.0151815

31. Das G, Shiras A, Shanmuganandam K, Shastry P. Rictor Regulates MMP-9 Activity and Invasion Through Raf-1-MEK-ERK Signaling Pathway in Glioma Cells. *Mol Carcinog* (2011) 50(6):412–23. doi: 10.1002/mc.20723

32. Lakka SS, Jasti SL, Gondi C, Boyd D, Chandrasekar N, Dinh DH, et al. Downregulation of MMP-9 in ERK-Mutated Stable Transfectants Inhibits Glioma Invasion *In Vitro*. *Oncogene* (2002) 21(36):5601–8. doi: 10.1038/sj.onc.I205646

33. Gjorgjevski M, Hannen R, Carl B, Li Y, Landmann E, Buchholz M, et al. Molecular Profiling of the Tumor Microenvironment in Glioblastoma Patients: Correlation of Microglia/Macrophage Polarization State With Metalloprotease Expression Profiles and Survival. *Biosci Rep* (2019) 39(6):BSR20182361. doi: 10.1042/bsr20182361

34. Cavallari C, Camussi G, Brizzi MF. Extracellular Vesicles in the Tumour Microenvironment: Eclectic Supervisors. *Int J Mol Sci* (2020) 21(18):6768. doi: 10.3390/ijms21186768

35. van Niel G, D'Angelo G, Raposo G. Shedding Light on the Cell Biology of Extracellular Vesicles. *Nat Rev Mol Cell Biol* (2018) 19(4):213–28. doi: 10.1038/nrm.2017.125

36. Hannen R, Selmansberger M, Hauswald M, Pagenstecher A, Nist A, Stiewe T, et al. Comparative Transcriptomic Analysis of Temozolomide Resistant Primary GBM Stem-Like Cells and Recurrent GBM Identifies Up-

37. Scharfenberg F, Helbig A, Sammel M, Benzel J, Schlomann U, Peters F, et al. Degradome of Soluble ADAM10 and ADAM17 Metalloproteases. *Cell Mol Life Sci* (2020) 77(2):331–50. doi: 10.1007/s00018-019-03184-4

38. McGeary SE, Lin KS, Shi CY, Pham TM, Bisaria N, Kelley GM, et al. The Biochemical Basis of microRNA Targeting Efficacy. *Science* (2019) 366(6472):eaav1741. doi: 10.1126/science.aav1741

39. Chen Y, Wang X. miRDB: An Online Database for Prediction of Functional microRNA Targets. *Nucleic Acids Res* (2020) 48(D1):D127–31. doi: 10.1093/nar/gkz757

40. Huang SX, Zhao ZY, Weng GH, He XY, Wu CJ, Fu CY, et al. The Correlation of microRNA-181a and Target Genes With Poor Prognosis of Glioblastoma Patients. *Int J Oncol* (2016) 49(1):217–24. doi: 10.3892/ijo.2016.3511

41. Wen X, Li S, Guo M, Liao H, Chen Y, Kuang X, et al. miR-181a-5p Inhibits the Proliferation and Invasion of Drug-Resistant Glioblastoma Cells by Targeting F-Box Protein 11 Expression. *Oncol Lett* (2020) 20(5):235. doi: 10.3892/ol.2020.12098

42. Wang XF, Shi ZM, Wang XR, Cao L, Wang YY, Zhang JX, et al. MiR-181d Acts as a Tumor Suppressor in Glioma by Targeting K-Ras and Bcl-2. *J Cancer Res Clin Oncol* (2012) 138(4):573–84. doi: 10.1007/s00432-011-1114-x

43. Priester M, Copanaki E, Vafaizadeh V, Hensel S, Bernreuther C, Glatzel M, et al. STAT3 Silencing Inhibits Glioma Single Cell Infiltration and Tumor Growth. *Neuro Oncol* (2013) 15(7):840–52. doi: 10.1093/neuonc/not025

44. Swiatek-Machado K, Mieczkowski J, Ellert-Miklaszewska A, Swierk P, Fokt I, Szymanski S, et al. Novel Small Molecular Inhibitors Disrupt the JAK/STAT3 and FAK Signaling Pathways and Exhibit a Potent Antitumor Activity in Glioma Cells. *Cancer Biol Ther* (2012) 13(8):657–70. doi: 10.4161/cbt.20083

45. Swiatek-Machado K, Kaminska B. STAT Signaling in Glioma Cells. *Adv Exp Med Biol* (2020) 1202:203–22. doi: 10.1007/978-3-030-30651-9_10

46. Guo YJ, Pan WW, Liu SB, Shen ZF, Xu Y, Hu LL. ERK/MAPK Signalling Pathway and Tumorigenesis. *Exp Ther Med* (2020) 19(3):1997–2007. doi: 10.3892/etm.2020.8454

47. Padfield E, Ellis HP, Kurian KM. Current Therapeutic Advances Targeting EGFR and EGFRvIII in Glioblastoma. *Front Oncol* (2015) 5:5. doi: 10.3389/fonc.2015.00005

48. Fu Y, Xin Z, Ling Z, Xie H, Xiao T, Shen X, et al. A CREB1-miR-181a-5p Loop Regulates the Pathophysiologic Features of Bone Marrow Stromal Cells in Fibrous Dysplasia of Bone. *Mol Med* (2021) 27(1):81. doi: 10.1186/s10020-021-00341-z

49. Urabe F, Kosaka N, Ito K, Kimura T, Egawa S, Ochiya T. Extracellular Vesicles as Biomarkers and Therapeutic Targets for Cancer. *Am J Physiol Cell Physiol* (2020) 318(1):C29–39. doi: 10.1152/ajpcell.00280.2019

50. Abels ER, Breakefield XO. Introduction to Extracellular Vesicles: Biogenesis, RNA Cargo Selection, Content, Release, and Uptake. *Cell Mol Neurobiol* (2016) 36(3):301–12. doi: 10.1007/s10571-016-0366-z

51. Nazimek K, Bryniarski K. Perspectives in Manipulating EVs for Therapeutic Applications: Focus on Cancer Treatment. *Int J Mol Sci* (2020) 21(13):4623. doi: 10.3390/ijms21134623

brain sciences

MDPI

Communication

Identification of Dysregulated microRNAs in Glioblastoma Stem-like Cells

Lara Evers [1,†], Agnes Schäfer [1,†], Raffaella Pini [2], Kai Zhao [1], Susanne Stei [1], Christopher Nimsky [1,3] and Jörg W. Bartsch [1,3,*]

1 Department of Neurosurgery, Philipps-University Marburg, University Hospital Marburg (UKGM), Baldingerstrasse, 35043 Marburg, Germany
2 Center for Omics Sciences, IRCCS San Raffaele Scientific Institute, Via Olgettina 58, 20132 Milan, Italy
3 Marburg Center for Mind, Brain and Behavior (MCMBB), 35032 Marburg, Germany
* Correspondence: jbartsch@med.uni-marburg.de
† These authors contributed equally to this work.

Abstract: Glioblastoma multiforme (GBM) is the most common malignant primary brain tumor in adults. Despite multimodal therapy, median survival is poor at 12–15 months. At the molecular level, radio-/chemoresistance and resulting tumor progression are attributed to a small fraction of tumor cells, termed glioblastoma stem-like cells (GSCs). These CD133-expressing, self-renewing cells display the properties of multi-lineage differentiation, resulting in the heterogenous composition of GBM. MicroRNAs (miRNAs) as regulators of gene expression at the post-transcriptional level can alter many pathways pivotal to cancer stem cell fate. This study explored changes in the miRNA expression profiles in patient-derived GSCs altered on differentiation into glial fiber acid protein (GFAP)-expressing, astrocytic tumor cells using a polymerase chain reaction (PCR) array. Initially, 22 miRNAs showed higher expression in GSCs and 9 miRNAs in differentiated cells. The two most downregulated miRNAs in differentiated GSCs were miR-17-5p and miR-425-5p, whilst the most upregulated miRNAs were miR-223-3p and let-7-5p. Among those, miR-425-5p showed the highest consistency in an upregulation in all three GSCs. By transfection of a 425-5p miRNA mimic, we demonstrated downregulation of the GFAP protein in differentiated patient-derived GBM cells, providing potential evidence for direct regulation of miRNAs in the GSC/GBM cell transition.

Keywords: glioblastoma multiforme; glioblastoma stem-like cells; differentiation; microRNA; GFAP; miR-425-5p; miR-223-3p; let-7; miR-17-5p

check for updates

1. Introduction

Glioblastoma multiforme, the most common malignant primary brain tumor in adults, is characterized by an aggressive and invasive growth pattern, rapid development of radio-/chemoresistance, and genetic heterogeneity [1]. The current therapeutic standard of care consists of maximum safe surgical resection, radiation, and temozolomide (TMZ) chemotherapy [2]. However, the median survival remains low at 12–15 months as tumor recurrence occurs rapidly [3].

Glioblastoma stem-like cells (GSCs) are currently viewed as modulators of the tumor microenvironment as well as the origin of radio-/chemoresistance thereby resulting in tumor progression [4]. Due to this small, but pluripotent self-renewing subpopulation of GBM tumor cells that typically reside in perivascular niches apart from the bulk tumor mass, GSCs cannot be sufficiently targeted by surgical resection [5]. As a result of GBM heterogeneity due to different GBM phenotypes, such as the classical, proneural, and mesenchymal types, patient-derived cell-cultured GSC lines might display diverging characteristics [6]. At the molecular level, GSCs express a unique pattern of stemness markers such as the transmembrane glycoproteins CD44 and CD133 or the transcription factor Sex-determining region Y-box2 (SOX2) [4,7]. In particular, CD133, an established

marker for neural progenitor cells and cancer stem-like cells, organizes the cell membrane topology [8]. Contrary to the bulk mass of astrocyte tumor cells, GSCs barely express the intermediate filament GFAP [9]. Therefore, GFAP is utilized as a marker for primary differentiated, astrocytic tumor cells in GBM [10].

Not only does the expression pattern of proteins change on GSC differentiation but recent studies also suggest that GSCs display a unique miRNA expression pattern [11]. MicroRNAs (miRNAs) as small noncoding RNA molecules regulate gene expression at the posttranscriptional level by binding to and thereby targeting their corresponding mRNAs [12]. As miRNAs can mediate many critical pathways to cancer progression such as proliferation, apoptosis, and angiogenesis, they can act as both tumor-suppressors (tumor-suppressor miRNAs) and oncogenes (onco-miRNAs) [13]. Clinically, miRNAs are receiving rising attention as their function as novel diagnostic and prognostic biomarkers, as well as future therapeutic agents, is discussed and given that they can affect multiple target genes involved in pathological processes [11].

For this reason, dysregulated miRNAs are intensely studied in GBM. However, the expression profile as well as the function of specific miRNAs in GSCs have not yet been adequately elucidated.

This study investigated changes in the miRNA expression profile in patient-derived, well-characterized, cultured, sphere-forming GSCs and their differentiated status as adherent GBM cells by utilizing a miRNA PCR array. As a result, a total of 31 dysregulated miRNAs were identified. Through a literature review and target prediction analyses, we closely investigated the most dysregulated miRNAs.

2. Materials and Methods

2.1. Cell Culture

After approval from the local ethics committee (Philipps University Marburg, medical faculty, file number 185/11), patient-derived GSCs as well as primary GBM cell lines were obtained during surgical resection. Each patient gave written informed consent before surgical resection. Isolation, preparation, and molecular characteristics of GSCs and primary GBM cell lines from resected tumor tissues were described previously [14,15]. GSC lines 2017/151, 2017/74, and 2016/240 were cultivated in non-cell-culture-treated Petri dishes. As a medium, DMEM/F12 (DMEM-12-A, Capricorn Scientific, Ebsdorfergrund, Germany), supplemented with 2% B27 (17504044, Thermo Fisher Scientific, Waltham, MA, USA), 1% amphotericin (15290026, Thermo Fisher Scientific, Waltham, MA, USA), 0.5% HEPES (H0887, Sigma-Aldrich, Taufkirchen, Germany), and 0.1% gentamycin (A2712, Biochrom, Berlin, Germany), was utilized. In addition, epidermal growth factor (EGF, 100-15, Pepro-tech, Hamburg, Germany) and basic fibroblast growth factor (bFGF, 100-18b, Peprotech, Hamburg, Germany) were both supplemented at a final concentration of 0.02 ng/μL. Primary differentiated GBM cell lines GBM100 and GBM42 were cultivated in phenol red-free DMEM (DMEM-HXRXA, Capricorn Scientific, Ebsdorfergrund, Germany) supplemented with 10% fetal calf serum (FCS, S0615, Sigma, Taufkirchen, Germany), 1% penicillin/streptomycin (2321115, Gibco, Carlsbad, CA, USA), 1 mM sodium pyruvate (NPY-B, Capricorn Scientific, Ebsdorfergrund, Germany), 1% L-glutamine (25030-024, Gibco, Carlsbad, CA, USA), and 1% non-essential amino acids (11140050, Gibco, Carlsbad, CA, USA). All cell lines were cultivated in a humidified atmosphere at 37 °C and 5% CO_2.

2.2. GSC Differentiation

To differentiate GSCs, cells of 2016/240, 2017/151, and 2017/74 were seeded in 6-well plates at a density of 750,000 cells in 2 mL. To initiate GSC differentiation, 10% FCS (S0615, Sigma-Aldrich, Taufkirchen, Germany) was supplemented in DMEM/F12. In addition, bFGF and EGF were withdrawn. After seven days of incubation, light-microscopy images were taken. Then, cells were harvested for further analyses.

2.3. miR-425-5p Mimic Transfection

For transient overexpression of miR-425-5p, primary GBM100 and GBM42 cell lines were transfected with 0.01 μM hsa-miR-425-5p miRCURY LNA miRNA (GeneGlobe ID: YM00471725-ADA, catalog no.: 339173, Qiagen, Hilden, Germany). In detail, cells were seeded in a 6-well format at a density of 300,000 cells in 2 mL. After 24 h of incubation and attaching, the transfection was performed with Lipofectamine 2000 Reagent (11668-030, Thermo Fisher Scientific, Waltham, MA, USA) according to the manufacturer's instructions. Meanwhile, 0.01 μM Allstar Negative Control siRNA (1027280, Qiagen, Hilden, Germany) was transfected as a control. The transfection was repeated after 24 h. Cells were harvested 48 h after the second transfection and further analyzed via qPCR and Western blot.

2.4. RNA and miRNA Isolation

Total RNA with an enriched fraction of miRNAs from cellular pellets was isolated using the miRNeasy Tissue/Cells Advanced Mini Kit (217684, Qiagen, Hilden, Germany) according to the manufacturer's instructions.

2.5. RNA Reverse Transcription (RT) and Quantitive Real-Time Polymerase Chain Reaction (qPCR)

To quantify gene expression on an mRNA level, total RNA was reverse transcribed using the RNA to cDNA EcoDryTM Premix (639548, TaKaRa, Saint-Germain-en-Laye, France) according to the manufacturer's instructions. Quantitative real-time PCR was performed with a total reaction volume of 20 μL/well, consisting of 10 μL SYBR Green/Rox Master Mix (PPLUS-R-10 ML, Primer Design, Eastleigh, UK), 2 μL *GFAP/CD133* primers (244900, Qiagen, Hilden, Germany), 6 μL nuclease-free water, and 2 μL cDNA. Expression of the ribosomal gene *RPLP0/XS13* (fw: 5′-TGG GCA AGA ACA CCA TGA TG-3′; rev: 5′-AGT TTC TCC AGA GCT GGG TTG T-3′) was used as a housekeeping gene for normalization [16]. PCR experiments were performed on the Applied Biosystems StepOne-Plus Real-Time PCR System (Thermo Fisher Scientific, Waltham, MA, USA). Relative gene expression was calculated utilizing the $2^{-\Delta\Delta Ct}$ method.

2.6. miRNA Reverse Transcription and miRNA PCR Array

First, pooled samples for GSCs and differentiated GBM cells consisting of 8.3 ng total RNA with an enriched miRNA fraction from each of the three cell lines (2017/151, 2016/240, and 2017/74) were generated. As a next step, reverse transcription of the pooled samples was performed utilizing a miScript II RT Kit (218161, Qiagen, Hilden, Germany). Then, following the manufacturer's instructions, a pathway-focused miRNA PCR array (331221 miScript, Qiagen, Hilden, Germany) was conducted utilizing the miScript SYBR Green PCR Kit (218073, Qiagen, Hilden, Germany). The miRNA PCR arrays were performed on the Applied Biosystems StepOnePlus Real-Time PCR System (Thermo Fisher Scientific, Waltham, MA, USA). Data analysis and scatter plot generation were performed using the corresponding online data analysis tool provided by Qiagen (miScript miRNA PCR Data Analysis, Qiagen, https://dataanalysis.qiagen.com/mirna/arrayanalysis.php?target=upload, accessed on 1 February 2023). Relative gene expression was calculated utilizing the $2^{-\Delta\Delta Ct}$ method. RNU6 was used for internal normalization. Results are presented in heatmaps, which were generated using the GraphPad PRISM 9 software, version 9.1 (Insight Partners, New York, NY, USA).

2.7. miRNA Reverse Transcription and qPCR

For verification of the miRNA PCR array results and further functional experiments on miR-425-5p, isolated RNA samples with an enriched fraction of miRNAs were reverse transcribed utilizing the miRCURY LNA RT Kit (339340, Qiagen, Hilden, Germany), according to the manufacturer's instructions. Quantitative real-time PCR was performed utilizing the miRCURY LNA SYBR® Green PCR Kit (339345, Qiagen, Hilden, Germany), according to the manufacturer's instructions. As miRNA primers, hsa-miR-17-5p miRCURY LNA miRNA PCR Assay (YP02119304, 339306, Qiagen, Hilden, Germany), hsa-miR-425-5p miRCURY

LNA miRNA PCR Assay (YP00204337, 339306, Qiagen, Hilden, Germany), hsa-miR-223-3p 5p miRCURY LNA miRNA PCR Assay (YP00205986, 339306, Qiagen, Hilden, Germany), and hsa-miR-7a-5p miRCURY LNA miRNA PCR Assay (YP00205727, 339306, Qiagen, Hilden, Germany) were used. For normalization, miR-24-5p (YP00203954, 339306, Qiagen, Hilden, Germany) and UniSp6 (YP00203954, 339306, Qiagen, Hilden, Germany) were used. Relative gene expression was calculated utilizing the $2^{-\Delta\Delta Ct}$ method.

2.8. Protein Extraction and Western Blot Analysis

For 30 min, whole cell lysates were incubated in RIPA buffer (50 mM HEPES pH 7.4; 150 mM NaCl; 1% (v/v) NP-40; 0.5% (w/v) natriumdeoxycholate; 0.1% (w/v) SDS; 10 mM phenantrolin; 10 mM EDTA; PierceTM Protease Inhibitor Mini Tablets, EDTA-free, Thermo Fisher Scientific; PierceTM Phosphatase Inhibitor Mini Tablets, Thermo Fisher Scientific). Then, protein samples were prepared in 5× Laemmli buffer (60 mM Tris HCl, pH: 6.8; 2% (w/v) SDS; 10% (w/v) glycerol; 5% (v/v) ß-mercaptoethanol; 0.01% (w/v) bromophenol blue) and 10× NuPAGETM sample reducing reagent (Thermo Fisher Scientific, Waltham, MA, USA). To separate proteins, samples were denatured at 95 °C for 5 min, then 12.5% SDS polyacrylamide gel was utilized for separation. Separated proteins were transferred onto nitrocellulose membranes (A29591442, GE Healthcare Life Science, Munich, Germany) followed by blocking in 5% (w/v) milk powder (MP) in TBST (50 mM Tris, pH 7.5; 150 mM NaCl; 0.1% (w/v) Tween-20), and then incubated for 1 h. The following primary antibodies were utilized: anti-PTEN (1:1000 in 5% MP in TBST, 9559T, Cell Signaling, Leiden, NL, USA), anti-GFAP (1:1000 in 5% bovine serum albumin in TBST, M0761, Dako GmbH, Jena, Germany), anti-SOX2 (1:2000 in 5% MP in TBST, ab97959, Abcam, Berlin, Germany), and anti-GAPDH (glyceraldehyde 3-phosphate dehydrogenase, 1:10,000 in 5% MP in TBST, 181602, Abcam, UK). After overnight incubation with primary antibodies at 4 °C, nitrocellulose membranes were washed three times with TBST. Then, membranes were incubated with horseradish peroxidase-conjugated antibodies (ab2116, Abcam, 1:5000) for 1 h. Membranes were washed again with TBST. By the addition of Western Bright Sirius substrate (K-12043-D10, Advansta, San Jose, CA, USA), chemiluminescence was detected using the ChemiDoc MP Imaging System (Bio-rad Laboratories GmbH, Feldkirchen, Germany). Western blot quantification was realized by using the Image J software version 1.53t (NIH, Bethesda, MD, USA).

2.9. Kyoto Encyclopedia of Genes and Genomes (KEGG) Analyses

To functionally characterize the most dysregulated miRNAs in patient-derived GSCs and their differentiated status, KEGG enrichment analysis was performed using the DIANAmiR-Path v3.0 web app, an online software suite dedicated to the evaluation of the regulatory role of miRNAs and the identification of controlled pathways [17]. The barplot and the chord diagram were built in the R environment (v. 4.1.3) with ggplot2, and circlize R packages [18,19].

2.10. Statistical Analysis

Results from multiple replicates are presented as the mean ± standard deviation (SD). The miRNA PCR array was conducted once. Paired Student's *t*-tests were applied for statistical comparison between the two groups. Results were considered as not significant (ns) ($p > 0.05$), significant (*) ($p < 0.05$), highly significant (**) ($p < 0.01$), or very highly significant (***) ($p < 0.001$) / (****) ($p < 0.0001$). Statistical analysis was performed utilizing GraphPad PRISM 9, version 9.1 (Insight Partners, New York, NY, USA).

3. Results

3.1. Differentiation of GSCs

GSC lines 2017/151, 2016/240, and 2017/74 were derived from resected tumor tissues of three patients with primary, isocitrate-dehydrogenase (IDH) wildtype GBM. Information regarding molecular-pathological features as well as clinical information is presented in Table 1. In cell culture, GSCs formed typical non-adherent neurospheres (Figure 1a, left).

On differentiation, cells acquired morphological features similar to those of glial cells. For instance, differentiated cells grew in monolayers attached to the bottom of six-well plates and developed long, star-shaped cellular protrusions (Figure 1a, right). As previously demonstrated, a side population analysis was conducted. Here, a population of cells with a higher efflux, hence a lower intracellular concentration of Hoechst dye, was identified. Inhibition of ABC transporters with verapamil and concomitant blockage of efflux confirmed the specificity of the side population as an efflux was no longer detectable [14]. At the molecular level, GSCs expressed high levels of the stem cell marker *CD133*. In contrast, differentiation resulted in a significant decrease in *CD133* expression on the mRNA level in all three GSC lines (Figure 1b, left). On the mRNA level, additional stem cell markers such as CD44, Sox2, and Nestin were tested with similar, but less consistent trends for Sox2 and Nestin, while CD44 was induced in differentiated GSCs (Supplementary Figure S1), similar to the significant increase observed for *GFAP* mRNA expression (Figure 1b, right).

Table 1. Clinical information and histopathological characteristics of patient-derived GSC lines. All three patients suffered from primary, isocitrate dehydrogenase (IDH) wildtype glioblastoma. Here, clinical parameters including age at diagnosis, sex, survival in days, and tumor localization are presented. Furthermore, histopathological data such as methylation status of the O6-methylguanine-DNA-methyltransferase (MGMT), p53 accumulation, and Ki67 labeling index (Ki67-Li) are presented.

GSC Line	Age at Diagnosis (in Years)	Sex	Survival in Days	Localization	MGMT Promotor Methylation Status	Ki67-Li	p53 Accumulation
2016/240	48	female	641	right frontal lobe	methylated	up to 10%	moderately accumulated
2017/151	66	male	126	right temporal lobe and right insula	methylated	up to 20%	accumulated
2017/74	61	male	398	right temporal lobe	not methylated	up to 50%	moderately accumulated
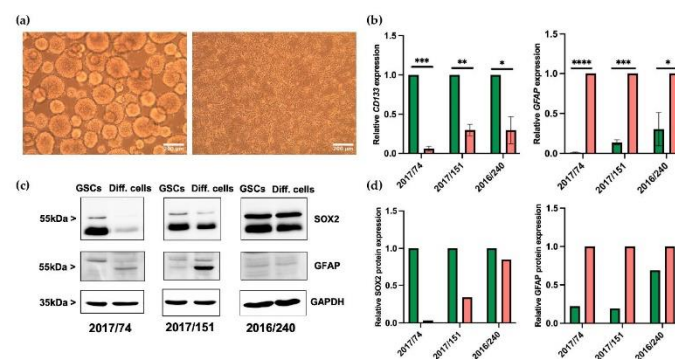
Figure 1. Differentiation of GSCs in astrocytic tumor cells. (**a**) Light microscopy images of 2017/151 spheroid GSCs (left) and adherent differentiated cells (Diff. cells, right). (**b**) Expression of *CD133* and *GFAP* on an mRNA level by RT-qPCR in GSCs (green bars) and corresponding differentiated, astrocytic cells (red bars). Results are given as mean ± SD of three independent experiments. A paired Student's *t*-test was applied to determine significance: * $p < 0.05$, ** $p < 0.01$, *** $p < 0.001$, **** $p < 0.0001$. (**c**) Western Blot of GSCs and Diff. cells showing SOX2 and GFAP expression, where GAPDH was used for internal normalization. (**d**) Western Blot quantification of stem cell marker SOX2 and differentiation marker GFAP in three GSCs lines (green bars) and differentiated cells (red bars).

In addition, Western blot analysis demonstrated that the stem cell marker SOX2 is more greatly expressed in GSCs compared to differentiated cells, while GFAP protein expression increases on differentiation (Figure 1c,d). To summarize, these data suggest that all three GSC lines were successfully differentiated into adherent, growing, astrocytic tumor cells, although to different extents.

3.2. Identification of Dysregulated miRNAs in GSCs and Differentiated Cells

As a screening method to identify changes in miRNA expression induced by GSC differentiation, a pathway-focused miRNA PCR array was conducted. This was realized by generating pooled samples of either GSCs or differentiated cells, containing an equal concentration of miRNAs from each of the three GSC lines and differentiated cell lines, respectively. Differences in miRNA expression based on fold regulation are presented for 84 tested miRNAs by a heatmap (Figure 2a). While green signals represent upregulation in GSCs, the red color indicates the downregulation of respective miRNAs in GSCs and consequently higher expression in differentiated cells. All miRNAs exhibiting fold regulation values > 2 or < −2 were interpreted to be dysregulated by the Qiagen analysis tool. A scatter plot analysis revealed that from a total of 84 tested miRNAs, 22 miRNAs were more greatly expressed in GSCs compared to differentiated cells. In contrast, nine miRNAs displayed lower expression in GSCs and were consequently more greatly expressed in differentiated cells (Figure 2b). A detailed analysis of these dysregulated miRNAs depicted by a heatmap revealed that 10 out of 31 miRNAs were particularly strongly dysregulated (Figure 2c and Table 2). Notably, miR-425-5p, miR-17-5p, miR-424-5p, miR-195-5p, and miR-30c-5p were highly expressed in GSCs. Meanwhile, miR-223-3p and four members of the let-7 miRNA family displayed higher expression in differentiated cells. A thorough literature research was conducted on these 10 miRNAs. Here, we focused on the general role of each miRNA in GBM and the current status of research concerning GSCs (Table 2).
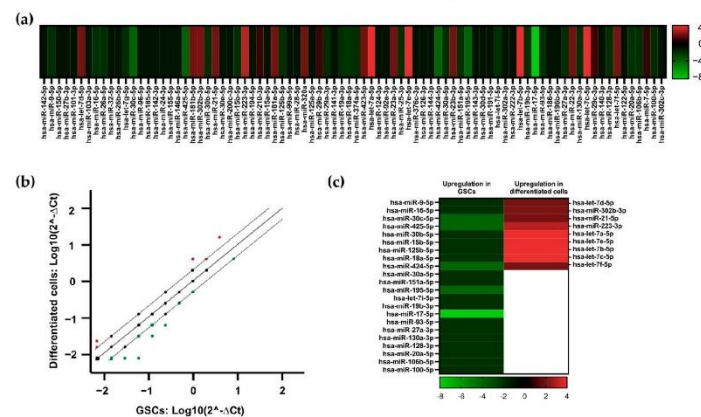
Figure 2. Differentially expressed miRNAs in GSCs and differentiated GBM cells. (**a**) Heatmap of differentially expressed miRNAs in pooled GSCs and pooled differentiated cells generated by fold expression values. Fold regulation values > 1 indicate lower miRNA expression in GSCs and overexpression in differentiated cells (red). Fold regulation values < 0 indicate higher expression in GSCs in comparison with differentiated cells (green). (**b**) Scatter plot analysis (log10 of 2^−delta Ct) of 84 miRNAs tested by the miRNA PCR array. Dotted lines equal log10 of fold regulation of 2 and −2. Green dots indicate upregulation in GSCs, black dots indicate no dysregulation, and red dots indicate overexpression in differentiated cells. (**c**) Heatmap of all tested miRNAs exhibiting fold regulation > 2 or < −2. Fold regulation values > 2 indicate miRNA overexpression in differentiated cells compared to GSCs (red). Fold regulation < −2 indicates miRNA overexpression in GSCs (green).

Table 2. Literature review results on highly dysregulated miRNAs identified in the PCR array. The table includes PCR array results indicated by fold regulation and published data on highly dysregulated miRNAs. We focused on the general role of each miRNA in GBM and their potential roles in GSCs. Plus, reported functionally relevant mRNA targets and predicted target genes directly involved in a GSC or differentiated state, respectively, are listed. For miRNA target prediction, the online software miRPathDB v2.0 was used.

miRNA	Upregulated in	Fold Regulation	Role in GBM	Role in GSCs	mRNA Target
miR-17-5p	GSCs	−8.05	Onco-miRNA [20] Highly expressed in GBM, correlated with poor prognosis [20]	Highly expressed in GSCs [21–23] Increases GSC proliferation [21]	PTEN [23] GFAP (predicted) [24]
miR-425-5p	GSCs	−4.00	Onco-miRNA [25] Associated with poor prognosis [25]	Highly expressed in GSCs [25] Promotes neurosphere formation and GSC survival [25]	PTEN [26] GFAP (predicted) [24]
miR-30c-5p	GSCs	−4.00	Conflicting data Promotes chemoresistance [27] Inhibition of proliferation, migration, and invasion [28] Downregulation in GBM tissue [28]	Unexplored	SOX-9 [28]
miR-424-5p	GSCs	−4.04	Conflicting data Effects on migration and proliferation, induction of apoptosis [29–31] Inhibition of epithelial-to-mesenchymal transition (EMT) and tumor growth [31] Enhances chemoresistance [30]	Unexplored	Akt-1, RAF1 [29] GFAP (predicted) [24]
miR-195-5p	GSCs	−4.05	Conflicting data Affects response to TMZ [32,33] Inhibits proliferation [34] Upregulated in recurrent GBM samples [35]	Unexplored	Cyclin E1 [32] Cyclin D1 [34] GFAP (predicted) [24]
let-7a-5p	Differentiated cells	4.01	Tumor-suppressor miRNA family [36,37] Inhibition of tumor cells' migration, proliferation, and invasion [36,37] Promotes cell cycle arrest and apoptosis [36]	Low expression in GSCs [38] Inhibition of neurosphere growth [37]	K-Ras [36] Musashi-2 (predicted) [24]
let-7e-5p		3.97			MMP9 [39] Musashi-2 (predicted) [24]
let-7b-5p		3.97			E2F2 [37] Musashi-2, Musashi-1 (predicted) [24]
let-7c-5p		4.00			Musashi-2 (predicted) [24]
miR-233-3p	Differentiated cells	3.09	Tumor-suppressor miRNA [40] Enhances radiation sensitivity of GBM cells [40]	Unexplored	ATM [40] Musashi-2 (predicted) [24]

Taken together, the PCR array identified a changed miRNA expression profile in GSCs and differentiated cells and revealed several candidate miRNAs for further investigation into GSC/GBM cell transition.

3.3. miR-425-5p Is Downregulated in Differentiated GSCs

From all dysregulated miRNAs, four miRNAs, miR-425-5p, miR-17-5p, let-7a-5p, and miR-223-3p, turned out to be functional candidates in GSCs for tumor cell differentiation. To validate the miRNA expression levels found in our PCR array screening using pooled miRNAs from all three GSCs (Figure 3a), we determined miRNA expression levels in all three GSC lines separately (Figure 3b and Supplementary Figure S2). Most consistently, miR-425-5p was significantly overexpressed in all three GSC lines compared to differentiated, astrocytic tumor cells (Figure 3b). miR-17-5p proved to be significantly overexpressed in GSCs (Supplementary Figure S2a). Meanwhile, let-7a-5p and miR223-3p downregulation in GSCs compared with differentiated cells could not be verified in the three GSC lines (Supplementary Figure S2b,c).
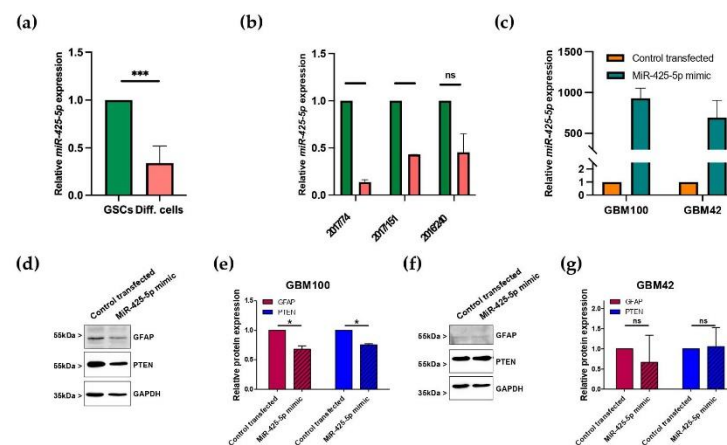
Figure 3. Expression of miR-425-5p in GSCs and effects on GFAP and PTEN protein levels in GBM cells. (**a**) Expression of miR-425-5p in GSCs (green) and their differentiated state (red). RT-qPCR results for differentiated 2017/74, 2017/151, and 2016/240 were normalized to undifferentiated controls. (**b**) Detailed depiction of miR-425-5p expression in each GSC line (green) and its corresponding differentiated state (red). Results are shown as mean values ± SD of two independent experiments. (**c**) miR-425-5p mimic transfection of primary GBM cell lines GBM100 and GBM42. (**d**) Representative Western blot demonstrating GFAP and PTEN expression after miR-425-5p mimic transfection in GBM100 cells. (**e**) Quantification of GFAP and PTEN protein expression in transfected GBM100 cells. (**f**) Representative Western blot demonstrating GFAP and PTEN expression after miR-425-5p mimic transfection in GBM42 cells. (**g**) Quantification of GFAP and PTEN protein expression in transfected GBM42 cells. Two independent experiments were conducted. Results are presented as mean values ± SD. A paired Student's *t*-test was applied to determine significance: ns $p > 0.05$, * $p < 0.05$, *** $p < 0.001$.

3.4. Transfection of miRNA Mimic Affects Protein Levels of GFAP in Patient-Derived GBM Cells

As shown in Table 2, miR-425-5p was identified to potentially target the GFAP gene, which is expressed as a marker of differentiated GBM cells, so that downregulation of miR-425-5p in GSCs could increase GFAP levels in the course of differentiation into GBM cells. To explore this, we transfected two patient-derived GBM cell strains (GBM100 and GBM42) with a miR-425-5p mimic miRNA (Figure 3c). About 48 h after transfection, cells

were lysed and analyzed for protein levels of GFAP and the known miR-425-5p target PTEN. In GBM100, both GFAP and PTEN protein levels were reduced after mimic transfection (Figure 3d,e), whereas the results for GBM42 were inconsistent (Figure 3f,g). Those first results suggested that GFAP is a target gene for miR-425-5p and could potentially regulate the differentiation state of GBM cells.

3.5. miRNA Profiling in GSC Maintenance and Differentiation

The 10 most regulated miRNAs were analyzed for their biological functions by KEGG enrichment analysis (Figure 4a). The most significant pathways were "Signaling pathways regulating pluripotency of stem cells", "Pathways in cancer", and "PI3K-Akt signaling", a pathway of high importance in GBM. In Figure 4b, the miRNA target relationship to pathways regulating the pluripotency of stem cells is shown in the form of a chord plot. All 10 miRNAs are connected to their mRNA targets, thereby showing their contribution to GSC maintenance or differentiation.
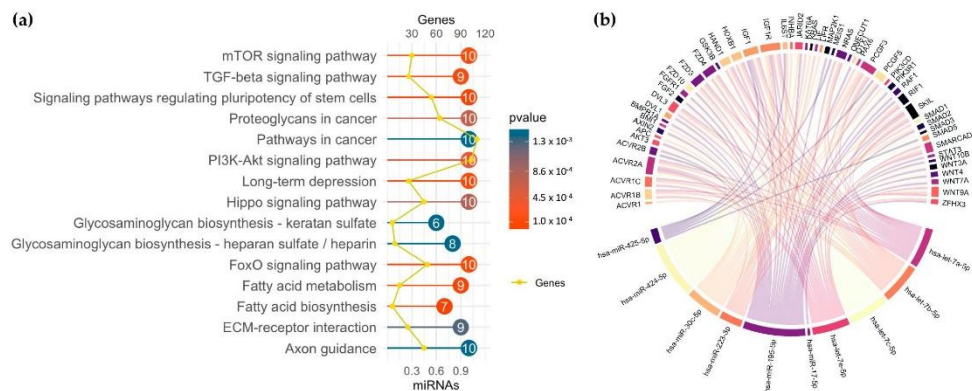
Figure 4. Bioinformatic analysis of the 10 most dysregulated miRNAs. (**a**) KEGG enrichment analysis of the 10 most dysregulated miRNAs. The x-axis reports the number of target genes and the fraction of miRNAs in the starting list involved in the pathway. The number within the dots represents the number of miRNAs. (**b**) The miRNA–target relationship in the KEGG_hsa04550 signaling pathway, "Signaling pathways regulating pluripotency of stem cells". Each link represents a miRNA–target interaction.

4. Discussion

Due to tumor heterogeneity and limited therapeutic options, GBM remains an incurable disease with a devasting prognosis. As modulators of the tumor microenvironment and radio-/chemoresistance, GSCs are considered putative future therapeutic targets [6]. Even though GSCs play a key role in tumor cell invasion, recurrence, and angiogenesis, many underlying signaling pathways remain elusive [41]. MicroRNAs (miRNAs) can act as central regulatory molecules of GBM hallmarks such as invasion or immune evasion [42]. Therefore, miRNAs are discussed as future therapeutic targets and diagnostic biomarkers [43]. Our study detected differences in the miRNA expression profile of GSCs and differentiated tumor cells by PCR array screening. Cultured patient-derived GSCs were stimulated to differentiate into astrocytic tumor cells. Although this in vitro differentiation model is commonly used in GSC research, in vivo GSC differentiation is a complex process as the tumor microenvironment is shaped by a variety of different cell types such as macrophages, microglia, and mesenchymal cells [44].

Based on our results from miRNA PCR array screening, a literature review of mRNA targets, and validating experiments in each GSC line, we present four suitable miRNA

candidates, miR425-5p, miR-17-5p, miR-223-3p, and let-7a-5p, which might be directly and indirectly involved in the regulation of GBM cell differentiation.

Firstly, miR-17-5p, the most dysregulated miRNA in the conducted array, is a known onco-miRNA in GBM [20]. Consistent with other studies, miR-17-5p was highly expressed in GSCs as it stimulates GSC proliferation [21–23]. As physically adjacent miRNA genes are often transcribed at the same time, they are summarized as a cluster. miR-17-5p is often analyzed as a part of the miR-17-92 cluster [45]. Notably, four of six miRNAs of the miR-17-92 cluster were consistently upregulated in our conducted PCR array. In GBM, the miR-17-92 cluster is highly expressed and correlated with a poor prognosis [20].

Secondly, miR-425-5p was upregulated in GSCs concordant with a study by La Rocha et al. [25]. MiR-425-5p is overexpressed in GBM tissue specimens in comparison to normal brain control specimens and acts as an onco-miRNA [25]. Both miR17-5p and miR-425-5p are known to target phosphatase and tensin homolog (PTEN) mRNA [23,26]. PTEN, a key tumor suppressor, is commonly mutated in GBM carcinogenesis [46]. As a predicted mRNA target based on miRPathDB v2.0, expression levels of GFAP could be regulated directly by miR-425-5p and miR-17-5p, suggesting that these miRNAs control astrocytic cell differentiation [24]. As an experimental proof, mimic miR-425-5p when transfected into differentiated patient-derived GBM cells, can regulate GFAP expression. Since these cells are also able to de-differentiate into GSCs, we interpret our findings to reveal that miR-425-5p is able to contribute, among other critical proteins, to GBM cell differentiation. Moreover, as chord analysis suggests, miR-425-5p is potentially involved in gene regulation of IGF1 (insulin growth factor 1), gp 130 (IL6ST), MEIS1 (a homeobox gene), SMAD5 (TGF-ß pathway), and PCGF5 (a polycomb transcription factor). All of them could be important mediators of growth signals and cell fate determination in GBM cells.

Furthermore, PCR array analysis identified nine miRNAs that were upregulated in differentiated cells. Notably, six of these nine miRNAs are members of the let-7 miRNA family. Published data revealed that the let-7 family acts as a tumor suppressor in GBM [11,36]. Overexpression of let-7 miRNAs leads to the inhibition of tumor cell migration and promotes apoptosis [36]. According to our PCR array, Degrauwe et al. demonstrated that the let-7 family is scarcely expressed in GSCs [38]. As an interesting mRNA target, Kirsten rat sarcoma virus oncogene homolog (K-Ras), an oncogene and activator of its downstream targets in the mitogen-activated protein kinase (MAPK) pathway, was identified [38]. According to miRPathDB v.2.0 target gene prediction, the stem cell marker Musashi-2 can be directly regulated by the let-7 family and miR-223-3p so that high expression of these miRNAs could suppress the GSC phenotype [24,47]. Additionally, miR-223-3p was overexpressed in differentiated cells. In GBM, miR-223-3p functions as a tumor-suppressor miRNA; its overexpression enhances radio-/chemosensitivity in cell culture models as miR-223-3p targets ataxia telangiectasia mutated (ATM) [40]. ATM initiates repair mechanisms after radio-/chemotherapy-induced DNA damage and thereby contributes to radio-/chemoresistance [48]. Since the role of miR-223-3p is currently uninvestigated in GSCs, future detailed analysis of miR-223-3p and ATM in GSCs is justified.

5. Conclusions

Our study detected a changed miRNA expression profile on GSC differentiation in a well-defined in vitro setup. Through a miRNA PCR array, 31 dysregulated miRNAs were identified. About 10 highly regulated miRNAs, including miR-425-5p, miR-17-5p, miR-223-3p, and the let-7 miRNA family, are promising miRNA candidates for further investigations aiming to manipulate the differentiation status of GSCs.

Supplementary Materials: The following supporting information can be downloaded at: https://www.mdpi.com/article/10.3390/brainsci13020350/s1, Figure S1: qPCR analysis of stem cell markers CD44, Sox2, and Nestin; Figure S2: qPCR analysis of miR425-5p, miR17-5p, let-7a-5p, and miR223-3p in individual GSC lines.

References

1. Vollmann-Zwerenz, A.; Leidgens, V.; Feliciello, G.; Klein, C.A.; Hau, P. Tumor Cell Invasion in Glioblastoma. *Int. J. Mol. Sci.* **2020**, *21*, 1932. [CrossRef] [PubMed]
2. Anjum, K.; Shagufta, B.I.; Abbas, S.Q.; Patel, S.; Khan, I.; Shah, S.A.A.; Akhter, N.; Hassan, S.S.U. Current status and future therapeutic perspectives of glioblastoma multiforme (GBM) therapy: A review. *Biomed. Pharmacother.* **2017**, *92*, 681–689. [CrossRef] [PubMed]
3. Alifieris, C.; Trafalis, D.T. Glioblastoma multiforme: Pathogenesis and treatment. *Pharmacol. Ther.* **2015**, *152*, 63–82. [CrossRef] [PubMed]
4. Garnier, D.; Renoult, O.; Alves-Guerra, M.-C.; Paris, F.; Pecqueur, C. Glioblastoma Stem-Like Cells, Metabolic Strategy to Kill a Challenging Target. *Front. Oncol.* **2019**, *9*, 118. [CrossRef]
5. Lathia, J.D.; Mack, S.C.; Mulkearns-Hubert, E.E.; Valentim, C.L.L.; Rich, J.N. Cancer stem cells in glioblastoma. *Genes Dev.* **2015**, *29*, 1203–1217. [CrossRef]
6. Gimple, R.C.; Bhargava, S.; Dixit, D.; Rich, J.N. Glioblastoma stem cells: Lessons from the tumor hierarchy in a lethal cancer. *Genes Dev.* **2019**, *33*, 591–609. [CrossRef] [PubMed]
7. Aghajani, M.; Mansoori, B.; Mohammadi, A.; Asadzadeh, Z.; Baradaran, B. New emerging roles of CD133 in cancer stem cell: Signaling pathway and miRNA regulation. *J. Cell. Physiol.* **2019**, *234*, 21642–21661. [CrossRef]
8. Barzegar Behrooz, A.; Syahir, A.; Ahmad, S. CD133: Beyond a cancer stem cell biomarker. *J. Drug Target.* **2019**, *27*, 257–269. [CrossRef]
9. Ricci-Vitiani, L.; Pallini, R.; Larocca, L.M.; Lombardi, D.G.; Signore, M.; Pierconti, F.; Petrucci, G.; Montano, N.; Maira, G.; de Maria, R. Mesenchymal differentiation of glioblastoma stem cells. *Cell Death Differ.* **2008**, *15*, 1491–1498. [CrossRef]
10. Aldaz, B.; Sagardoy, A.; Nogueira, L.; Guruceaga, E.; Grande, L.; Huse, J.T.; Aznar, M.A.; Díez-Valle, R.; Tejada-Solís, S.; Alonso, M.M.; et al. Involvement of miRNAs in the differentiation of human glioblastoma multiforme stem-like cells. *PLoS ONE* **2013**, *8*, e77098. [CrossRef]
11. Shea, A.; Harish, V.; Afzal, Z.; Chijioke, J.; Kedir, H.; Dusmatova, S.; Roy, A.; Ramalinga, M.; Harris, B.; Blancato, J.; et al. MicroRNAs in glioblastoma multiforme pathogenesis and therapeutics. *Cancer Med.* **2016**, *5*, 1917–1946. [CrossRef]
12. O'Brien, J.; Hayder, H.; Zayed, Y.; Peng, C. Overview of MicroRNA Biogenesis, Mechanisms of Actions, and Circulation. *Front. Endocrinol.* **2018**, *9*, 402. [CrossRef] [PubMed]
13. Buruiană, A.; Florian, Ș.I.; Florian, A.I.; Timiș, T.-L.; Mihu, C.M.; Miclăuș, M.; Oșan, S.; Hrapșa, I.; Cataniciu, R.C.; Farcaș, M.; et al. The Roles of miRNA in Glioblastoma Tumor Cell Communication: Diplomatic and Aggressive Negotiations. *Int. J. Mol. Sci.* **2020**, *21*, 1950. [CrossRef] [PubMed]
14. Hannen, R.; Selmansberger, M.; Hauswald, M.; Pagenstecher, A.; Nist, A.; Stiewe, T.; Acker, T.; Carl, B.; Nimsky, C.; Bartsch, J.W. Comparative Transcriptomic Analysis of Temozolomide Resistant Primary GBM Stem-Like Cells and Recurrent GBM Identifies Up-Regulation of the Carbonic Anhydrase CA2 Gene as Resistance Factor. *Cancers* **2019**, *11*, 921. [CrossRef]

15. Dong, F.; Eibach, M.; Bartsch, J.W.; Dolga, A.M.; Schlomann, U.; Conrad, C.; Schieber, S.; Schilling, O.; Biniossek, M.L.; Culmsee, C.; et al. The metalloprotease-disintegrin ADAM8 contributes to temozolomide chemoresistance and enhanced invasiveness of human glioblastoma cells. *Neuro Oncol.* **2015**, *17*, 1474–1485. [CrossRef] [PubMed]
16. Schlomann, U.; Koller, G.; Conrad, C.; Ferdous, T.; Golfi, P.; Garcia, A.M.; Höfling, S.; Parsons, M.; Costa, P.; Soper, R.; et al. ADAM8 as a drug target in pancreatic cancer. *Nat. Commun.* **2015**, *6*, 6175. [CrossRef]
17. Vlachos, I.S.; Zagganas, K.; Paraskevopoulou, M.D.; Georgakilas, G.; Karagkouni, D.; Vergoulis, T.; Dalamagas, T.; Hatzigeorgiou, A.G. DIANA-miRPath v3.0: Deciphering microRNA function with experimental support. *Nucleic Acids Res.* **2015**, *43*, W460–W466. [CrossRef]
18. Wickham, H. *ggplot2: Elegant Graphics for Data Analysis*; Springer International Publishing: New York, NY, USA, 2016; ISBN 978-3-319-24275-0.
19. Gu, Z.; Gu, L.; Eils, R.; Schlesner, M.; Brors, B. circlize Implements and enhances circular visualization in R. *Bioinformatics* **2014**, *30*, 2811–2812. [CrossRef] [PubMed]
20. Gruszka, R.; Zakrzewska, M. The Oncogenic Relevance of miR-17-92 Cluster and Its Paralogous miR-106b-25 and miR-106a-363 Clusters in Brain Tumors. *Int. J. Mol. Sci.* **2018**, *19*, 879. [CrossRef]
21. Ernst, A.; Campos, B.; Meier, J.; Devens, F.; Liesenberg, F.; Wolter, M.; Reifenberger, G.; Herold-Mende, C.; Lichter, P.; Radlwimmer, B. De-repression of CTGF via the miR-17-92 cluster upon differentiation of human glioblastoma spheroid cultures. *Oncogene* **2010**, *29*, 3411–3422. [CrossRef]
22. Schraivogel, D.; Weinmann, L.; Beier, D.; Tabatabai, G.; Eichner, A.; Zhu, J.Y.; Anton, M.; Sixt, M.; Weller, M.; Beier, C.P.; et al. CAMTA1 is a novel tumour suppressor regulated by miR-9/9* in glioblastoma stem cells. *EMBO J.* **2011**, *30*, 4309–4322. [CrossRef]
23. Li, H.; Yang, B.B. Stress response of glioblastoma cells mediated by miR-17-5p targeting PTEN and the passenger strand miR-17-3p targeting MDM2. *Oncotarget* **2012**, *3*, 1653–1668. [CrossRef]
24. Kehl, T.; Kern, F.; Backes, C.; Fehlmann, T.; Stöckel, D.; Meese, E.; Lenhof, H.-P.; Keller, A. miRPathDB 2.0: A novel release of the miRNA Pathway Dictionary Database. *Nucleic Acids Res.* **2020**, *48*, D142–D147. [CrossRef]
25. De La Rocha, A.M.A.; González-Huarriz, M.; Guruceaga, E.; Mihelson, N.; Tejada-Solís, S.; Díez-Valle, R.; Martínez-Vélez, N.; Fueyo, J.; Gomez-Manzano, C.; Alonso, M.M.; et al. miR-425-5p, a SOX2 target, regulates the expression of FOXJ3 and RAB31 and promotes the survival of GSCs. *Arch. Clin. Biomed. Res.* **2020**, *4*, 221–238. [CrossRef]
26. Zhou, J.-S.; Yang, Z.-S.; Cheng, S.-Y.; Yu, J.-H.; Huang, C.-J.; Feng, Q. miRNA-425-5p enhances lung cancer growth via the PTEN/PI3K/AKT signaling axis. *BMC Pulm. Med.* **2020**, *20*, 223. [CrossRef] [PubMed]
27. Quintavalle, C.; Donnarumma, E.; Iaboni, M.; Roscigno, G.; Garofalo, M.; Romano, G.; Fiore, D.; de Marinis, P.; Croce, C.M.; Condorelli, G. Effect of miR-21 and miR-30b/c on TRAIL-induced apoptosis in glioma cells. *Oncogene* **2013**, *32*, 4001–4008. [CrossRef] [PubMed]
28. Liu, S.; Li, X.; Zhuang, S. miR-30c Impedes Glioblastoma Cell Proliferation and Migration by Targeting SOX9. *Oncol. Res.* **2019**, *27*, 165–171. [CrossRef]
29. Gheidari, F.; Arefian, E.; Adegani, F.J.; Kalhori, M.R.; Seyedjafari, E.; Kabiri, M.; Teimoori-Toolabi, L.; Soleimani, M. miR-424 induces apoptosis in glioblastoma cells and targets AKT1 and RAF1 oncogenes from the ERBB signaling pathway. *Eur. J. Pharmacol.* **2021**, *906*, 174273. [CrossRef] [PubMed]
30. Xu, H.; Zhang, H.; Tan, L.; Yang, Y.; Wang, H.; Zhao, Q.; Lu, J. FAM87A as a Competing Endogenous RNA of miR-424-5p Suppresses Glioma Progression by Regulating PPM1H. *Comput. Math. Methods Med.* **2021**, *2021*, 7952922. [CrossRef] [PubMed]
31. Zhao, C.; Wang, X.-B.; Zhang, Y.-H.; Zhou, Y.-M.; Yin, Q.; Yao, W.-C. MicroRNA-424 inhibits cell migration, invasion and epithelial-mesenchymal transition in human glioma by targeting KIF23 and functions as a novel prognostic predictor. *Eur. Rev. Med. Pharmacol. Sci.* **2018**, *22*, 6369–6378. [CrossRef]
32. Wang, H.; Ren, S.; Xu, Y.; Miao, W.; Huang, X.; Qu, Z.; Li, J.; Liu, X.; Kong, P. MicroRNA-195 reverses the resistance to temozolomide through targeting cyclin E1 in glioma cells. *Anticancer. Drugs* **2019**, *30*, 81–88. [CrossRef]
33. Xu, N.; Liu, B.; Lian, C.; Doycheva, D.M.; Fu, Z.; Liu, Y.; Zhou, J.; He, Z.; Yang, Z.; Huang, Q.; et al. Long noncoding RNA AC003092.1 promotes temozolomide chemosensitivity through miR-195/TFPI-2 signaling modulation in glioblastoma. *Cell Death Dis.* **2018**, *9*, 1139. [CrossRef]
34. Liu, K.; Deng, Y.; Yang, Y.; Wang, H.; Zhou, P. MicorRNA-195 links long non-coding RNA SEMA3B antisense RNA 1 (head to head) and cyclin D1 to regulate the proliferation of glioblastoma cells. *Bioengineered* **2022**, *13*, 8798–8805. [CrossRef] [PubMed]
35. Yu, W.; Liang, X.; Li, X.; Zhang, Y.; Sun, Z.; Liu, Y.; Wang, J. MicroRNA-195: A review of its role in cancers. *OncoTargets Ther.* **2018**, *11*, 7109–7123. [CrossRef]
36. Wang, X.-R.; Luo, H.; Li, H.-L.; Cao, L.; Wang, X.-F.; Yan, W.; Wang, Y.-Y.; Zhang, J.-X.; Jiang, T.; Kang, C.-S.; et al. Overexpressed let-7a inhibits glioma cell malignancy by directly targeting K-ras, independently of PTEN. *Neuro Oncol.* **2013**, *15*, 1491–1501. [CrossRef]
37. Song, H.; Zhang, Y.; Liu, N.; Zhang, D.; Wan, C.; Zhao, S.; Kong, Y.; Yuan, L. Let-7b inhibits the malignant behavior of glioma cells and glioma stem-like cells via downregulation of E2F2. *J. Physiol. Biochem.* **2016**, *72*, 733–744. [CrossRef]
38. Degrauwe, N.; Schlumpf, T.B.; Janiszewska, M.; Martin, P.; Cauderay, A.; Provero, P.; Riggi, N.; Suvà, M.-L.; Paro, R.; Stamenkovic, I. The RNA Binding Protein IMP2 Preserves Glioblastoma Stem Cells by Preventing let-7 Target Gene Silencing. *Cell Rep.* **2016**, *15*, 1634–1647. [CrossRef] [PubMed]

39. Ventayol, M.; Viñas, J.L.; Sola, A.; Jung, M.; Brüne, B.; Pi, F.; Mastora, C.; Hotter, G. miRNA let-7e targeting MMP9 is involved in adipose-derived stem cell differentiation toward epithelia. *Cell Death Dis.* **2014**, *5*, e1048. [CrossRef] [PubMed]
40. Liang, L.; Zhu, J.; Zaorsky, N.G.; Deng, Y.; Wu, X.; Liu, Y.; Liu, F.; Cai, G.; Gu, W.; Shen, L.; et al. MicroRNA-223 enhances radiation sensitivity of U87MG cells in vitro and in vivo by targeting ataxia telangiectasia mutated. *Int. J. Radiat. Oncol. Biol. Phys.* **2014**, *88*, 955–960. [CrossRef]
41. Boyd, N.H.; Tran, A.N.; Bernstock, J.D.; Etminan, T.; Jones, A.B.; Gillespie, G.Y.; Friedman, G.K.; Hjelmeland, A.B. Glioma stem cells and their roles within the hypoxic tumor microenvironment. *Theranostics* **2021**, *11*, 665–683. [CrossRef]
42. Karsy, M.; Arslan, E.; Moy, F. Current Progress on Understanding MicroRNAs in Glioblastoma Multiforme. *Genes Cancer* **2012**, *3*, 3–15. [CrossRef] [PubMed]
43. He, B.; Zhao, Z.; Cai, Q.; Zhang, Y.; Zhang, P.; Shi, S.; Xie, H.; Peng, X.; Yin, W.; Tao, Y.; et al. miRNA-based biomarkers, therapies, and resistance in Cancer. *Int. J. Biol. Sci.* **2020**, *16*, 2628–2647. [CrossRef]
44. Da Ros, M.; de Gregorio, V.; Iorio, A.; Giunti, L.; Guidi, M.; de Martino, M.; Genitori, L.; Sardi, I. Glioblastoma Chemoresistance: The Double Play by Microenvironment and Blood-Brain Barrier. *Int. J. Mol. Sci.* **2018**, *19*, 2879. [CrossRef]
45. Olive, V.; Jiang, I.; He, L. mir-17-92, a cluster of miRNAs in the midst of the cancer network. *Int. J. Biochem. Cell Biol.* **2010**, *42*, 1348–1354. [CrossRef] [PubMed]
46. Montano, N. Biomarkers in Glioblastoma multiforme. Evidences from a literature review. *J. Clin. Transl. Res.* **2016**, *2*, 3–10. [CrossRef]
47. Kudinov, A.E.; Karanicolas, J.; Golemis, E.A.; Boumber, Y. Musashi RNA-Binding Proteins as Cancer Drivers and Novel Therapeutic Targets. *Clin. Cancer Res.* **2017**, *23*, 2143–2153. [CrossRef]
48. Ferri, A.; Stagni, V.; Barilà, D. Targeting the DNA Damage Response to Overcome Cancer Drug Resistance in Glioblastoma. *Int. J. Mol. Sci.* **2020**, *21*, 4910. [CrossRef]

8 Appendix

8.1 Curriculum Vitae

8.2 Verzeichnis akademischer Lehrer

Meine akademischen Lehrer waren die Damen und Herren in Marburg:

Adamkiewicz, Adamus, Adhikary, Aktuna, Bodgan, Bopp, Bouazoune, Brandt, Braun, Brehm, Brendel, Burchert, C. Bauer, Del Rey, D. K. Bartsch, Di Fazio, Elsässer, Frech, Greene, Grgic, Hänze, Huber, J. W. Bartsch, Jacob, Dörsam, Lauth, Lieber, Lill, Maisner, Mandic, Moll, Mühlenhoff, Müller, Müller-Brüsselbach, Neubauer, Nimsky, Oberwinkler, Oehrn, Oliver, Pagenstecher, Pankuweit, Plant, Pogge von Strandmann, Ponath, Preußer, Purvanov, Roth, Rust, S. Bauer, Schäfer, Schlomann, Schmeck, Schmidt, Schmuck, Schnare, Schötz, Schulte, Schütz, Slater, Sommer, Stehling, Steinhoff, Stiewe, Strauer, Suske, Timmesfeld, Timofeev, Visekruna, Wanzel, Weihe, Westermann, Worzfeld, Wrocklage, Wüstenhagen

8.3 Danksagung

8.4 Ehrenwörtliche Erklärung